# INFLUENCE OF BRACING SYSTEMS ON THE BEHAVIOR OF CURVED AND SKEWED STEEL I-GIRDER BRIDGES DURING CONSTRUCTION

A Dissertation
Presented to
The Academic Faculty

By

Telmo Andres Sanchez Grunauer

In Partial Fulfillment
Of the Requirements for the Degree
Doctor of Philosophy in the
School of Civil and Environmental Engineering

Georgia Institute of Technology

December 2011

# INFLUENCE OF BRACING SYSTEMS ON THE BEHAVIOR OF CURVED AND SKEWED STEEL I-GIRDER BRIDGES DURING CONSTRUCTION

Approved by:


Dr. Donald W. White, Advisor
School of Civil and Environmental Engineering
*Georgia Institute of Technology*

Dr. Roberto T. Leon, Advisor
School of Civil and Environmental Engineering
*Georgia Institute of Technology*

Dr. Bruce R. Ellingwood
School of Civil and Environmental Engineering
*Georgia Institute of Technology*

Dr. Kenneth M. Will
School of Civil and Environmental Engineering
*Georgia Institute of Technology*

Dr. Dewey H. Hodges
School of Aerospace Engineering
*Georgia Institute of Technology*



Date Approved: August 18, 2011

To Stephanie and her lovely and contagious smile

# ACKNOWLEDGEMENTS

Pursuing a doctoral degree at Georgia Tech has been a wonderful experience, where I have met people that have changed my life in many aspects. In this regard, I would like to start expressing my gratitude to my advisor, Dr. Donald W. White. I do not know of any other person that can combine the understanding that Dr. White has in all the aspects of our profession, with an extraordinary sense of humor. It has been an honor to work for whom I consider to be one of the most prominent researchers in the field of steel structures. I also would like to thank my thesis committee members, Dr. Roberto Leon, Dr. Bruce Ellingwood, Dr. Kenneth Will, and Dr. Dewey Hodges. Their input and guidance helped me improve several parts of my research and of the thesis manuscript.

The financial support of the National Cooperative Highway Research Program is gratefully acknowledged. Similarly, I would like to thank Domenic Coletti and Dr. Brandon Chavel from HDR Engineering, Inc., for the valuable input provided in various topics of this thesis.

In special, I would like to thank my friend and colleague Cagri Ozgur. Cagri has been a good friend since my first day in Atlanta. He and my other great friend, Efe Guney, have helped me in many ways, and have been always there to work, to have fun, or do anything else. My officemates Yoon-Duk, Akhil, Cliff, Juan Manuel, Towhid, and Yavuz will also be deeply remembered for their friendship and all the great moments that we spent together.

I want to express my gratitude to my family and in special to my daughter Stephanie. She came to this world to become my largest inspiration. It is because of her that I have been able to pursue my dreams.

Finally and foremost, I would like to thank my future wife, Eva, for her love and all the wonderful moments that we have shared in Atlanta. Without doubts, meeting her was the most important aspect of pursuing a doctorate degree at Georgia Tech.

# TABLE OF CONTENTS

# LIST OF TABLES

# LIST OF FIGURES

# SUMMARY

The construction of horizontally curved bridges with skewed supports requires careful consideration. These types of bridges exhibit three-dimensional response characteristics that are not commonly seen in straight bridges with normal supports. As a result of this behavior, engineers may face difficulties during the construction, when the components of the bridge do not fit together or the final geometry of the structure does not correspond to that intended by the designer. These complications can lead to problems that compromise the serviceability aspects of the bridge and in some cases, its structural integrity.

The three dimensional response that curved and skewed bridges exhibit is directly influenced by the bracing system used to configure the structure. In I-girder bridges, cross-frames are provided to integrate the structure, transforming the individual girders into a structural system that can support larger loads than when the girders work separately. In general, they facilitate the construction of the structure. However, they can also induce undesired collateral effects that can be a detriment to the performance of the system. These effects must be considered in the design of a curved and skewed bridge because, in some cases, they can modify substantially its response.

This research is focused on understanding how the bracing system affects the performance of curved and skewed I-girder bridges, as well as, the ability of the approximate analysis methods to capture the structural behavior. In this research, techniques that can be implemented in the creation of 2D-grid models are developed to overcome the limitations of this analysis method. In addition, efficient cross-frame

arrangements that mitigate the collateral effects of skew are developed. These mitigation schemes reduce the undesired cross-frame forces and flange lateral bending stresses associated with the transverse stiffness of the structure, while ensuring that the bracing system still performs its intended functions.

# CHAPTER I

# INTRODUCTION

## 1.1. Background

The construction of a steel bridge has five fundamental phases: The analysis and design of the structure, the detailing and elaboration of the fabrication drawings, the fabrication of the bridge components, the erection of the steel structure, and the placement of the concrete deck and appurtenances.

In horizontally curved bridges with skewed supports the completion of each of these phases requires careful considerations. These types of bridges exhibit three-dimensional response characteristics that are not commonly seen in straight bridges with normal supports. As a result of this behavior, engineers may face difficulties during the structure erection, when the components of the bridge do not fit together or the final geometry of the structure does not correspond to that intended by the designer. These complications can lead to problems that compromise the serviceability aspects of the bridge and in some cases, its structural integrity.

The three dimensional response that curved and skewed bridges exhibit is directly influenced by the bracing system that is used to configure the structure. In I-girder bridges, cross-frames are provided to consolidate the structure, transforming the individual girders into a structural system that can support larger loads than when the girders work separately. Beyond stabilizing the girders, the cross-frames perform other functions in the system. During the placement of the concrete deck, the cross-frames help

control the girder deflections and the profile of the deck. They also provide the load path necessary to resist wind actions. In general, they facilitate the construction of the structure. However, they can also induce undesired collateral effects that can be a detriment to the performance of the system. These effects must be considered in the design of a curved and skewed bridge because, in some cases, they can substantially modify its response.

Another factor that merits consideration is the presence of the stay-in-place (SIP) metal deck forms in the system. These forms provide the surface necessary to pour the concrete and also facilitate its placement. Traditionally, engineers have not considered the forms as a means to provide stability bracing, so they are ignored in the analysis. However, the forms are part of the system and in some cases their effects may not be negligible. In some bridges they may influence the girder deflections during the deck placement.

This research is focused on understanding how the bracing systems and the SIP forms affect the performance of curved and skewed I-girder bridges, as well as the ability of the available analysis methods to capture the structural behavior. Most of the studies and recommendations provided in this thesis are based on an evaluation of the physical aspects that impact the three-dimensional response in curved and skewed bridges.

With respect to analysis methods, these studies explore the attributes necessary to predict the structural responses during construction. Approximate 1D line-girder and 2D-grid analyses are investigated to determine their applicability in the design of complex bridge systems. Additionally, research is conducted to propose practices that can improve

the accuracy of the analysis of I-girder bridges using 2D-grid models. Specifically, better representations of the I-girder torsional properties and of the cross-frame stiffness contributions are proposed for use in 2D-grid analyses.

## 1.2. Research Objective

The objective of this research is to improve the practices used to analyze and design curved and/or skewed steel I-girder bridges for construction, with particular attention to the influence of the bracing system on the structural behavior. The following are the activities pursued to achieve this objective:

1) **Investigate the influence of skew on the behavior of I-girder bridges:** The support skew induces torsion in the girders. The unequal lateral and vertical displacements that occur due to the skew at locations where the girders are connected with cross-frames are accommodated in the form of girder twists. This can result in undesired large forces in the cross-frames and lateral bending stresses in the girder flanges that need to be considered in the structural design. In addition, the girder twists or layovers can complicate the construction of a skewed bridge in its different phases. Specifically, the steel erection and the deck placement are stages that require special consideration since the structure's assembly and the control of the deck profile can be affected by the skew. As illustrated in Figure 1.1(a), when the girder layovers are excessive they can cause misalignments in the bearings, which can result in bearing damage. Similarly, as shown in Figure 1.1(b), girder layovers affect the structure’s profile, complicating the deck placement, and the control of the deck thickness.

(a) Bearing misalignment

(b) Excessive girder layovers

Figure 1.1. Complications associated with skew effects in the construction of I-girder bridges

The above discussion shows that skewed supports may induce an undesirable behavior of the structure. An understanding of the associated mechanisms that cause twisting of the girders is essential to determine practices that can mitigate the impact of the skew effects. In this research, studies are conducted of structures of different

characteristics to identify the basic parameters that control the behavior of a skewed bridge and how each of them influences the system performance.

2) **Develop methods to reduce the collateral effects of skew:** In curved and/or skewed bridges, the bracing system has a direct effect on the structural responses. In straight and skewed bridges, in addition to stabilizing the girders during the noncomposite stages, the cross-frames provide an alternate load path that affects the bridge behavior. In this research, efficient arrangements of the cross-frames that mitigate the collateral effects of skew are developed. The techniques proposed to improve the structural performance are based on a mechanistic evaluation of the skew effects. The objective is to reduce the undesired cross-frame forces and flange lateral bending stresses associated with the transverse stiffness of the structure, while ensuring that the bracing system still performs its intended functions.

3) **Investigate the virtues and limitations of the methods used to analyze and design I-girder bridges:** Line girder (1D) and grid (2D) methods are commonly used in the industry to analyze and design bridge structures. The inherent three-dimensional behavior that curved and/or skewed bridges exhibit, however, is not always properly captured by these methods. In this research, the virtues and limitations of these procedures are studied to establish limits of their applicability. In the study of the 2D-grid methods, the investigation is focused on determining the capabilities of the elements implemented in computer programs to model the bridge components. The elements and techniques used to simulate the behavior of I-girders and cross-frames are investigated to highlight their deficiencies and propose techniques that can improve the accuracy of the results obtained from analyses conducted with this

method. In particular, the development of elements that can accurately capture the behavior of cross-frames and techniques that better simulate the torsional stiffness of the girders are proposed.

4) **Develop methods to predict the responses associated with girder flange lateral bending due to skew effects:** In current practice (2011), there is limited guidance on how the effects of skew should be included in the design of I-girder bridges. Estimates on the magnitude of cross-frame forces, levels of flange lateral bending stresses, and girder twists that can be produced by skew are widely varied. One of the main reasons for this state of affairs is the difficulty to characterize the effects of skew in terms of the bridge geometry. The span length, width, skew angle, and the configuration of the bracing system are some of the variables that have a direct influence on the bridge performance. Another reason is that the approximate methods of analysis used for design often are not able to properly capture the structural responses related to skew. In this research, techniques to recognize potential difficulties due to skew in early stages of the design process are provided. Another outcome of the research is a set of procedures to quantify the different responses associated with skew effects.

5) **Investigate the influence of stay-in-place (SIP) metal deck forms on the behavior of I-girder bridges:** SIP forms are attached to the top flanges of the girders prior the deck placement, participating as a potential source of stiffness in the noncomposite structure. Traditionally, this incidental source of stiffness is ignored in the structural analysis of I-girder bridges. Even though research efforts have been dedicated to study the potential use of the forms as a method to provide stability bracing, their

stiffness contributions are highly variable and depend on unpredictable factors. These attributes deter engineers from using the SIP forms for this purpose. However, under certain circumstances, the SIP forms can participate in the control of the bridge geometry; namely, they can influence the displacements that occur in the noncomposite structure due to the weight of the reinforcing steel, the construction equipment, and the wet concrete. This research focuses on identifying the conditions when the participation of the SIP forms in the structural response can be considerable. The studies provide an insight to the different aspects that need to be considered with regard to SIP forms and their influence in the control of the deformed geometry of a bridge during construction. In addition, recommendations for the configuration of the bracing systems are provided that lead to better overall performance of the steel I-girder bridges during construction.

## 1.3. Summary of Original Contributions

The activities described in the previous section can be summarized as points that represent the contributions of this research. Specifically, the outcomes of the studies reported in this thesis are the following:

- Explanation of the interaction between the bracing system and the support skew from a mechanistic perspective:
    - Identification of the mechanisms involved in the transverse load path that induce forces in the cross-frames, lateral bending stresses in the flanges, and girder twists.
    - Development of an index to determine the expected levels of the responses associated with the skew effects based on the bridge geometry.

  - Determination of limits for the applicability of 1D line-girder analysis for the design of straight and skewed bridges.

- Development of two methods to mitigate the skew effects during the construction of straight and skewed bridges.
- Improvement of modeling techniques used to conduct 2D-grid analyses of curved and/or skewed bridges:
  - Implementation of an equivalent torsion constant to account for the contributions of flange warping to the torsional stiffness of I-girders.
  - Development of two-node elements that capture the physical structural properties of different types of cross-frames used in I-girder bridges.
- Development of procedures to predict flange lateral bending stresses and girder layovers due to skew effects.
- Clarification of the influence of SIP forms on the performance of I-girder bridge structures:
  - Identification of the circumstances where the SIP forms participate in the structural responses of a bridge.
  - Development of procedures and practices that reduce the effects of the SIP forms on the control of the deformed geometry of a bridge during construction.

The contributions of this research are focused on practical aspects of the engineering of steel I-girder bridges. The explanations of the interaction between the bracing system and support skew provide engineers with criteria to evaluate the repercussions of using a given cross-frame layout on the structure's response. In addition,

the solutions proposed to mitigate the skew effects and improve the structural performance can be applied readily in the design of bridges of this kind. Similarly, the new 2D-grid analysis techniques can be implemented with minor effort in design offices. The elements developed to represent the cross-frames can be programmed and introduced in the element library of any commercial software used for bridge engineering. In summary, it is expected that the developments proposed in this thesis can find immediate applicability in the bridge industry.

## 1.4. Organization

This thesis is organized in six main chapters. Chapter 2 presents the different functions of the cross-frames in a bridge structure. The discussions focus on how the bracing system participates during the construction and when the bridge is in service. It is emphasized that in certain circumstances, the cross-frames are not only structural components that provide stability bracing to the girders, but also they participate as primary load carrying members. Specifically, it is shown that the bracing system provides a path to distribute the transverse forces due to curvature and/or skew effects as well as lateral loads (e.g., wind or seismic loads). Also, the discussions illustrate how the bracing system helps control the bridge geometry during the different construction stages.

Chapter 3 introduces the bridge structures studied in this research and the analytical tools used for this purpose. The first part of the chapter shows the description of nine bridges of different geometries that are selected for the studies conducted to investigate the structural performance of I-girder bridges during construction. The second part describes the analytical procedures used for the finite element simulations. The

characteristics of the refined computer models are discussed, along with their capabilities to represent the physical behavior of a bridge structure.

Chapter 4 discusses the behavior and analysis of curved and skewed I-girder bridges. In this chapter, the approximate line-girder (1D) and grid (2D) methods of analysis are introduced first to illustrate their capabilities and limitations for representing the behavior of bridges with complex geometries. The assumptions used in the derivations of the methods are studied to highlight the cases where the results obtained from these analysis methods can be misleading. The second part of the chapter focuses on the effects of skew on the behavior of I-girder bridges. Studies are conducted on a basic structure that illustrates the behavioral aspects of a skewed bridge. The observations are extended to more complex skewed structures with simple and multiple spans. The findings of these studies are used to develop schemes that reduce the undesired effects of skew. They are tested in two study cases that show how the configuration of the bracing system can be modified to improve the structural performance.

Chapter 5 discusses in detail the pitfalls of conventional 2D-grid analysis, and how they can affect the response predictions of a curved and/or skewed bridge. The modeling practices that are commonly used in grid analyses are introduced to demonstrate that, under certain circumstances, they are insufficient to properly represent the structural behavior of these types of bridges. These studies set the background for improved techniques that can be implemented to overcome the limitations of the traditional 2D-grid models. Elements that represent more accurately the contributions of the cross-frames to the system are formulated for three different cross-frame configurations. In addition, an equivalent torsion constant is introduced as an

approximate method to simulate the contributions of warping to the girder torsional stiffness. The recommended practices are implemented in the analysis of three bridges with complex geometries to demonstrate how they can increase the accuracy of the predicted responses. The chapter closes with the development of procedures to determine the flange lateral bending stresses and girder layovers that result from skew effects.

Chapter 6 addresses the consideration of SIP forms in the analysis of I-girder bridges. Studies are conducted on two structures that, due to specific characteristics, are more susceptible to the stiffness contributions of the SIP forms. The analyses show that in bridges where the girders are not properly braced, the effects of the SIP forms and other nonstructural components can be considerable. The conclusions of this part of the research demonstrate that when the global second-order effects are small, which is generally desirable once the complete structural steel system is erected, the influence of the SIP forms is negligible; therefore, it is not necessary to include them in the analysis.

Chapter 7 summarizes the findings and contributions reported in this thesis. The chapter concludes with recommendations for future studies that can be conducted to extend the scope of this research. Appendices A, B, and C show certain details of the development of the stiffness matrices of the two-node elements used to represent cross-frames.

# CHAPTER II

# ROLES OF CROSS-FRAMES IN THE STRUCTURAL BEHAVIOR OF I-GIRDER BRIDGES

## 2.1. Cross-Frame Functions during Various Periods of the Structure's Life

Structural stability is one of the most relevant aspects that engineers have to address when designing steel structures. In the case of I-girder bridges, the stability of each individual girder between braced points and the stability of the entire system are the main concerns. These two limit states are of particular interest during the construction of the bridge, when the steel framing has to resist the combination of its own weight, the weight of the wet concrete, and other construction loads. At this point there is no composite action and the chance of a stability failure is higher than when the bridge is in service. To prevent failure, cross-frames are provided along the length of the bridge, consolidating the structural system.

In curved and/or skewed bridges, the presence of these components, however, has more implications than those described above. Either as an intended attempt to control the effects of the horizontal curvature and the skew at the supports, or as an undesired side effect due to providing an unintended stiff secondary load path, the distribution of cross-frames can substantially modify the behavior of an I-girder bridge both during construction and during service. That is, there is much more to consider in the design of the cross-frames than just the consideration of structural stability, particularly in horizontally-curved and/or skewed I-girder bridges. Being aware of this, engineers have

developed various ad hoc principles to select the cross-frame types that best suit a particular application and distribute them along the bridge geometry.

Historically, cross-frames and diaphragms have been mainly addressed as the components that provide stability bracing, a load path for the distribution of the wind load, and restraint of the torsion due to eccentric loadings on the overhangs during the deck placement. In simple bridge geometries, as in straight bridges with straight supports, moderate span lengths, and identical girders, these components do not have major influence in the system other than the mentioned above. As the geometry of the bridge deviates from this basic scheme, the functions and effects that cross-frames and diaphragms have in the structure become more important, up to the point where the structural integrity of the bridge depends on them. Horizontal curvature, support skews, large spans and widths, unbalanced construction loads, unequal girder lengths among many other characteristics subject the girders to torsion, increasing the significance of cross-frames and diaphragms.

To determine efficient methods to layout and dimension cross-frames, it is necessary to identify all the functions of these components in the structure. Satisfaction of these requirements with a smaller number of cross-frames leads to more efficient designs. Sections 6.7.4 and 4.6.2.7 of the AASHTO 2010 LRFD Bridge Design Specifications (AASHTO 2010) describe some of the functions and requirements for cross-frames in I-girder bridges. These functions and others discussed in the literature can be classified in two different groups: functions during the various periods of the structure's life and functions associated with different characteristics of the bridge geometry. The following are the roles related to each of these classifications.

### 2.1.1. Functions during Construction

- **Provide stability bracing:** During the steel erection, the cross-frames provide the lateral and torsional bracing required to prevent overall buckling of the system. The unbraced length, given by the distance between cross-frames, also controls the lateral torsional buckling strength of individual girders. The stability bracing provided by the cross-frames is also fundamental during the deck casting, considering that in many bridges, a large part of the construction dead loads corresponds to the weight of the concrete deck. Furthermore, this load is applied to the top flanges, which in positive moment regions increases the susceptibility of the structure to lateral torsional buckling.
- **Provide torsional restraint to the fascia girders:** During the deck placement, the fascia girders are subjected to torsion due to overhang eccentric loads. The spacing between cross-frames limits the stress levels in the flanges due to the corresponding lateral bending and also controls the layover in these girders.
- **Prevent bending of the deck due to differential vertical displacements between adjacent girders without corresponding girder torsional rotations:** When the girders are not well connected by cross-frames, differential vertical displacements can occur between adjacent girders without corresponding torsional rotations of the girders. This can result in bending deformations of the deck during its placement, potentially causing problematic undercutting or over-run of the deck thickness if these relative displacements become too large. The cross-frames force the girders to act together as a unit, and thus assist the contractor in controlling the thickness of the deck during concrete placement.

- **Provide a load path for wind loadings during construction:** As discussed in Section 3.8.4 of the G13.1 Guidelines for the Analysis of Steel Girder Bridges (AASHTO/NSBA 2011), the stability of the bare steel structure subjected to its self-weight, weight of the deck forms, and wind loads should be considered in the design, especially, in long-span bridges. The cross-frames integrate the structural system, making it work as a unit. In the absence of a flange level lateral bracing system, the cross-frames are the only components that provide the load path required to transfer and distribute the lateral load applied to the exterior girders to the rest of the girders and to the bearings.

### 2.1.2. Functions during Service

- **Provide stability bracing in negative moment regions:** In the negative moment regions of continuous span bridges, the girders are susceptible to distortional buckling. To prevent stability related problems, bracing is required at the bottom flange of the girders. Cross-frames are usually provided at pier locations; therefore, bracing is warranted at these positions.
- **Provide a load path for wind loadings during service:** As mentioned in Section 4.6.2.7.1 of AASHTO (2010), the interior cross-frames transfer the portion of the wind load that acts in the lower part of the exterior girders to the deck and from the deck to the bearings. Section 2.3 discusses in further detail the participation of the cross-frames in the structure's wind load resistance.
- **Distribute the live loads applied to the structure:** Live loads are distributed in the I-girders through bending action of the deck and in a minor scale, through the cross-frame diagonals and bottom chords. Previous research demonstrates that due to the

presence of the deck, the top chords have a negligible influence in the live load distribution (Fasl et al. 2009). Section 2.4 presents an extended discussion on the mechanisms involved in the live load distribution and the cross-frame influence.

### 2.1.3. Functions during Maintenance and Demolition

- **Provide stability bracing during deck removal:** As the deck is removed, the composite action in the system decreases, and the steel structure by itself resists the remaining dead load plus the weight of the machinery used in the process. Similar to the construction stages, the cross-frames are the components that provide the bracing required to prevent stability related problems during re-decking and demolition operations.

### 2.1.4. Functions Associated with Characteristics of the Bridge Geometry

- **Load transfer from the interior to the exterior girder in curved bridges:** Due to curvature effects, vertical loads are transferred from the inside to the outside girder through the cross-frames or diaphragms, as shown in Figure 2.1. These vertical loads, also known as V-loads, develop internal forces in the cross-frame components that need to be considered in the design. A more detailed explanation of the load transferring process in curved bridges is presented in Chapter 4.

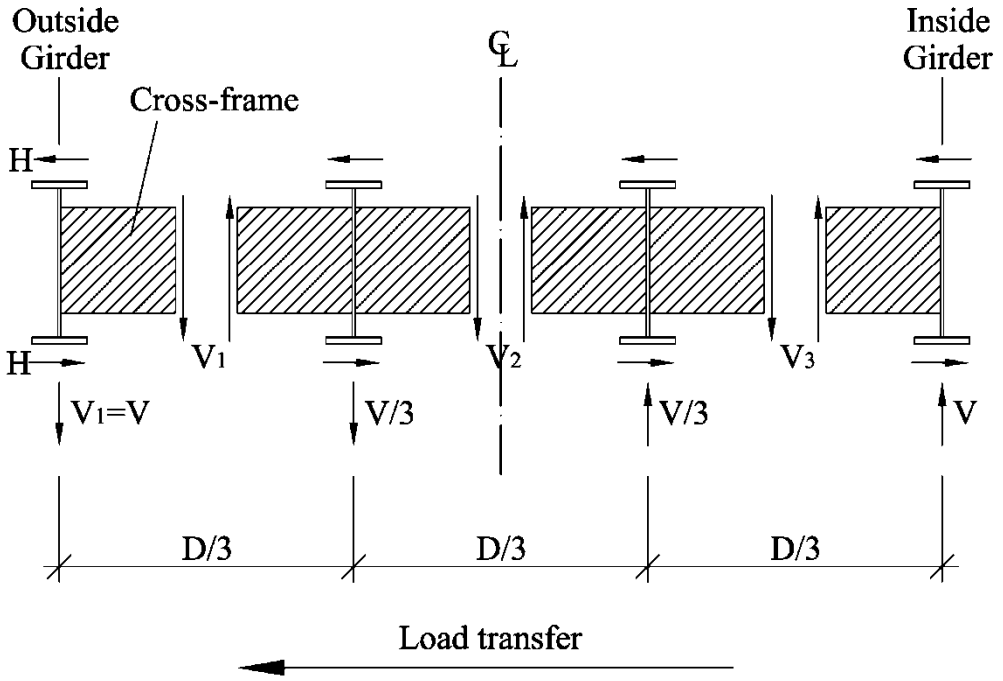


Figure 2.1. Forces in multiple girder system (Adapted from Poellot, 1987)

- **Control of flange lateral bending response in curved bridges:** As a result of horizontal curvature, vertical loads also cause lateral bending stresses in the girder flanges. Figure 2.2 shows a typical stress response in the top flange of the exterior girder in a three girder system. In the figure, the stress responses are plotted versus the normalized length of the girder. As shown, the flange lateral bending stresses, $f_\ell$, can be a significant part of the total stress ($f_b$ plus $f_\ell$). The lateral bending stresses are controlled by placing a sufficient number of cross-frames in the structure. As the number of cross-frames increases, the stresses are reduced.

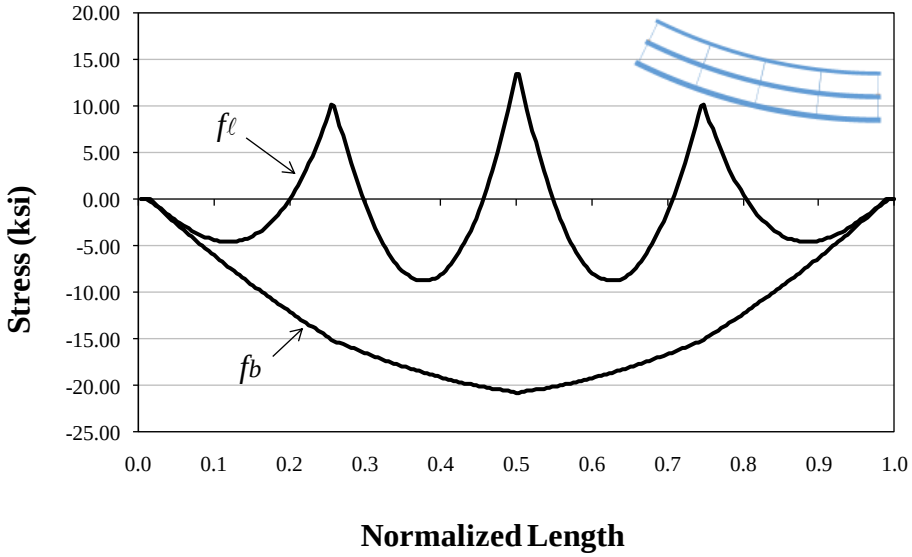


Figure 2.2. Major-axis and lateral bending stresses, $f_b$ and $f_\ell$, in a curved bridge

- **Control differential deflections and girder layovers:** In bridges with skew supports, there are differences in the vertical stiffness of the I-girders at any section perpendicular to the bridge longitudinal axis. Figure 2.3 shows a skewed bridge and the initial and deformed geometry due to the structure's self-weight at a selected interior line of cross-frames. As shown in the figure, the cross-frames force the girders to rotate as a group to accommodate the differential vertical deflections. Due to this behavior, large forces can develop in the cross-frame elements, especially in the cross-frames located in the vicinity of the supports. Similar to the curvature effects, the cross-frames in skewed bridges provide a secondary load path that can affect considerably the system behavior, as explained in detail in Chapter 4.

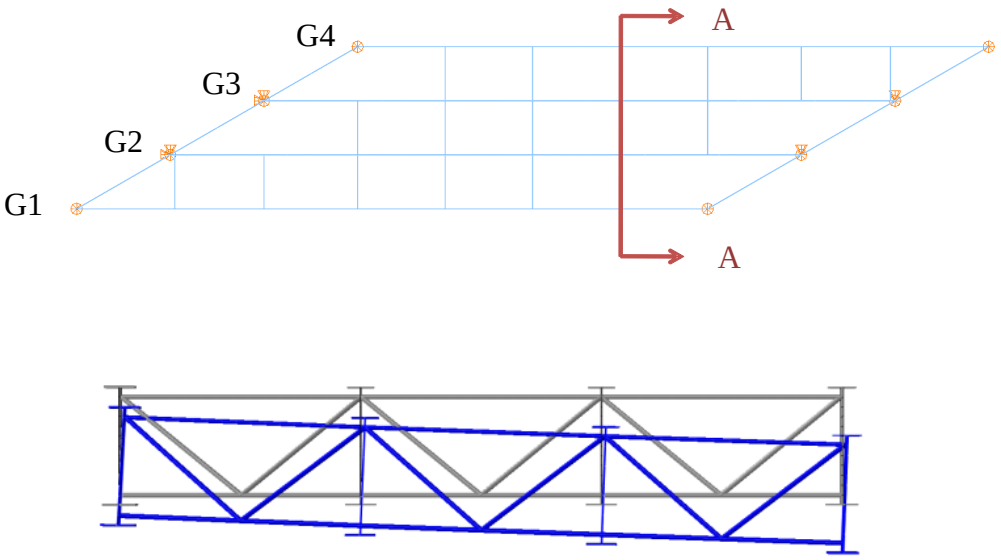


Section A-A

Figure 2.3. Effects of support skew in girder displacements

## 2.2. Considerations Regarding the Layout of the Bracing System in I-Girder Bridges

The layout of the intermediate cross-frames in a bridge can have a significant impact on the structural properties of the system. This section introduces the terminology associated with the distribution of cross-frames in the structure's layout and the types of configurations used in this research. Figure 2.4 depicts a typical distribution of cross-frames in a curved and skewed multiple span bridge. The common terms related to their position throughout the bridge geometry are illustrated in the figure.

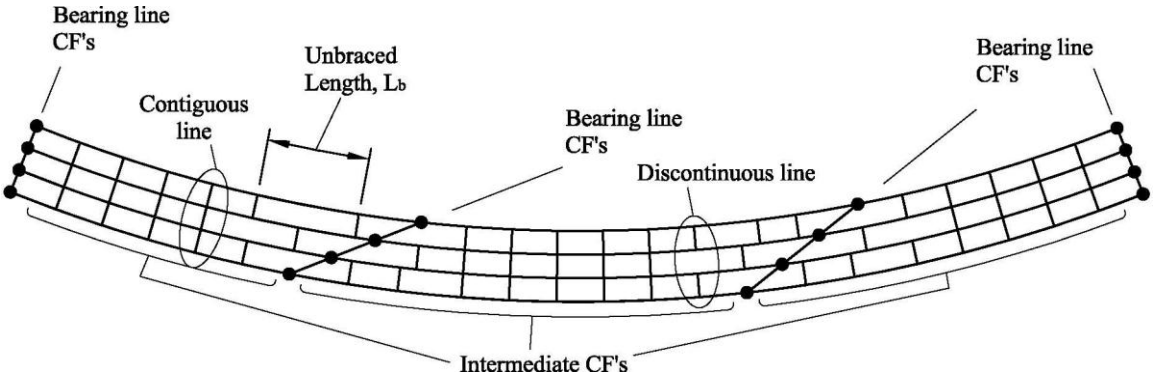


Figure 2.4. Typical distribution of cross-frames in a bridge layout

The cross-frames represent a small part of the total weight of the bridge structure, however, the cost associated with their fabrication and erection is generally higher than the cost of other structural components. Therefore, it is desired to find a trade-off between the number of cross-frames considered in the bridge design and the requirements discussed in Section 2.1. Similarly, the *"Load and Resistance Factored Design and Analysis of Skewed and Curved Steel Bridges Manual"* (NHI/FHWA 2011b) indicates that the impact of the cross-frame spacing in curved and/or skewed bridges is as follows:

Closer spacing:

- Lower cross-frame forces
- Lower flange lateral moments (and girder layovers)
- Higher compression-flange capacity

vs.

- Higher cross-frame cost

Larger spacing:

- Lower cross-frame cost

vs.

- Larger cross-frame forces
- Larger flange lateral moments (and girder layovers)
- Lower compression-flange capacity

Past editions of the AASTHO Bridge Design Specifications limited the spacing between cross-frames to a maximum of 25.0 ft for any type of bridge geometry. This requirement was removed in the 1994 LRFD Specifications. Instead, the distribution of cross-frames in the bridge layout is determined by rational analysis, considering the aspects discussed in Section 2.1. For the case of curved bridges, AASHTO (2010) Article 6.7.4.2 limits the unbraced length to a maximum of 30.0 ft.

### 2.2.1. Types of Cross-Frame Configurations

There are three types of cross-frame configurations that are most commonly used in design; namely, the X-type, V-type, and inverted V-type. These are shown in Figure 2.5. Another configuration used in practice is the Z-type, composed of top and bottom chords and a single diagonal. In the context of this thesis, this configuration is classified as an X-type cross-frame with a diagonal removed.

The selection of a given configuration depends on the ratio between the girder depth and the distance between girders. Typically, an X-configuration is selected for the intermediate cross-frames when the angle between the bottom chord and the diagonals is more than 25 degrees. At smaller angles the efficiency of the diagonal members to carry vertical load decreases, and larger gusset plate dimensions are required to accommodate the connection of the diagonals. Due to these limitations, the other two options are preferred when the girder spacing is large in comparison to the girder depth.

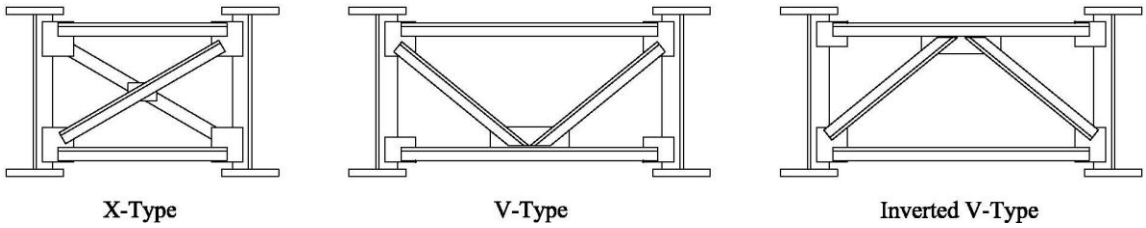


Figure 2.5. Cross-frame configurations used for steel I-girder bridges

At the bearing lines, it is common to use the inverted V-configuration given that at these locations, the expansion device will be supported by the top chord (see Figure 2.6). Having the diagonals framing into the top chord at mid-point develops a load path that will take the wheel load directly into the bearings, preventing large flexural stresses in the top chord that otherwise will occur using other configurations, as depicted in the figure. Another option commonly used to connect the girders at the bearing lines is via diaphragms. These components consist of hot-rolled W-sections, channels, or fabricated members from steel plates.

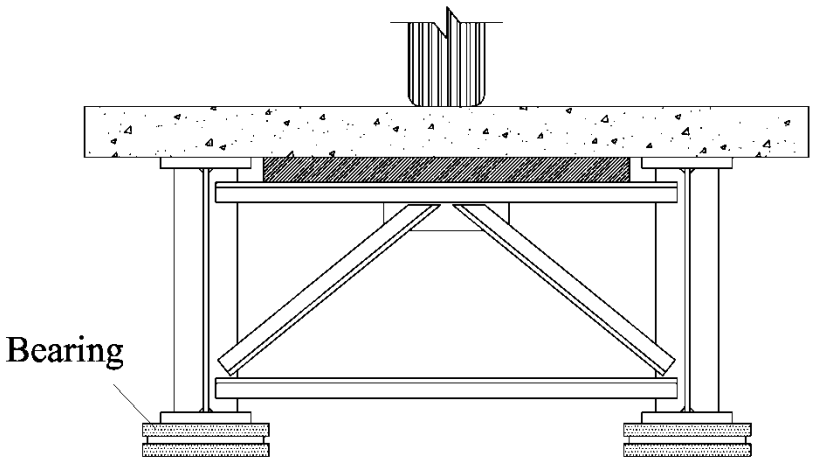


Figure 2.6. Inverted V-type configuration at the bearing lines

For intermediate cross-frames and when the girder spacing does not allow the use of the X-type cross-frame, the use of V-type configurations is advisable. Usually, the designer will pick the configuration that he or she is more familiar with or will follow the recommendations given by DOT's standards. In some cases, when either the X-type or V-type configurations are used for intermediate cross-frames, the top chords may be removed. This practice reduces the number of cross-frame elements. As shown in Section 4.2.2.2, the removal of the top chord in the X-type configuration also helps reduce the transverse stiffness of the bridge, mitigating the collateral effects of the support skew, while still providing the required girder stability bracing. Removing the top chord in V-type configurations, however, may have a detrimental effect on the bridge performance. As discussed in Sections 4.3.3 and 6.4.2, due to the large reduction in the cross-frame stiffness, this practice may change the structural response significantly and compromise the stability of the system.

## 2.3. Wind Load Resistance

The resistance of the structure due to wind loads must be considered in the design of steel girder bridges. The AASHTO Bridge Design Specifications, Article 4.6.2.7.1, describes the procedure for wind load analysis. It is mentioned that in a composite system, a possible mechanism for the wind load distribution is to assume that the wind load acting above the upper half of the girders (including parapets and vehicles) is transmitted directly to the deck. The wind load acting in the lower half is applied to the bottom flange. The wind actions cause lateral bending of the bottom flange. In this case, the cross-frames work as the supports of a continuous beam subjected to a uniformly distributed load. Hence, the lateral forces in the bottom flange are transferred to the cross-

frames, from the cross-frames to the deck, and then by diaphragm action of the deck to the bearings.

In the noncomposite structure, the distribution of the wind load depends entirely on the bracing system. In long span bridges (usually 200 ft and longer), flange level braces are provided to increase the lateral stiffness of the structure during construction. The weight of a flange level bracing system is a minor part of the structure's total weight; however, the costs associated with the fabrication and erection of its components can be significant. Hence, the use of flange level bracing, is limited to bridges where the stability of the structure under gravity and lateral loads cannot be warranted with cross-frames. In the absence of flange level braces, the cross-frames are the only structural components that integrate the system, such that under wind load actions the bridge deflects laterally as a unit. In this case, the pressure exerted by the wind in the fascia girders is resisted by lateral bending of both top and bottom flanges. The bracing system collects and distributes the forces to the interior girders, and then to the bearings.

Analyses conducted with 1D or 2D models do not capture this force distribution in the system. Instead, ad hoc procedures are used to determine the cross-frame forces. The reactions at the cross-frame locations determined from the approximate analysis that considers the flanges as continuous beams are used to calculate the forces that are used to dimension the cross-frame components.

In the design of cross-frames for strength, the live and dead load actions are not properly captured, unless a 3D model that evaluates their effects is constructed. In 1D line-girder analyses of straight and skewed bridges, for example, the cross-frames are not

modeled; hence, it is not possible to capture the cross-frame forces due to gravity loads. Similarly, as discussed in Sections 5.1 and 5.2, 2D-grid analyses conducted with current practices underestimate the forces in the cross-frames significantly. Due to the limitations of the approximate 1D line-girder and 2D-grid models, generally it is not possible to properly predict the cross-frame forces induced by gravity loads. For this reason, the AASHTO Specifications state that "At a minimum, diaphragms and cross-frames shall be designed to transfer wind loads according to the provisions of Article 4.6.2.7 and shall meet all the applicable slenderness requirements in Article 6.8.4 or Article 6.9.3." Additionally, the forces that result from the overhang eccentricity should be included in the cross-frame design.

## 2.4. Live Load Distribution

In a bridge, live loads are transferred from girder to girder through the deck and in a minor scale through the diaphragms or cross-frames. The AASHTO Specifications provide procedures to determine factors that can be used in the structural analysis to consider the live load distribution among the girders. The number of lanes, the type of girder (fascia or interior girder), the characteristics of the flexure regions (positive or negative moment regions), are some of the variables considered in the analysis.

Figure 2.7 depicts the mechanisms involved in the load distribution. The predominant of these mechanisms is bending of the concrete deck. Racking of the cross-frames is a secondary source of stiffness that also participates in the load distribution. NCHRP 592 *"Simplified Live Load Distribution Factor Equations"* (NCHRP/TRB 2007) discusses the influence of the cross-frames in the live load distribution. This report shows

that variations in the cross-frame position and stiffness have a relatively small impact on the way the live load is transferred from girder to girder. In addition, studies have been conducted in existing bridges to determine the changes in the structural behavior due to the removal of the intermediate diaphragms (Stallings et al. 1999). The experiments conducted in a three-span steel I-girder bridge show that the diaphragms have a small effect on the transverse distribution of truck loads.

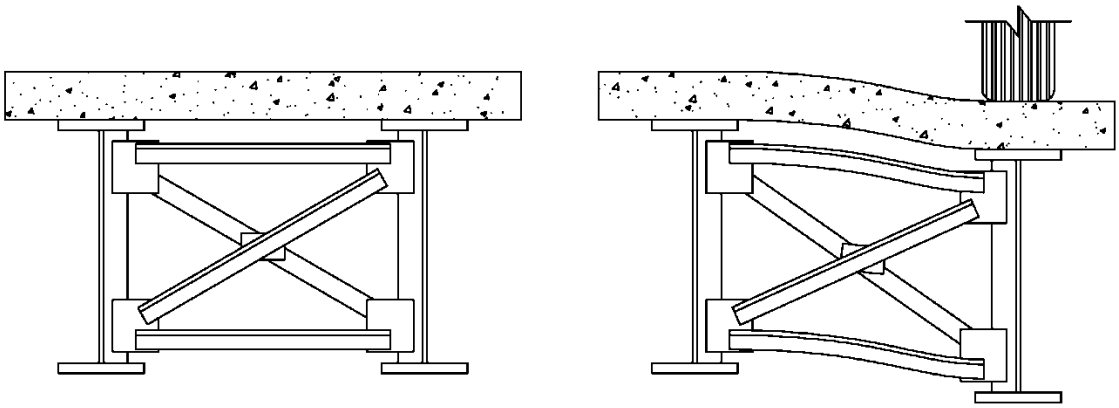

System unloaded System under live load action

Figure 2.7. Live load actions in I-girder bridges

Even though conclusive results are not available regarding the influence of the bracing system in the live load distribution, the existing experimental and analytical investigations conducted on this topic, suggest that the participation is minor. However, there is an important aspect to consider with respect to cross-frames and diaphragms. As illustrated in Figure 2.7, the differential vertical deflections between adjacent girders are accommodated by racking of the cross-frame. This mechanism can induce large stress concentrations in the welds between the cross-frame/diaphragm connection plates and the girder web, which in some cases result in fatigue related problems (Fisher and Keating 1989, Dexter and Wright 2004). Furthermore, given that support skews induce larger

vertical differential deflections between the girders, the probability of abrupt failure due to fatigue is increased in these types of bridges (Berglund and Schultz 2006).

In summary, the bracing system can have a relatively small effect on the distribution of live loads. The transverse force transfer is dominated by the contributions of the deck. Due to differential deflections, stress concentrations can occur in the girders at the cross-frame locations. Skewed bridges require particular attention in this regard since the differential deflections are larger in these systems. This is an undesired collateral effect of the skew that can affect the structural performance of the bridge.

# CHAPTER III

# ANALYTICAL STUDY OF I-GIRDER BRIDGES

This chapter introduces the I-girder bridge structures studied in this research and the analytical techniques used for the investigation. The chapter is organized by first introducing the different geometries and characteristics of the considered structures and the criteria for the bridge selection. The second part of the chapter describes the finite element simulations used in the studies.

## 3.1. Description of the Case Studies

The influence of the horizontal curvature, the skew, and the bracing system can be studied by analyzing how each of these parameters participates in the overall response of a bridge structure. There is a wide range of span lengths, horizontal curvatures, bridge widths and skew angles that are used for the design of highway bridges. Therefore, a comprehensive study of how these parameters affect the behavior of a bridge must consider this large spectrum of geometries. For the studies conducted in the NCHRP 12-79 Project *"Guidelines for Analytical Methods and Erection Engineering of Curved and Skewed Steel Deck-Girder Bridges"*, hereafter referred to as NCHRP Project 12-79, a matrix comprised of 58 I-girder bridges representative of a wide range of practical structural configurations is investigated. The NCHRP Project 12-79 studies include bridges currently in service and bridges that have been published as design examples. Also, parametric cases of simple and continuous span bridges are included in the research. The study matrix is composed of six groups, as shown in Figures 3.1 to 3.6.

These figures depict the overall deck plan geometry of the structures. The cases studied vary from simple span straight and skewed bridges to more complex continuous span curved and skewed bridges. The nomenclature to categorize the bridges is the following. The first letter defines whether the structure is an existing (E), an example (X), or a parametric (N) bridge. The second letter, I, stands for I-girder bridge to differentiate them from the box-girder bridges that form another part of the NCHRP Project 12-79 studies. The third letter indicates whether the bridge is a simple (S) or continuous (C) span. The fourth letter, S or C, defines if the bridge is straight or curved, respectively. The last letter represents the orientation of the supports and is abbreviated as N, if the supports are normal to the longitudinal axis of the bridge, R for curved bridges with radial supports, and S, if at least one of the supports is skewed. The number next to the letter code denotes the specific case study. The numbers in parentheses summarize the geometry of the bridges. The titles for each of the groups shown in Figure 3.1 to Figure 3.6 include the key to illustrate the meaning of the numbers in the parentheses. For all the bridges shown in the matrix, girder G1 is the one that is closest to the bottom of the page. In the curved bridges, G1 is also the girder with the largest radius of curvature. A detailed discussion of the criteria used to select the 58 configurations and the details of each structure are documented in Ozgur (2011).

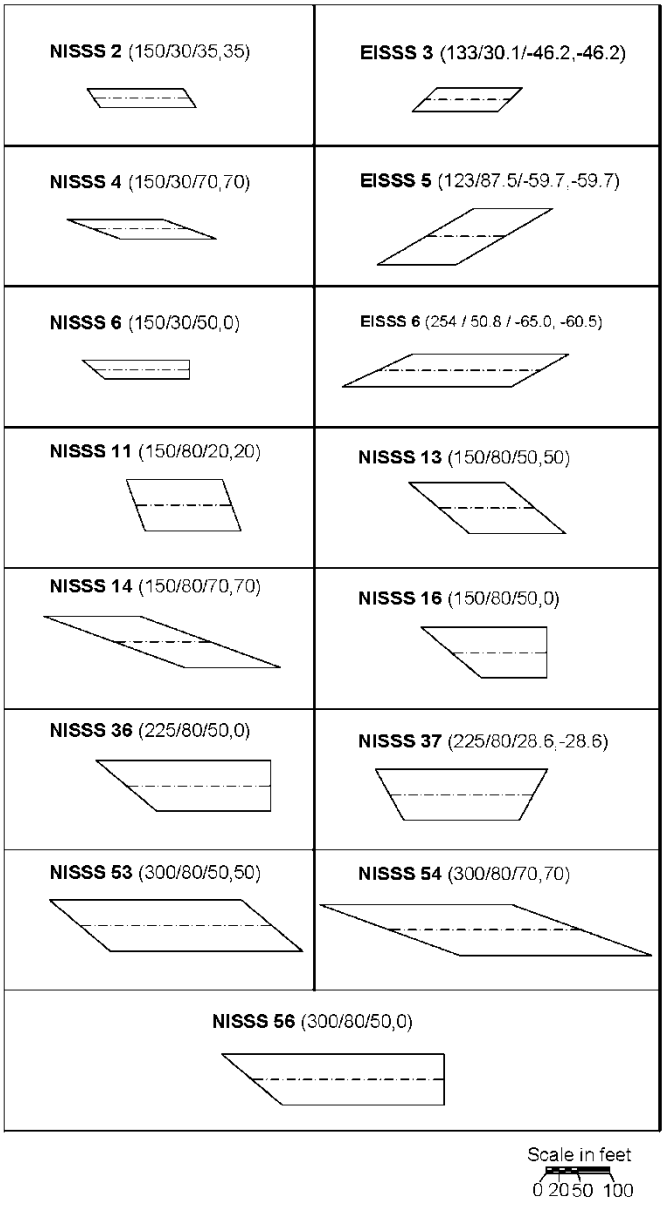


Figure 3.1. Schematic representation of the case studies, Project NCHRP 12-79, simple-span, straight with skewed supports
(Length / Width / $\theta_{left}$, $\theta_{right}$)

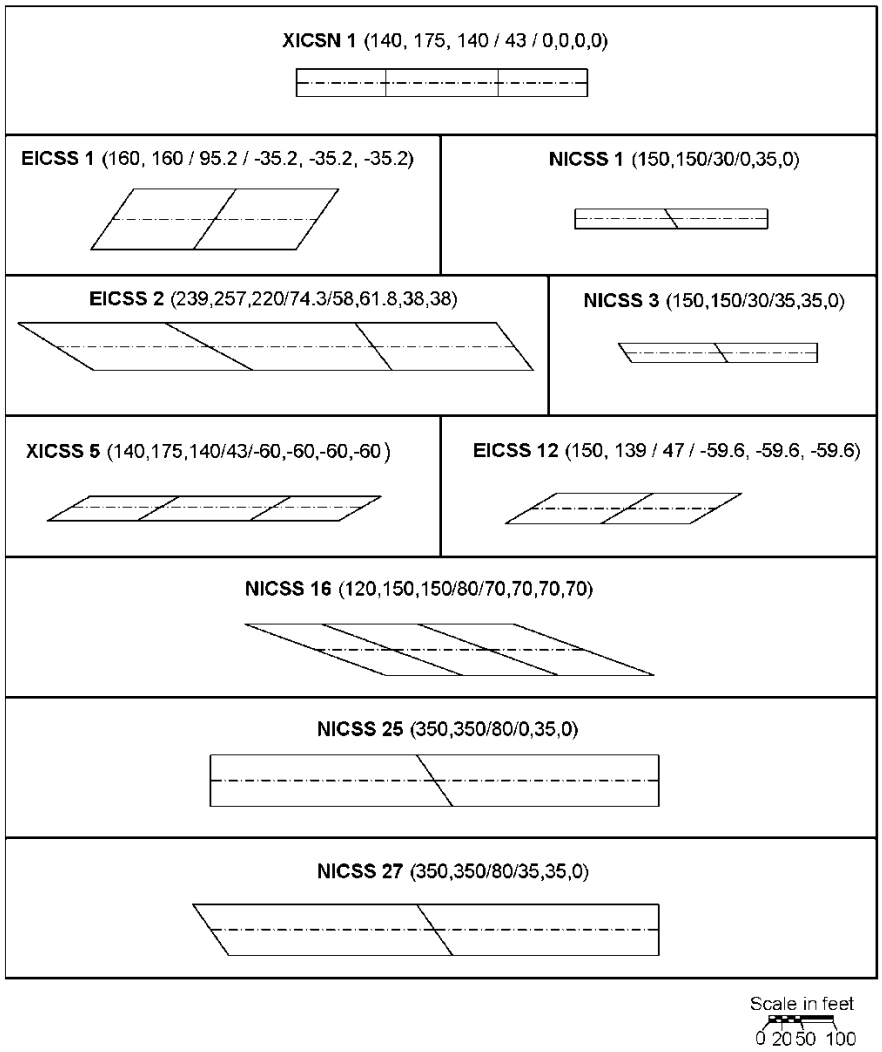


Figure 3.2. Schematic representation of the case studies, Project NCHRP 12-79, continuous-span, straight with skewed supports
(Length$_1$, Length$_2$,…/ Width / $\theta_{left}$…,$\theta_{right}$)

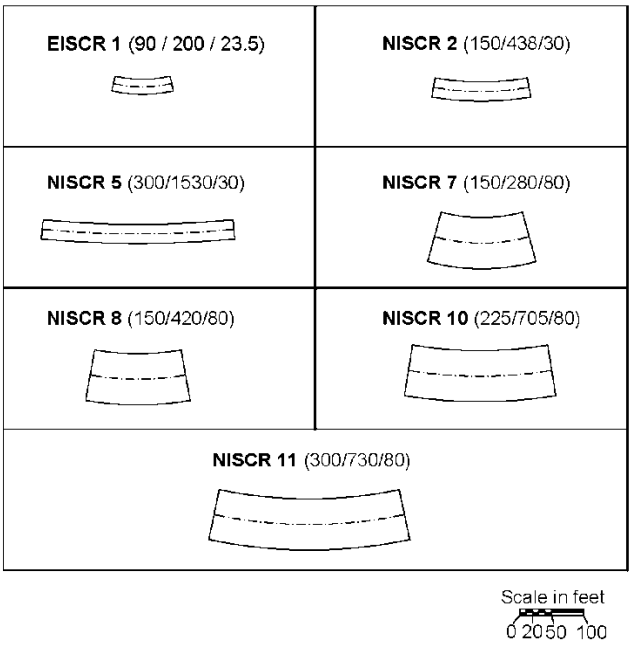


Figure 3.3. Schematic representation of the case studies, Project NCHRP 12-79, simple-span, curved with radial supports
(Length / Radius / Width)

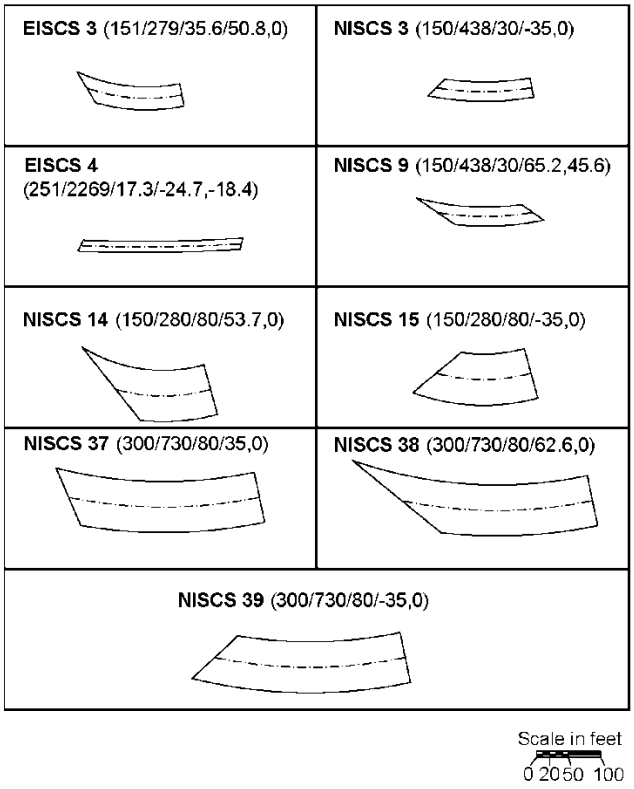


Figure 3.4. Schematic representation of the case studies, Project NCHRP 12-79, simple-span, curved with radial supports
(Length / Radius / Width)

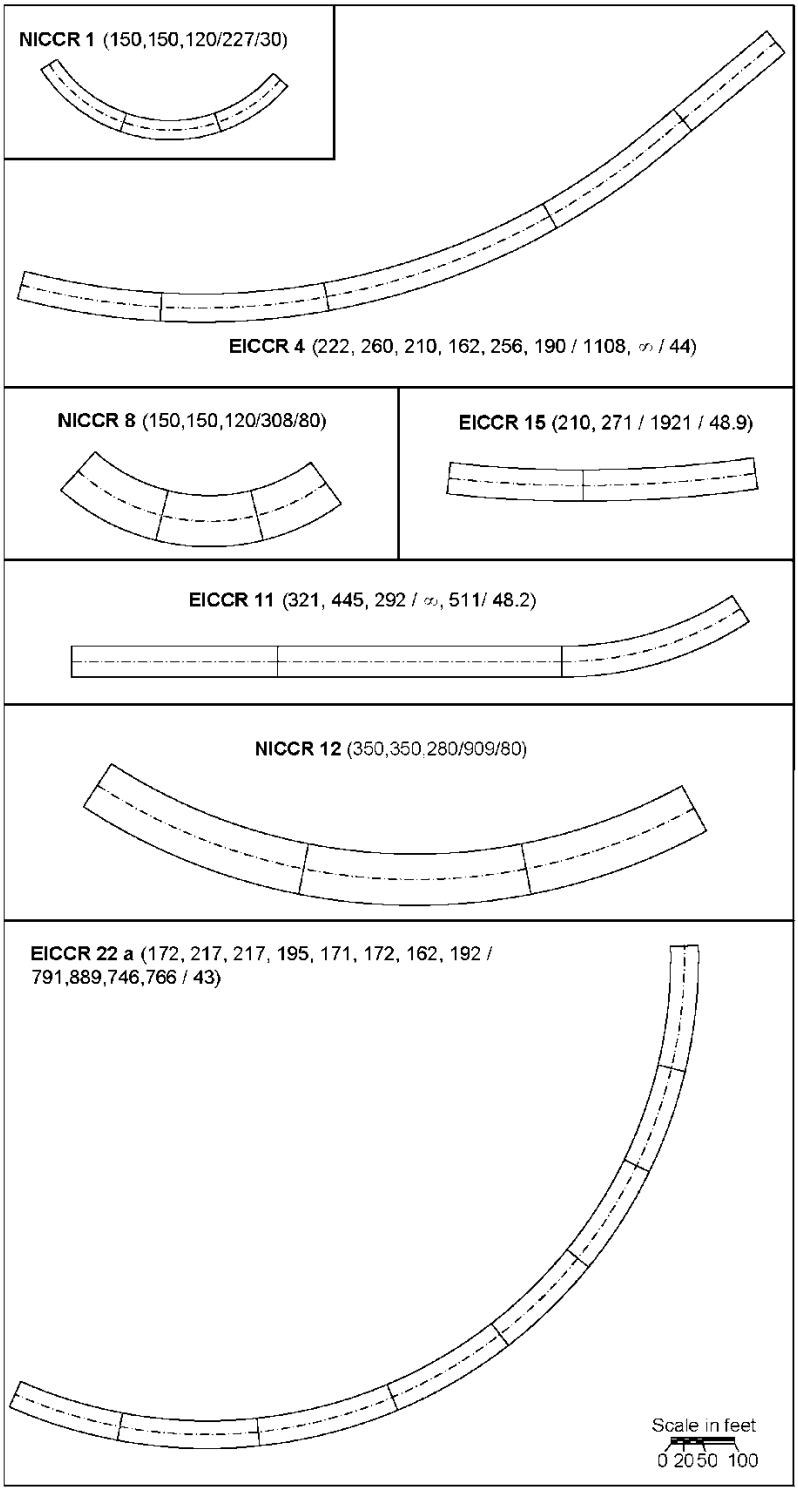


Figure 3.5. Schematic representation of the case studies, Project NCHRP 12-79, continuous-span, curved with radial supports
(Length$_1$, Length$_2$, …/ Radius / Width)

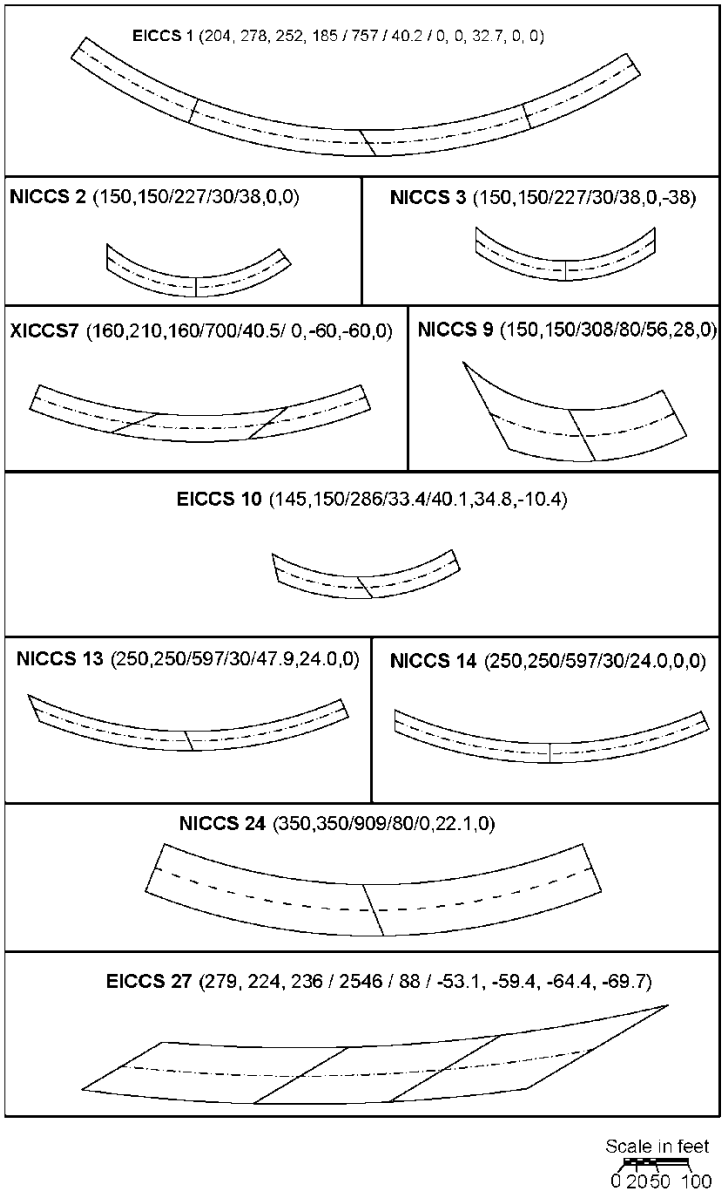


Figure 3.6. Schematic representation of the case studies, Project NCHRP 12-79, continuous-span, curved with skewed supports
(Length$_1$, Length$_2$, …/ Radius / Width / $\theta_{left}$, …, $\theta_{right}$)

Nine of the 58 bridges depicted in Figure 3.1 to Figure 3.6 are selected for the studies discussed in this thesis; these are:

1. XICSN1
2. EISSS3
3. NISSS14
4. NISSS16
5. NICSS16
6. NISCR8
7. EISCS3
8. EISCS4
9. XICCS7

Bridges 1 and 6 are discussed in Section 4.1.1 to illustrate the approximate 1D line-girder method of analysis and evaluate its ability to capture the structural response of these systems. Bridges 4, and 5 are analyzed in Sections 4.2.2 and 4.2.3 to investigate the collateral effects of support skew on the behavior of straight bridges and methods to mitigate them. Bridges 2, 7, and 9 are studied in Section 4.3 to determine the influence of different cross-frame configurations in the response of these structures during construction. In Section 5.4, Bridges 4, 5, and 9 are revisited to show the implementation of procedures proposed to improve and extend the applicability of the 2D-grid methods of analysis. In Chapter 6, the influence of the SIP forms on the behavior of I-girder bridges is explored by analyzing several construction scenarios for Bridges 2 and 8. The following sections present a complete description of the nine bridges selected for this research.

### 3.1.1. Description of Bridge XICSN1

This bridge is a design example documented in AISI (1997). It is a three span structure with lengths of 140 ft, 175 ft, and 140 ft, a width of 43 ft, and normal supports. It has four girders connected with V-type cross-frames at the abutments and the interior supports, and all the intermediate cross-frames are inverted V-type. This structure is the simplest case studied in the NCHRP 12-79 Project. This bridge is studied to introduce the 1D line-girder analysis in Section 4.1.1. Figure 3.7 shows the perspective and plan views of this bridge.

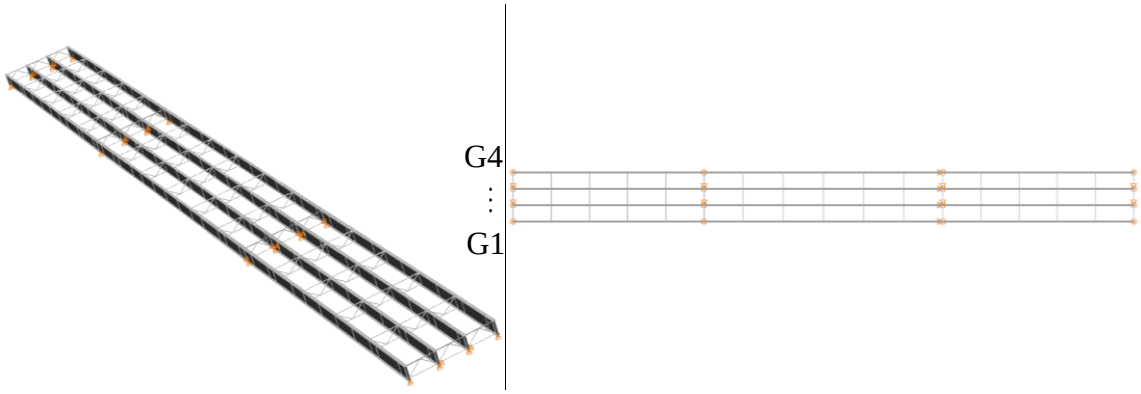


Figure 3.7. Perspective and plan views of XICSN1

### 3.1.2. Description of Bridge EISSS3

Bridge EISSS3 is located on SR 1003 (Chicken Road) over US74 between SR 1155 & SR 1161, Robeson Co., NC. This bridge is a relatively simple structure with a span of 133 ft, a width of 30.1 ft, and parallel supports skewed at 46.2 degrees. A particular characteristic of this bridge is that the interior cross-frames are of the inverted V-type without a top chord. This structure was first studied by Morera and Sumner (2009). These researchers instrumented the bridge to monitor the behavior during construction. As discussed in Morera (2010), the SIP forms had a significant participation

in the bridge response. This structure is analyzed in Chapters 4 and 6 to study the stability bracing effectiveness of the inverted V-type cross-frame without top chords and the effect of the permanent metal deck forms on the behavior of I-girder bridges. Plan and perspective views of EISSS3 are shown in Figure 3.8.

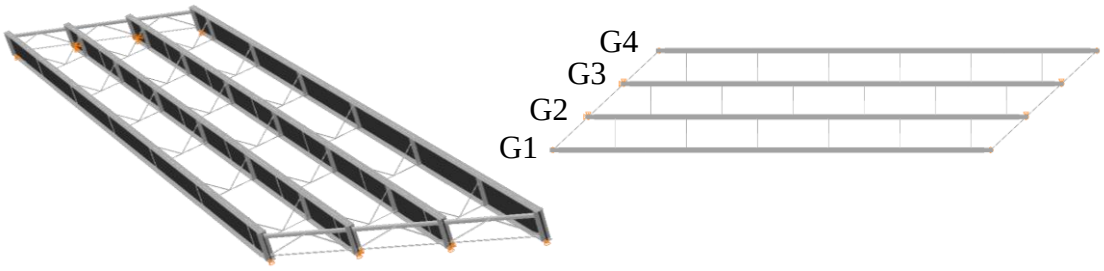


Figure 3.8. Perspective and plan views of EISSS3

### 3.1.3. Description of Bridge NISSS14

This parametric bridge represents an extreme case of a high skew combined with a large width. The structure has a span length of 150 ft, and a width of 80 ft. The supports are parallel with a 70 degree skew. The nine girders are connected using V-type cross-frames in a staggered pattern. Figure 3.9 depicts the bridge geometry.

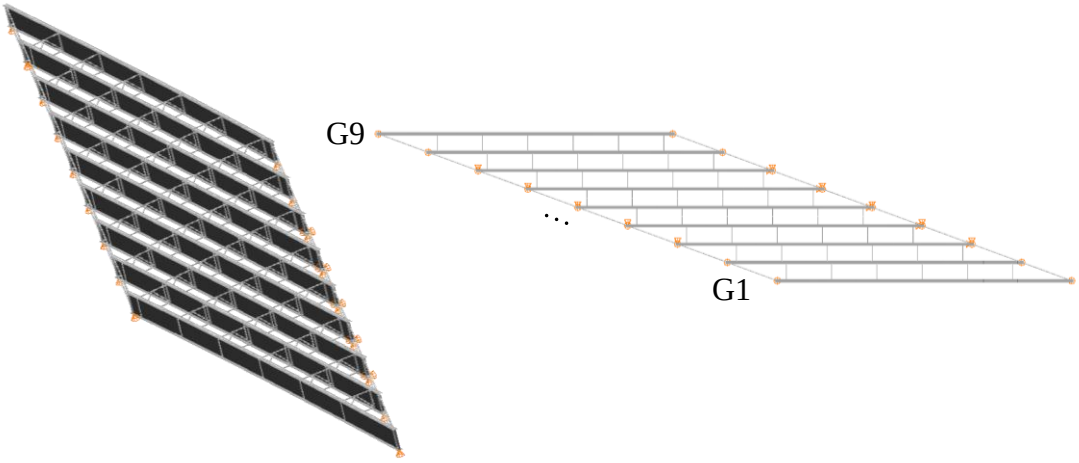


Figure 3.9. Perspective and plan views of NISSS14

This structure is studied in Chapter 4 to illustrate the behavior of a highly skewed bridge with a staggered cross-frame pattern. The erection sequence of the bridge is also simulated to observe the capability of the analysis methods to capture the skew effects, as the structure is constructed.

In this bridge, the steel erection starts with the placement of girder G1. At the supports, the girder displacements are restrained with tie-downs, and a holding crane is provided at mid-span to prevent stability failure problems. The next girder, G2, is placed and connected to girder G1 with the cross-frames, and then, the holding crane is released. The rest of girders are added sequentially following the same scheme.

Stages 2, 3, 4, 5, and 9 are selected to study the construction of this bridge. Three of these stages are depicted in Figure 3.10. Stage 2 corresponds to the state where two girders are in place without the holding crane. In Stage 5, the first five girders are positioned on the bearings. The response of the structure is also evaluated at the end of the steel erection, Stage 9. At this point, the only loading in the system is its self-weight or Steel Dead Load (SDL). Finally, in Stage 10, the behavior of the structure is studied when the Total Dead Load (TDL) is acting on the noncomposite system. In this stage, composite action has not been reached, and only the steel structure is resisting the loadings.

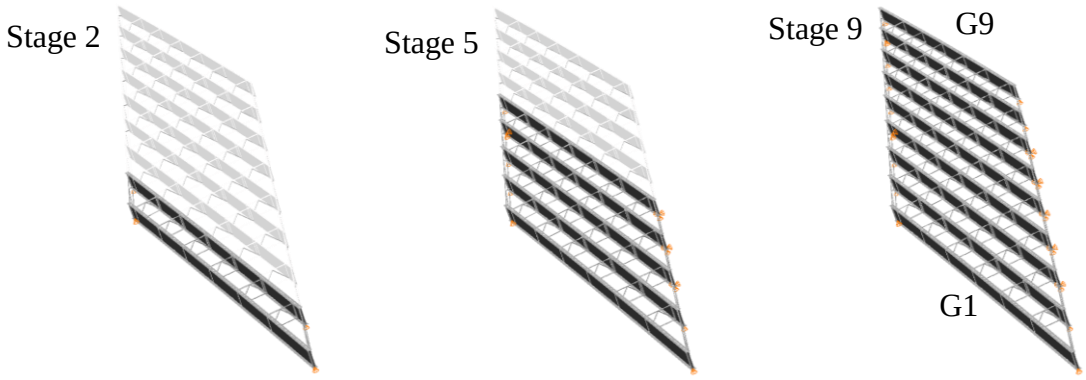


Figure 3.10. Erection stages investigated in Bridge NISSS14

### 3.1.4. Description of Bridge NISSS16

NISSS16 is a nine girder bridge connected with inverted V-type cross-frames. It has a span of 150 ft and a width of 80 ft. This bridge has unequal skews, with one support oriented at 50 degrees and the other oriented normal to the girders. Figure 3.11 illustrates the geometry of the structure.

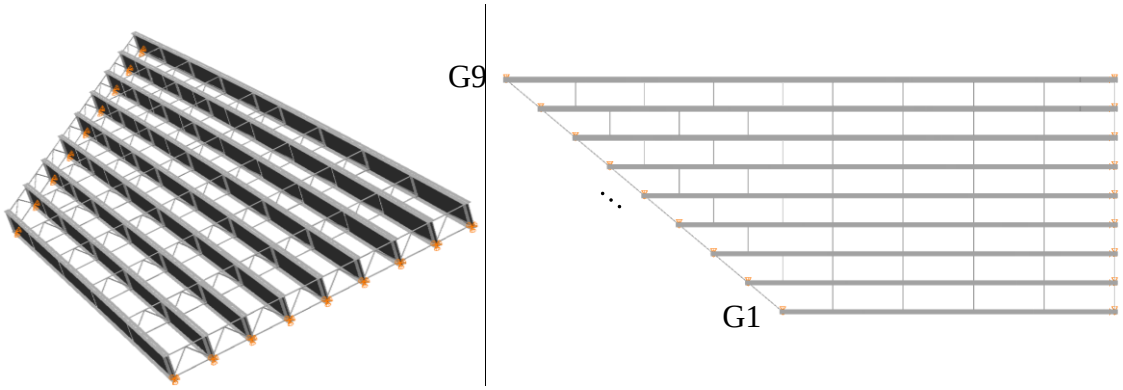


Figure 3.11. Perspective and plan views of NISSS16

One of the attributes investigated in this system is the interaction between the staggered pattern in the left part of the bridge and the contiguous lines of cross-frames in the right part. Due to the skew, the cross-frames are staggered near the left abutment to avoid “nuisance stiffness” effects (Krupicka and Poellot, 1993). Due to this cross-frame

layout, the staggered cross-frames act as point loads near the girder flanges that cause flange lateral bending stresses. In the right part of the bridge, where the cross-frame lines are contiguous, the resultant of cross-frame forces coming from both sides of the girders are small since these forces tend to cancel each other. Therefore, the flange lateral bending stresses should be larger in the left part of the girders and it should be relatively small in the right part. This structure is studied in Chapter 4 to illustrate methods that can be implemented to reduce the undesired effects of the skew. This bridge is revisited in Chapter 5 to demonstrate response prediction enhancements in the analysis of I-girder bridges using 2D-grid models. It is desired to study the ability of the 2D models to capture the fluctuations in the flange lateral bending response described above.

### 3.1.5. Description of Bridge NICSS16

This continuous-span bridge represents an extreme case of a high skew combined with a large width. The span lengths in this bridge are 120 ft, 150 ft, and 150 ft. The bridge is composed of nine I-girders spaced 9.25 ft. The overhangs in the bridge are 3 ft wide, producing a total width of the structure of 80 ft. The supports are parallel and skewed 70 degrees. Figure 3.12 shows the steel structure of the bridge in perspective, as well as its plan view.

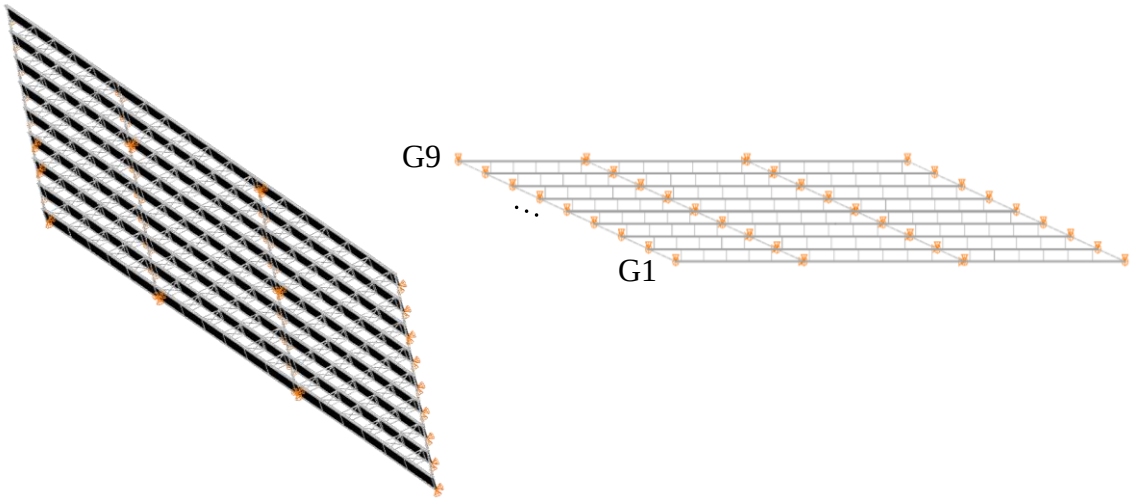


Figure 3.12. Perspective and plan views of NICSS16

NICSS16 is studied in Chapter 4 to illustrate the effects of skew in a multi-span bridge. Also, this bridge is studied in Chapter 5 to show the ability of the improved 2D-grid methods of analysis to predict the behavior of a structure with a challenging geometry. The staggered cross-frame pattern and the large skew makes of this an ideal scenario to analyze the distribution of forces in the cross-frames, as well as the associated flange lateral bending stresses.

### 3.1.6. Description of Bridge NISCR8

This structure is a parametric case used to introduce the application of the V-load method in Section 4.1.1.1. Its relatively simple geometry makes it an ideal case to demonstrate the attributes of the 1D line-girder analysis method. The bridge has a simple span of 150 ft. The radius of curvature is 420 ft and the total width is 80 ft. The nine girders are connected with contiguous lines of X-type cross-frames, all oriented radially. Figure 3.13 shows the framing plan and 3D view of the bridge.

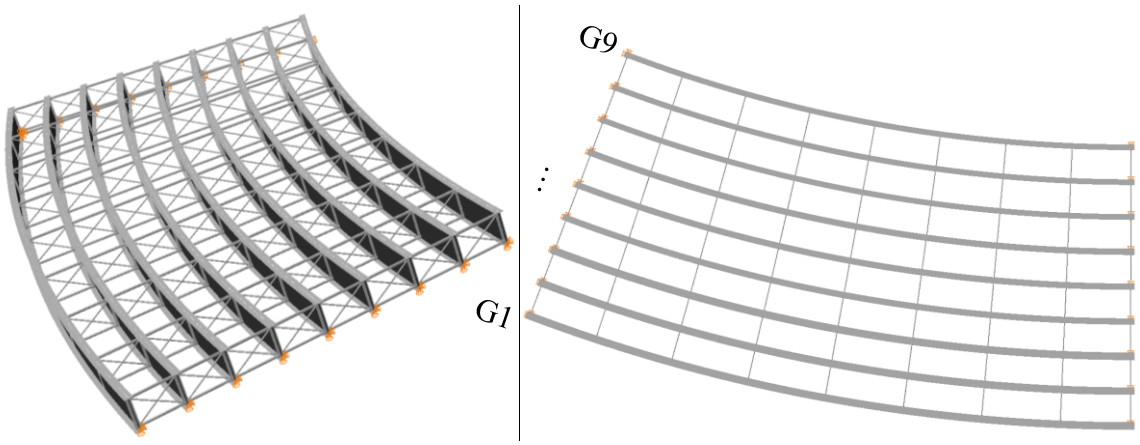


Figure 3.13. Perspective and plan view of NISCR8

### 3.1.7. Description of Bridge EISCS3

The inventory name of this bridge is SR8002 Ramp A-1, and it is located in King of Prussia, PA. This structure was studied originally by Chavel (2008). Figure 3.14 shows the perspective and plan views of the bridge. The structure has a span of 151 ft, a radius of 279 ft, and a width of 35.6 ft. The left support is skewed 50.8 degrees, and the right support is radial. The bridge is composed of six I-girders connected with V-type cross-frames at the left abutment and a diaphragm at the other abutment. The diaphragm is an I-section fabricated with ½-in. by 9-in. plates for the flanges and a ½-in. by 43-in. plate for the web. All the intermediate cross-frames are of the X-type. This curved and skewed structure is selected for the studies presented in Section 4.3 to show the influence of different cross-frame configurations on the behavior of the bridge during construction.

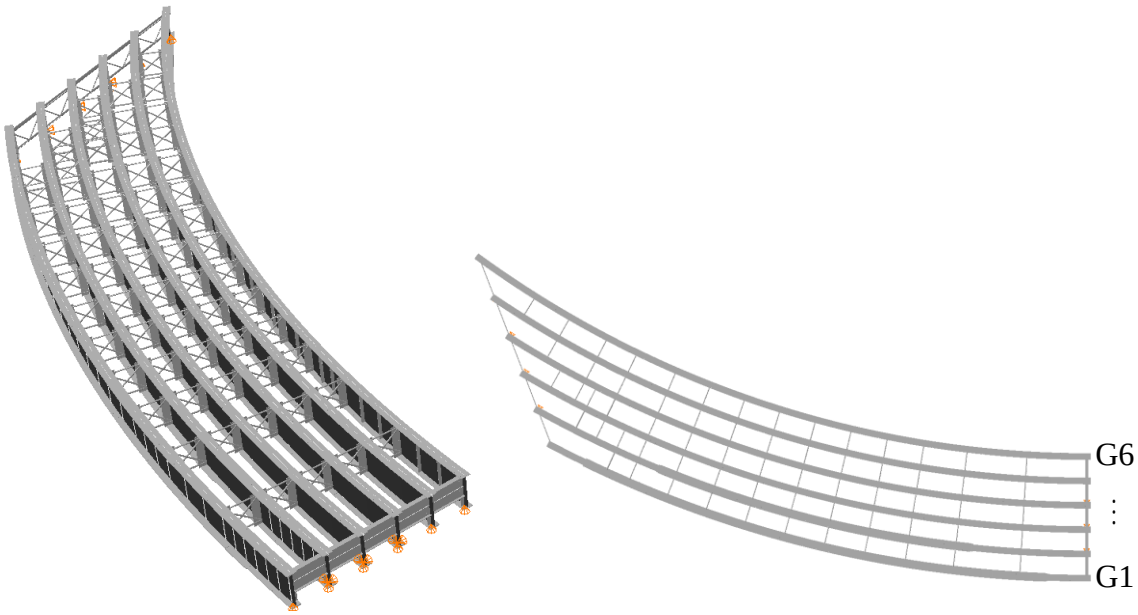


Figure 3.14. Perspective and plan view of EISCS3

### 3.1.8. Description of Bridge EISCS4

This bridge is located in NC 146 (Long Shoals Road) between Blue Ridge Parkway and SR 3495, Asheville, NC. The framing plan of the bridge is shown in Figure 3.15. The structure has 17 girders that were erected in three phases. During its construction, Phase III experienced large response amplifications.

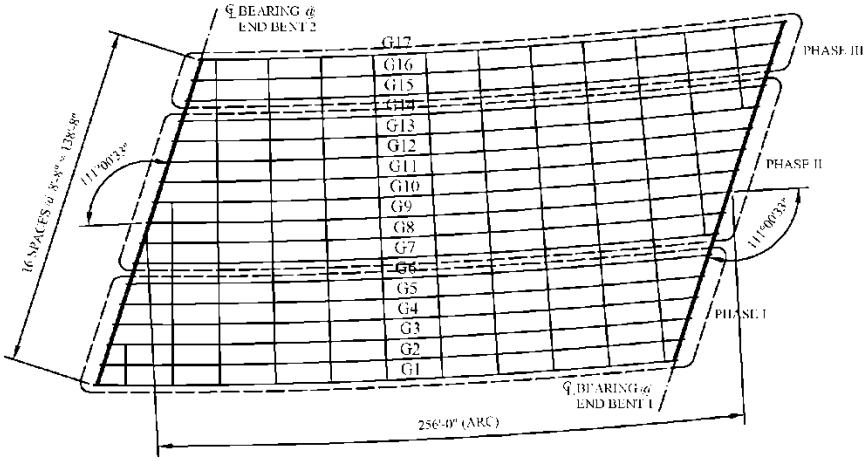


Figure 3.15. Framing plan of EISCS4

In Phase I the first six girders were erected, followed by placement of the concrete slab. Subsequently, in the second phase, eight additional I-girders were erected and the deck was placed. At this point 14 girders had been erected. Next, cross-frames were inserted in the bay between girders G6 and G7 and a closure pour was made to finalize the construction of the first two phases. The next step was to construct Phase III, which consisted of three girders (girders G15 to G17), following the same scheme as used in Phase II. The concrete deck in Phase III was to be placed over the three girders in a single pour, from Bent 1 to Bent 2. Then, the cross-frames between girders G14 and G15 were to be installed, followed by a closure pour.

During the concrete placement on Phase III, it was observed that the vertical deflections were considerably larger than in the girders of Phase II. By the time that approximately two thirds of the concrete deck had been placed, the top-of-slab on Phase III was approximately six inches lower than the corresponding location on Phase II. At this point, it was decided to stop the deck placement. The bridge had deformed more than expected and was potentially at a point of incipient instability. Figure 3.16 shows the three girder unit after the placement of two thirds of the deck and the corresponding rotation at one of the bearings.

Figure 3.16. Photos of the three girder Phase III unit after placement of 2/3 of the deck (Courtesy of NCDOT)

The behavior of the three unit structure erected in Phase III is scrutinized in Chapter 6. EISCS4 is a structure where the participation of the metal deck forms and other implements used to place the concrete deck could have influenced the overall behavior of the system. Figure 3.17 shows the perspective and plan view of the three-girder system considered for the studies.

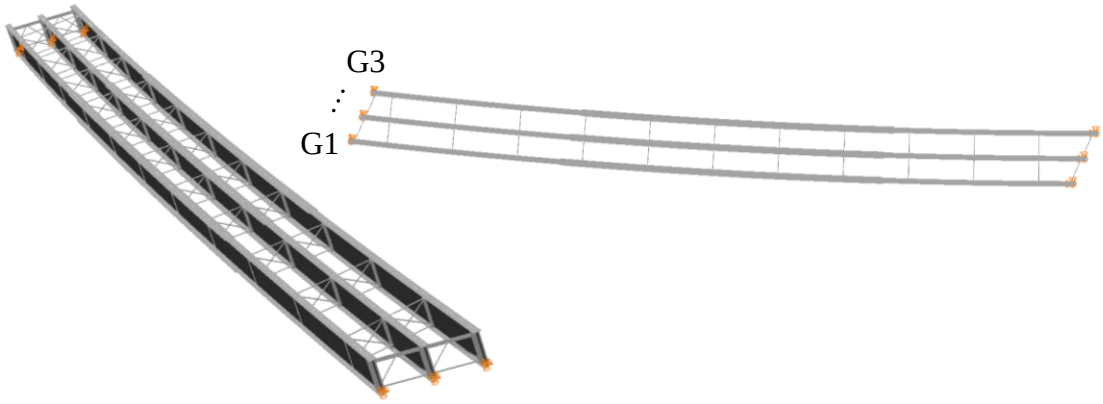


Figure 3.17. Perspective and plan views of EISCS4 Phase III

### 3.1.9. Description of Bridge XICSS7

This structure is an example bridge studied in *"Load and Resistance Factored Design and Analysis of Skewed and Curved Steel Bridges"* (NHI/FHWA 2011a & 2011b). It is a three-span four-girder bridge with the interior supports skewed 60 degrees. The span lengths are 160 ft, 210 ft, and 160 ft. The radius of curvature is 700 ft, and the girders are spaced every 11 ft. Figure 3.18 shows the perspective and the plan view of the structure. This bridge is analyzed in Section 4.3 to study the influence of different types of cross-frame configurations on the structural responses. Also, this system is studied in Section 5.4 to illustrate the improvements in the structural response predictions obtained from a 2D-grid analysis by implementing the recommendations of this research.

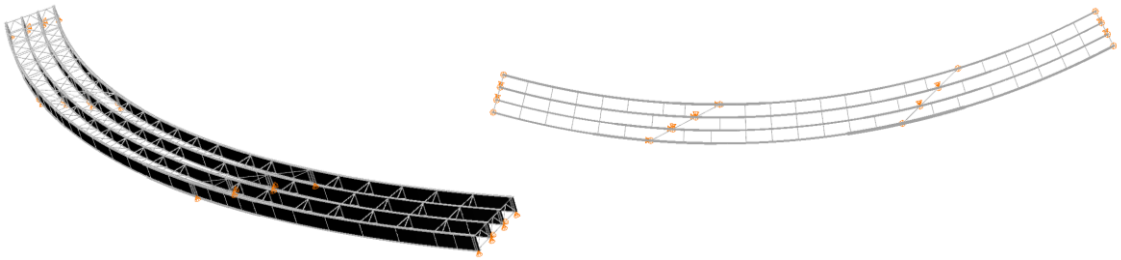

Figure 3.18. Perspective and plan view of XICSS7

## 3.2. Procedures for Finite Element Simulations

Refined 3D finite element analyses (FEA) are used in this research as the reference to determine the accuracy of the 1D and 2D models to capture the response of curved and/or skewed I-girder bridges. FEA models are also used in Chapter 6 to investigate the influence of the permanent metal deck forms on the response of an I-girder bridge. The FEA models are implemented in the ABAQUS 6.10 software package (Dassault Systèmes 2010).

### 3.2.1. Elastic Finite Element Models

Most of the analyses discussed in this research are elastic solutions of the bridge responses. The analyses include geometrically linear and geometrically nonlinear models to determine the influence of second-order effects on the behavior of the case studies. Figure 3.19 shows the characteristics of a typical finite element model. The I-girders are modeled using the general purpose four-node S4R shell elements for the web and the compatible B31 beam elements for the flanges. These element utilize a linear interpolation of the displacements. Preliminary studies demonstrated that 12 shell elements through the depth of the web are necessary to obtain adequate convergence of strains and displacements. The reinforced concrete deck is also modeled with S4R shell

elements. A smeared layer within the depth of the shell is defined to represent the steel reinforcement and capture the orthotropic behavior of the slab reinforcing.

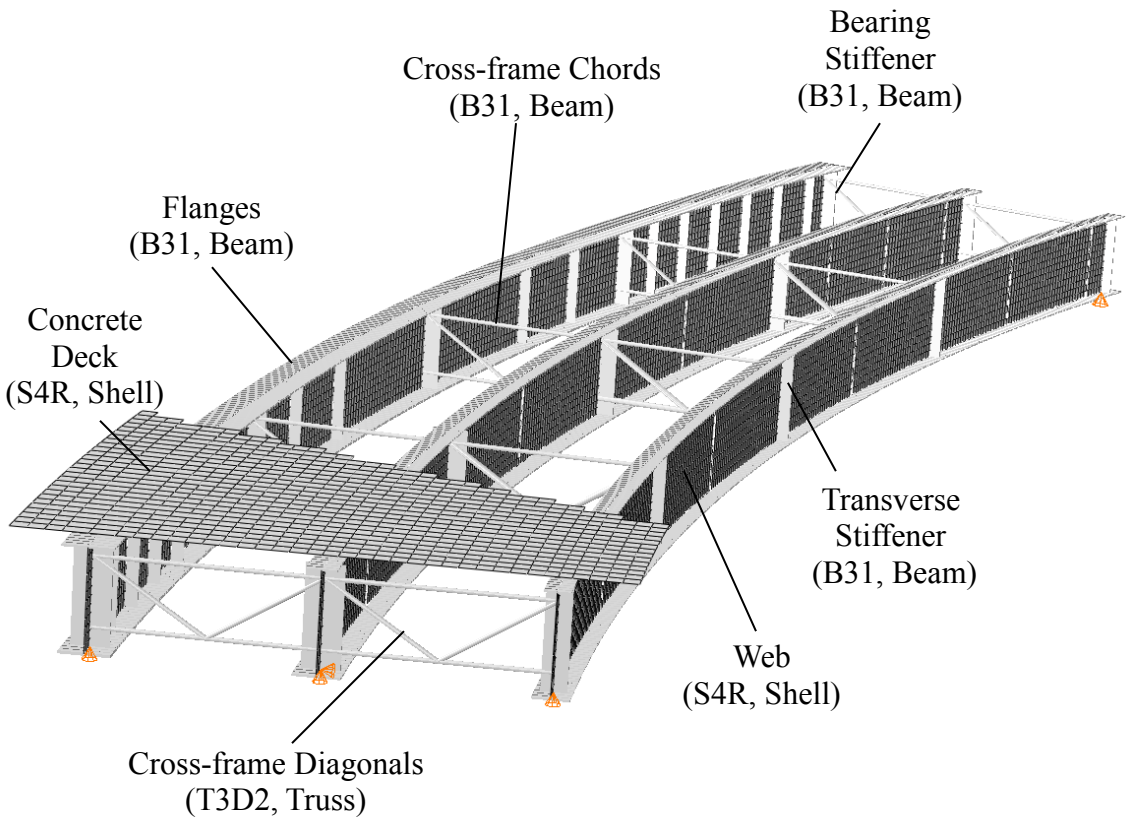


Figure 3.19. Characteristics of a typical FEA used for the elastic models

The transverse stiffeners and the cross-frame connection plates are modeled using B31 beam elements that are connected to the web shell elements. In the cases where there is a stiffener or connection plate at one side of the web only, the local cross-section axis of the beam element is shifted a distance equal to half-width from the section centroid. This practice is used to simulate the actual location of the stiffeners and connection plates in the girders.

The cross-frame top and bottom chords are modeled using B31 beam elements, and the cross-frame diagonals are modeled with the T3D2 truss elements. In the cross-frame elements, the most important source of deformation is axial straining since these components can be considered as trusses that connect the girders at discrete locations. The need for elements that are capable of capturing bending deformations in the chords of the cross-frames is important to capture the poor performance of some cross-frame configurations considered in the research. In particular, the in-plane stiffness of the inverted V-type configuration without top chord (see Section 4.3.3) depends on the flexural properties of the bottom chord.

The top and bottom chords in the cross-frames are subjected to a linear variation of moments between the ends, if the self-weight of the chords is neglected. This condition resembles the case of a cantilever beam subjected to a point load at the tip. Tests conducted with the B31 element show that one element is sufficient to capture the deformations on a cantilever beam subjected to a point load at the tip. Therefore, in the analyses conducted in this research, a single B31 beam element is used to represent the top and bottom chords in X-type cross-frames, the bottom chord in the inverted V-type cross-frames, and the top chord in the V-type cross-frames. The top chord in the inverted V-type cross-frames and the bottom chord in the inverted V-type cross-frames are modeled with two beam elements since the diagonals are connected at mid-length of the chords (see Figure 2.5).

In the FEA models, the location of the cross-frame element nodes usually does not coincide with the location of the web shell nodes. Therefore, linear multi-point constraint equations are used to couple the degrees-of-freedom of the cross-frame nodes

with the shell nodes. The deck shell elements and the flange B31 elements are connected using beam multi-point constraints, providing a rigid link between the beam and shell nodes that constrain both the displacement and rotation degrees-of-freedom. The length of the rigid link is equal to the distance between the centroids of the connected elements. The support conditions are modeled to represent the structural constraints that the physical bearings impose to the system. For example, to represent a guided bearing, where the girders can displace longitudinally, only the vertical and transverse degrees-of-freedom (dofs) are restrained.

These modeling techniques to simulate the elastic behavior of I-girder bridges have been validated and used in previous research to predict the behavior of a full scale I-girder bridge tested in FHWA Turner-Fairbank Highway Research Center (Jung 2006).

### 3.2.2. Test Simulations

For the analyses conducted in Chapter 6 to assess the participation of the permanent metal deck forms on the response of I-girder bridges, the elastic models described previously are not sufficient. As discussed in Chapter 6, the structures analyzed in this part of the research are susceptible to large response amplifications due to second-order effects. Due to the nonlinear response characteristics, the stresses in the bridge components can be beyond the yielding limit. Hence, for these analyses, virtual tests that represent more accurately the physical structural behavior are required. The virtual simulation is a full nonlinear FEA (e.i., geometric and material nonlinear analysis) that captures the plastic deformations that may occur in the girders, considering the influence

of residual stresses from the fabrication of the girders and the geometric imperfections that are inherent to the manufacturing processes.

The modeling attributes of the virtual test simulations are the same as those implemented by Kim (2010). In these test both the girder flanges and webs are modeled using S4R shell elements. Twelve elements are used across the girder flange widths and 20 are used through the web depths for the analyses. The other structural components are modeled as described in the previous section. As discussed in Kim (2010), the mesh refinement used to model the girders depends not only on the density required to capture the stress and displacements properly but also, on the minimum number of elements required to model the initial residual stress pattern adequately.

The fabrication processes involved in cutting and welding the steel plates to produce the I-girders induce residual stresses that affect their strength. The residual stresses are introduced in the FEA by specifying initial stresses in the models. The pattern used is the one proposed by Kim (2010), which is based on the research conducted by Prawel et al. (1974). It is important to notice that the residual stresses shown in the figure are self-equilibrating at the cross-section level. Due to these stresses, the tips of the flanges are in compression and the middle segment is in tension, as illustrated in Figure 3.20. In the web, the distribution is positive (tension) near the web-flange juncture. Towards the middle, the web is subject to compression. The compressive stress used to model the residual stresses in the web is taken as the smaller value of $0.176F_y$ and the idealized web buckling strength, $F_{crw}$, under a uniform axial compression force, $P$, assuming simply-supported boundary conditions, as shown in Figure 3.20(b). In I-girders with slender webs, such as the used in bridges, web plate buckling can control over the $0.176F_y$ limit.

In these cases, tension residual stresses are scaled such that the web cross-section is in equilibrium.

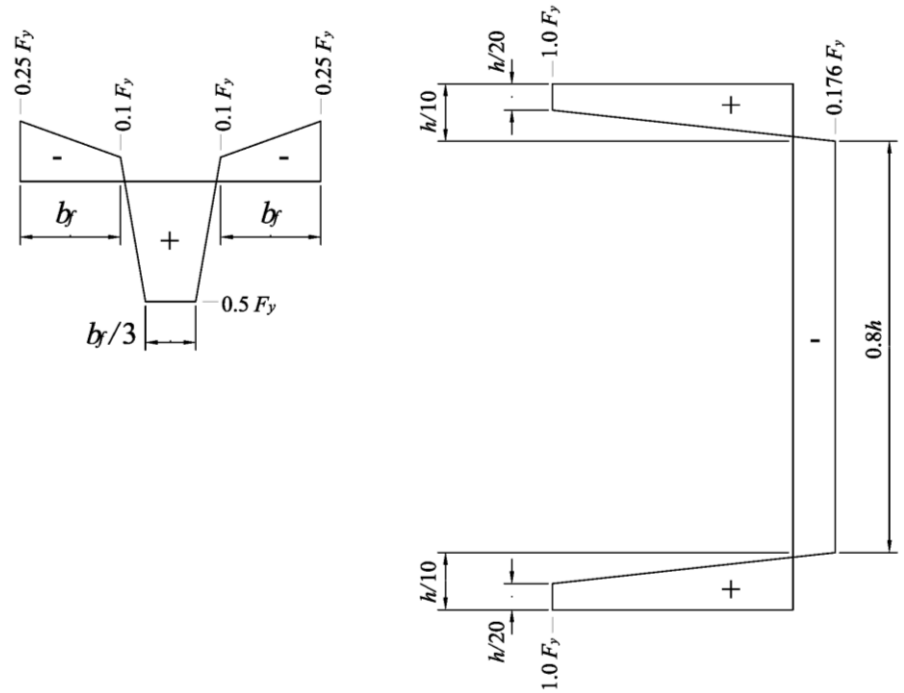


Flange distribution Web distribution

Figure 3.20. Nominal residual stress pattern (adapted from Kim (2010))

For Grade 50W steel ($F_y$ = 50 ksi and $F_u$ = 65 ksi), the material stress-strain curves used in the virtual simulations are depicted in Figure 3.21. In these curves, the strain hardening region is represented by two straight segments. In the figure, the dashed curve corresponds to the engineering stress-strain response whereas the solid curve corresponds to the true stress-strain response. The true stress, $\sigma_{true}$, also known as Cauchy stress, is calculated as

$$\sigma_{true} = \sigma_{eng}\left(1+\varepsilon_{eng}\right) \quad \text{(Eq. 3.1)}$$

where $\sigma_{eng}$ is the engineering stress and $\varepsilon_{eng}$ is the engineering strain. The corresponding work conjugate strain measure is the true or logarithmic strain, $\varepsilon_{true}$, which is calculated as

$$\varepsilon_{true} = \ln\left(1+\varepsilon_{eng}\right) \quad \text{(Eq. 3.2)}$$

In the FE analyses conducted in this research, the true stress-strain curves are implemented to represent the material properties since the S4R shell element is derived for large strain applications.

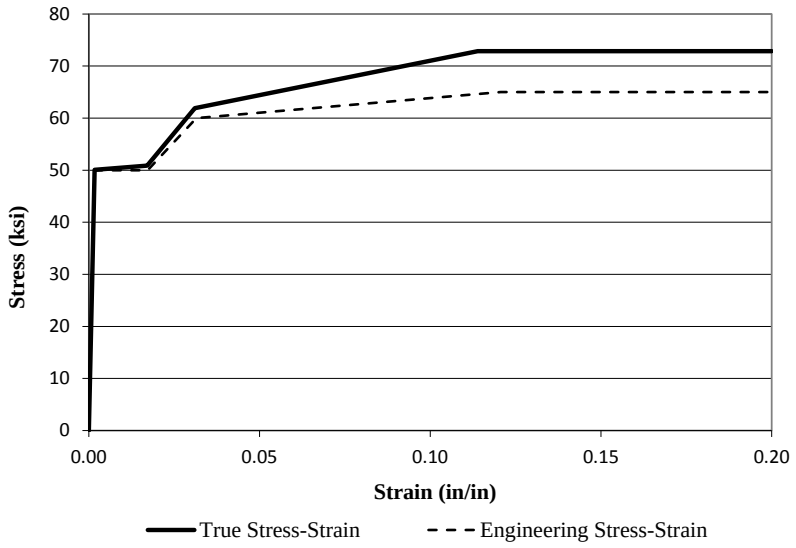


Figure 3.21. Stress-strain diagram for a Grade 50W steel ($F_y$=50 ksi)

In some cases, the geometric imperfections in the girders resulting from the fabrication processes need to be considered in the virtual tests. The Code of Standard Practice for Steel Buildings and Bridges (AISC 2010) specify that the maximum admissible lateral deformation in a girder within the unbraced length, $L_b$, is $L_b$/1000. In systems with straight girders, normal supports, and balanced loads, the lateral deformations can have a large influence in the structural response and the ultimate

strength. For the bridges studied in this research, however, the horizontal curvature and the support skew impose lateral-torsional deflections that are significantly larger than the imperfections associated with the fabrication processes. Therefore, the virtual test simulations conducted in Chapter 6 do not include initial geometric imperfections.

# CHAPTER IV

# BEHAVIOR AND ANALYSIS OF HORIZONTALLY CURVED AND SKEWED I-GIRDER BRIDGES

Chapter 2 provides a concise description of the different functions that bracing systems have in I-girder bridges. This chapter focuses on the interaction between the bracing systems, curvature, and skew and the repercussions on the behavior of these structures. This chapter is organized by first introducing the different analysis methods used in the design of I-girder bridges, highlighting their attributes, differences, and limitations. In the second part, studies are conducted to understand the factors that control the structural behavior on straight and curved skewed bridges. Next, practices that can be implemented in straight and skewed bridge to mitigate the skew effects are introduced. In the last part of the chapter, three I-girder bridges are analyzed to study the influence of different cross-frame configurations on the system responses.

## 4.1. Assessment of Current Practices used for the Analysis of Steel Bridges

Three methods of analysis are commonly used for the prediction of the structural response of I-girder bridges. The simplest is the line-girder or 1D analysis method, where the bridge girders are studied independently. Due to this modeling simplification, the line-girder analysis cannot capture the interaction between the different components of the structure. The second method commonly used for bridge design is 2D-grid analysis. With this method, both the girders and the bracing system are considered in the models. However, for bridges of certain characteristics, the simplifications in the computational

models used to represent girders and cross-frames can result in a false prediction of the real behavior. The 1D and 2D methods are known as approximate or simplified analyses because in certain cases, they cannot represent the physical behavior of a bridge. In particular, the inherent three-dimensional response associated with support skew, horizontal curvature, and the configuration of the bracing systems is not always properly captured by the simplified methods. The last method is a three-dimensional finite element representation of the bridge, where all the structural components are modeled explicitly. This method is more sophisticated than the previous, and is usually the best option for the analysis of complex structures. The next sections introduce each of these three analysis techniques, exploring their attributes and limitations.

### 4.1.1. Approximate 1D Line Girder Analysis

In this analysis method, the girders are analyzed individually, and the interaction between the girders and the bracing system is ignored. For the noncomposite structure, the loadings considered in the analysis are the girder self-weight, the weight of the SIP forms and other devices used to facilitate the concrete placement, and the weight of the wet concrete. In this research, these loads are also referred to as steel dead load (SDL), additional dead load (ADL), and concrete dead load (CDL), respectively. The sum of these three loads is known as the total noncomposite dead load (TDL).

In addition to the TDL, in the fascia girders, the torsion imposed by the overhang brackets is also considered. The loads associated with the concrete deck placement are modeled as uniformly distributed loads based on tributary areas in this research.

The bridge XICSN1 introduced in Section 3.1.1 is used to illustrate the line-girder method. Girder G2 is isolated from the rest of the structure, and it is analyzed as a continuous beam. The plots in Figure 4.1 compare the responses captured by the nonlinear FEA and the approximate 1D analysis at the TDL level. In the plots, the horizontal axis is normalized with respect to total length of the bridge. Figure 4.1(a) shows that the line-girder analysis accurately captures the major-axis bending stresses, $f_b$, predicted by the FEA. Figure 4.1(b) shows that the vertical displacements obtained from the 1D analysis are also an accurate representation of the benchmark.

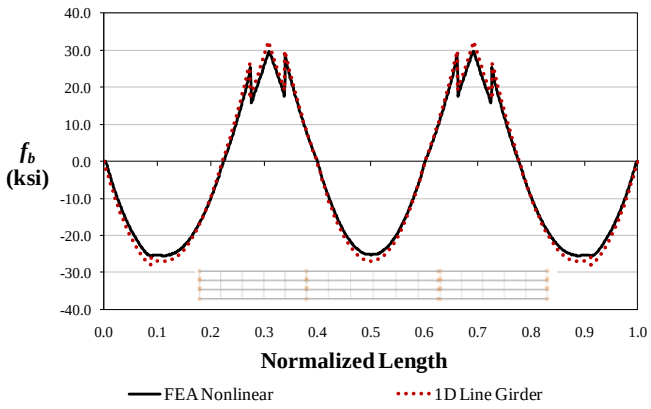


(a) Major-axis bending stresses, $f_b$

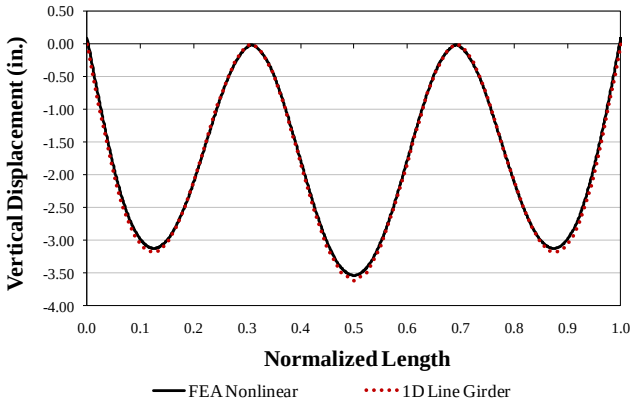


(b) Vertical displacements

Figure 4.1. Comparison of the response predictions obtained from a refined 3D FEA model and a 1D line-girder analysis for girder G2 of bridge XICSN1

This example shows that for simple geometries, the 1D analysis is sufficient to predict the structural behavior of an I-girder bridge. In straight bridges with normal supports, the cross-frames serve mainly as girder braces; they do not participate in the load distribution, and their contribution to the behavior of the system is negligible. In the fascia girders, the cross-frames help limit the levels of flange lateral bending stress, $f_\ell$, that result from the torsion imposed by the overhang brackets. Figure 4.2 shows the stress response in the top flange of girder G1. As shown, the $f_\ell$ stresses resemble the response of a continuously supported beam. In this case, the cross-frames represent the supports.

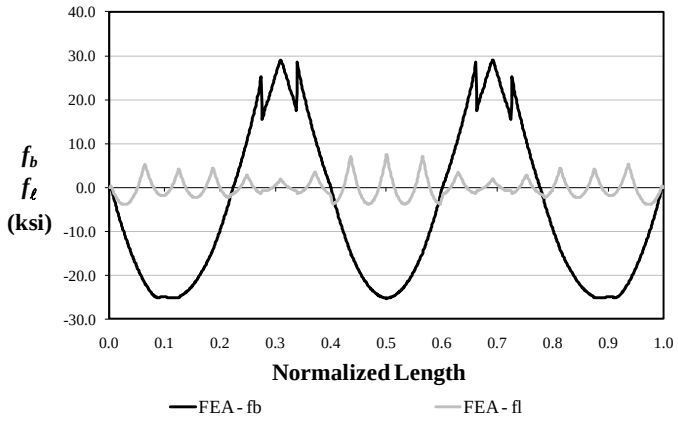


Figure 4.2. Major-axis bending and flange lateral bending stresses predicted by the refined 3D FEA model for girder G1 of bridge XICSN1

AASHTO (2010) provides specific ad hoc procedures to determine the $f_\ell$ response in the fascia girders when designing a bridge structure using 1D analysis. The stress level at the cross-frame location is calculated as

$$f_\ell = \frac{w_\ell L_b^{\,2}/12}{S_{yf}} \qquad \text{(Eq. 4.1)}$$

where $w_\ell$ is the uniformly distributed load imposed in the flange by the overhangs, $L_b$ is the distance between cross-frames, and $S_{yf}$ is the elastic section modulus of the flange under consideration. In this equation, the value of 12 in the denominator is sometimes changed to 10, to recognize that the flange is not fully fixed (per symmetry boundary conditions) at the bracing locations. For many bridges, the highest levels of flange lateral bending stress occur at the bracing points; therefore, the stresses calculated with Eq. 4.1 represent a reasonable estimate for design. As illustrated in Figure 4.3, $w_\ell$ is obtained by calculating the magnitude and location of the overhang dead load resultant, $w_b$, and summing moments about the web-flange juncture.

In Figure 4.2, it is shown that the maximum $f_\ell$ stress in the top flange of girder G1 (bridge XICSN1) is 7.4 ksi at the center of the bridge (i.e., $x$ = 0.5). Applying Eq. 4.1 with the values of 12 and 10 in the denominator, the predicted stresses are 7.8 ksi and 9.3 ksi, respectively. As in this structure, the values predicted with Eq. 4.1 are generally a reasonable approximation of the expected $f_\ell$ stresses provided that the girder does not experience large second-order response amplifications.

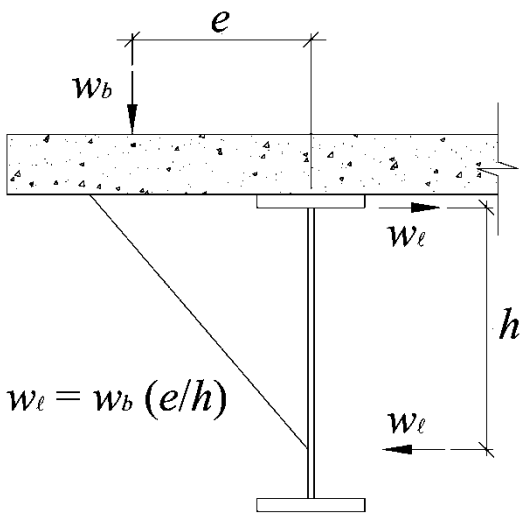


Figure 4.3. Determination of the uniformly distributed load $w_\ell$

4.1.1.1. The V-Load Method for Analysis of Curved Bridges

The V-load method extends the capabilities of the 1D line-girder analysis to consider the effects of the horizontal curvature. The method was originally developed by HDR Engineering Inc. (1963) (previously Richardson, Gordon, and Associates) and published in the *"USS Structural Report, Analysis and Design of Horizontally Curved Steel Bridge Girders."* The V-load method is an analysis tool that has been used for more than four decades in the preliminary and final design of curved I-girder bridges. This section discusses the derivation of the method to highlight its attributes and applicability to the analysis of I-girder bridges. The derivations are based on the work presented in Grubb (1984) and Poellot (1987).

The simply supported curved I-girder shown in Figure 4.4(a) is subject to a major-axis uniform moment, *M*, that is applied at the ends. The axial forces acting in the flanges, *T*, are approximately equal to $M/h_o$, where $h_o$ is the distance between the flange

centroids. A differential element of the top flange with an arc length equal to *ds* is extracted from the girder. Figure 4.4(b) shows the free body diagram (FBD) of the flange segment. The horizontal components of the forces, $T_x$, cancel each other. The vertical components, $T_y$, are additive, so a uniformly distributed internal force, $q$, that is transferred through the web is necessary to balance these components. In the context of the flange segment depicted in Figure 4.4(a), the axial forces and the uniformly distributed force are self-equilibrating, and can be compared to the hoop tension observed in thin-walled pressure vessels. Thus, the axial force, $T$, is equal to $qR$, where $R$ is the radius of curvature of the girder, so $q = M/Rh_o$.

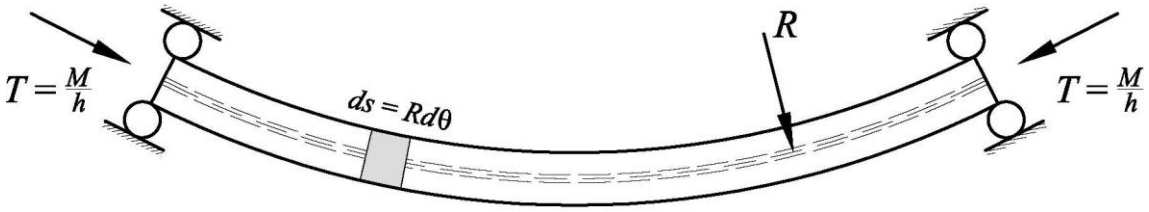


(a) Axial forces in the top flange due to uniform moment

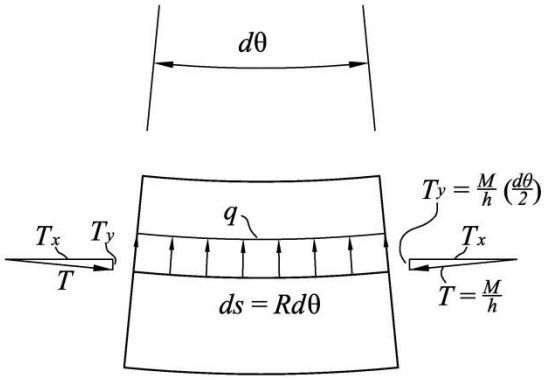


(b) Free body diagram of the flange segment

Figure 4.4. Curved girder subject to a uniform major-axis bending moment

The uniformly distributed force, $q$, subjects the flanges to lateral bending. Hence, in a two-girder system such as the one depicted in Figure 4.5(a), the flanges behave as

continuous beams, where the cross-frames work as supports. The girders G1 and G2 in this figure are subject to moments $M_1(x)$ and $M_2(x)$, respectively, where $x$ is the coordinate measured along the length of the girders. The FBD of the first intermediate cross-frame in Figure 4.5(b) shows that the reaction at this position or force in the cross-frame, $H_1$, is equal to $q_1 L_{b1} = M_1 L_{b1} / R_1 h_o$, where $L_{b1}$ is the distance between cross-frames measured along the centerline of G1, and $R_1$ is the curvature radius of the girder. The moment in this equation, $M_1$, is taken as the moment at the cross-frame position, i.e., $M_1 = M_1(L_{b1})$.

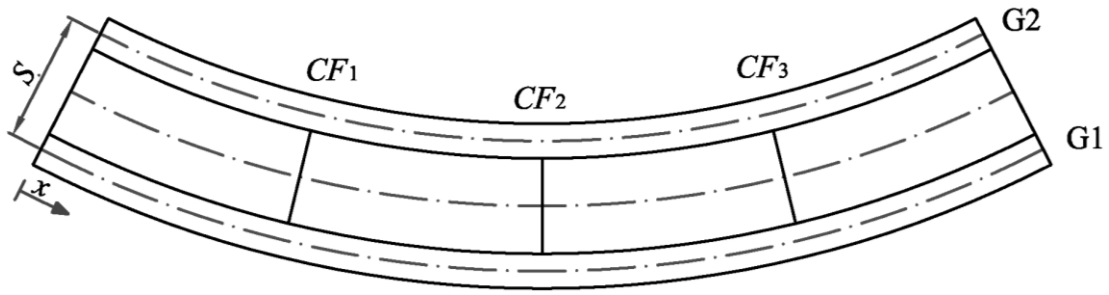


(a) Plan view of the two-girder system

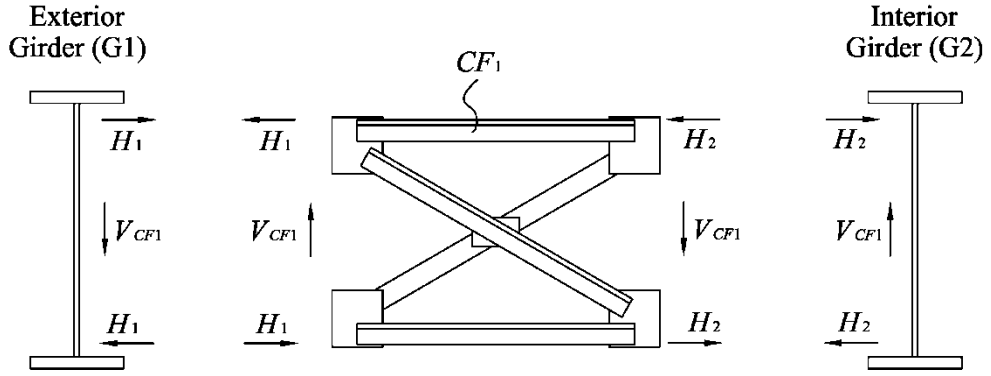


(b) Free body diagram of the first intermediate cross-frame

Figure 4.5. Interaction of forces in a curved girder system

The reaction at the bottom flange level is the same as $H_1$, but is in the opposite direction since the moment causes compression in the top flange and tension in the

bottom flange or vice versa. Similarly, in the interior girder, G2, the reaction, $H_2$, is taken equal to $q_2 L_{b2} = M_2 L_{b2} / R_2 h_o$, where $M_2 = M_2(L_{b2})$. Notice that $L_{b1}/R_1 = L_{b2}/R_2$ is taken as a constant value $L_b/R$, so $H_1 = M_1 L_b/Rh_o$ and $H_2 = M_2 L_b /Rh_o$. In the cross-frame, moment equilibrium requires that

$$V_{CF1} = \frac{(H_1 + H_2)h_o}{S} = \frac{M_1 + M_2}{RS/L_b} \qquad \text{(Eq. 4.2)}$$

These vertical forces are a direct result of the horizontal curvature effects, and they are known as V-loads. In the last equation, the subscript *CF*1 is used to emphasize that this is the V-load at the first intermediate cross-frame position. Similarly, the loads at the other cross-frame locations can be found by replacing the moments $M_1$ and $M_2$, accordingly. In the exterior girder, G1, the secondary moments that result from the V-loads, $M_{1s}$, have to be added to the primary moments produced by the gravity loadings, $M_{1p}$. In the interior girder, G2, these loads are in opposite direction, so the resulting moments have to be subtracted from the gravity load moments. Therefore, the total moment in a particular cross-section of girder G1, $M_1$, is equal to $M_{1p}+ M_{1s}$. Likewise, for the interior girder, $M_2 = M_{2p}+ M_{2s}$. Moreover, at any cross-frame position, $M_{1s} = -M_{2s}$ $(L_1/L_2)$, where $L_1$ and $L_2$ are the developed lengths of G1 and G2, respectively. For practical cases, the term in parenthesis in the last equation is close to one, so $M_{1s} \approx -M_{2s}$. With this approximation, the sum of the total moments in G1 and G2, $M_1 + M_{2,}$ is approximately equal to $M_{1p} + M_{2p}$. Substituting the last result in Eq. 4.2,

$$V = \frac{M_{1p} + M_{2p}}{RS/L_b} \qquad \text{(Eq. 4.3)}$$

With this procedure, the girders can be analyzed independently using a line-girder analysis. The curved girders are represented with equivalent straight girders of length $L_1$ and $L_2$, and they are subject to the gravity loadings plus the V-loads. This development can be extended to consider cases with more than two girders. As discussed by Poellot (1987), the V-loads in a multi-girder system can be calculated as

$$V = \frac{\sum M_p}{CRS/L_b} \qquad \text{(Eq. 4.4)}$$

In Eq. 4.4, the subscript *CF*1 is dropped to highlight that a V-load is calculated at each cross-frame position. The constant *C* in this equation depends on the number of girders in the structure. Table 4.1 shows the values of *C* for systems with up to ten girders. These constants are obtained assuming that there is a linear distribution of the V-loads from the interior to the exterior girder. This means that in a system with more than two girders, the V-loads in the intermediate girders are determined by linear interpolation of the V-loads in the exterior and interior girders.

Table 4.1. Values of the *C* coefficient

| **Girders** | **Coefficient** |
|---|---|
| 2 | 1 |
| 3 | 1 |
| 4 | 10/9 |
| 5 | 5/4 |
| 6 | 7/5 |
| 7 | 14/9 |
| 8 | 12/7 |
| 9 | 15/8 |
| 10 | 165/81 |

The flange lateral bending stresses due to the horizontal curvature in any girder, $f_\ell$, can be calculated at the cross-frame locations with the formula

$$f_\ell = \frac{ML_b^{\,2}/12\,Rh_o}{S_y} \qquad \text{(Eq. 4.5)}$$

which has essentially the same form as Eq. 4.1, but substituting $w_\ell$ with the assumed uniformly distributed lateral load, $q = M/Rh_o$. In Eq. 4.5, the moment $M$ is taken as the total moment at a particular section of the girder that result from the action of the gravity loads, and the V-loads, i.e, $M = M_p+M_s$. In fascia girders the effects of the curvature and the overhang brackets can be considered simultaneously by adding the results of Eqs. 4.1 and 4.5.

In Eq. 4.5, the elastic flange section modulus, $S_y$, is equal to $(t_f\, b_f^3/12)/(b_f/2)$, where $b_f$ and $t_f$ are the flange width and thickness, respectively. Since the flange area, $A_f$, is equal to $b_f \cdot t_f$, the section modulus can be expressed as $S_y = A_f \cdot b_f / 6$. In addition, the moment, $M$, is equal to $f_b \cdot S_x$, where $f_b$ is the major-axis bending stress and $S_x$ is the strong-axis elastic section modulus of the girder. Substituting these parameters in Eq. 4.5, the flange lateral bending stress can be expressed as

$$f_\ell = \frac{1}{2}\frac{f_b S_x}{A_f h_o}\frac{L_b}{R}\frac{L_b}{b_f} \qquad \text{(Eq. 4.6)}$$

This form of the equation shows the basic parameters that control the $f_\ell$ stresses induced by the horizontal curvature. Notice that if the girder is doubly symmetric, $S_x/(A_f\, h_o) \approx 1$. Hence, the $f_\ell$ stress response is controlled by the $f_b$ stresses and the ratios $L_b/R$ and $L_b/b_f$.

The application of the V-load method is demonstrated next. The exterior girder, G1, of bridge NISCR8 presented in Section 3.1.6 is analyzed here to illustrate the use of

the method. The geometry of this structure and the arrangement of the cross-frames make it ideal for this analysis. This is a simple span bridge that has radial supports and contiguous cross-frames; hence, it satisfies all the basic assumptions considered in the derivation of the V-load formulas.

Figure 4.6 shows an elevation view of girder G1 of the bridge NISCR8, with the gravity loads corresponding to the girder self-weight (SDL), the concrete dead load (CDL), and the additional dead load (ADL). The sketch also shows the V-loads at the cross-frame positions that are calculated from the gravity loads. It is worth mentioning that the CDL and the ADL are modeled as uniformly distributed loads that are calculated based on tributary areas, while the SDL is calculated considering the section changes in the girder. The sum of these three loads is the total noncomposite dead load (TDL).

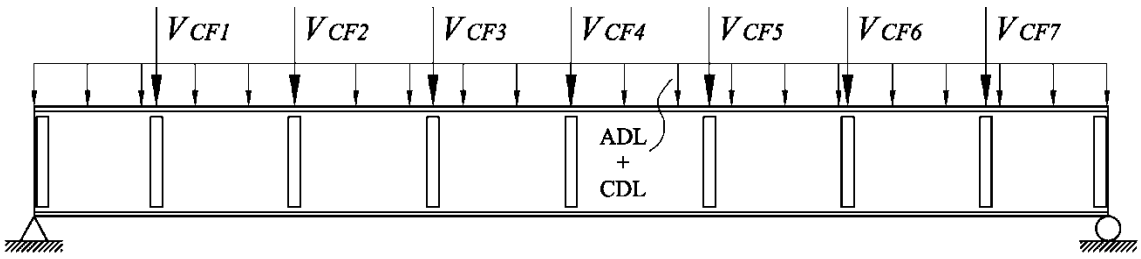


Figure 4.6. Schematic representation of girder G1 in bridge NISCR8 with the loadings required for the line-girder analysis

Table 4.2 summarizes the procedure to calculate the V-load at mid-span, i.e., CF4. In the table, the second and third columns show the uniformly distributed loads corresponding to the ADL and CDL. The three next columns show the moments at mid-span due to each of the loadings, and the last column shows the TDL moment. The sum of the TDL moments is 39308.3 kip-ft. Therefore, according to Eq. 4.2, the V-load is equal to

$$V_{CF4} = \frac{39308.3\,\text{kip - ft}}{(15/8)420\,\text{ft}\;9.25\,\text{ft}/19.3\,\text{ft}} = 104.1\,\text{kips}$$

Similarly, the V-loads at the other cross-frame positions are calculated following the same scheme.

Table 4.2. Principal moments obtained from a line-girder analysis for the calculation of the V-loads at mid-span (CF4)

| Girder | $w_{ADL}$ (kip/ft) | $w_{CDL}$ (kip/ft) | $M_{SDL}$ (kip-ft) | $M_{ADL}$ (kip-ft) | $M_{CDL}$ (kip-ft) | $M_{TDL}$ (kip-ft) |
|---|---|---|---|---|---|---|
| G1 | 0.0596 | 0.9838 | 1739.7 | 198.5 | 3275.9 | 5214.1 |
| G2 | 0.0758 | 1.0916 | 1669.5 | 242.3 | 3489.2 | 5401.0 |
| G3 | 0.0758 | 1.0916 | 1601.6 | 232.4 | 3346.5 | 5180.5 |
| G4 | 0.0758 | 1.0916 | 1088.0 | 222.7 | 3206.8 | 4517.5 |
| G5 | 0.0758 | 1.0916 | 993.9 | 213.2 | 3070.1 | 4277.2 |
| G6 | 0.0758 | 1.0916 | 950.3 | 203.9 | 2936.4 | 4090.6 |
| G7 | 0.0758 | 1.0916 | 811.0 | 194.8 | 2805.6 | 3811.4 |
| G8 | 0.0758 | 1.0916 | 774.2 | 185.9 | 2677.8 | 3637.9 |
| G9 | 0.0596 | 0.9838 | 737.8 | 139.4 | 2300.9 | 3178.1 |
| | | **Total** | 10366.0 | 1833.1 | 27109.2 | 39308.3 |

Figure 4.7 shows the results obtained from the 1D line-girder analysis and a refined 3D FEA for girder G1. As shown in the first plot, the major-axis bending stress response is accurately captured by the simplified method. Likewise, the vertical displacements obtained from the approximate solution are a good representation of the benchmark response. These results are expected since the bridge geometry and the configuration of the bracing system match the assumptions in the development of the V-load method.

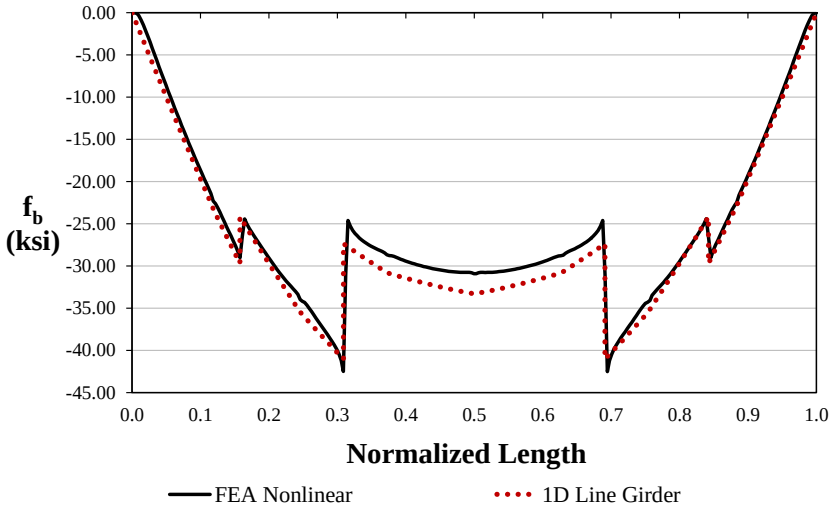


(a) Major-axis bending stresses

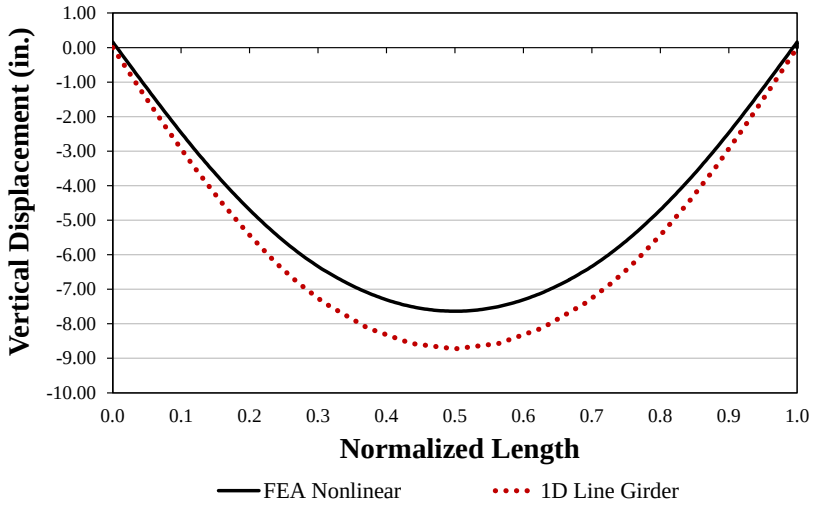


(b) Vertical Displacements

Figure 4.7. Comparison of results obtained from the approximate 1D line-girder analysis and the 3D nonlinear FEA for bridge NISCR8, girder G1

The other response that is of interest for the design of this curved bridge is the flange lateral bending stress. For illustration, this response is evaluated at CF4, which is located at mid-span, the point of maximum major-axis bending moment. At CF4, the

stress due to the effects of horizontal curvature and the overhang loading eccentricity, calculated according to Eqs. 4.1 and 4.5 is equal to

$$f_{\ell\_o} = \frac{0.097 \text{ kip - ft} \left(19.3 \text{ ft}\right)^2 / 12}{0.0868 \text{ ft}^3} = 0.24 \text{ ksi}$$

$$f_{\ell\_c} = \frac{12117.4 \text{ kip - ft} \left(19.3 \text{ ft}\right)^2 / 12 \cdot 420 \text{ ft} \cdot 6.69 \text{ ft}}{0.0868 \text{ ft}^3} = 10.71 \text{ ksi}$$

$$f_{\ell\_\text{total}} = 0.24 \text{ ksi} + 10.71 \text{ ksi} = 10.95 \text{ ksi}$$

The $f_\ell$ stress level obtained from the refined 3D FEA is 10.14 ksi, which is close to the 10.95 ksi value obtained from the approximate analysis.

A final remark with regard to the behavior of this structure is the influence of the second-order effects on the system responses. Figure 4.8 shows the stress and deflection responses predicted from a linear and a nonlinear FEA. The plots show that the responses are essentially the same; therefore, the second-order amplifications are negligible. In this case, the results from the line-girder analysis, based on the V-load method discussed previously, match almost exactly the benchmark responses because the geometry of the bridge is relatively simple and the amplifications associated with the nonlinear response are insignificant. In general, the method is accurate for cases that closely satisfy the assumptions used for its derivation. However, for bridges with unequal girder spacing, staggered cross-frame patterns, skewed supports, bridges that exhibit significant nonlinear responses, etc., a line-girder analysis based on the V-load method may not be sufficient. For those cases, models based on 2D-grid analyses conducted with the techniques discussed in Chapter 5 or 3D FEA, which capture more accurately the

interaction between the structural components and second-order amplifications, may be required. These aspects are further discussed in the next sections.

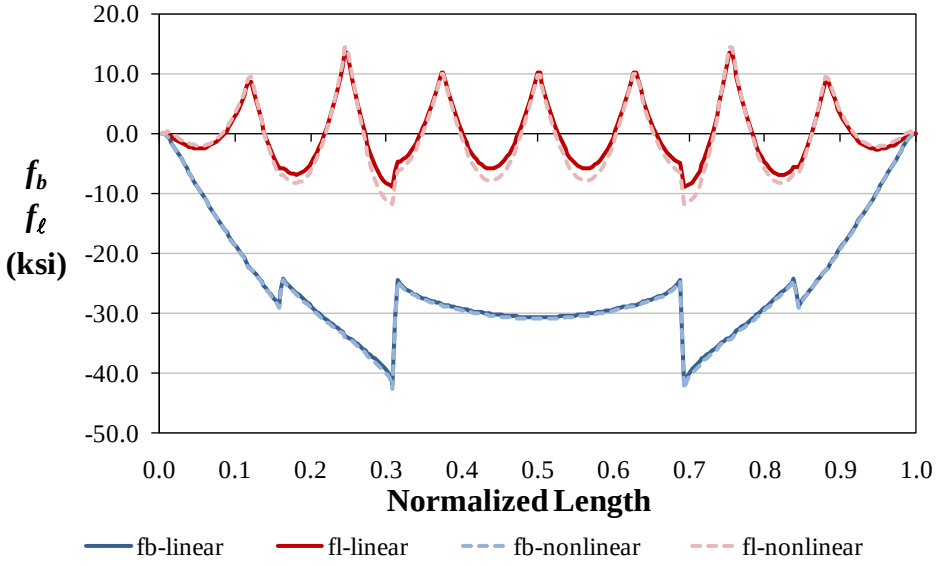


(a) Stress responses

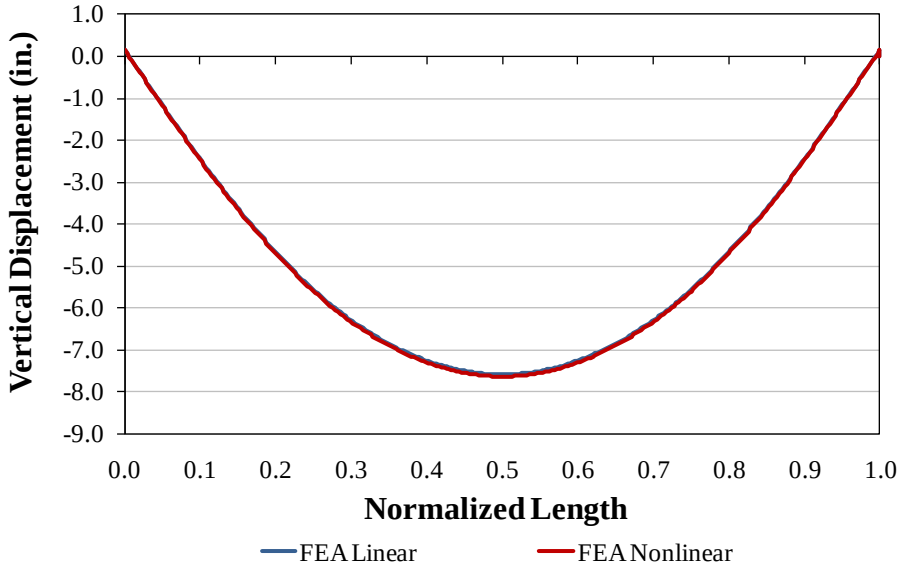


(b) Vertical displacements

Figure 4.8. Comparison of responses obtained from a linear and a nonlinear FEA for bridge NISCR8, girder G1

### 4.1.2. Approximate 2D-Grid Analysis

The 2D-grid method is another approximate analysis technique used to design steel I-girder bridges. In the most basic 2D-grid methods, also known as traditional 2D-grid methods, girders and cross-frames are modeled as line elements that have three degrees-of-freedom (dofs) per node, two rotational and one translational. As shown in Figure 4.9(a), the rotational dofs capture the bending and torsion responses, and the translational dof corresponds to the vertical displacements. In some computer programs, the 2D-grid models are constructed using frame elements that have six dofs per node. As shown in Figure 4.9(b), these elements have three translational and three rotational dofs at each node.

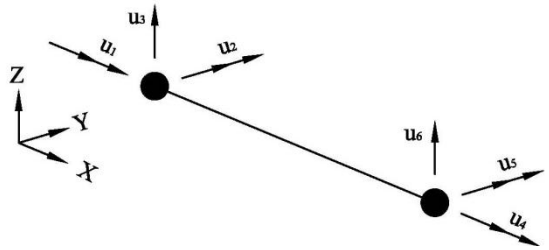


(a) Traditional 2D-grid element

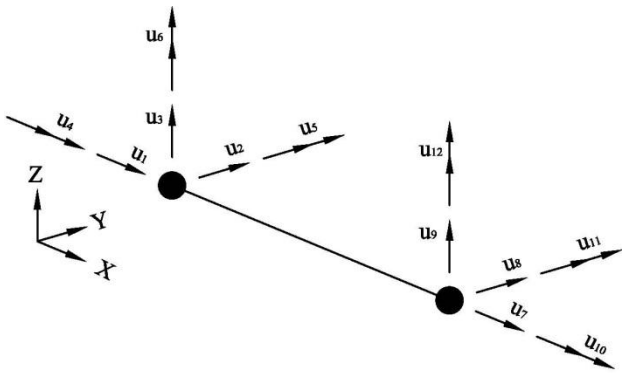


(b) Frame element

Figure 4.9. Schematic representation of the general two-node elements implemented in computer programs for grid analysis of I-girder bridges

In grid analyses, the girders and cross-frames are included in the model to capture their structural interaction. Even though this in-plane representation of the structure can capture more attributes of the bridge behavior than the 1D line-girder model, it has several limitations. The formulation of the element used to represent the structural components in many computer software packages used for the analysis and design of steel girder bridges is commonly based on the Euler-Bernoulli beam theory. The kinematic assumptions of this formulation are:

- The deformations are small
- The cross-sections normal to the girder axis remain planar and normal during the deformation
- The girder is straight and prismatic
- The loadings are applied through the shear center

In I-girder bridges with simple geometries these assumptions have a minor effect, and the classic beam theory is sufficient to predict the expected behavior. The first assumption is usually satisfied for practical cases. If the second-order amplifications are negligible, the deflections in the bridge are much smaller than its dimensions, so the small deformation assumption is generally met. The second assumption implies that during the deformations there is no distortion of the girder cross-sections due to shear straining. In I-girder bridges, the flexural deformations are the main contributors to the system response, so the effects of the shear deformations have a minor impact in the response. In many cases, the shear deformations may be negligible for practical purposes, but as the span-to-depth ratio decreases, they gain importance. Some computer programs do also implement beam elements that account for shear deformations. The derivation of

these elements is typically based on Timoshenko's beam theory, which captures the contribution of the shear deformations to the girder response.

I-girders generally do not have prismatic sections since they are dimensioned to optimize the design. The girders are generally more robust near mid-span, where the bending moments are the largest, and the cross-section dimensions decrease towards the abutments, where the flexural strength requirements are smaller. Therefore, the third assumption is not satisfied if a girder is modeled with a single element. In 2D models the girders are discretized such that they are prismatic within the element length. Hence there is always a node connecting the elements at a section change. In most computer programs, the elements are connected at the cross-section centroids, which is not the case in stepped girders. This modeling limitation, however, does not affect significantly the prediction of the system response, so it is an acceptable approximation for design purposes.

The fourth assumption implies that the girders are not subject to significant torsion. In the elements with 12 dofs used for grid analysis, the predictions for the major-axis bending, minor-axis (or lateral) bending, and torsion responses are analyzed independently. This implies that in the formulation of the element stiffness matrix there is no coupling between these three responses. Hence, the Euler-Bernoulli theory is used to develop the stiffness coefficients for each orthogonal direction considering that the loads are acting through the shear center, while the torsion coefficients are formulated separately. It is well known that in an open section thin-walled beam there are two sources of torsion resistance; namely the pure or St. Venant and the warping torsion resistance. In the formulation of the two-node beam implemented in most computer

commercial programs only the first source is considered. This can have a detrimental effect in the response prediction for cases where the torsion deformations have a significant influence in the behavior of the structure. A complete discussion of the torsion model in 2D analyses is presented in Chapter 5.

In 2D analyses of I-girder bridges, both the girders and cross-frames are modeled using the Euler-Bernoulli beam element or in a few cases, the Timoshenko beam element. Figure 4.10 shows the cross-frame representations used in the 2D models. The standard practice is to model the cross-frames with equivalent beam elements that capture their behavior in an approximate fashion (Coletti and Yadlosky 2007, NHI/FHWA 2011a). As shown in the figure, the cross-frame is represented with a single beam element that is connected to the girder elements at Nodes 1 and 2. Various ad hoc procedures are used to determine the section properties of the equivalent beam, as discussed in Section 5.2. Another practice that is occasionally used is to model all the cross-frame elements explicitly. For this purpose, rigid links or rigid multi-point constraints are included in the model. As illustrated in the figure, at the left end the links are connected between Nodes 1 and 3, and 1 and 5, and the cross-frame components are connected to Nodes 3 and 5. The kinematics of the left girder and the cross-frame are coupled through these links. Similarly, at the right end, the links between Nodes 2 and 4, and 2 and 6, couple the kinematics of the cross-frame and the girder. By modeling the cross-frames using this technique, a more realistic representation of the system is attained; however, constructing these kinds of models can be laborious if it is not automated within the software. For this reason, in common practice, the equivalent line element is used for 2D-grid analyses.

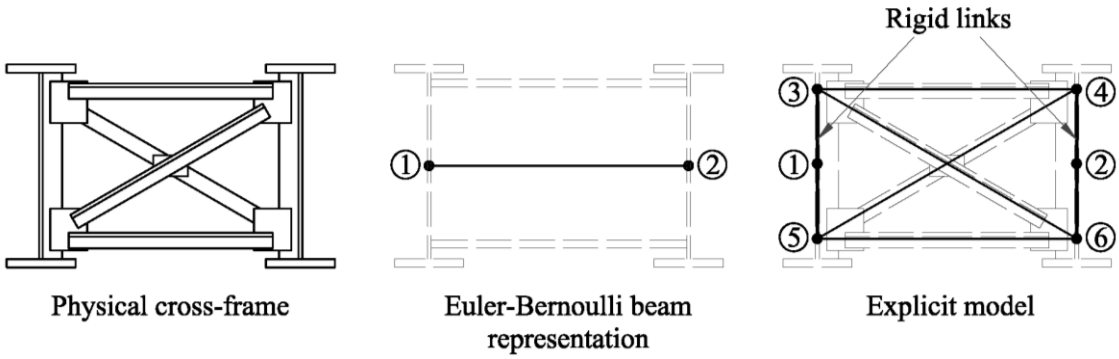


Figure 4.10. Modeling techniques used in 2D-grid analyses to represent the cross-frames

The foregoing discussion highlights the characteristics of the elements and the modeling techniques used in grid analyses. This analysis method has been successfully used in the design of highway bridges for several decades. However, for structures with tight curvatures, sharp skews, complex cross-frame layouts, or cases where the geometric nonlinearities influence the structural behavior, a 2D-grid analysis may not be sufficient. In these cases, the limitations in the element formulations, particularly limitations regarding the torsion model, and the simplifications used for modeling the cross-frames can be a detriment to the accuracy of the analysis. The recommendations provided in Chapter 5 can be implemented in computer programs to improve the predictions obtained with this analysis method.

### 4.1.3. Three-Dimensional Finite Element Analysis

The 3D finite element analysis (FEA) is the most sophisticated method of analysis available. With this analysis method, all the components of the structure are modeled explicitly, including all attributes associated with the structural depth. Cross-frame elements, transverse stiffeners, connection plates, etc., are all included in the models. Although a model constructed with this method can provide the most accurate

representation of the physical structure, it has its limitations. In recent years, commercial software providers have improved significantly the efficiency of the programs to create 3D FEA models of steel girder bridges. However, the cost of the software, the inclusion of different loading scenarios for live load analysis, and the time required to post-process the analysis results are some of the reasons why 3D FEA often has been reserved for the design of special structures. Therefore, 3D FEA tends to be used in cases where it is suspected that the approximate methods described previously cannot represent accurately the structural behavior of a bridge. Another limitation is the ability of the user to conduct this type of analyses. FE software requires the user to be familiar with the theory behind the program development and the various assumptions in the model formulations. All 3D FEA models are not the same, and a 3D FEA of a bridge by itself does not warrant accurate predictions; more importantly, the analyst must have the ability to scrutinize the model and its results.

The levels of sophistication in FEA are unlimited. Depending on the purpose of the analysis, a basic linear-elastic model could be sufficient for the design of many structures. More advanced models include the effects of second-order amplification and material inelastic behavior. Also, the representation of special loadings acting in the bridge (including their locations), the weight of construction equipment and nonstructural components used during the deck placement, and the effects of the early concrete hardening are a few of many factors that can be included in the 3D model. The most refined FEA models include all the factors above plus residual stresses and initial imperfections that result from the girder fabrication processes. A FEA of these characteristics is known as a virtual model since it provides the closest representation of

the physical behavior of the bridge. Due to the level of complexity, these analyses are predominantly used for research purposes. Section 3.2 introduces the characteristics of the 3D FEA models presented in this research. Key 3D FEA results along with the results of the approximate methods for different bridge structures are discussed in the sections below.

## 4.2. Influence of the Support Skew on the Structural Behavior

Depending on the geometry of the bridge and the relationship between the span length, the width, the skew angle, and the distribution of the intermediate cross-frames in the structure, skew effects can have different levels of importance. Some of the most relevant effects that the skewed supports may have on the structural behavior of an I-girder bridge include: out-of-plumbness of the webs, large cross-frame forces, high levels of flange lateral bending stress, bearing misalignments, fit-up problems during the steel erection, and difficulties with the control of the overall bridge geometry during the deck placement. All these effects are related to each other; for example, the torsional rotations or twist that the girders experience at the bearing lines due to the skew, result in girder layovers, webs with an out-of-plumbness, and possibly, misalignments of the bearings. Similarly, because the cross-frames are connected to the girders, the forces on these elements are transferred to the girders in the form of nodal forces that are applied at the connections. These nodal forces can induce significant levels of flange lateral bending stress.

In the following sections the skew effects are analyzed in detail. The mechanisms involved in the flow of transverse forces that cause girder layovers, large cross-frame

forces, flange lateral bending stresses, and other undesirable effects of skew are studied to investigate possible methods that can be implemented to reduce their influence in the structural responses of an I-girder bridge. In addition, the studies conducted in the next sections serve to propose a method that can be used to identify cases where the skew may have an important participation on the behavior of an I-girder bridge during construction.

### 4.2.1. Mechanistic Explanation of the Skew Effects

#### 4.2.1.1. Skew Effects in a Two-Girder System

The skew effects are first analyzed considering a simple two-girder system. In this study, the structure is scrutinized to determine the changes in the system response, as the intermediate cross-frames are connected sequentially to the girders. Figure 4.11 shows a perspective view of the finite element model of the structure, including all the intermediate cross-frames. The structure has a span length of 52 ft, the separation between girders is 8 ft, the supports are skewed at 70 degrees, and the intermediate cross-frames are spaced at 6.5 ft. The cross-frame spacing in this system does not reflect the actual distance that would be used in the design of a bridge of these characteristics, which is usually of at least 15 ft. The intention of including more intermediate cross-frames than necessary to provide stability bracing and to satisfy the other requirements discussed in Chapter 2 is to observe the changes that the structure experiences due to the skew, as the transverse stiffness of the system is increased. As illustrated in the figure, girder G1 is the one that forms the acute angle with the cross-frame at the left support, and G2 is the other girder. The intermediate cross-frames have been numbered from CF1 to CF5, with CF1 being the one that is next to the left support.

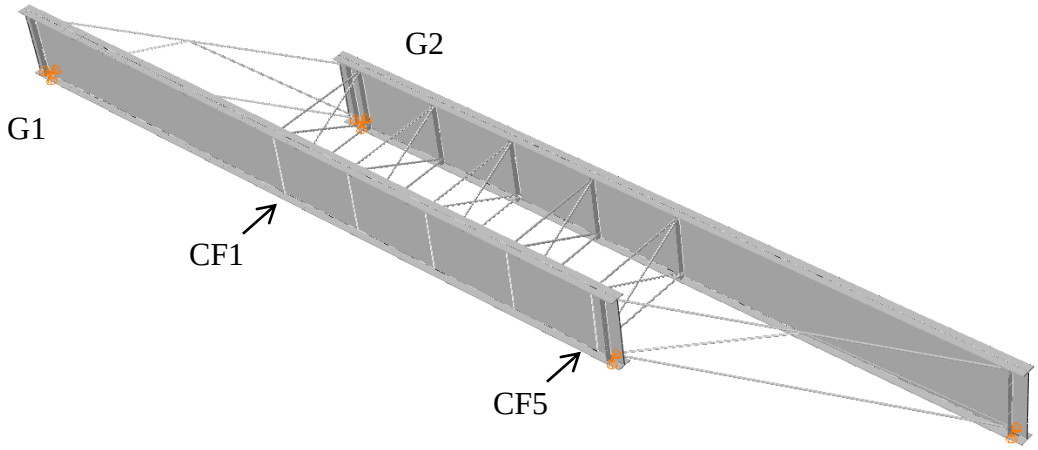


Figure 4.11. 3D view of the finite element model of the two I-girder system

In the first step of the study, the intermediate cross-frames are removed from the structure. Only the bearing line cross-frames are left in place, and the structure is subjected to its self-weight. Next, the first intermediate cross-frame, CF1, is connected to the girders, and the response of the system is captured to observe the changes in behavior. Following the same scheme, the other four intermediate cross-frames are added sequentially.

Linear elastic finite element analyses are conducted following the sequence described above. The intention of conducting linear analyses is to isolate the effects of the skew from the second-order amplifications that the structure can experience as a result of the loadings. The conclusions of the research, however, are applicable for any type of structure with skewed supports, as shown in Sections 4.2.1.4 and 4.2.1.5. Figure 4.13 shows plots of the relative lateral displacement between the top and bottom flanges (or layover) versus the position of the girders with respect to a Cartesian coordinate system with its origin located at the left end of girder G1. In the plots, G1 is positioned

between $x$ = 0 ft and $x$ = 52 ft, and G2 between $x$ = 22 ft and x = 74 ft. The dashed lines illustrate the position of the intermediate cross-frames in the structure. Next to each plot, a perspective view and a plan view of the system's deflected shape obtained from the FEA and amplified by a factor of five, are also included.

In Figure 4.13(a), it is shown that when the girders are connected with cross-frames only at the bearing lines, the layover in both girders varies linearly between the connection points. At the bearing lines, the layover is -1.37 inches and 1.37 inches for the left and right supports, respectively, since the bearing lines have equal skew. Notice that the end cross-frames enforce the rotation of the girders at the supports to be the same. As discussed in Section 4.3, the in-plane rigidity of cross-frames is much larger that the torsional rigidity of the girders; therefore, the cross-frames rotate as a quasi-rigid body (effectively rigid in the cross-frame plane) as the girders twist. By comparing the responses of the girders, it is evident that the girders are twisted the same amount along their length. For example, the layover at the mid-length of both girders is zero. This characteristic is also observed in the plan view of the deformed shape.

The layover of the girders imposed by the end cross-frames can be defined as a global effect of the skew. When the girders deflect vertically due to the gravity loads, they also must rotate to accommodate the effects of the skew. This concept is further illustrated in Figure 4.12. The figure shows schematically the deflections and rotations at the left support of the two-girder system. When the girders deflect vertically, a relative longitudinal displacement, $u_{long}$, occurs between the top and the bottom flange. Since the cross-frame can only rotate about the axis defined by the bearing line, it accommodates this *longitudinal* displacement by imposing a relative *lateral* displacement, $u_{lat}$, between

the flanges. Hence, the girder layover at the bearing lines can be estimated in terms of the major-axis bending response such that $u_{lat} = u_{long} \cdot \tan(\theta)$, where $\theta$ is the skew angle (Ozgur and White 2007). The relative flange lateral displacement is the girder layover, and it induces twist in the girders since at the other support, the girders displace laterally in the opposite direction. This global effect concept is fundamental to understand the collateral effects of skew and the methods to mitigate them since it controls the behavior of a skewed structure, as will be discussed in the next sections.

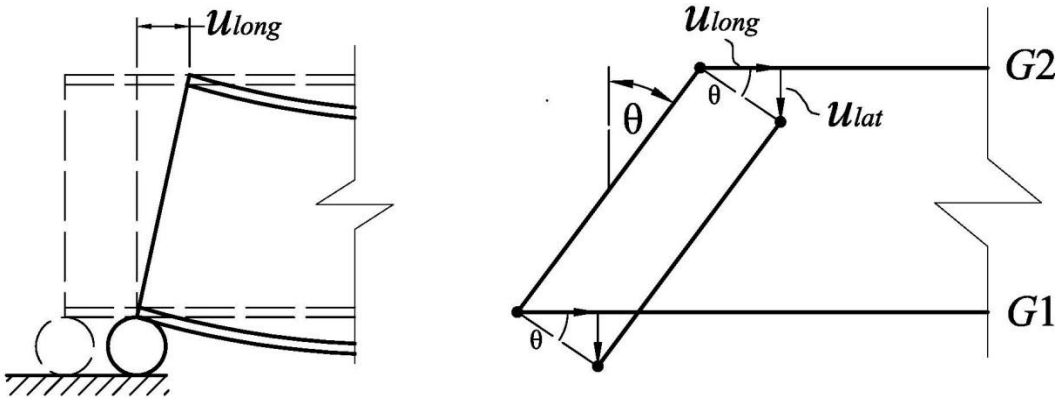


Figure 4.12. Relative flange lateral displacement (layover) in a skewed bridge

The plot in Figure 4.13(b) shows the girder layovers when the first intermediate cross-frame, CF1, is connected. As shown in the plot, the cross-frame enforces the relative lateral displacements in both girders to be the same at the connection. When the girders are connected only at their ends, the displacements at the location of CF1 are -0.11 inches and -1.27 inches for G1 and G2, respectively. With the inclusion of CF1, the girders twist, and the resulting layover is -1.15 inches in both girders. As with the end cross-frames, because of its large in-plane stiffness, the deformations in CF1 due to straining in the chords and diagonals are much smaller than the deflections that result from the girder twist. Therefore, the addition of the first intermediate cross-frame

enforces compatibility in the girder layover at that location. It is worth mentioning that while, with the inclusion of CF1, the layovers in the girders vary with respect to the case without intermediate cross-frames; at the supports they remain essentially unchanged.

Figure 4.13(c) to Figure 4.13(f) illustrate the change in the girder layovers as the rest of intermediate cross-frames are connected to the system. The plots show that as with CF1, the addition of the intermediate cross-frames requires the relative lateral displacements to be compatible at the bracing points, "sewing" the structure together at these locations. Notice that the inclusion of the rest of the intermediate cross-frames does not affect significantly the layovers at the bearing lines, which remain essentially the same during the process.

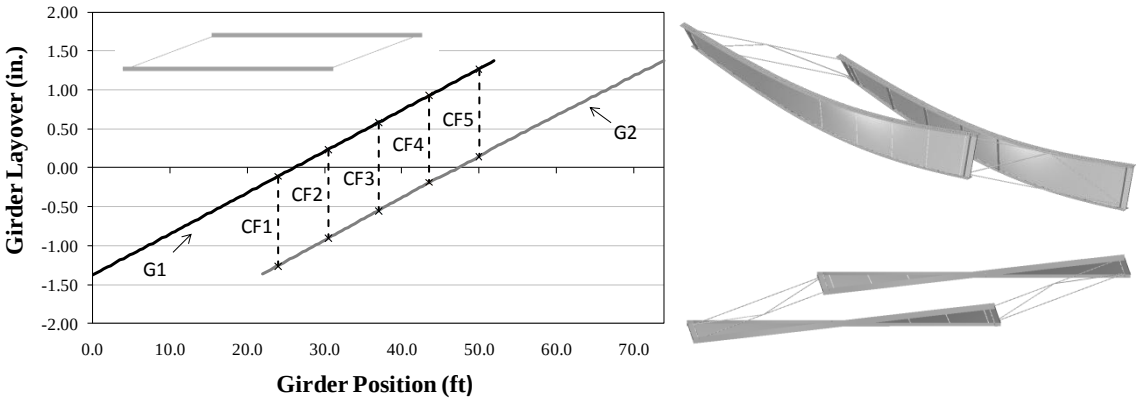


(a) Two-girder system without intermediate cross-frames

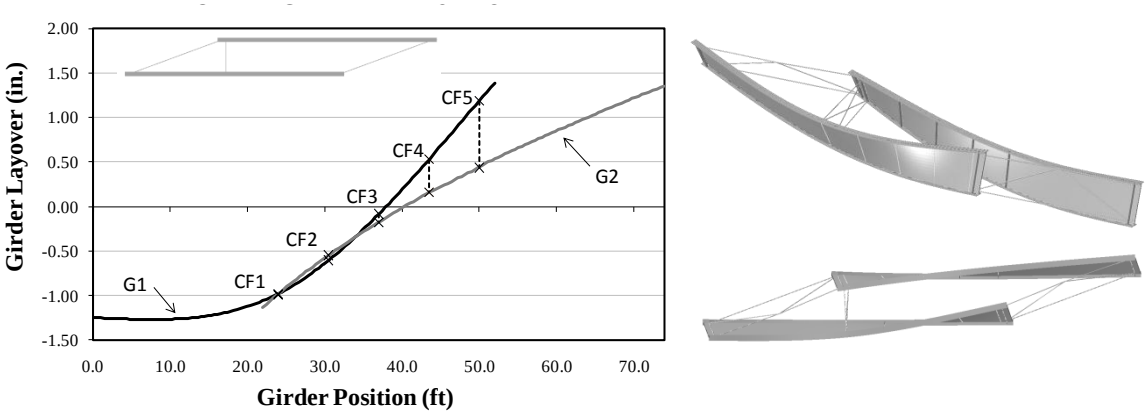


(b) Erection of the intermediate cross-frame CF1

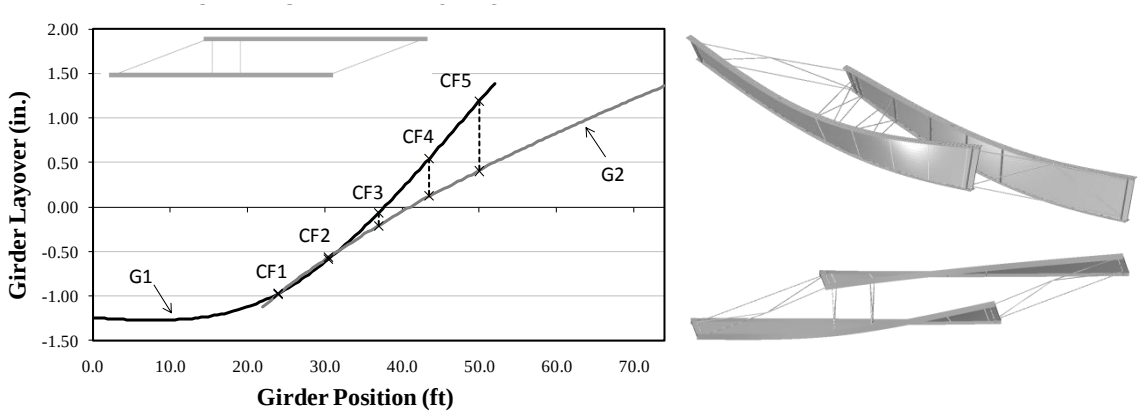


(c) Erection of the intermediate cross-frame CF2

Figure 4.13. Relative flange lateral displacements (or girder layover) obtained from the linear FEA simulation of the intermediate cross-frame erection in a skewed I-girder system

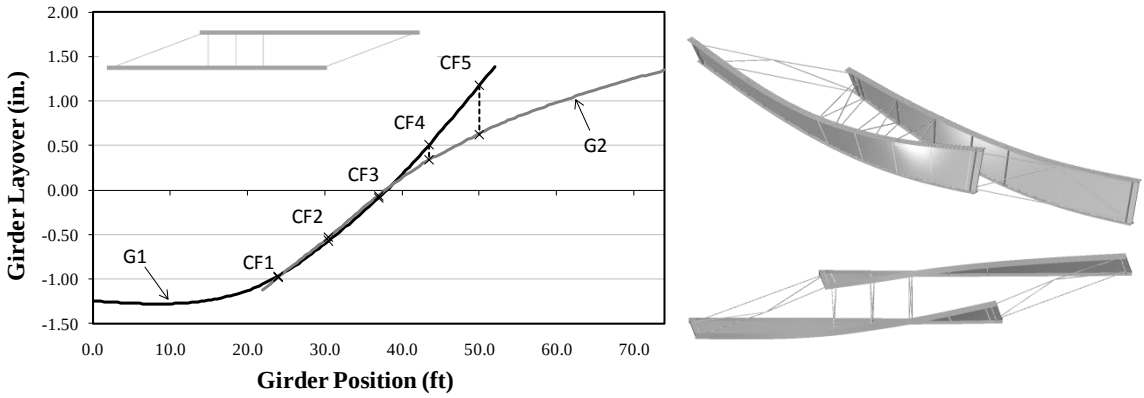


(d) Erection of the intermediate cross-frame CF3

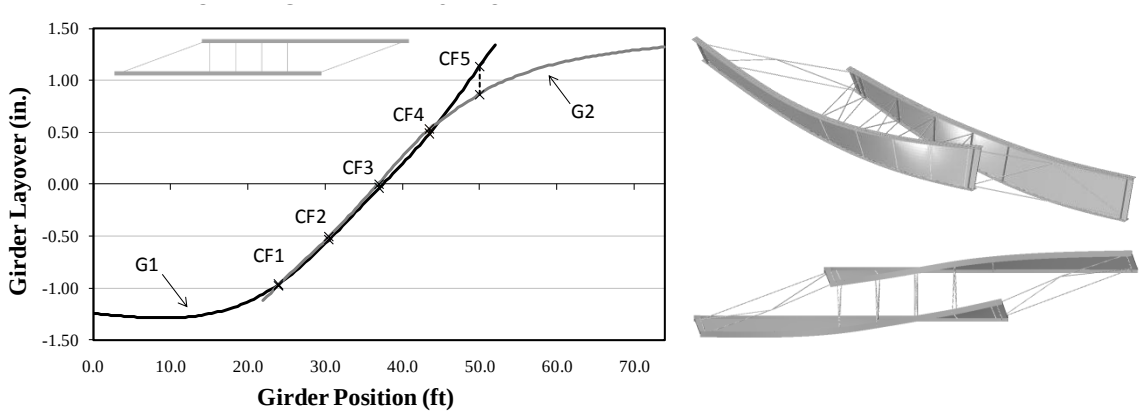


(e) Erection of the intermediate cross-frame CF4

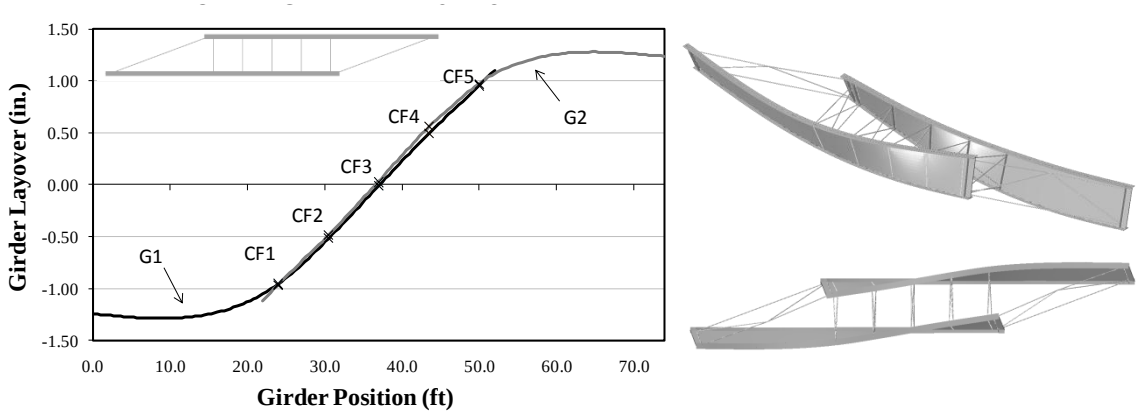


(f) Erection of the intermediate cross-frame CF5

Figure 4.13. Relative flange lateral displacements (or girder layover) obtained from the linear FEA simulation of the intermediate cross-frame erection in a skewed I-girder system (continued)

This study shows that the behavior of a skewed I-girder system may be represented as the sum of two factors. First, the end cross-frames induce a global effect in the system that results in a linear variation of the girder layovers between the ends. Since at the supports, the girders are connected through the bearing line cross-frames, the twist of both girders is the same at these positions. The second factor relates to the addition of the intermediate cross-frames. With the erection of the intermediate cross-frames, the gap in the layovers created by the global effect is closed, enforcing the compatibility of the relative lateral displacements at the bracing points. The forces needed to displace and twist the girders such that the layover compatibility is obtained, depend on the transverse or lateral-torsional stiffness of the girders. These forces are proportional to the girder transverse stiffness and to the twists and lateral displacements they have to undergo to equate their layovers. As shown in the next section, this fundamental behavior explains the source of the large cross-frame forces and the high levels of flange lateral bending stresses that can affect the behavior of some skewed girder bridges, and also, affect the constructability.

The analyses conducted in the two-girder system also highlight an important aspect related to the efficiency of the cross-frame layout. From this study, it is inferred that the most efficient approach for laying out the intermediate cross-frames is to erect them parallel to the skew rather than perpendicular to the longitudinal axis of the girders. If the intermediate cross-frames are parallel to the skew, the relative layover between the girders at the connection points is already zero before making the connection, so the forces required to frame them are essentially zero, as well. For instance, at 10 ft from the left bearing, the layover in girder G1 imposed by the global effect is -0.85 inches, as

shown in Figure 4.13(a). A line parallel to the skew drawn from this location intersects girder G2 at $x$ = 32 ft. From the figure, it is determined that the layover in G2 at that position is also -0.85 inches; therefore, the compatibility of layovers between these two points is a natural result of the global effect induced by the bearing line cross-frames. The girders do not have to be twisted any more than they already are to be connected at these locations. As a result, the forces in the components of an intermediate cross-frame erected parallel to the skew will be smaller than when they are framed perpendicular to the girder axis. The only forces acting on these components result from the elastic response due to the vertical and longitudinal deflections in the girders; these deflections, however, do not represent a substantial source of deformation for the cross-frame components. In general, the magnitudes of the cross-frame forces are dominated by the in-plane deformations that they experience when they enforce the girder lateral displacements to be equal at the connection points.

From this discussion it is apparent that a recommended strategy to mitigate the effects of the skew is to install the internal cross-frames at the same angle as the skew. In cases where the skews at each support are different, the cross-frames could be oriented such that there is a smooth transition in the angle defined by the cross-frames and the girders. In all cases, the objective should be to connect two points that have approximately the same layovers as imposed by the global effect since this practice would reduce the internal forces in the cross-frames. The AASHTO Specifications (AASHTO 2010), however, limit the use of skewed intermediate cross-frames to angles of up to 20 degrees. Beyond this limit, it is required to place the cross-frames perpendicular to the longitudinal axis of the girders. One of the reasons for this limitation

is the difficulty to weld the connection plates to the girders. At angles larger than 20 degrees, the access to weld the connection plates to the girder web becomes narrow. Extensive research has been conducted at the University of Texas at Austin (Quadrato et al. 2010) to test an innovative solution that, besides improving the overall performance of a bridge structure, eliminates the execution of this weld. In their studies, a half-pipe stiffener is welded to the girders at the cross-frame locations. Then, the rectangular connection plate is welded to the stiffener. Since the contour of the stiffener is circular, it is possible to weld the connection plate at angles larger than 20 degrees, eliminating the constructability limitation. The researchers conducted tests with the half-pipe stiffener only at the bearing lines. This detail, however, may be considered to connect the cross-frames at angles larger than 20 degrees in the interior of a bridge. In addition, a detail that can be used to overcome the difficulties of welding the connection plate at angles larger than 20 degrees is discussed in Section 4.2.2.1.

In addition to the fabrication difficulties, there are aspects related to the structural performance that need to be considered when the intermediate cross-frames are oriented at large angles. As the orientation angle increases, so does the length of the cross-frame. As a result, the load carrying efficiency of the cross-frame elements subjected to compression forces decrease. Additionally, the bracing stiffness and strength of the cross-frames tends to decrease, as discussed by Wang and Helwig (2008). Therefore, while skewing the cross-frames can improve the system performance by relaxing the internal forces, a check of their strength and stiffness requirements must be considered due to the above reasons.

The previous analyses are mainly focused on the study of the girder layovers. Another response related to the deformed geometry that is important to consider in a skewed bridge is the girder vertical displacements. Figure 4.14 shows the vertical displacement response in girders G1 and G2 for the case where there are cross-frames only at the bearing lines. By comparing the deflection curves, it is observed that the response of each individual girder is the same since both girders have the same dimensions and the only loading is their self-weight. The plot shows that as in the case of the girder layovers, due to the skew, the vertical displacements at the intermediate bracing points do not match when the cross-frames are connected perpendicular to the girders. At CF1, for example, the deflection of girder G1 is 1.57 inches, while in girder G2, it is 0.11 inches. The differential deflections at the bracing points are a result of the skew angle. In a case where the structure has normal supports, i.e., the skew angle is zero, the differential deflections vanish.

In general, the girder vertical deflections are less sensitive to the addition of the intermediate cross-frames than the girder layovers. For the case shown in Figure 4.14, the vertical displacement at mid-span is 1.61 inches. The results of the FEA for the case when all the intermediate cross-frames are in place indicate that this displacement is 1.59 inches; therefore, the change is negligible.

In the context of the cross-frames, the differential vertical deflections are not the main source of the internal forces. As illustrated for this simple structure, the major-axis bending deflections are rather insensitive to the addition of the internal cross-frames and in general, to the skew effects. The forces in the cross-frames are mainly the result of enforcing compatibility of the girder layovers. This type of behavior is typical for most

straight and skewed I-girder bridges (NCHRP/TRB 2011). However, there are situations where the skew effects have an influence not only in the lateral but also in the vertical displacements. These cases are discussed in Section 4.2.1.6. It is important to mention that the above observations apply only to structures in their noncomposite conditions. When the bridge deck is in place, the girders are highly restrained against rotation relative to one another As discussed in Berglund and Schultz (2006), the effects of the skew are accommodated through the relative vertical displacement between girders in the composite structure.

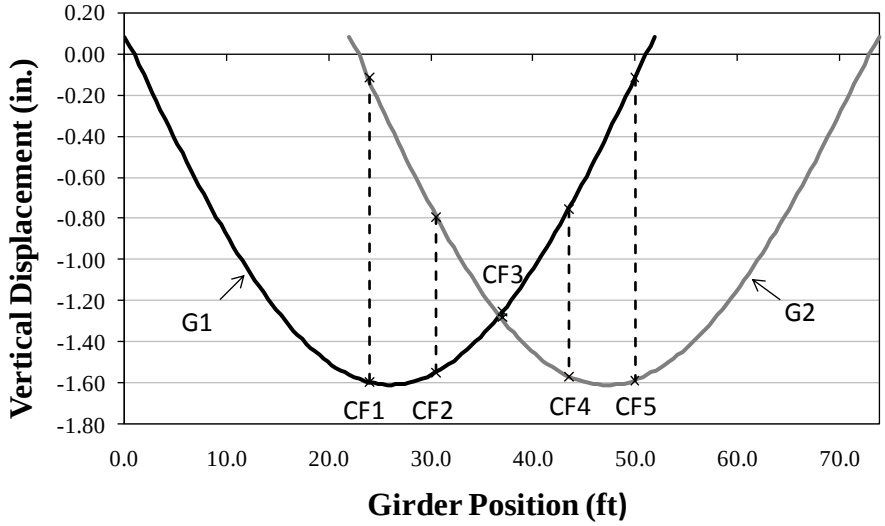


Figure 4.14. Vertical deflection response in the two-girder system when cross-frames are provided only at the bearing lines

4.2.1.2. Effects of Support Skew on the Cross-Frame Forces and the Flange Lateral Bending Stresses

From the two-girder system discussed in the previous section, it is concluded that for the girders to have compatible layovers at the brace points, they need to be twisted and displaced laterally. The forces required to achieve the layover compatibility depend on the lateral-torsional stiffness of the girders at the cross-frame positions. The

intermediate cross-frames serve as the ties that enforce these displacements to be essentially the same, and also provide the load path for the transverse forces needed to make the girders twist. These concepts are further illustrated by analyzing the layovers and differential deflections of the two-girder system at the CF1 location. Figure 4.15 shows the deflected shape of the girders at this location for the cases when only the bearing line cross-frames are in place and after all the intermediate cross-frames have been erected. For the first case, the girder layovers in G1 and G2 are -0.11 inches and -1.25 inches, respectively. When CF1 is connected, the girders twist, and the resulting layover is -0.96 inches in both of them. Notice that for both cases, the differential deflections remain practically the same, i.e., 1.46 inches.

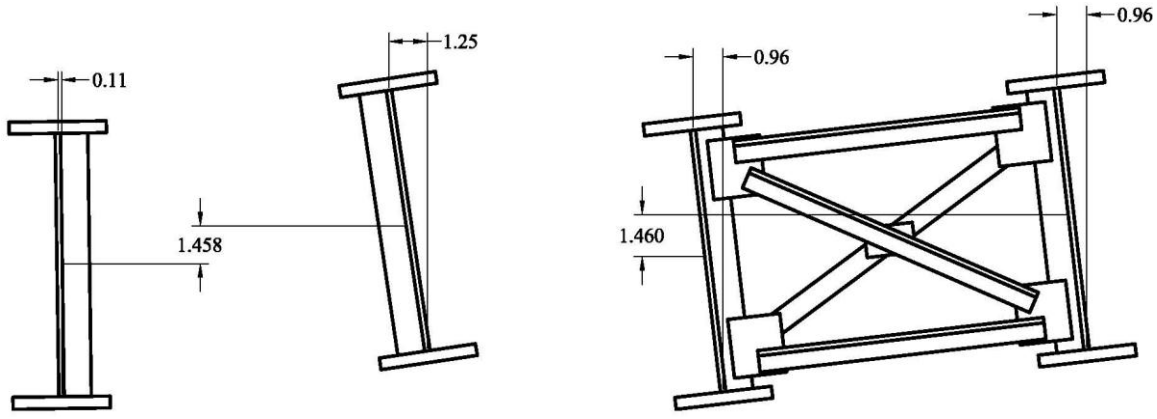


(a) No intermediate cross-frames (b) All intermediate cross-frames in place

Figure 4.15. Differential deflections and girder layovers at the first intermediate cross-frame position, CF1

To study the forces acting on the girders, a free body diagram of the cross-frame and the girders is shown in Figure 4.16. As shown in the figure, the cross-frame imposes the internal forces needed to enforce compatibility of the layovers in the girders. These

forces, named A, B, C, and D, are transferred from girder to girder through the cross-frame chords and diagonals. Except for some extreme cases as the discussed in Section 5.4.2, the vertical components of these forces ($A_y$, $B_y$, $C_y$, and $D_y$) have a negligible participation on the girder responses since their effects are much smaller than the effects of the gravity loads that are applied to the system. In skewed bridges these vertical force components are equivalent to the V-loads induced by the curvature effects.

The transverse load path, associated with the horizontal components of these loads ($A_x$, $B_x$, $C_x$, and $D_x$), is a secondary effect of the gravity loads. The components of the structure that participate in this load path need to be designed to resist these secondary forces. In the case of the I-girders, the horizontal components of the forces induce lateral bending stresses, $f_\ell$. When they are significant, these stresses must be considered in combination with the major-axis bending stresses in proportioning the I-girders, according to the requirements of AASHTO (2010). In the case of the cross-frames, the chords, the diagonals, and the connections to the girders must be dimensioned such that they can resist both the vertical and the horizontal components of the forces. In many cases, these requirements control over the stability bracing requirements, which should also be considered to dimension the cross-frame components.

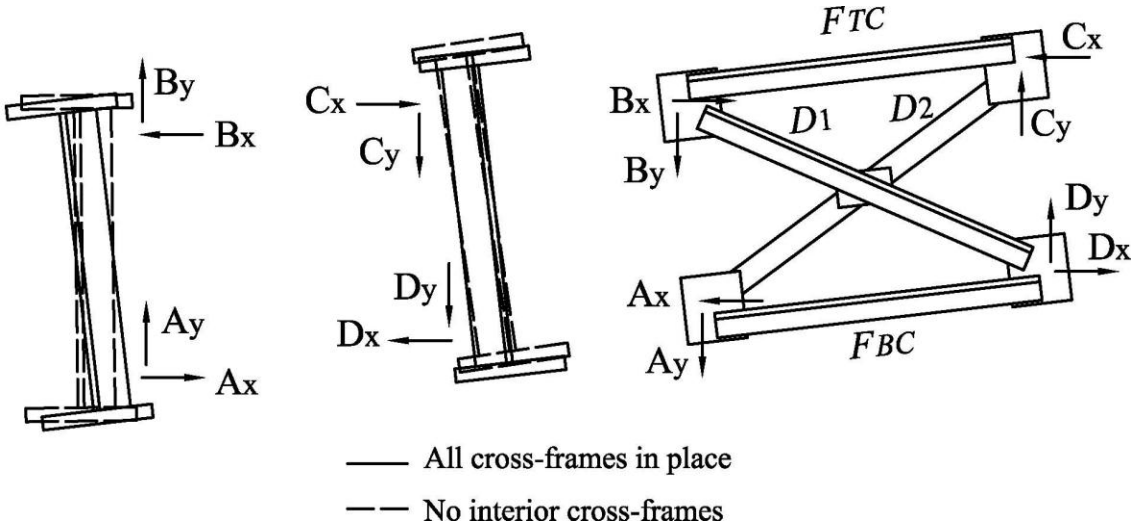


Figure 4.16. Schematic representation of the internal forces in the girders and the cross-frame that result from the skew effects

In some cases, the forces required to twist the girders and connect the intermediate cross-frames can be very large, depending on the transverse stiffness of the girders at the connections. This is an important aspect to consider during the construction stages of the structure. “Come-alongs” and lever hoists are devices used to connect the internal cross-frames and handle the fit-up problems that may occur in the field. Another technique used by steel erectors to connect the cross-frames at the points where fit-up is a concern is to install the chords and diagonals individually. Figure 4.17 illustrates the use of some of these tools during the erection of a skewed bridge, where a come-along at the top flange level and provisional cable braces are used to control the layover of the girders before the cross-frame is placed.

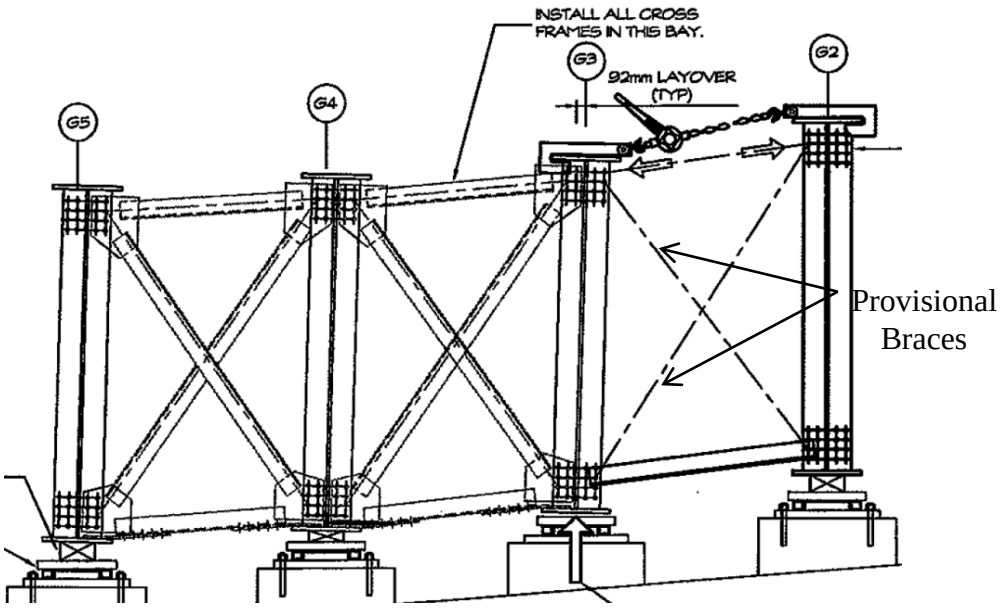


Figure 4.17. Schematic representation of the techniques used to control the position of the girders and connect the cross-frames in skewed bridges (Courtesy of Mr. Robert Cisneros, High Steel Structures, Inc.)

4.2.1.3. Transverse Force Path in a Skewed Bridge

The previous discussion highlights the importance of considering the cross-frame forces and their effects in the structure's behavior. In the following analysis, a quantitative assessment of these forces and their expected magnitude at different locations along the length of the girders is presented.

To study the transverse load path induced by the gravity loads, the two I-girder system introduced in the previous section is analyzed here by considering a modification. The diagonals and the bottom chord of the internal cross-frames are removed from the system, leaving the top struts as the only elements that connect the girders at the bracing locations. The objective of this practice is to simplify the structure at a basic level and observe the manner in which the transverse forces flow within the system. This study is only intended to illustrate the aspects that control the magnitude of the forces at the

different bracing locations and does not represent a recommendation for the analysis and the design of real bridges.

The first step of the study involves the determination of the girder lateral stiffness at the location of the intermediate cross-frames. For this purpose, the structure is analyzed under the influence of the uniformly distributed load, and with the girders connected with cross-frames only at the supports. Then, a unit load is applied at the node where the first internal strut is framed, as depicted in Figure 4.18. The deflections that result from the application of the point load represent the coefficients of the flexibility matrix that is used later to compute the transverse forces. For example, the coefficient, $\delta_{21}$, represents the displacement in Node 2 due to a unit force applied at Node 1. Following the same procedure, unit loads are applied at the other nodes to form a ten-by-ten flexibility matrix, *D*. The stiffness matrix of this simplified system, *K*, is the inverse of the flexibility matrix, such that $K = D^{-1}$. The stiffness matrix obtained from this analysis is an approximate representation of the transverse stiffness of the system at the connection points.

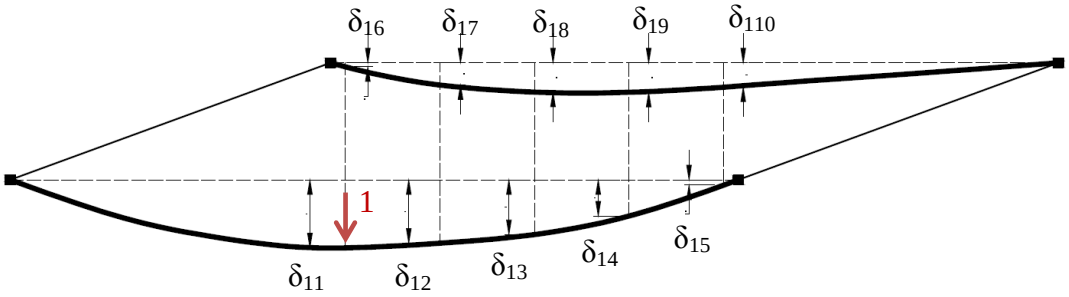


Figure 4.18. Coefficients of lateral deflection due to a unit force applied at Node 1 measured at the nodes that connect the struts to the girders

Next, an analysis is conducted introducing the five top struts in the system. The lateral displacements at the connection points resulting from the application of the

structure's self-weight are captured in this analysis. Figure 4.19 shows the plots of the relative lateral displacement between the top and bottom flanges (or layover) versus the position of the girders with respect to an absolute reference that is located at the left end of girder G1. Figure 4.19(a) corresponds to the case where the girders are connected only at the supports, and Figure 4.19(b) shows the girder layovers once the struts are erected. Next to the plots, the three dimensional and plan views of the deflected shape of the system are also included. Notice that the plots of Figure 4.13(f) and Figure 4.19(b) are essentially the same. For this particular structure, the elimination of the diagonals and the bottom chords did not have a significant influence in the girder layovers. The reason is that in this system, the bottom flanges do not deflect laterally, as shown in the plan view of the deflected shape in both figures. Therefore, for this system, the girder layover is dominated solely by the displacement of the top flanges.

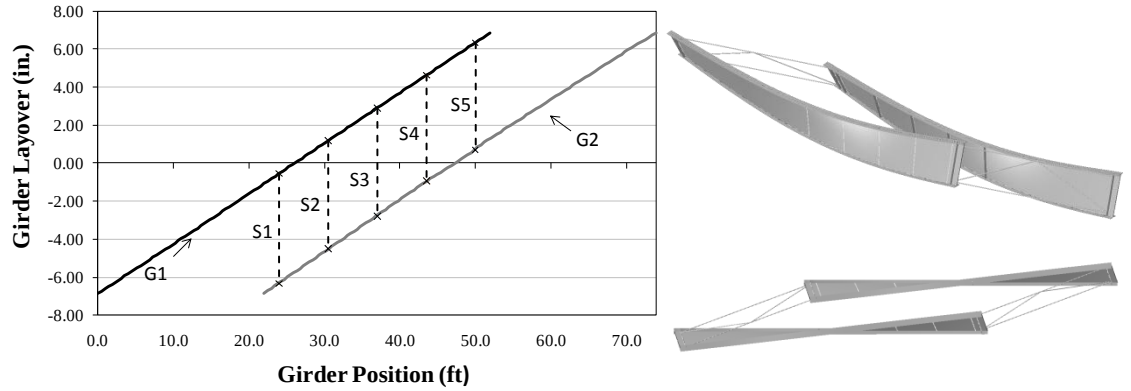


(a) Two-girder system without intermediate struts

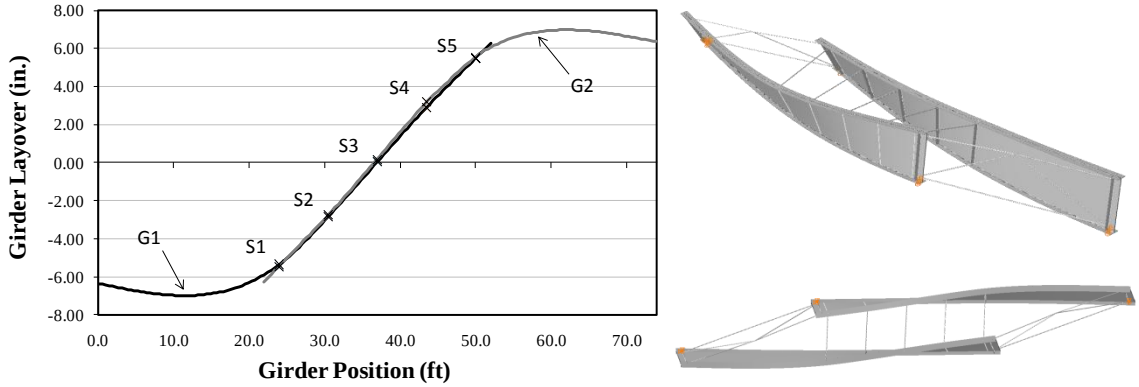


(b) Two-girder system with intermediate struts

Figure 4.19. Relative flange lateral displacements (or girder layover) obtained from the linear FEA for the system with the intermediate struts

The lateral displacements required to enforce the compatibility of the layovers at the bracing points are equal to the difference between the displacements in the girders when they are connected with the struts and the displacements imposed by the global effect. For example, from Figure 4.19(a), the layover at the location of the second strut, S2 in G1, is 1.16 inches From Figure 4.19(b), the resulting layover at this position is -2.84 inches The differential lateral displacement is 1.16 - (-2.84) = 4.00 inches. Following the same procedure, the displacements obtained at the other locations are calculated and stored in the vector $\Delta$, such that

$$\Delta = \begin{Bmatrix} 4.82 \\ 4.00 \\ 2.81 \\ 1.65 \\ 0.74 \\ -0.74 \\ -1.64 \\ -2.80 \\ -3.99 \\ -4.80 \end{Bmatrix} \text{in.}$$

The information obtained from the two analyses described previously is used to obtain approximate values of the forces required to attain the compatibility of lateral displacements imposed by the struts. By applying the direct stiffness method, the internal forces, *F*, are equal to $F=K\cdot\Delta$. In Figure 4.20, the strut forces obtained from this approximate analysis are compared to the forces obtained from the linear 3D FEA. The forces corresponding to the approximate analysis are shown in parentheses. Ideally, the magnitude of the forces obtained from both analyses should be the same. However, the ten degree-of-freedom system is a coarse model that represents approximately the behavior of the entire structure.

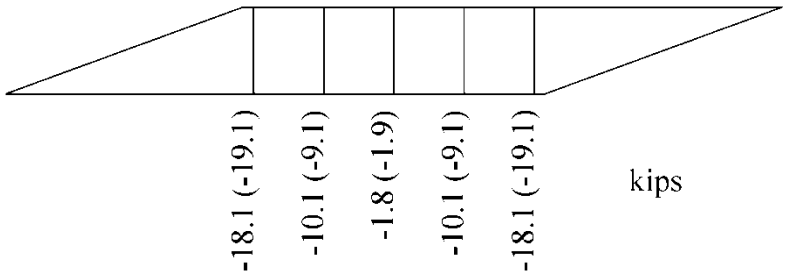


Figure 4.20. Strut forces in the two-girder system

This study shows that the struts provide the path to transfer the forces between girders, enforcing the layover compatibility. In addition, the analyses show that the

largest forces are concentrated near the supports, where the transverse stiffness of the girders is also the largest. Kupricka and Poellot (1993) describe this behavior as "nuisance stiffness" because of the lateral-torsional stiffness of the girders that cause these undesired forces in the cross-frames and subject the girders to lateral bending.

The observations from this study, conducted with top struts as bracing elements, can be extended to more realistic cases with cross-frames composed of chords and diagonals. In general, the forces in the cross-frames are proportional to the transverse or lateral and torsional stiffness of the girders. Therefore, in skewed bridges, if the first intermediate cross-frame is connected too close to a bearing, high internal forces should be expected. Engineers are aware of this problem, and they layout the intermediate cross-frames considering this aspect. One commonly applied rule of thumb is to place the first intermediate cross-frame at least at 1.5 times the girder depth. It is expected that at this location the girders are flexible enough to accommodate the cross-frame and make the connection. Ozgur (2011) provides improved recommendations on how to layout the cross-frames near the skew and reduce the nuisance stiffness effect, based on a simplified analysis of girder lateral stiffness. However, it is not possible to develop rules to determine precisely how far from the support the first intermediate cross-frame has to be placed to overcome this limitation. This depends on the elastic interaction of all the structural components of the system, so it varies depending on the characteristics of the bridge. An approximate analysis, such as the one discussed above, can be done to determine the expected cross-frame forces near the abutments and in the rest of the system. The internal forces obtained with the representation of the lateral rigidity of the structure with a ten degree-of-freedom system are close to the values predicted by the

FEA. However, developing approximate models like the one discussed above to determine the cross-frame positions where the transverse forces are admissible is impractical for design purposes.

There is an additional aspect to consider relating to the position of the first intermediate cross-frame. A factor to ponder regarding which should be the minimum distance between the support and the cross-frame is the lateral-torsional buckling capacity of the girders for the segment defined between these two points. During construction, the actions on the girders are generally defined by their self-weight and distributed loads that act at the top flange level. In simple span bridges, the bending moments that result from these loadings around the support area are smaller than the moments expected around the mid-length of the girders. Therefore, the strength requirements at this segment are smaller than in the rest of the bridge. The first estimate for the location of the cross-frame could be obtained by checking the lateral-torsional resistance of the girder segment versus the required moment. Since this moment is smaller than in other segments of the girders, it may be possible to increase the unbraced length, while still having the strength required to prevent a stability failure or large amplifications of the structure's deformations due to second order effects. Moving the cross-frame a few feet from the abutment towards the interior of the bridge can have a minor impact on the girder strength and reduce the cross-frame internal forces to acceptable magnitudes. At the intermediate supports, bridges with multiple spans have larger strength requirements than bridges with one span. At the pier locations, the bottom flanges are in compression, and the moments can be significantly larger than the

moments near the abutments. In these cases, the bracing requirements are more severe, and the position of the cross-frame may be controlled by the strength requirements.

In all the cases, the best practice to evaluate the forces in the cross-frames, determine the locations where they are most effective and in general, conduct an integral assessment of the bridge response is to analyze the structure considering the skew effects. This is accomplished by constructing a 2D or 3D model of the system and capturing the interaction of the structural components. As shown in Chapter 5, a 2D model with proper representations of the torsional rigidity of the I-girders and the cross-frame contributions can capture the expected forces accurately.

#### 4.2.1.4. Skew Effects in Multi-Girder Bridges

The discussions in the foregoing section illustrate the concepts of transverse stiffness and layover compatibility by focusing on the study of a two-girder system. These concepts can be extended to systems with multiple girders. For this purpose, the bridge NISSS14, introduced in Section 3.1.3, is analyzed in the studies presented next. This bridge is selected because the skew effects in this structure are severe. Figure 4.21 shows the plan view of the bridge assuming that, initially, the intermediate cross-frames that connect girder G5 to the rest of the system, CF1 to CF12, have not been erected. This hypothetical erection scheme is used to study the transverse stiffness concept, the associated cross-frame forces, and the flange lateral bending stresses in a multi-girder bridge. This scheme is chosen to illustrate the behavior of a multi-girder system; it does not necessarily represent a recommended procedure for the erection of this structure.

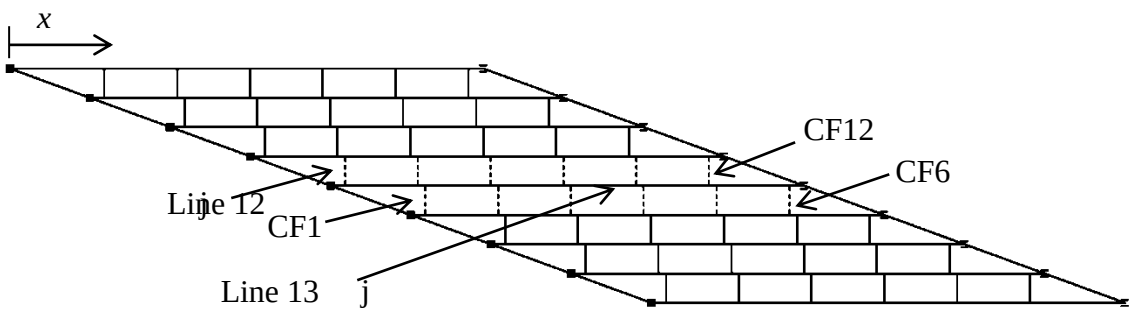


Figure 4.21. NISSS14 Bridge with girder G5 connected only at the abutments

The girder layovers when the structure is subject to the total dead load obtained from a linear elastic FEA model are shown in Figure 4.22. The plot shows that the system is split into two groups defined between girders G1 to G4 and girders G6 to G9. The intermediate cross-frames in each of these groups enforce the compatibility of lateral displacements. The layovers in girder G5 are different from those in the rest of the system since this girder is connected only at the bearing lines. To erect cross-frames CF1 to CF12, it is necessary to displace both groups of girders and close the gap at each bracing location. As depicted in the plot, these gaps vary from 1.35 inches at CF1 to 2.57 inches at CF5.

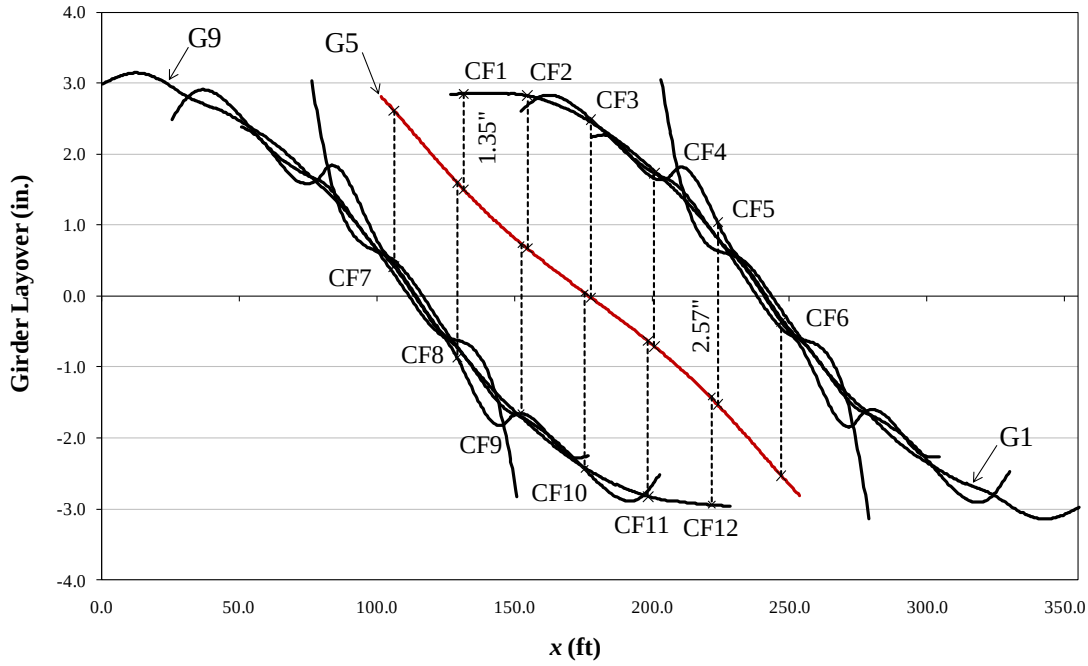


Figure 4.22. Girder layovers in bridge NISSS14 at the TDL condition, assuming that girder G5 is connected only at the ends

Figure 4.23 shows the girder layovers once the intermediate cross-frames are erected. As shown in the plot, when cross-frames CF1 to CF12 are placed, they seam the girders together, leading to a small axial deformation of the cross-frame elements. These deformations result from connecting girder G5 to the two girder groups. From the FEA of this bridge, it is determined that the forces in the cross-frames elements required to connect G5 to the rest of the system ranges from 153.5 kips in compression to 158.1 kips in tension. These large forces are due to the resistance of the bridge units, G1-G4 and G6-G9, to the lateral displacements.

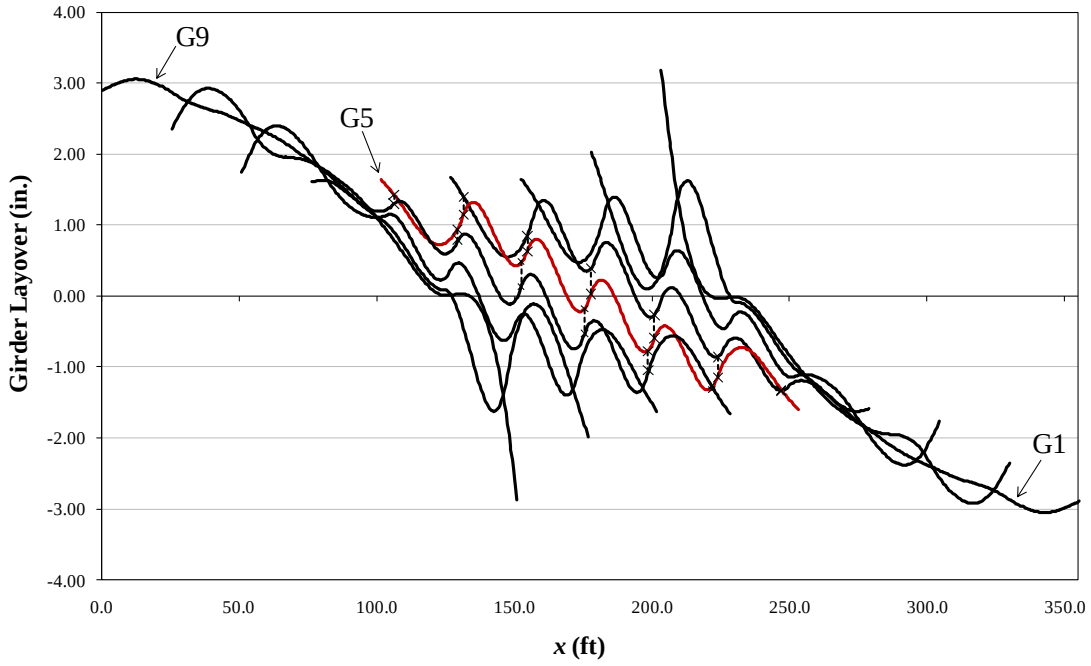


Figure 4.23. Girder layovers in bridge NISSS14 at the TDL condition, after the placement of the intermediate cross-frames at girder G5

The above forces cause high levels of flange lateral bending stress, as shown in Figure 4.24, for the top flange of girder G5. In this plot, the major-axis and flange lateral bending stresses, $f_b$ and $f_\ell$, are plotted versus the normalized girder length. As depicted in the figure, the stress levels associated with lateral bending are significantly larger than the major-axis bending stress levels. For this girder, the $f_\ell$ stresses are largest near mid-span. In the context of the internal forces, this means that larger forces are necessary to connect the cross-frames near mid-span than to make the connections near the abutments.

It is important to mention that the $f_\ell$ levels in girder G5 can be reduced significantly if the cross-frames are slightly shifted, so that the staggered pattern becomes a contiguous line. With this practice, the positive and negative peaks in the response

cancel each other out, so the stress resultant is small. For example, near mid-span, at the locations of cross-frames CF3 and CF10, the stresses are -58.2 ksi and 57.8 ksi, respectively. If the cross-frames are shifted so they are collinear, the forces cancel each other, and the resultant stress is approximately equal to -0.4 ksi. However, this practice mitigates only one of the collateral effects of the skew. The forces in the cross-frames would still be large if the contiguous cross-frame pattern is used, so the cross-frame components and connections would need to be designed to resist such forces. Similarly, the possible fit-up issues that may occur during the steel erection would still be present.

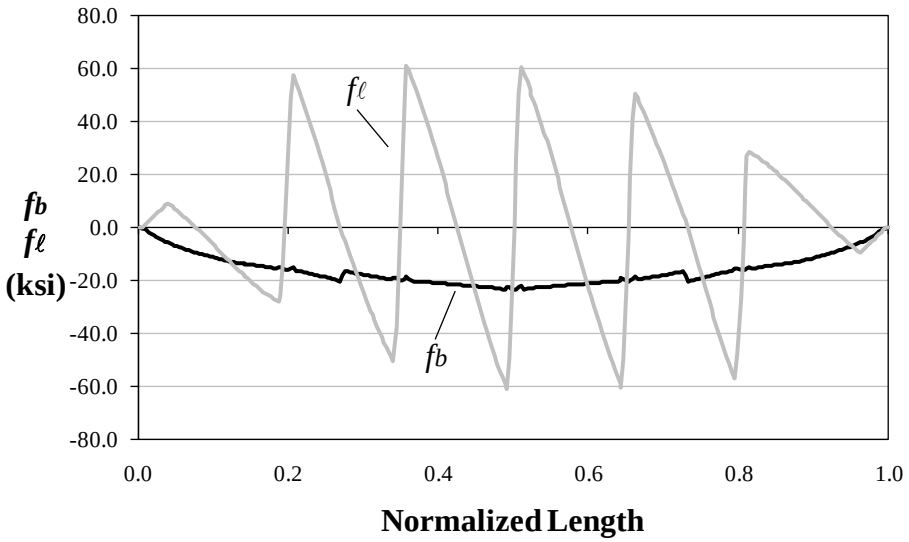


Figure 4.24. Stress levels at the top flange of girder G5 after the erection of the intermediate cross-frames

In the two-girder system discussed previously, the largest cross-frame forces are concentrated near the abutments, where the transverse stiffness of the girders is also the largest. Near mid-span, the forces are smaller since the girders are more flexible at this region. However, in multi-girder systems it is not as easy to identify the flexible and stiff zones, as in the simpler two-girder system. The results of the 24 straight and skewed

bridges studied in the NCHRP 12-79 Project indicate that in heavily skewed bridges, the $f_\ell$ stresses in the fascia girders are concentrated around the supports; while in the interior girders, the largest $f_\ell$ stress values occur near mid-span. To illustrate this concept, Figure 4.25 shows the stress responses in the top flange of the nine girders of the case study. As shown in this figure for girders G1, G2, G8, and G9, the largest peaks in the lateral bending stress response occurs near the supports where the girders form an obtuse angle with the bearing line cross-frames. Intuitively, this is expected since the outer girders are stiffer transversely near the supports. For the rest of girders the $f_\ell$ stress responses grow towards the interior of the structure, as shown for girders G3 to G7. As previously illustrated for girder G5, when the girders are connected with the intermediate cross-frames, they form a group that is stiffer around the mid-span zone. Therefore, for the cross-frames it is more difficult to deform the structure and impose the compatibility of girder layovers, which results in larger cross-frame forces and higher $f_\ell$ stress levels.

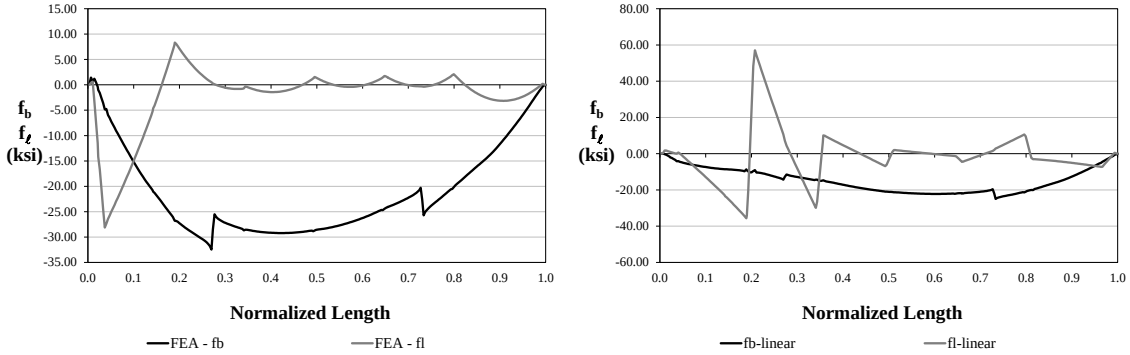


Girder G1




Girder G2

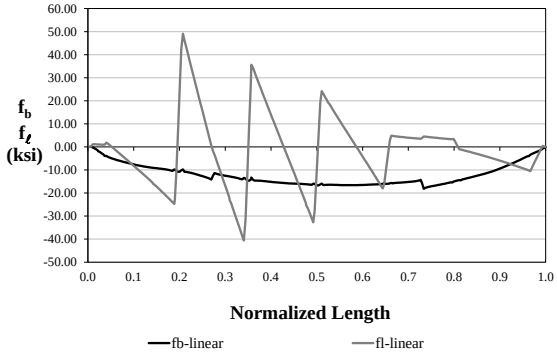


Girder G3

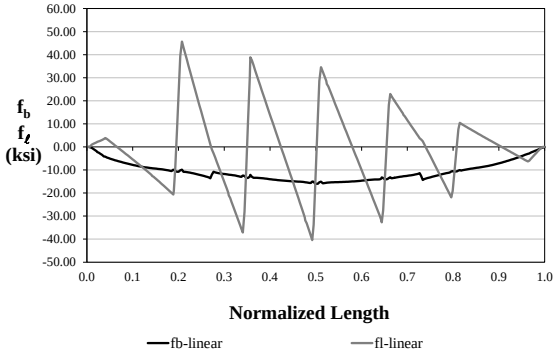


Girder G4

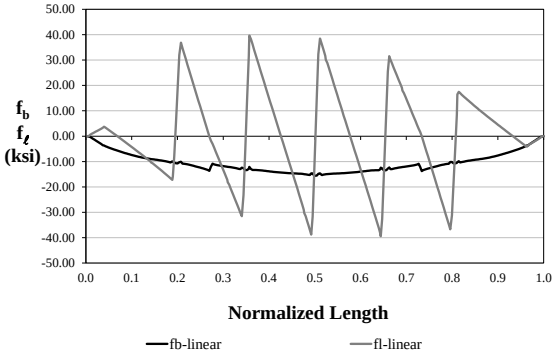


Girder G5

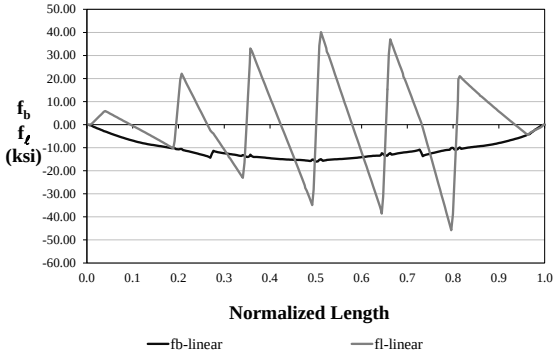


Girder G6

Figure 4.25. Stress responses in the girders of bridge NISSS14 at the TDL level

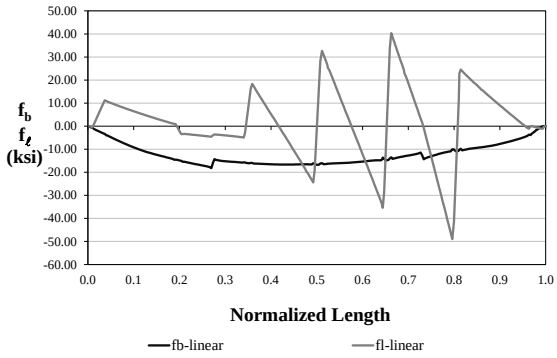


Girder G7

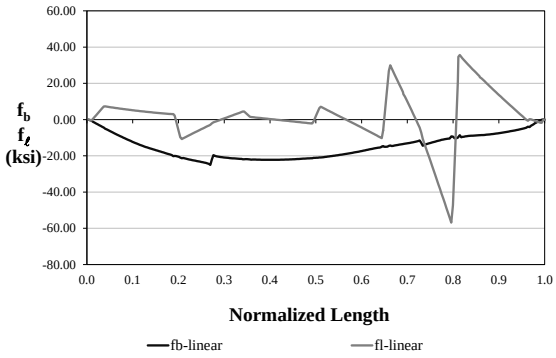


Girder G8

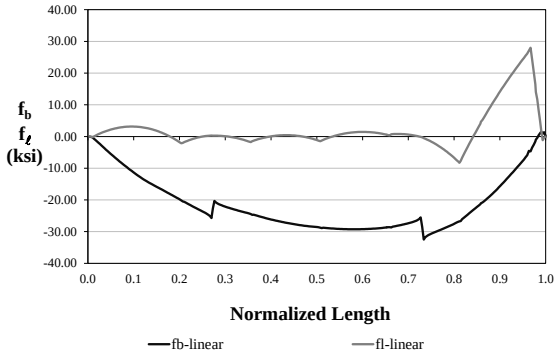


Girder G9

Figure 4.25. Stress responses in the girders of Bridge NISSS14 at the TDL level (continued)

The above analysis also can be conducted by studying the lateral deformations and the cross-frame forces when the structure is subject to the total deal load (TDL). Figure 4.26 depicts the plan view of the deformed shape and a plot of the cross-frame forces in gray scale. The deformed shape shows that the top flanges in girders G1, G2, G8, and G9 undergo large lateral displacements near the supports that form an obtuse angle with the end cross-frames. In the interior girders, the largest deformations occur in the mid-span area. The contour plot shows that the cross-frame forces are also the largest at these regions. These results are consistent with the stress plots shown previously and demonstrate how the different effects of the skew interact with each other.

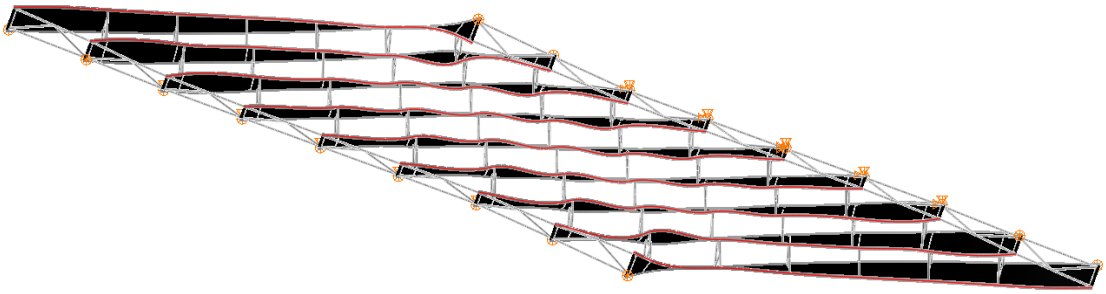

(a) Plan view of the deformed shape

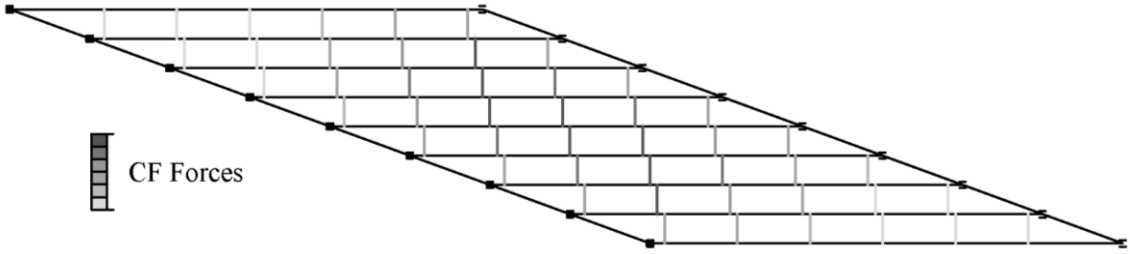


(b) Cross-frame forces

Figure 4.26. Effects of the skew on the behavior of bridge NISSS14

The bridge analyzed in this section illustrates the influence of the skew on the behavior of a simple span multi-girder bridge. In the next section, a straight and skewed continuous span bridge is studied to observe the interaction between the skew and the continuity over the supports.

4.2.1.5. Skew Effects in Continuous-Span Bridges

The influence of the skew in continuous span bridges is studied in this section. The structure considered for the analyses is bridge NICSS16; this structure is introduced in Section 3.1.5. The plan view of the bridge is shown in Figure 4.27. The second and third spans of the structure have the same dimensions as the simple span bridge NISSS14. Hence, these two structures are compared here to observe the effects of the girder continuity over the supports.

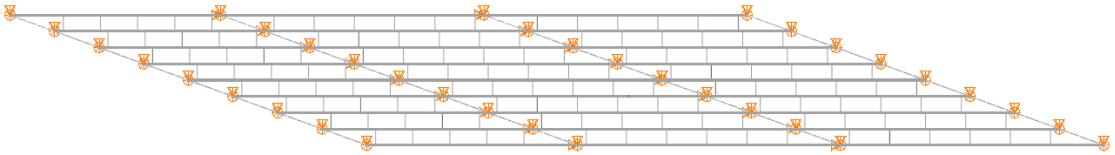

Figure 4.27. Plan view of NICSS16

Figure 4.28 shows the stress plots for the top flange of girders G5 and G9 at the TDL level. As depicted in these plots, the behavior of the structure is similar to that of the simple span NISSS14 Bridge. In the interior girder G5, the $f_\ell$ stresses are larger in the interior regions of the spans, where the transverse stiffness of the bridge is the largest. In girder G9, the largest flange lateral bending stress occurs near the Span 3 abutment. As observed in the two-girder system and the simple span presented previously, the stiffer points in the fascia girders are near the supports. Also, in Span 3, due to the global effects imposed by the end cross-frames, the lateral displacement and twist required to obtain the layover compatibility in the intermediate cross-frame that is closest to the right end abutment are the largest. At this location, girder G9 forms an obtuse angle with the end cross-frame. Hence, the large deformations imposed at this stiff point result in the 11.2 ksi peak in the $f_\ell$ stress response.

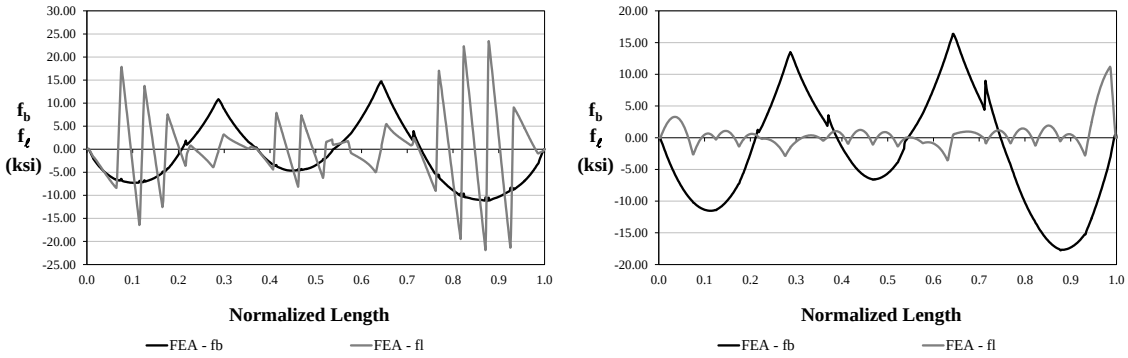


Girder G5 Girder G9

Figure 4.28. Stress responses in the girders of bridge NISSS14 at the TDL level

The deformed shape of the bridge and the cross-frame force contours shown in Figure 4.29 also indicate that the behavior of the continuous span bridge is similar to the response of the simple span structure discussed previously. The deformed shape shows that the flanges in the interior girders undergo large lateral deformations near the middle of each of the spans; while in the exterior girders, the most significant deformations occur near the simple supports. The cross-frame force contour shows the same trend, with the largest forces concentrated in the middle of the spans and near the corners with obtuse angles.

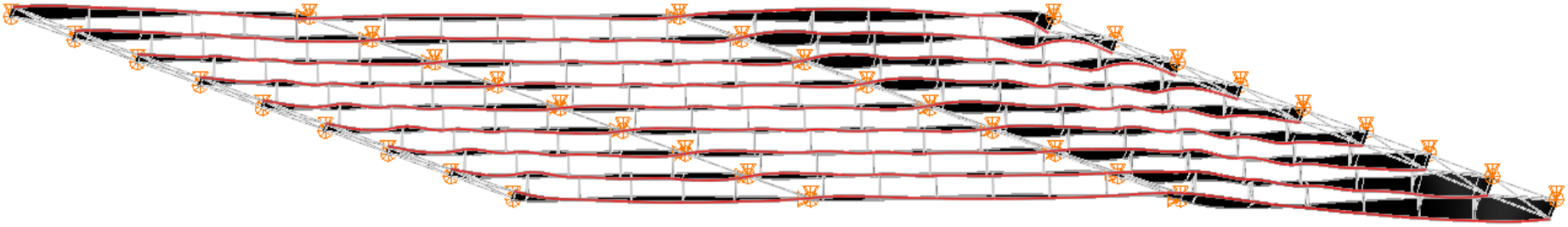

(a) Plan view of the deformed shape

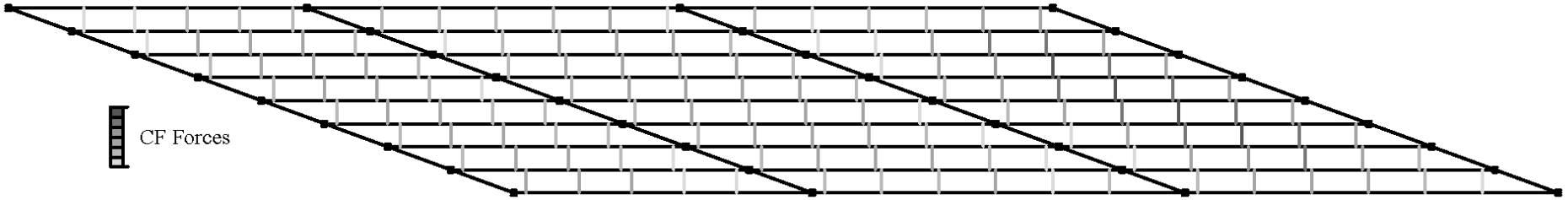


(b) Cross-frame forces

Figure 4.29. Effects of the skew on the behavior of bridge NISSS16

4.2.1.6. General Assessment of Skew Effects

The structures investigated in Sections 4.2.1.4 and 4.2.1.5 serve to illustrate the effects of the skew on the behavior of simple and continuous span bridges. These bridges are ideal cases for this purpose because their skew effects have a large participation in the structural behavior. However, these structures are specific scenarios of the wide range of the geometries and bracing system configurations used in the design of highway bridges. Fortunately, for the design of a particular structure a complete assessment of the skew effects, as conducted in the previous cases, is not always necessary. In many bridges, the skew does not affect the structural performance as significantly as in the case studies. In fact, in many of the 24 straight and skewed structures analyzed in the NCHRP 12-79 Project (NCHRP/TRB 2011), the effects of the skew are minor. From a study of these structures it is observed that a possible index to differentiate the bridges that experience large skew effects from the ones that are less sensitive to the skew is

$$I_S = \frac{w_g \times tan\theta}{L_s} \qquad \text{(Eq. 4.7)}$$

where $I_S$ is the skew index, $w_g$ is the width of the bridge measured between fascia girders, $\theta$ is the skew angle, and $L_s$ is the span length. Figure 4.30 illustrates the variables required to calculate the skew index. In bridges with unequal skew of at the bearing lines, $\theta$ is taken as the angle of the support with the largest skew. In continuous span bridges, one index is determined for each span.

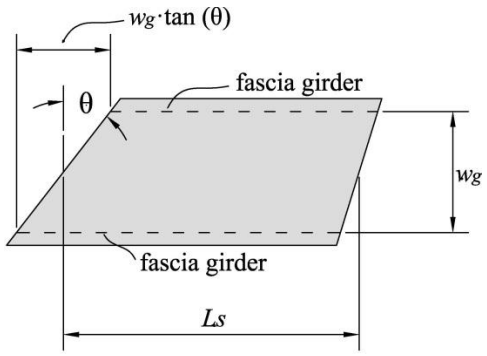


Figure 4.30. Parameters for the calculation of the skew index

Table 4.3 shows the results at the TDL level for the 24 straight and skewed bridges studied in the NCHRP 12-79 Project. This table illustrates how this index can be used to identify bridges that may be susceptible to large skew effects due to their geometry. The bridges are ordered according their skew index, with the bridge having the largest index listed first. The third to sixth columns of the table include the values of several responses that are influenced by the skew. The third column shows the maximum $f_\ell$ stress in the bridge, which is obtained by looking at the responses in all the girders of the bridge and selecting the maximum absolute value. The next column shows the ratio between the $f_\ell$ and $f_b$ stresses. In this case, the flange major-axis bending stress, $f_b$, is the maximum absolute value in the girder where the $f_\ell$ stress is selected. This normalizes the $f_\ell$ response since the TDL considered in the analyses of the bridges varies depending on the structure. The fifth and sixth columns show the maximum tension and compression forces in the cross-frame components, respectively. These forces are obtained by observing the distribution of the cross-frame forces in the bridge and selecting the ones with the largest magnitudes.

Table 4.3 shows that in general, as the skew index increases, so do the magnitudes of the responses associated with the skew effects. Also, the results show that, except for NISSS56 and NICSS25, bridges with $I_S \leq 0.30$ are much less sensitive to skew effects. For the structures with $I_S \leq 0.30$, the $f_\ell$ / $f_b$ ratio, which is one of the most suitable parameters to investigate the skew effects, is considerably smaller than in bridges with skew indices larger than 0.30. Similarly, the cross-frame forces in the structures included in this group are relatively small.

In Bridges NISSS56 and NICSS25 the cross-frame forces are larger than in the rest of bridges with $I_S \leq 0.30$ due to nuisance stiffness effects (see Section 4.1.2.3). In these two structures, some of the intermediate cross-frames that are close to the skewed supports can be removed to relax the transverse stiffness of the bridge while still providing the required stability bracing to the girders. As illustrated in Figure 4.31, in Bridge NICSS25 the cross-frame with the largest forces is located in the first contiguous line in Span 2 (Line 13). In this cross-frame, the forces in the top and bottom chords are 177.7 kips in tension and 119.0 kips in compression, respectively. These are the forces reported in Table 4.3. A separate analysis conducted in this structure, removing the cross-frames in Lines 12 and 13 that connect girders G2 to G3 and G7 to G8 show that the maximum cross-frame forces are reduced to 86.1 kips in compression and 129.2 kips in tension. This example shows the influence of the bracing system in the structural response. Even though bridges with skew indices smaller or equal than 0.30 are less sensitive to skew effects, the cross-frame forces can be considerably large, depending on the cross-frame layout used to connect the girders.

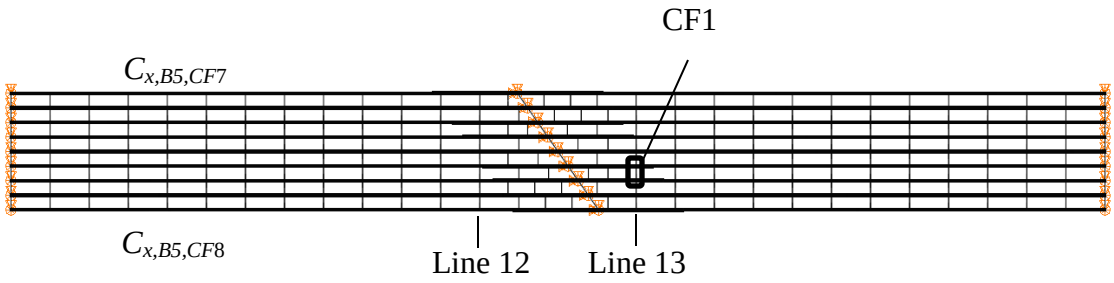


Figure 4.31. Plan view of Bridge NICSS25

The results in Table 4.3 show that in bridges with $I_S > 0.30$, at least one of the responses associated with skew effects is significant. In NICSS16, NISSS14, NISSS54, NISSS16, EICSS12, NISSS36, and EISSS6, both the $f_\ell$ / $f_b$ ratio and the cross-frame forces are large. In NISSS13, the stress ratio is large (i.e., $f_\ell / f_b = 0.35$), but the cross-frame forces are smaller than in bridges with similar skew indices. The reason for having small cross-frame forces is the staggered cross-frame pattern. In this structure, all the cross-frames are staggered and placed at 11 ft from each other. Therefore, the transverse stiffness of the bridge at the connection points is considerably smaller than when the cross-frame lines are contiguous or staggered by a small distance, as in the case of NISSS14. For NISSS13, however, the reduction of the internal forces obtained by staggering the cross-frames is overcome by the fact that the $f_\ell$ / $f_b$ ratio is large. Characteristics similar to NISSS13 are also observed in XICSS5, NISSS4 and EICSS1.

The influence of the cross-frame configuration is also noticeable in the responses of EICSS2 and EISSS5. In EICSS2 all the cross-frame lines are contiguous; therefore, even though the flange lateral bending stresses are small, the cross-frame forces are large. In the case of EISSS5, the intermediate cross-frames are V-type cross-frames without top

chords. As shown in the results of EISSS5, removing the top chord in V-type cross-frames is a practice that may relax the transverse stiffness of the bridge and reduce the effects of skew. In this structure, even though the skew index is relatively large, both the stress ratio and the cross-frame forces are small. The results obtained for EISSS5 suggest that this is a technique that can be used to mitigate the skew effects; however, as discussed in Sections 4.3.3 and 6.4.2, the in-plane stiffness of the V-type cross-frame is severely reduced by removing the top chord. This practice can compromise the ability of the cross-frames to provide stability bracing. In addition, due to the poor bracing properties of this cross-frame configuration, structures designed with V-type cross-frames without top chords are prone to experience significant second order amplifications of the structural responses. For these reasons, the use of this cross-frame configuration should be avoided.

A second limit where the skew effects not only cause large values in the responses associated with the transverse stiffness of a bridge but also can influence the major-axis bending responses is 0.65. In bridges where $I_S$ is above this limit, the vertical components of the nodal forces, $A_y$, $B_y$, $C_y$, and $D_y$, (see Section 4.2.1.2) are large enough to be considered in combination with the gravity loads for the prediction of the major-axis bending stresses, $f_b$, and the vertical displacements. The construction sequence simulation of Bridge NISSS14 described below and the studies presented in Section 5.4 for Bridge NICSS16, which has a skew index equal to 1.36, show that these nodal forces have a significant contribution to the major-axis bending responses.

Table 4.3 shows that there is no definite limit in the index that can be used to categorize the bridges. The reason is that even though the index can serve as a parameter

to determine when a bridge may be susceptible to large skew effects, it does not consider the fundamental influence that the bracing system has on the structural performance. As discussed previously, the orientation of the cross-frames, the use of a staggered or continuous pattern, the distance from the support to the first intermediate cross-frame, the use of flange-level bracing systems, among others, are parameters that influence the responses in a skewed bridge. Also, the type of cross-frame configurations, such as the X, V, and inverted V with their variations (cross-frames without top chords, lean-on bracing) influence the response of the system. All these parameters, of course, cannot be included in a single index. Instead, the index highlights structures that due to their geometry are more susceptible to the collateral effects of skew, for the reasons discussed in the previous sections.

Table 4.3. Summary of results for selected responses in the straight and skewed I-girder bridges studied in Project NCHRP 12-79, TDL level

| Bridge | Skew Index, $I_S$ | Max. $f_\ell$ Stress (ksi) | Ratio $f_\ell/f_b$ | Maximum Tension CF Force (kips) | Maximum Comp. CF Force (kips) |
|---|---|---|---|---|---|
| NICSS16 | 1.69, 1.36, 1.36 | 25.3 | 1.62 | 61.5 | 74.0 |
| NISSS14 | 1.36 | 60.1 | 2.73 | 158.1 | 153.4 |
| NISSS54 | 0.67 | 64.9 | 2.53 | 466.8 | 324.0 |
| NISSS13 | 0.58 | 9.3 | 0.35 | 14.9 | 15.2 |
| NISSS16 | 0.58 | 8.2 | 0.33 | 73.3 | 70.7 |
| EICSS2 | 0.49, 0.57, 0.23 | 4.4 | 0.12 | 102.0 | 116.5 |
| EISSS5 | 0.54 | 1.8 | 0.08 | 8.7 | 8.2 |
| EICSS12 | 0.46, 0.51 | 5.7 | 0.37 | 52.3 | 49.8 |
| XICSS5 | 0.44, 0.36, 0.44 | 3.7 | 0.25 | 44.3 | 40.4 |
| NISSS4 | 0.43 | 9.1 | 0.56 | 34.7 | 20.4 |
| NISSS36 | 0.39 | 7.3 | 0.34 | 114.9 | 110.2 |
| EICSS1 | 0.38, 0.38 | 6.7 | 0.23 | 38.9 | 41.5 |
| EISSS6 | 0.36 | 21.2 | 0.42 | 112.2 | 105.6 |
| NISSS53 | 0.29 | 3.1 | 0.13 | 15.6 | 15.8 |
| NISSS56 | 0.29 | 6.6 | 0.18 | 113.3 | 105.7 |
| EISSS3 | 0.24 | 4.2 | 0.13 | 8.0 | 6.5 |
| NISSS6 | 0.19 | 3.1 | 0.16 | 23.0 | 23.8 |
| NISSS11 | 0.18 | 4.0 | 0.09 | 9.5 | 9.9 |
| NISSS37 | 0.18 | 3.3 | 0.17 | 73.0 | 25.6 |
| NICSS25 | 0.15, 0.15 | 5.1 | 0.23 | 177.7 | 119.0 |
| NICSS27 | 0.15, 0.15 | 3.3 | 0.13 | 64.4 | 63.1 |
| NISSS2 | 0.11 | 1.4 | 0.07 | 3.0 | 3.6 |
| NICSS1 | 0.11, 0.11 | 2.9 | 0.18 | 47.1 | 41.6 |
| NICSS3 | 0.11, 0.11 | 1.8 | 0.08 | 30.5 | 30.4 |

To further illustrate the use of the index, the construction sequence of bridge NISSS14, introduced previously, is revisited here. The structure's construction is scrutinized during five stages (Stages 2, 3, 4, 5, and 9). Figure 4.32 shows three of the five stages considered in the analyses.

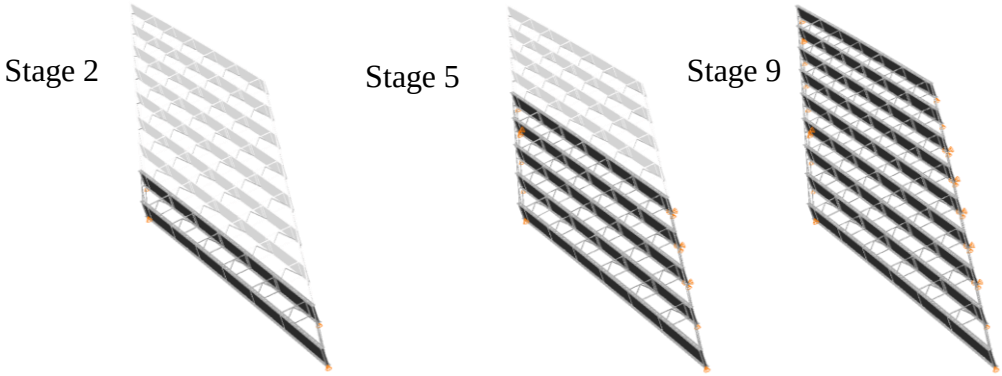


Figure 4.32. Erection stages investigated in bridge NISSS14

In this bridge, the spacing between girders is 9.25 ft, the span length is 150 ft, and the skew angle is 70 degrees. Hence, the skew index for Stage 2 is

$$I_S = \frac{9.25 \text{ ft} \times \tan(70)}{150 \text{ ft}} = 0.17$$

Similarly, for Stages 3, 4, 5, and 9 the index is 0.34, 0.51, 0.68, and 1.36, respectively.

Figure 4.33 shows the $f_b$ and $f_\ell$ plots of girders G1 and G2 for each of the stages. The plots contain three responses; the $f_b$ and $f_\ell$ traces obtained from the 3D FEA and the $f_b$ trace obtained from a line-girder analysis. The responses obtained from the 1D analyses consider loadings that are only based on the self-weight of the structure. These analyses do not consider the influence of the internal forces in the cross-frames resulting from the skew effects. Since the dimensions of G1 and G2 are the same and the only loading considered is the structure's self-weight, the line-girder analyses predictions for G1 and G2 are also the same and do not change during the construction simulation.

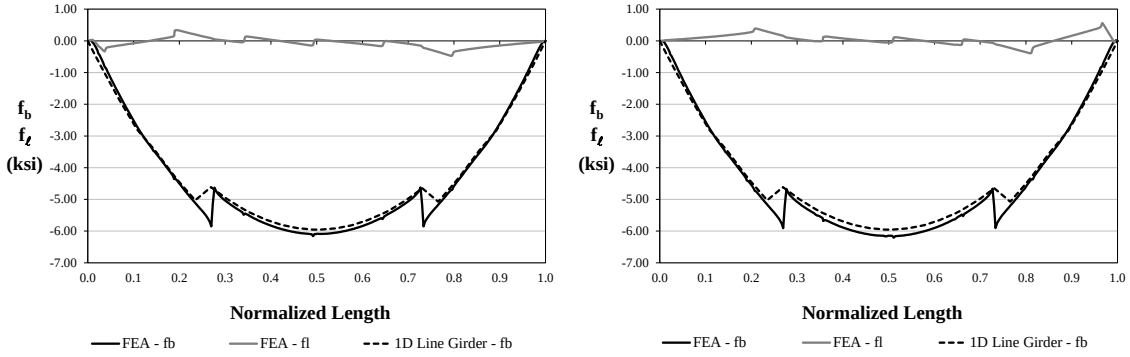


Girder G1 Girder G2

(a) Stage 2 ($I_S$ = 0.17)

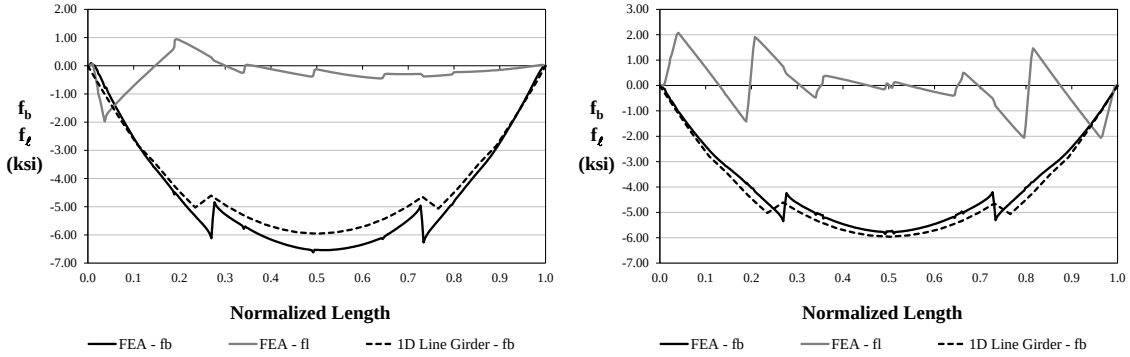


Girder G1 Girder G2

(b) Stage 3 ($I_S$ = 0.34)

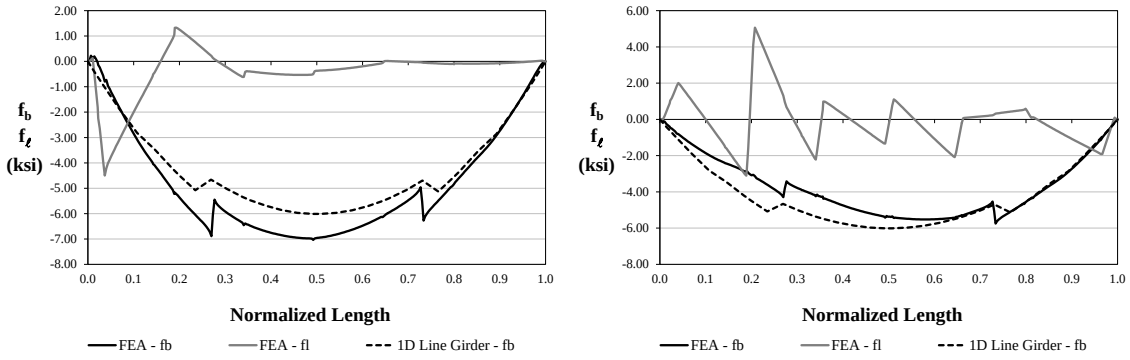


Girder G1 Girder G2

(c) Stage 4 ($I_S$ = 0.51)

Figure 4.33. Stress responses in the top flanges of girders G1 and G2 of bridge NISSS14 during five construction stages

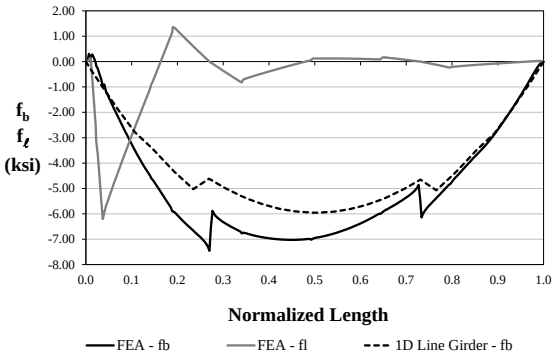


Girder G1

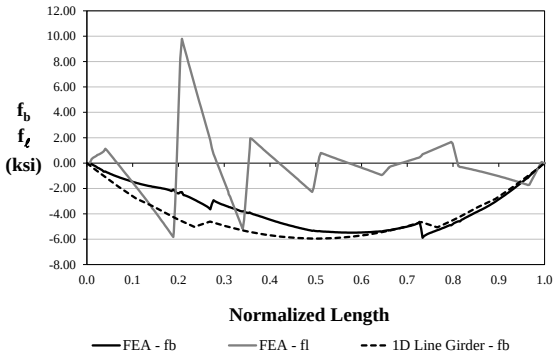


Girder G2

(d) Stage 5 ($I_S$ = 0.68)

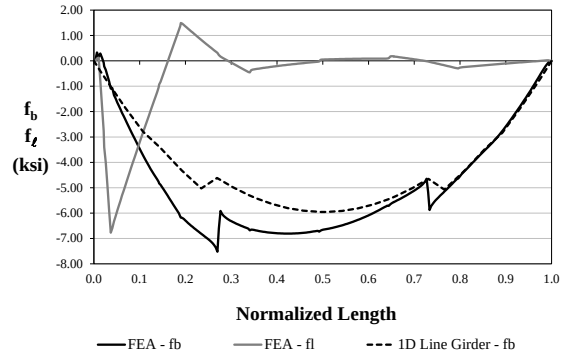


Girder G1

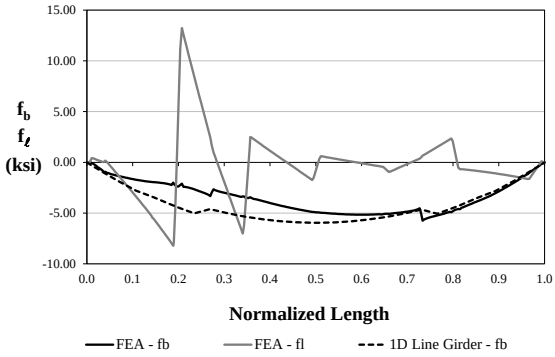


Girder G2

(e) Stage 9 ($I_S$ = 1.36)

Figure 4.33. Stress responses in the top flanges of girders G1 and G2 of bridge NISSS14 during five construction stages (continued)

From these plots, it is evident that as the construction progresses and the geometry of the bridge changes, the skew effects gain more importance. It is observed that in Stage 2, the influence of the skew is negligible, so the horizontal components of the nodal forces do not cause considerable levels of $f_\ell$. Also, the $f_b$ stresses associated with major-axis bending are solely dominated by the gravity loads. The vertical components of the nodal forces coming from the cross-frames are too small to influence the response. Hence, the 1D line-girder analysis is a good match of the benchmark. As more girders are

erected, the influence of the skew is more noteworthy. In Stage 5 for example, when five girders have been erected, the level of $f_\ell$ stresses is significant as compared to the $f_b$ response. As shown in the plots, the effect of the nodal force vertical components is also noticeable since the line-girder analysis prediction deviates considerably from the expected response. In the 1D analysis, the participation of the cross-frames is not included, so the forces transferred by the bracing system do not participate in the predictions. A similar trend is observed for Stage 9, when the structure's erection is completed. The plots show that the forces transferred through the cross-frames have a considerable impact in the performance of the structure.

This analysis demonstrates that the behavior of a skewed bridge not only depends on the severity of the skew. The skew angle by itself does not determine the magnitude of the collateral skew effects. Instead, it is the relationship between the span length, the width, the skew angle, and the distribution of the cross-frames in the bridge layout that determines the structural behavior. The proposed skew index relates the first three parameters that define the geometry of the bridge. As shown, as the index increases, so does the influence of the skew on the system response. It is also noticeable that in the construction stages investigated in this bridge, the responses in Stages 3, 4, 5, and 9, which have indices of 0.34, 0.51, 0.68 and 1.36, respectively, are more affected by the skew compared to Stage 2, where the index is below 0.30.

The construction simulation also highlights an important aspect regarding the accuracy of the 1D model predictions. Comparing the predictions obtained from the 1D and 3D analyses, it is observed that even when the line-girder solution deviates from the

expected response, in general, the difference in stress magnitudes tends to be minor. For example, at mid-span of girder G1, Stage 9, the $f_b$ stress obtained from the 3D model is -6.65 ksi. At the same position, the 1D model predicts a stress of -5.96 ksi, so the difference is 0.69 ksi. For design purposes, this difference is negligible, thus many engineers would conclude that the 1D model is sufficient to represent the expected structural behavior of this bridge. However, it is important to notice that the 1D model does not provide any information regarding the flange lateral bending response, which according to the AASHTO Specifications must be included in the construction checks, when the lateral bending is significant. Similarly, the approximate analysis does not predict the internal cross-frame forces, which are an important response to consider, especially during the construction of the structure. Hence, although the 1D analysis may capture approximately the major-axis bending response of the girders, it does not provide all the information needed to evaluate the structural components.

The results obtained from the 24 studied bridges and from the construction simulation discussed above show that the skew index could be used for several purposes. First, it could be used to determine when an approximate 1D line-girder model may be adequate to analyze and design a skewed bridge. If the structure's geometry is such that the index is more than 0.30, it is suggested to conduct a more elaborate 2D-grid analysis following the recommendations discussed in Chapter 5 or to analyze the structure by constructing a 3D FEA model. In the case of continuous span bridges, it would be sufficient for one span to have an index above this value to consider conducting a more detailed analysis. In addition, the index could serve to determine when it may be necessary to implement one of the mitigation schemes proposed in Section 4.2.2. As

previously discussed, understanding the global effect imposed by the bearing line cross-frames on the deformed shape of a bridge is crucial to configure the bracing system and reduce the undesired collateral skew effects. Lastly, the proposed index can be used to anticipate the erection stages in which the steel erector may have problems to assemble a skewed structure.

4.2.1.7. Summary of the Skew Effects in Straight I-Girder Bridges

The analyses conducted in the above case studies show that the effects of the skew in simple span and continuous span multi-girder bridges follow the same trend as in the basic two-girder bridge studied initially. In general, the end cross-frames impose a global effect that twists all the girders in the same direction. The inclusion of the intermediate cross-frames with large in-plane rigidities forces the girders to have approximately the same layovers at the bracing points. Due to this effect, the cross-frames may develop large internal forces. These forces depend on the transverse stiffness of the system at the connection points and on the amount of twist and lateral displacement that the girders have to undergo to reach the layover compatibility.

The cross-frame forces are transferred to the girders in the form of nodal forces that flow through the connections. The horizontal components of the forces induce lateral bending stresses, $f_\ell$, in the flanges that in certain cases could be larger than the major-axis bending stresses, $f_b$, that result from the gravity loads. The use of contiguous lines of cross-frames reduces the levels of $f_\ell$ stress, but it does not help decrease the cross-frame forces.

The vertical components of the nodal forces are equivalent to the V-loads in curved bridges, and should be considered in combination with the gravity loads when predicting the major-axis bending response of the girders. In bridges with a skew index less than 0.30, the vertical force components are comparatively smaller than the gravity loads, and have a minor influence in the $f_b$ stresses and the vertical displacements. For bridges with indices equal to or larger than 0.30, the overall response of the structure may be considerably affected by the skew. Above this limit, the transverse load path can increase rapidly, inducing lateral bending stresses in the girders and generating large $f_\ell / f_b$ stress ratios. Line girder analyses of bridges with $0.30 \leq I_s \leq 0.65$ may properly predict the major-axis bending responses, but cannot capture the transverse load effects since it does not include the participation of the cross-frames. In bridges with skew indices above 0.65, the cross-frame forces may also have a considerable influence in the vertical displacements and $f_b$. Therefore, if the skew index is larger than 0.30, it is recommended to conduct a 2D-grid analysis following the procedures discussed in Chapter 5 or a 3D finite element analysis. Alternately, for a bridge with a large index, one of the mitigation schemes proposed in Section 4.2.2 could be implemented to diminish the collateral effects of the skew.

### 4.2.2. Mitigation Schemes to Reduce the Skew Effects

In the previous sections the factors that control the behavior of a skewed bridge are introduced. In general, it is demonstrated that the configuration of the cross-frames in the bridge layout is one of the principal factors that influence the structural response. The mitigation schemes discussed in this section are based on determining efficient methods

to layout the cross-frames, such that they provide stability bracing, help control the bridge geometry, and at the same time, reduce the collateral effects of the skew.

In this section, two case study bridges are presented to implement practices that could be used in the design of steel I-girder bridges to minimize the undesired collateral effects of skew. Namely, the bridges NISSS16 and NISSS14 introduced in Section 3.1 are studied for this purpose.

4.2.2.1. Case Study I: NISSS16 – Implementation of Fanned Cross-Frames

This structure was introduced in Section 3.1.4. Figure 4.34 shows the plan view of the bridge with the original cross-frame layout. The cross-frames are oriented perpendicular to the girder longitudinal axes, as required by the AASHTO Bridge Design Specifications for bridges with skews larger than 20 degrees. In this structure, the left abutment is oriented at 50 degrees, while the other abutment is normal. The span length is 150 ft, the distance between fascia girders is 74 ft, and the skew index is 0.59. In the left part of the bridge, the cross-frames are staggered to relax the transverse rigidity of the structure and diminish the nuisance stiffness effects. In the right part of the structure, the cross-frames are configured using contiguous lines since the effects of the skew are smaller in that region.

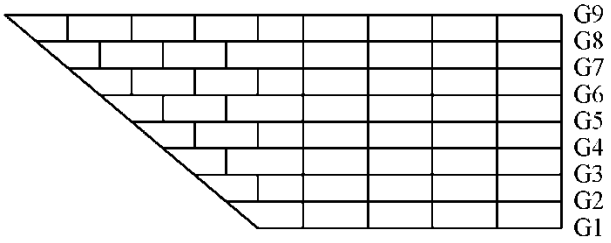


Figure 4.34. Framing plan of NISSS16 with the cross-frames oriented perpendicular to the longitudinal axis of the girders (Layout 1)

The bridge structural components were dimensioned following the AASHTO Bridge Design Specifications, using Grade 50 steel ($F_y$ = 50 ksi). In the design of the girders, one of the parameters that determine the distance between cross-frames (or bracing points) is their lateral-torsional buckling (LTB) resistance. The design of the structure indicates that the cross-frame layout shown in Figure 4.34 provides sufficient bracing to prevent a stability failure between the braced points. In this study, however, the original layout is modified to find a more efficient distribution of the cross-frames. For this purpose, it is necessary to first determine the maximum allowable distance between bracing points, $L_b$, for the limit state of LTB in each of the girders.

According to the AASHTO Specifications, Section 6.10.8, the LTB strength of the structure is checked using the "one third rule" given by the following equation:

$$f_{bu} + \frac{1}{3} f_{\ell} = \phi_f F_{nc} \qquad \text{(Eq. 4.8)}$$

where $f_{bu}$ and $f_{\ell}$ are the major-axis and lateral bending stresses in the compression flange, and $\phi_f$ is the resistance factor that for flexure related limit states is equal to one. For the purpose of this study, the nominal flexural resistance of the compression flange, $F_{nc}$, is the LTB strength, for $f_{\ell} = 0$.

Girder G5 is considered to illustrate the determination of the maximum allowable unbraced length. The calculations are conducted using an approximate analysis to estimate a lower limit for $L_b$. From a 1D line-girder analysis, it is determined that the maximum $f_{bu}$ stress due to the TDL is equal to 23.10 ksi, at mid-span. At this point, it has not been decided if the cross-frame line at mid-span of G5 (or near) is contiguous or not.

Thus, it is conservative to assume that the cross-frame line is discontinuous, and that the girder is subjected to lateral bending at this location. Section C6.10.1 of the AASHTO Specifications recommends an $f_\ell$ value of 10.0 ksi for interior girders and 7.5 ksi for exterior girders of bridges with skew angles of up to 60 degrees and a $D/b_f$ ratio of approximately 4.0, which is the case for NISSS16. The stress values recommended above correspond to the total unfactored stress, including live load.

The AASHTO Specifications also require the constructability checks to be conducted at 1.5 times the nominal dead loads for the STRENGTH IV load combination. This load combination often controls the constructability checks for the noncomposite structure. Assuming that the ratio between the total unfactored loads and the noncomposite dead loads is 3, $f_\ell$ in girder G5 is 10.0/3 = 3.33. Therefore, for G5 at mid-span, the left hand-side of Eq. 4.7 is equal to 1.5(23.10 +3.33/3) = 36.32 ksi. Since for flexure $\phi_f$ = 1.0, the nominal flexural resistance of the compression flange, $F_{nc}$, has to be at least equal to 36.32 ksi. Next, it is necessary to determine the unbraced length limits, $L_p$ and $L_r$, that define the inelastic and elastic LTB regions, respectively. From Section 6.10.8.2.3 of the AASHTO Specifications, these limits are defined as

$$L_p = 1.0 r_t \sqrt{\frac{E}{F_{yc}}} \qquad \text{(Eq. 4.9)}$$

and

$$L_r = \pi r_t \sqrt{\frac{E}{F_{yr}}} \qquad \text{(Eq. 4.10)}$$

where $r_t$ is the effective radius of gyration for lateral torsional buckling, $E$ is the modulus of elasticity of the steel, $F_{yc}$ is the yielding strength of the compression flange, and $F_{yr}$ is the compression flange stress at the onset of nominal yielding, including residual effects. The $F_{yr}$ strength is taken as the minimum between $0.7F_{yc}$ and $F_{yw}$, where $F_{yw}$ is the yielding strength of the web.

For the mid-span section of girder G5, it is determined that $r_t$ = 4.48 in. Since the girders are fabricated with Grade 50 steel, $F_{yc}$ = 50 ksi and $F_{yr}$ = 0.7·50 = 35 ksi. Substituting these values in Eqs. 4.8 and 4.9, the limiting unbraced lengths are $L_p$ = 9.00 ft and $L_r$ = 33.8 ft. In general, the unbraced length in bridge girders is around 25 ft. Therefore, it is reasonable to assume that for girder G5, $L_b$ is between $L_p$ and $L_r$, so at the strength level, the failure mode is inelastic LTB. Hence, according to Section 6.10.8.2.3 of the AASHTO Specifications the flexural resistance of the compression flange is

$$F_{nc} = C_b\left[1-\left(1-\frac{F_{yr}}{R_b F_{yc}}\right)\left(\frac{L_b - L_p}{L_r - L_p}\right)\right]R_b R_h F_{yc} \le R_b R_h F_{yc} \qquad \text{(Eq. 4.11)}$$

For the approximate analysis, it is assumed that the moment gradient modifier, $C_b$, is equal to 1.0, which is reasonable at the vicinity of mid-span. For the mid-span section of girder G5, the web-load shedding factor, $R_b$ is equal to 1.0. Likewise, the hybrid factor, $R_h$ is equal to 1.0 since all the components in the bridge are fabricated with Grade 50 steel. The value of the minimum required nominal strength, $F_{nc}$ = 39.65 ksi, and the values of $R_b$, $R_h$, $F_{yc}$, $F_{yr}$, $L_p$ and $L_r$ are substituted in Eq. 4.10 to determine the maximum unbraced distance:

$$F_{nc} = 1.0\left[1-\left(1-\frac{35}{1.0\cdot 50}\right)\left(\frac{L_b - 9.0}{33.8-9.0}\right)\right]1.0\cdot 1.0\cdot 50 = 36.32$$

From the above equation, it is determined that the maximum unbraced length required to prevent LTB at mid-span segment of girder G5 is equal to 31.5 ft. The bracing requirements along the girder length vary depending on the bending moment, decreasing towards the supports (zero-moment regions). In addition, the girder cross-sections are reduced accordingly since the strength requirements decrease. For the purpose of this analysis, it is assumed that for girder G5, the maximum unbraced distance is 31.5 ft at any location along its length. Following the same procedure, the maximum unbraced lengths are determined for the other girders, as shown in Table 4.4. The cross-frames in NISSS16 must be placed considering these limits. An additional aspect that has to be considered with respect to the admissible unbraced length in the fascia girders is the effect of the eccentric overhang loadings. The $f_\ell$ stresses due to these loadings can be calculated using Eq. 4.1. These stresses should be added to those imposed by the skew effects. The values shown in the table for girders G1 and G9 consider these additional stresses.

Table 4.4. Maximum unbraced lengths to prevent LTB in the girders of Bridge NISSS16

| Girder | $f_{bu}$ (ksi) | $f_\ell$ (ksi) | $1.5(f_{bu}+ f_\ell/3)$ (ksi) | $L_b$ (ft) |
|---|---|---|---|---|
| G1 | 13.3 | 3.52 | 21.71 | 42.0 |
| G2 | 17 | 3.33 | 27.17 | 37.5 |
| G3 | 19.7 | 3.33 | 31.22 | 35.0 |
| G4 | 20.3 | 3.33 | 32.12 | 35.0 |
| G5 | 23.1 | 3.33 | 36.32 | 31.5 |
| G6 | 25.8 | 3.33 | 40.37 | 25.0 |
| G7 | 25.4 | 3.33 | 39.77 | 30.0 |
| G8 | 28.2 | 3.33 | 43.97 | 22.0 |
| G9 | 29.5 | 3.52 | 46.01 | 18.0 |

The next step to configure the bracing system is to identify possible cross-frame layouts that minimize the effects of skew. As discussed in Section 4.2.1.1, the end cross-frames impose a global effect that result in girder layovers. An effective method to reduce the cross-frame forces and the flange lateral bending stresses is to connect the girders at locations that have approximately the same layovers. In a bridge with parallel skewed supports, this is achieved by placing the intermediate cross-frames at the same angle as the end cross-frames. In the case study, the left support is inclined 50 degrees, while the right support is normal; therefore, it is not feasible to position all the cross-frames parallel. A possible method that can reduce the effects of the skew in this bridge is to orient the cross-frames in a fanned arrangement. Figure 4.35(a) shows this scheme for the cross-frame layout, where the cross-frame lines fan out from Point A. Figure 4.35(b) and Figure 4.35(c) show two possible configurations based on this criterion. In the configuration shown in Figure 4.35(b) (Layout 2), 48 intermediate cross-frames are provided considering the maximum unbraced length limits determined previously to prevent LTB. The four contiguous lines (CF2, CF4, CF6, and CF8) are sufficient to control the profile of the structure during the concrete placement. The intention is to keep all the interior girder top flanges aligned with the line that joins the top flanges of the fascia girders at the connection points. Hence, with the contiguous cross-frame lines, the girder top flanges are forced to stay in the same plain, providing a surface that is suitable for deck placement.

The configuration shown in Figure 4.35(c) has 44 intermediate cross-frames. The unbraced lengths in the girders are the same as in the first configuration; however, the

second arrangement, besides having four less cross-frames, takes advantage of one of the attributes studied in the foregoing sections, as explained next.

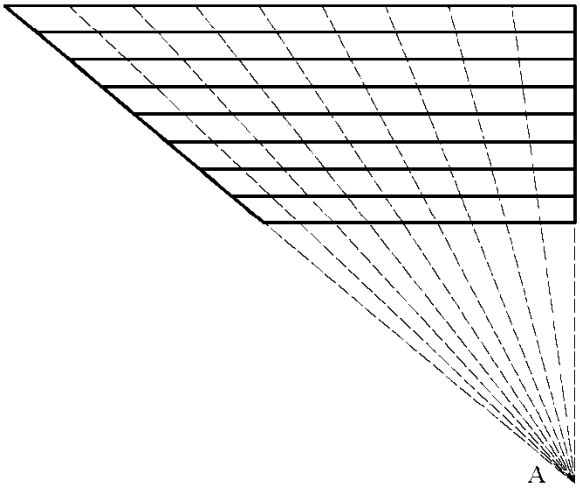


(a) Sketch of the fanned cross-frame lines

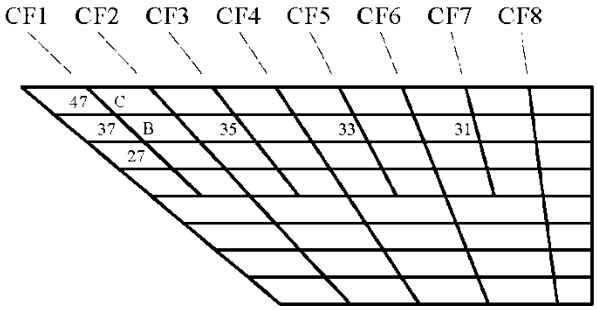


(b) Fanned configuration with continuous cross-frame lines between girders G5 and G9 (Layout 2)

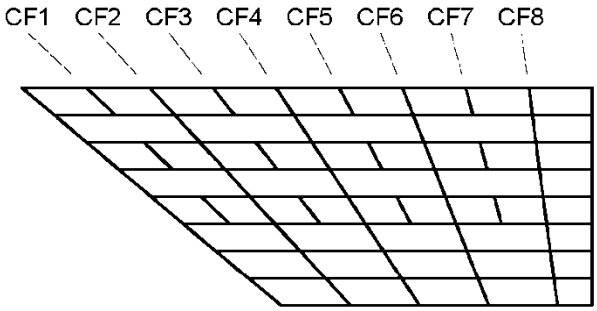


(c) Fanned configuration with girders grouped in pairs to diminish the skew effects (Layout 3)

Figure 4.35. Configurations with fanning cross-frame lines implemented in NISSS16

In the configuration of Figure 4.35(b), lines CF1, CF3, CF5, and CF7 connect girders G5 to G9 continuously. This pattern unnecessarily increases the transverse stiffness of the bridge, inducing large cross-frame forces. For example, consider a hypothetical case where cross-frames 31, 33, 35, and 37 are the last components to be erected in the structure. To place cross-frame 37, it is necessary to displace laterally and twist the groups formed by girders G5-G7 and G8-G9, so the layovers at the connection points, B and C, are the essentially same. Hence, the forces in this cross-frame are proportional to the transverse stiffness of the girder groups and to the displacements required to obtain the layover compatibility at the connection points. From the functionality standpoint, however, it is not necessary to include this cross-frame in the system. In the case of girder G8, Cross-frame 47 provides the stability bracing required at C to prevent LTB. Similarly, at Point B in girder G7, the bracing provided by Cross-frame 27 is sufficient for stability purposes. The same observations apply to cross-frames 31, 33, and 35.

In general, for stability bracing purposes, it is preferable to brace the girders in pairs rather than connecting several girders. This practice relaxes the transverse rigidity of the structure at the connection points since the stiffness of a pair of girders is smaller than the stiffness of a multi-girder group. Thus, less effort is required to connect the cross-frames. Also, the internal cross-frame forces and the levels of flange lateral bending stress are reduced since the girders are less restricted and can move to accommodate the lateral displacements and twists induced by the global effect without generating stress concentrations. This concept is applied in the framing layout depicted in Figure 4.35(c). Except for the contiguous lines necessary to control the deformed geometry of the

noncomposite structure under the noncomposite dead loads, the cross-frames in the bridge are arranged such that they connect the girders in pairs.

An important aspect that must be considered when using the fanned pattern to layout the cross-frames is the efficiency of these components to provide stability bracing. Generally, in skewed bridges, the design of the cross-frame elements is controlled by the forces induced by the skewed effects rather than by the stability bracing requirements. However, when the cross-frames are skewed, their efficiency to brace the girders decreases and the bracing checks can control their design. Hence, when the cross-frames are configured with a fanned arrangement, it is necessary to check that in addition to having the strength required to resist the internal forces they also satisfy the stability bracing requirements. Moreover, the flexibility of the bent-plate connection detail commonly used to connect cross-frames with large skews is another aspect to consider. As shown by Quadrato et al. (2010), the ability of the cross-frames to provide efficient stability bracing is significantly reduced due to the flexibility of this detail. To overcome this limitation, a detail such as the one depicted in Figure 4.36 could be implemented. As shown in the figure, the bent plate can be reinforced to reduce its flexibility by providing stiffeners near the top and bottom flange. Also, a stiffener at the web mid-depth could be provided to increase the rigidity of the bent plate.

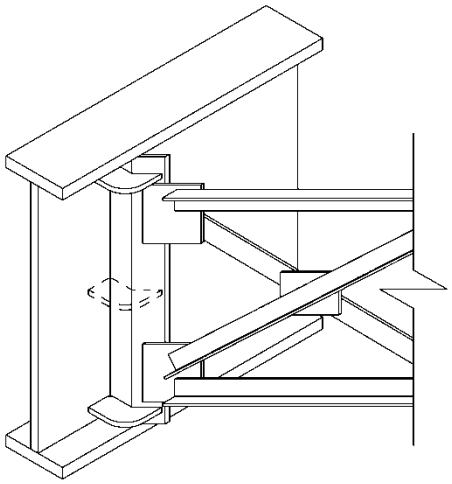

Figure 4.36. Detail implemented to reduce the flexibility of the bent plate connection

In addition, Quadrato et al. (2010) developed a connection detail to connect skewed cross-frames that may be implemented in combination with the recommendations provided in this section. In these tests, a half-pipe stiffener is welded at each side of the web. Due to the circular contour of this stiffener it is possible to weld the connection plates at any practical angle.

The stiffened bent-plate and the half-pipe stiffener details are not implemented in the models discussed next. Instead, for the analyses conducted in bridges with fanned cross-frame arrangements, the cross-frames are connected to the girders using connection plates that are skewed the same angle as the intermediate cross-frames.

Table 4.5 shows the forces in the intermediate cross-frames obtained from 3D nonlinear analyses for each of the three layouts at the TDL level. The values in the table are the maximum compression and tension forces in the chords and diagonals of the intermediate cross-frames, which are a measure of the skew effects. The table shows that the fanned systems, Layouts 2 and 3, result in smaller cross-frame forces compared to the

forces in the original configuration, Layout 1. For example, the maximum tension force in the top chords is reduced from 73.3 kips to 51.6 kips for Layout 2 and to 47.9 kips for Layout 3.

Table 4.5. Maximum forces in the intermediate cross-frames predicted for the layouts considered in bridge NISSS16 at the TDL level

| Element | Cross-Frame Arrangement Type | Number of Interior Cross-Frames | Maximum Compression Force (kips) | Maximum Tension Force (kips) |
|---|---|---|---|---|
| Top Chord | (1) | 48 | 13.0 | 73.3 |
| | (2) | 48 | 6.0 | 51.6 |
| | (3) | 44 | 5.6 | 47.9 |
| Diagonals | (1) | 48 | 70.7 | 39.6 |
| | (2) | 48 | 50.4 | 17.9 |
| | (3) | 44 | 45.6 | 16.7 |
| Bottom Chord | (1) | 48 | 70.7 | 11.3 |
| | (2) | 48 | 50.4 | 0.1 |
| | (3) | 44 | 45.6 | 0.1 |

Another measure that can be studied to evaluate the effects of the different cross-frame layouts is the girder stress responses. Figure 4.37 shows the $f_b$ and $f_\ell$ stress predictions obtained from the nonlinear FEA models for the top flange of girder G5 for each of the three layouts. In the plot, the horizontal axis corresponds to the normalized length of the girder. The peaks in the $f_\ell$ response for the configuration with the cross-frames oriented perpendicular to the girders (Layout 1) are a consequence of the staggered pattern used in the left part of the bridge. These stresses vanish in the zone framed with contiguous lines. The plots show that the flange lateral bending stresses decrease when the fanned configurations are implemented. As shown in the table

included in the plot, the $f_b/f_\ell$ ratio is reduced from 0.33 to 0.12, highlighting the benefits of the proposed methods. It is worth mentioning that the major axis bending stress remains almost the same for the three cases since the skew index in this bridge is less than 0.65. This response is insensitive to the modifications in the bracing system configuration.

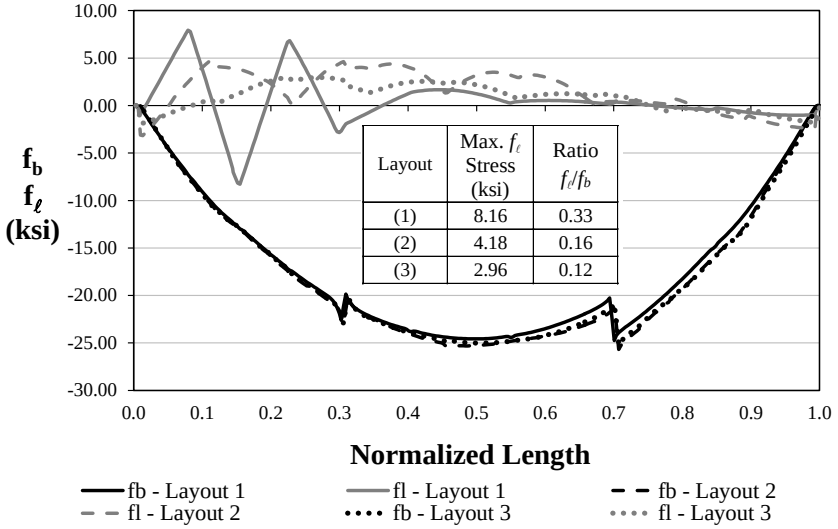


| Layout | Max. $f_\ell$ Stress (ksi) | Ratio $f_\ell/f_b$ |
|---|---|---|
| (1) | 8.16 | 0.33 |
| (2) | 4.18 | 0.16 |
| (3) | 2.96 | 0.12 |

Figure 4.37. Stress responses in the top flange of girder G5 in NISSS16 at the TDL level, considering different cross-frame layouts

The studies conducted in the above case study demonstrate that the configuration of the cross-frames has a strong impact in the bridge performance. Comparing the results obtained from Layouts 1, 2, and 3, it is evident that the last layout is the most efficient to diminish the effects of the skew. The use of a fanned configuration reduces the lateral deformations required to connect the cross-frames. Additionally, a practice that helps reduce the transverse stiffness of the bridge and mitigate the skew effects is to brace the girders in pairs. In general, the internal cross-frame forces are expected to be smaller when the bracing system is oriented such that it does not interfere with the natural

rotations that the girders experience due to the global effect. When the cross-frames are connected perpendicular to the girders, they disturb the girder rotations that are originated by the global effect, imposing additional lateral deformations that result in larger cross-frame forces and $f_\ell$ levels. In bridges with unequal skew angles, the fanned configuration is a method to lessen the collateral impact of the cross-frames in the bridge response, while still providing the required stability bracing and controlling the bridge geometry during the deck placement.

Based on these observations, a possible procedure to diminish the collateral effects of the skew in straight simple-span bridges is:

1. Determine the maximum unbraced lengths, $L_b$, in the girders, based on the LTB check specified in the AASHTO Specifications, Section 6.10.8. The $f_{bu}$ stresses are obtained from the major-axis bending moment requirements due to the factored TDL. The $f_\ell$ stresses can be obtained from either the recommendations provided in Section C6.10.1 of the AASHTO Specifications or using the method presented in Section 5.5.1 of this thesis. In the calculation for the fascia girders, include the $f_\ell$ stresses that result from the eccentricity of the overhang loads.
2. Study possible cross-frame layouts that do not interfere with the girder rotations imposed by the global effect. If the supports are skewed and parallel, the best alternative is to also connect the intermediate cross-frames parallel to the skew. If the skew at the supports are not the same, it is recommended to

orient the cross-frames in a fanned configuration. For this purpose, the bearing lines are projected to find the point where they intersect. The fanned cross-frame lines are drawn with respect to the intersection point, considering the unbraced length limits determined in Step 1. In cases where the skew angle is larger than 20 degrees, the connection detail shown in Figure 4.36 or the recommended by Quadrato et al. (2010) can be implemented to overcome the fabrication difficulties related to the welding of the connection plate.

3. Provide contiguous cross-frame lines following the fanned pattern. Use the minimum number of contiguous lines required to control the bridge profile during the deck placement. In some of the girders additional bracing beyond that provided by the contiguous lines may be necessary to ensure lateral stability of the girders. In these cases, connect the girders in pairs with the cross-frames oriented in the fanned configuration. If it is possible, avoid connecting more than two girders along the same cross-frame line since this increases the transverse stiffness of the structure unnecessarily, resulting in larger cross-frame forces and possible fit-up problems during the steel erection.
4. In many skewed structures, the strength requirements due to the gravity loads control the design of the cross-frames over the stability bracing requirements. However, it is important to keep in mind that due to the skewed orientation of the cross-frames, their ability to provide stability bracing is reduced. Therefore, in a bridge where the cross-frame member sections are kept the

same, it is necessary to check that the cross-frames with the largest skew angle satisfy the bracing requirements.

4.2.2.2. Case Study II: NICSS16 – Interior X-Type Cross-Frames without Top Chords

The functions of cross-frames in steel girder bridges are in introduced in Chapter 2. As mentioned there, one of the most important functions of cross-frames is to stabilize the girders during the deck placement. Also, they are necessary to control the profile of the structure, so the concrete deck is placed evenly and with a uniform thickness. In addition, cross-frames increase the transverse stiffness of the structure, which in the case of a skewed bridge, creates a spurious secondary load path that can complicate the bridge construction. Hence, it is desirable to investigate alternatives that reduce the secondary effects of the skew while still providing with the required functions of the bracing system. In the studies conducted in this research, it is determined that the use of X-type cross-frames without top chords is a potential mechanism that can be implemented for this purpose, as demonstrated in the following discussion.

The first consideration focuses on the bracing properties of the cross-frames. The models that are commonly used in practice to design bracing systems for beams and girders are the ones proposed by Yura (2001). These models assume that the X-type cross-frames can work either as a tension-only or a tension-compression system. Figure 4.38 depicts the principles of both of of these models. In the tension-only system, it is assumed that the diagonals are only effective when they work in tension. Then, the torsional stiffness of the brace, $\beta_b$, depends only on the properties of the diagonals and the bottom chord. In this model, the contribution of the top chord is not included in the stiffness calculation, but the top chord is needed to transfer the force *F* to the tension

diagonal. The second model is the tension-compression system, which considers the axial stiffness of the diagonals when working in compression. In this model, the participations of the cross-frame chords are ignored in the torsional brace stiffness calculation, and $\beta_b$ are function the diagonal properties, only. If the tension-compression model is used to design the bracing system, the presence of the top chord is irrelevant. Hence, although in reality the stiffness of cross-frames with and without top-chord is different, from the tension-compression *design* model perspective, they are the same.

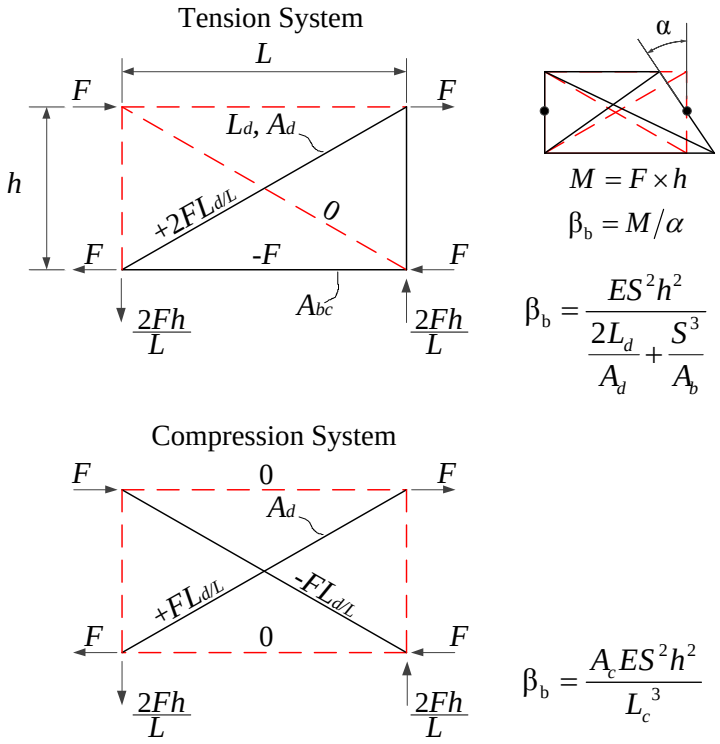


Figure 4.38. Stiffness models for X-type cross-frames (adapted from Yura (2001))

The next consideration focuses on the stiffness properties of the X-type cross-frames with and without top chords. Figure 4.39 shows the flexion and the shear modes of the cross-frames. The shear stiffness of the cross-frame, $k_s$, is insensitive to the

presence of the top chord since it only depends on the stiffness of the diagonals, and is equal to

$$k_s = \frac{Eh^2}{L_d^{\,3}}\left(A_{d1} + A_{d2}\right) \qquad \text{(Eq. 4.12)}$$

where $E$ is the steel modulus of elasticity. The other variables are defined in Figure 4.38. The shear stiffness is the parameter that controls the differential vertical displacements between adjacent girders. Hence, to control the profile of a bridge during the deck placement and achieve a uniform deck thickness, the top chord may not be needed.

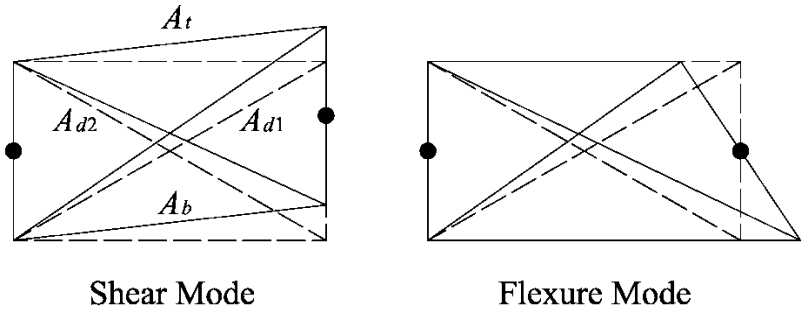


Figure 4.39. Flexure and shear modes in the X-type cross-frame

The other source of stiffness that is of interest is the flexural stiffness, $k_f$, since it is a major contributor to the transverse rigidity of a bridge. This stiffness is

$$k_f = \frac{Eh^2}{4L}\left(A_b + A_t\right) + \frac{Eh^2L^2}{4L_d^{\,3}}\left(A_{d1} + A_{d2}\right) \qquad \text{(Eq. 4.13)}$$

To simplify the discussion, it is assumed that the diagonals and chords have the same area. Hence, for the case where the top chord is present in the cross-frames, the flexure stiffness reduces to

$$k_{f\,\mathrm{TC}} = \frac{Eh^2}{2L} A\left(\frac{1}{L} + \frac{L^2}{L_d{}^3}\right) \qquad \text{(Eq. 4.14)}$$

Similarly, for the case where the top chord is removed from the cross-frame, the flexure stiffness is equal to

$$k_{f\,\mathrm{NC}} = \frac{Eh^2}{2L} A\left(\frac{1}{2L} + \frac{L^2}{L_d{}^3}\right) \qquad \text{(Eq. 4.15)}$$

The ratio of Eq. 4.15 to Eq. 4.14, $r_f$, is a parameter that shows the reduction in the flexure stiffness due to the top chord removal. By substituting $L = L_d \cdot \cos(\theta)$ in Eqs. 4.14 and 4.15, and by simplifying terms, the ratio $r_f$ reduces to

$$r_f = \frac{1 + 2\cos^3(\theta)}{2 + 2\cos^3(\theta)} \qquad \text{(Eq. 4.16)}$$

In X-type cross-frames, the angle θ usually varies between 25 to 50 degrees. At angles less than 25 degrees, this configuration becomes inefficient. In those cases, a V-type or inverted V-type cross-frame is more suitable. Hence, for practical cases, the stiffness ratio, $r_f$, is bounded between 0.71 and 0.61.

The flexural stiffness of the cross-frames has a direct impact on the transverse stiffness of a bridge since it is more difficult to displace laterally and twist the girders to accommodate the girder layovers once they are in place. Therefore, the reduction of the cross-frame bending stiffness is a method that can be implemented to mitigate the undesired collateral effects of skew. In this context, the use of X-type cross-frames without top chords, which reduces the bending stiffness in a range between 61 and 71 percent, is a potential solution. As demonstrated in the analyses above, X-type cross-

frames with and without top-chords are equally capable of controlling the structure's profile, and have the same bracing capacity if they are designed as a compression system.

This mitigation scheme is implemented in one of the bridges introduced in Section 3.1 to explore its benefits. The structure considered for this analysis is Bridge NICSS16. This structure was studied in Section 4.2.1.5 to observe the effects of the skewed supports in continuous I-girder bridges. This is a nine-girder three-span bridge, with skew indices of 1.69, 1.36, and 1.36. The bridge plan view and the dimensions of a typical interior cross-frame are illustrated in Figure 4.40.

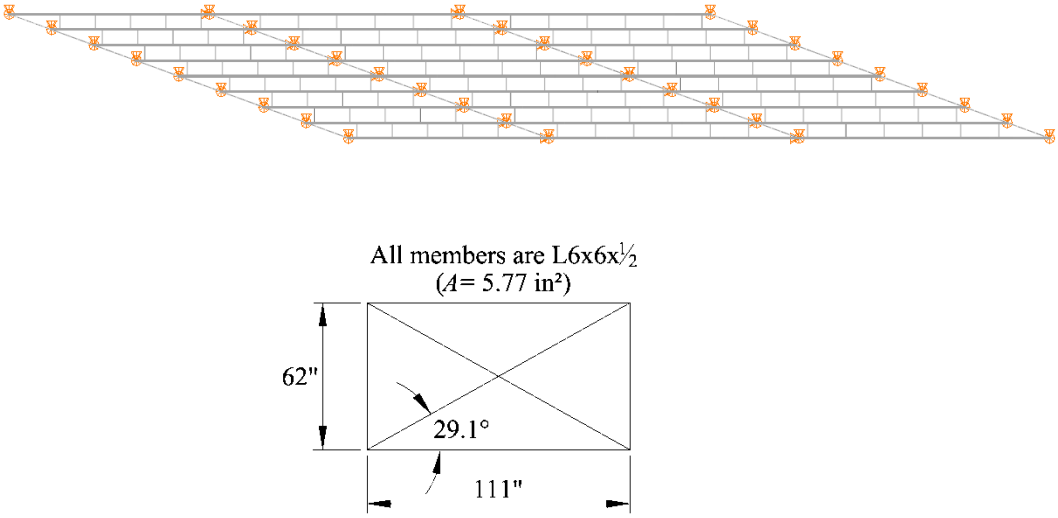


Figure 4.40. Plan view of NICSS16 and cross-frame dimensions

The interior cross-frames in this bridge have an angle of $\theta = 29.1^{o}$, so the $r_f$ ratio is equal to 0.70. Hence, when the top-chord is removed, the cross-frame bending stiffness is reduced to a 70 %. The impact of this modification is illustrated in Figure 4.41 that shows the stress responses in the top and bottom flanges of girder G5. These responses are obtained from refined nonlinear 3D FEA. The stress plots show that the reduction in $f_\ell$

is considerable. For example, the maximum $f_\ell$ value in the top bottom flange, which is located in the positive moment region of Span 3, is reduced from 17.0 ksi to 9.5 ksi. Similarly, in the top flange, $f_\ell$ decreases from 23.4 ksi to a value of 14.7 ksi. The plots also show that the major-axis bending stress responses are almost insensitive to this modification. Except for minor changes in the third span, $f_b$ remains essentially the same. The behavior described for this girder is observed in the rest of girders of the bridge, as well. In general, the top-chord removal results in a significant decrement of $f_\ell$.

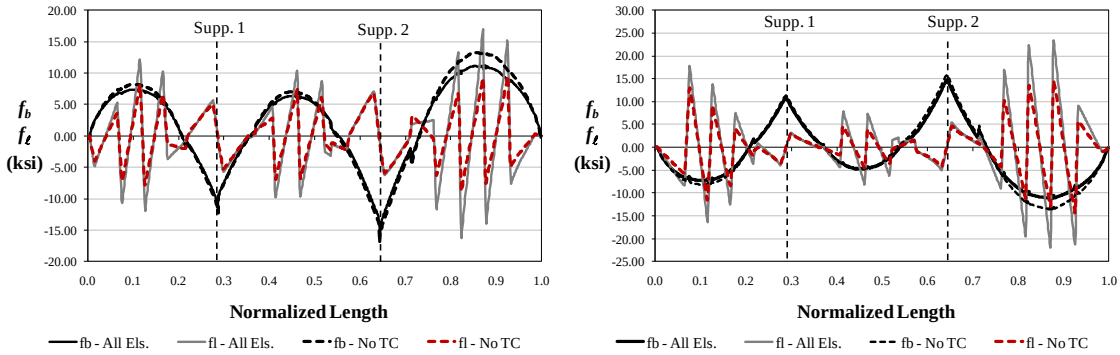


Figure 4.41. Stress responses in girder G5 of NICSS16 at the TDL level for cross-frames with and without top chords

Other responses of interest are the vertical displacements and the girder layovers. These two responses are shown in Figure 4.42. As depicted in the plots, the behavior of the system in terms of the girder displacements and girder rotations is slightly changed with the top-chord removal. The layover plot also shows that the cross-frames without top chords are bracing the girder properly. If the bracing efficiency of the modified cross-frames were insufficient, the girder layovers would increase considerably since large

rotations are associated with amplifications due to second-order effects and stability related problems.

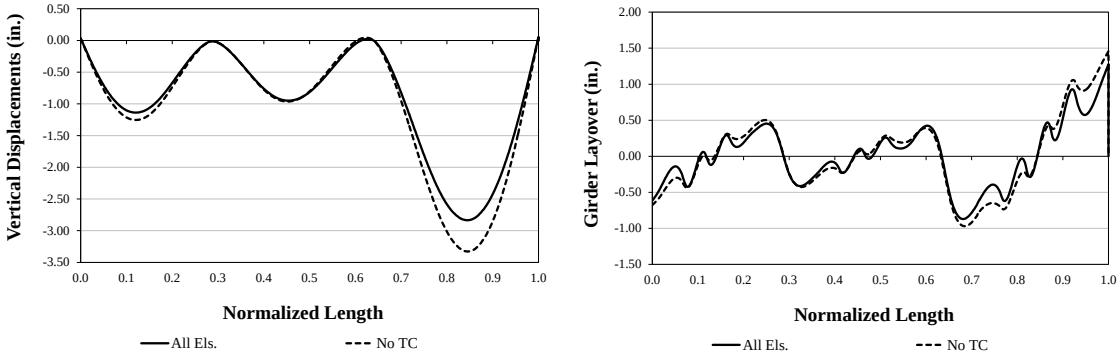


Figure 4.42. Vertical displacements and layovers in girder G5 of NICSS16 at the TDL level for cross-frames with and without top chords

The derivations and the case study discussed in this section demonstrate that the use of X-type cross-frames without top-chords is a measure that helps mitigate the adversities of skew. This practice relaxes the transverse stiffness of the bridge while not affecting the functions of the bracing system. Depending on the severity of the skew, the improvements in the overall structural performance may vary from bridge to bridge. For structures with a skew index less that 0.50 the changes may not be noticeable, but in bridges where the skew effects are large, the top-chord removal can be a potential solution to improve the bridge behavior.

### 4.3. Influence of Cross-Frame Configurations on Bridge Responses

In this section three bridges are analyzed to study the influence of the bracing system on the structural behavior. The intermediate cross-frames are modified by removing certain elements, and the system responses are captured to evaluate how significant are the variations on the performance of the structures. In all the analyses, the

vertical displacements, girder layovers, $f_b$ and $f_\ell$ stress responses, and cross-frame forces are presented for the total dead load (TDL) condition.

### 4.3.1. Case Study I: Continuous Curved and Skewed Bridge (XICSS7)

This structure has a challenging geometry that includes the horizontal curvature and highly skewed internal supports. The bridge layout and the parameters that define the bridge geometry are shown in Figure 4.43.

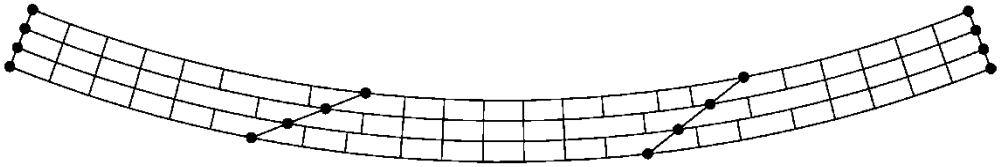

$L_1$ = 160 ft, $L_2$ = 210 ft, $L_3$ = 160 ft / $R$ = 700 ft / $w$ = 40.5 ft / $\theta_1$= 0 ˚, $\theta_2$= -60 ˚, $\theta_3$= -60˚, $\theta_4$= 0˚

Figure 4.43. XICSS7 Bridge Layout – Case Study 1

The structure is designed using the X-configuration for the intermediate cross-frames and the interior bearing lines, while the inverted V-configuration is used at the abutments. Three analyses are conducted in this bridge modifying the cross-frames. In this study, the elements in the intermediate cross-frames are sequentially removed to observe the changes in the bridge behavior. The first analysis is conducted with all the elements of the intermediate cross-frames in place. In the second analysis, one of the diagonals is removed from the interior X-type cross frames. Finally, a third analysis is performed removing only the top chord. Figure 4.44 shows the studied variations in the cross-frames.

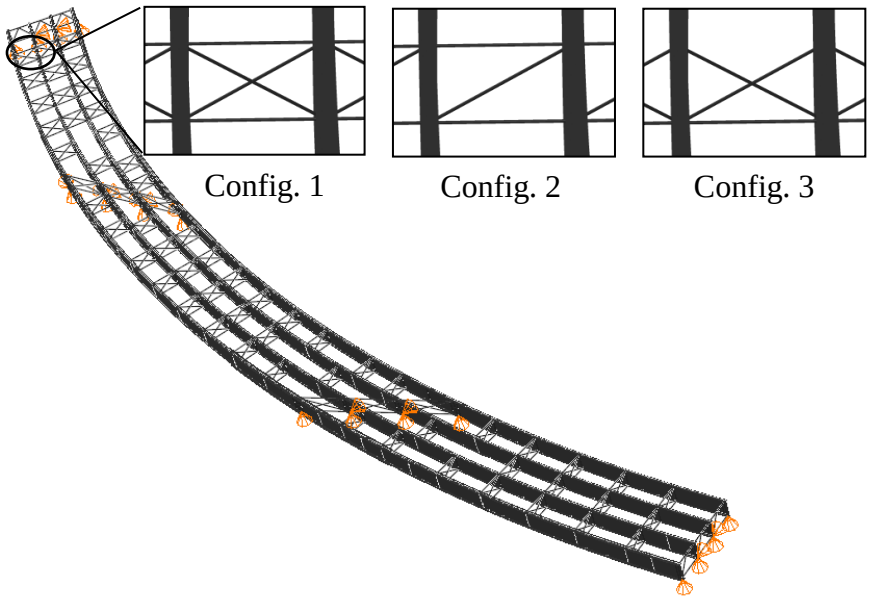


Figure 4.44. Intermediate cross-frame configurations used in the analyses – Case Study 1

The plots in Figure 4.45(a) and Figure 4.45(b) show a comparison of the major-axis bending and flange lateral bending stress responses in the exterior girder of the bridge for the different analyses described above. Only the results for the exterior girder are presented. Similar responses are observed in the other three girders of the structure. As shown in these figures, there is no appreciable difference in the response of the bridge girder between the analyses. The removal of one diagonal or the top chord has little effect in the behavior of the bridge. This means that even though the cross-frame stiffness is reduced with the removal of a diagonal or the top chord, they are still comparably rigid with respect to the girder stiffness. Hence, for this bridge regardless the modifications the cross-frames behave essentially as rigid bodies.

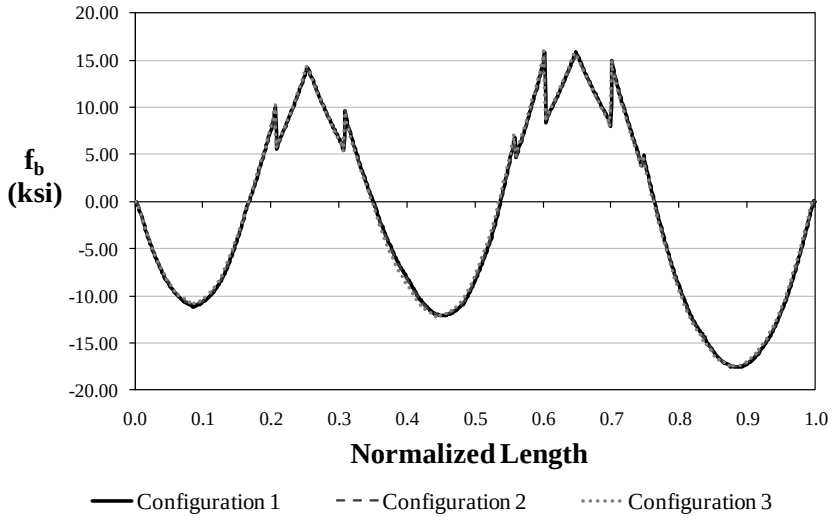


a) Major-axis bending stresses, $f_b$

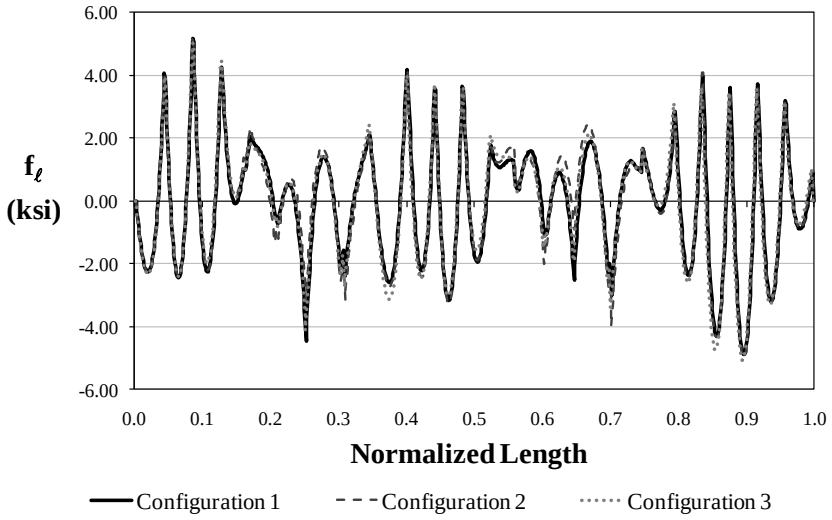


b) Flange lateral bending stresses, $f_\ell$

Figure 4.45. Comparison of stress predictions in the top flange of girder G1 of Bridge XICSS7

The forces in the cross-frame elements are also investigated for each of the cases. Table 4.6 shows the maximum tension and compression forces in the cross-frames across the bridge, as predicted by the different analyses. These values would be used in the strength checks, considering that this bridge has been designed using the same element

cross sections for all the cross-frames. As observed in the table, for the three analyses, the forces vary between 78.39 kips in compression and 70.07 kips in tension, which could be considered as an acceptable range for a bridge of these characteristics. The table also shows that as with the girder stresses, with the fourth cross-frame configuration excessive forces would be developed in the diagonals.

Table 4.6. Forces in the cross-frame elements (kips) – Case Study 1

| | Analysis | (1) | (2) | (3) |
|---|---|---|---|---|
| Top Chord | Compression | -28.71 | -64.93 | NA |
| | Tension | 42.84 | 44.83 | NA |
| Diagonals | Compression | -54.14 | -39.20 | -78.39 |
| | Tension | 48.39 | 70.07 | 66.56 |
| Bottom Chord | Compression | -44.22 | -56.91 | -56.85 |
| | Tension | 31.40 | 29.41 | 42.97 |

A similar comparison is done for the vertical displacements and layovers of the exterior girder. Figure 4.46 shows that as with the stress predictions, the girder responses do not change for the different scenarios. The structure's performance is insensitive to the cross-frame modifications.

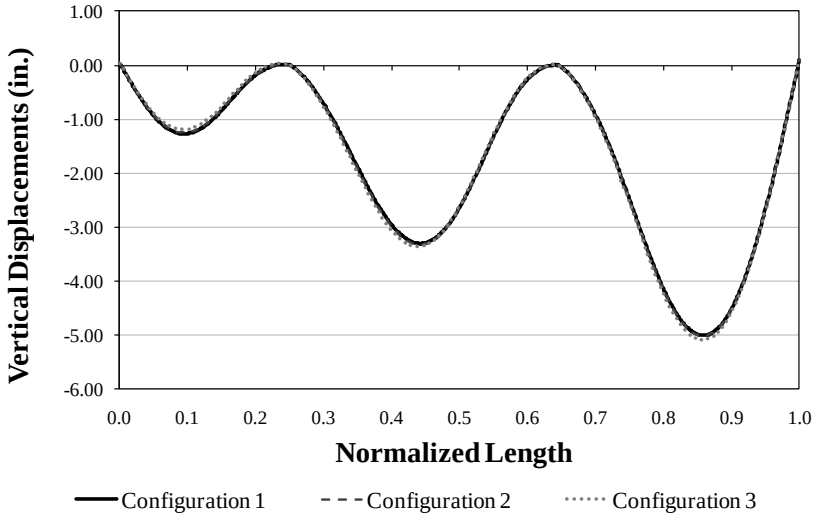


a) Vertical displacements

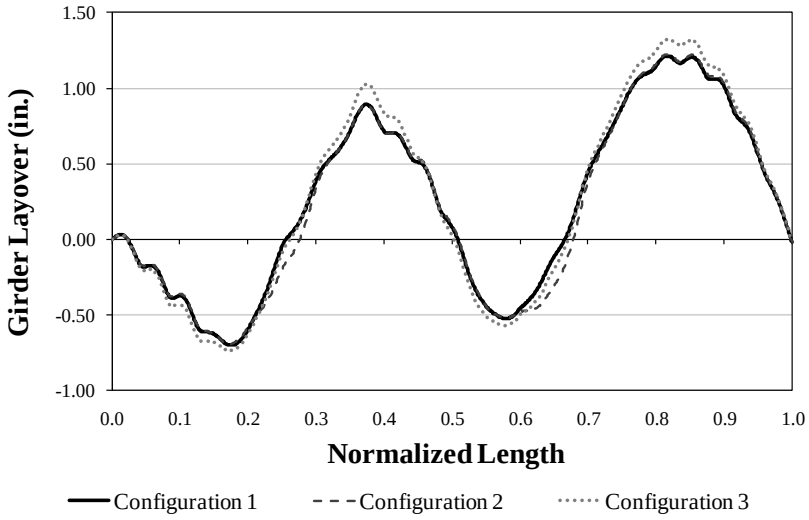


b) Girder layovers

Figure 4.46. Comparison of displacement predictions in the top flange of girder G1 of Bridge XICSS7

The results for this bridge show that the configurations of the cross-frames have a minimal impact in the structure's behavior. The system is insensitive to the removal of one of the diagonals or to the removal of the top chord. The explanation of the almost invariable behavior of the bridge is that these three cross-frame configurations are

effectively rigid compared to the stiffness properties of the girders and the overall structure. From these analyses, it is also important to notice that the forces in the cross-frame elements for Configurations 2 and 3 remain in a range considered as practical for design. Hence, the analyses reveal that the cross-frame designs can be refined without affecting the intended behavior of the system, while still keeping the cross-frame forces within acceptable levels. From a design perspective, the use of any of the first three options is sufficient in this bridge. With respect to economy, however, options two and three are the most efficient.

### 4.3.2. Case Study II: Simple Span Curved and Skewed I-Girder Bridge (EISCS3)

The next case study is the SR8002 Ramp A-1, King of Prussia, PA, introduced in Section 3.1.7. It is a single span curved bridge with a skewed support. Figure 4.47 depicts its layout and the parameters that define the geometry of the bridge. An important aspect of this bridge is that it has a severe staggered cross-frame pattern near the skewed support. As depicted in the layout of the structure, there are several cross-frames that are located close to one another near the left abutment. In this study, the intermediate cross-frames are modified to observe how the changes influence the behavior of the bridge; especially at the skewed end.

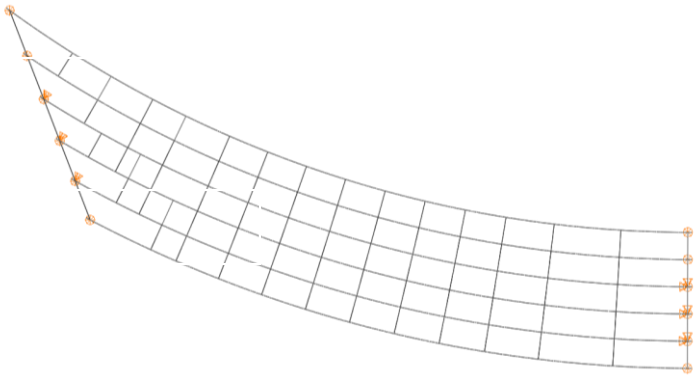

$L_1$ = 153 ft / $R$ = 279 ft / $w$ = 35.6 ft / $\theta_1 = 52.4^0$, $\theta_2 = 0^0$

Figure 4.47. EISCS3 Bridge Layout – Case Study 2

As in the previous case study, analyses were conducted for this bridge to assess the influence of different intermediate cross-frame configurations. Figure 4.48 shows the four studied designs. The first one is the as-built condition. The bridge was constructed with X-type intermediate cross-frames, V-type cross-frames at the left support, and diaphragms at the right support. For the next analysis, all the top chords of the intermediate cross-frames were removed. Since this is a simple span bridge, bracing is required at the top flanges along the entire length of the girders. This analysis was conducted to determine if the diagonals were sufficiently stiff to provide stability bracing and ensure the integrity of the structure during the deck placement. The third analysis was conducted removing both diagonals from the cross-frames located between girders G3 and G4. The intention was to separate the structure into two units that lean on each other through the intermediate horizontal struts. In this study, only the cross-frame in the first interior line between girders G3 and G4 was left with all its elements in place. The diagonals were not removed since there are no more cross-frames at that line where the

girders can lean on. Finally, a fourth analysis was conducted removing the majority of cross-frame diagonals between girders G2 and G3, G3 and G4, and G4 and G5. This is a scenario where a minimum number of intermediate cross-frames are left in the structure. The cross-frame distribution in this analysis is an extreme application of the lean-on bracing concept in bridges (Wang and Helwig, 2008).

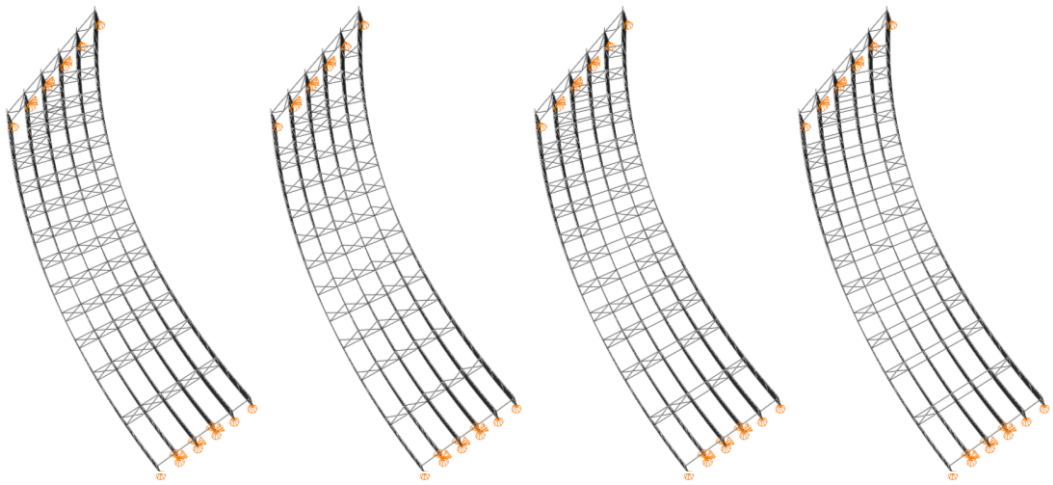

Figure 4.48. Intermediate cross-frame configurations implemented in the analyses – Case Study 2

The stress responses in the top flange in the exterior girder, G1, are shown in Figure 4.49. Similar responses are observed in the other five girders. As shown in the plots, the girder is insensitive to the variations in the cross-frame configurations used in the study. The larger differences are observed between the responses of the analyses conducted with Configurations 1 and 2 that compare the as-built structure versus the structure without top chords in the intermediate cross-frames.

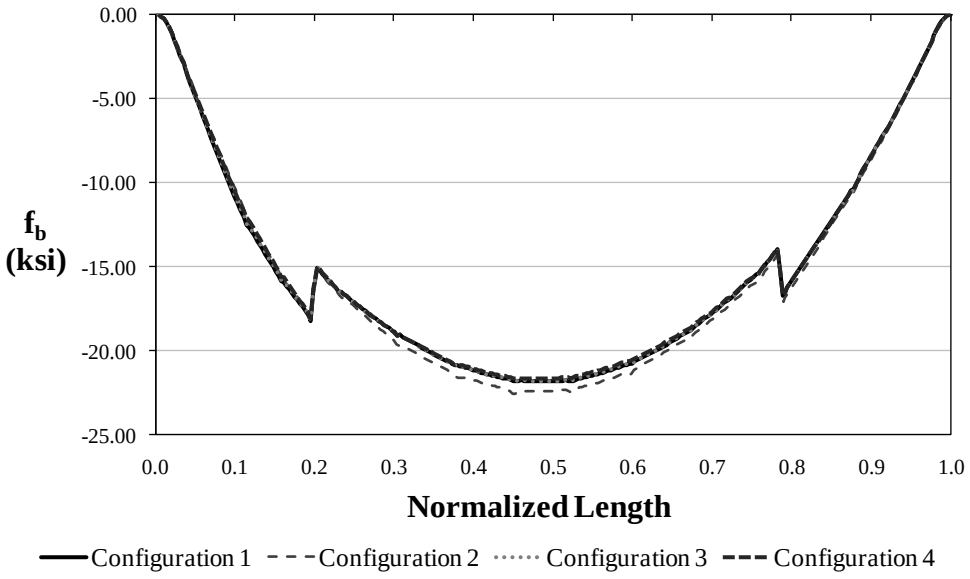


a) Major-axis bending stresses, $f_b$

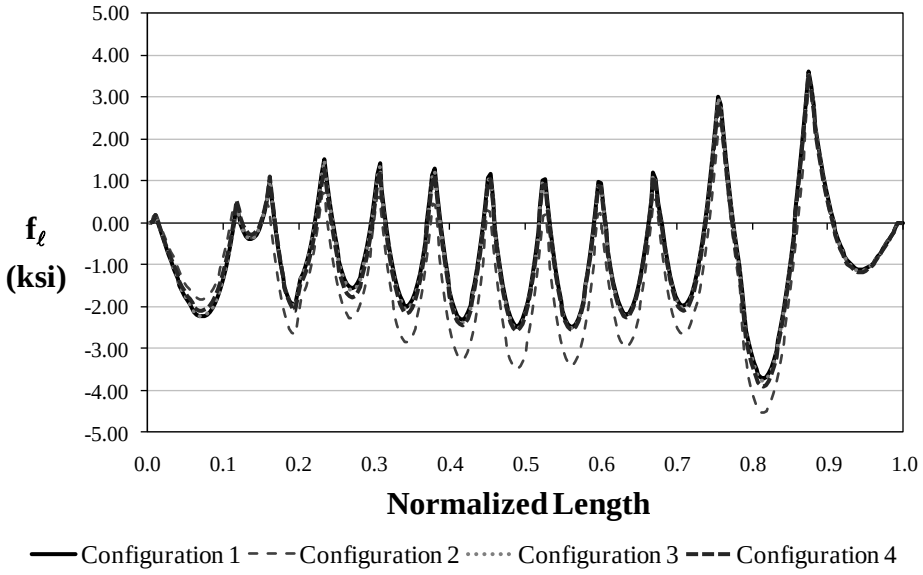


b) Lateral bending stresses, $f_\ell$

Figure 4.49. Comparison of stress predictions in the top flange of girder G1 of Bridge EISCS3

A comparison of the cross-frame forces is also necessary to determine the influence of the studied variations. As in Case Study 1, the maximum tension and

compression forces for the top chords, diagonals, and bottom chords are shown in Table 4.7. These values would be the required strengths used for the design of the cross-frames.

As observed in the table, the forces fluctuate between 93.57 kips in compression and 80.67 kips in tension. It is important to note that both values correspond to Configuration 2, where the top chords were removed from the intermediate cross-frames. As in the girder stress comparisons, this design is slightly more demanding than the others for the cross-frames. In all the cases, the stresses are within ranges that are suitable for design.

Table 4.7. Forces in the cross-frame elements (kips) – Case Study 2

| | Configuration | (1) | (2) | (3) | (4) |
|---|---|---|---|---|---|
| Top Chord | Compression | 44.14 | NA | 45.70 | 44.40 |
| | Tension | 48.56 | NA | 48.63 | 49.41 |
| Diagonals | Compression | 33.37 | 41.45 | 31.68 | 30.61 |
| | Tension | 34.37 | 80.67 | 33.07 | 29.68 |
| Bottom Chord | Compression | 50.32 | 93.57 | 50.47 | 48.29 |
| | Tension | 49.49 | 60.00 | 46.64 | 48.51 |

A comparison of the girder vertical displacements and layovers is shown in Figure 4.50. These plots show the minor influence that the different configurations have on the behavior of the bridge. An important aspect of the layover plots is that for the cases where the bracing system is modified, there is no substantial increase in the girder rotations with respect to the original configuration. This indicates that all the configurations provide adequate stability bracing to the girders since large rotations are associated with an unstable condition of the system.

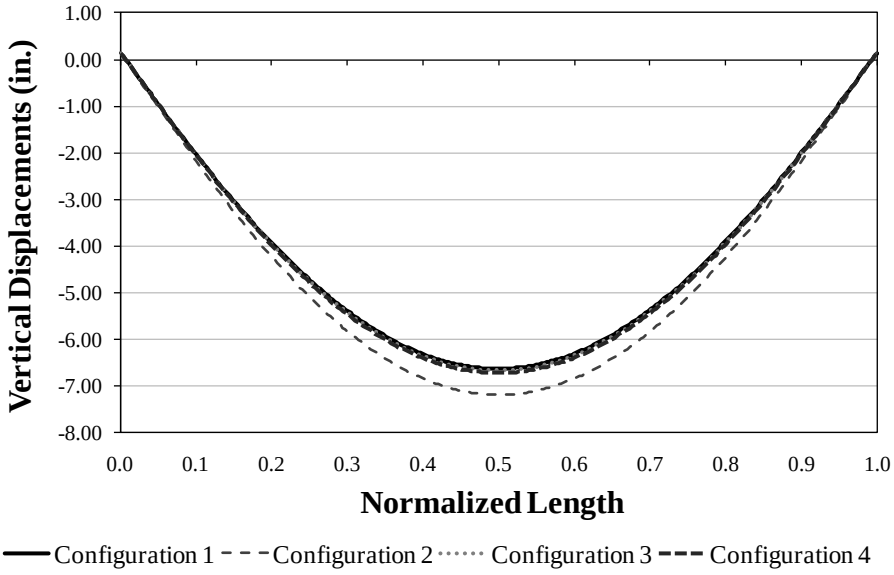


a) Vertical displacements

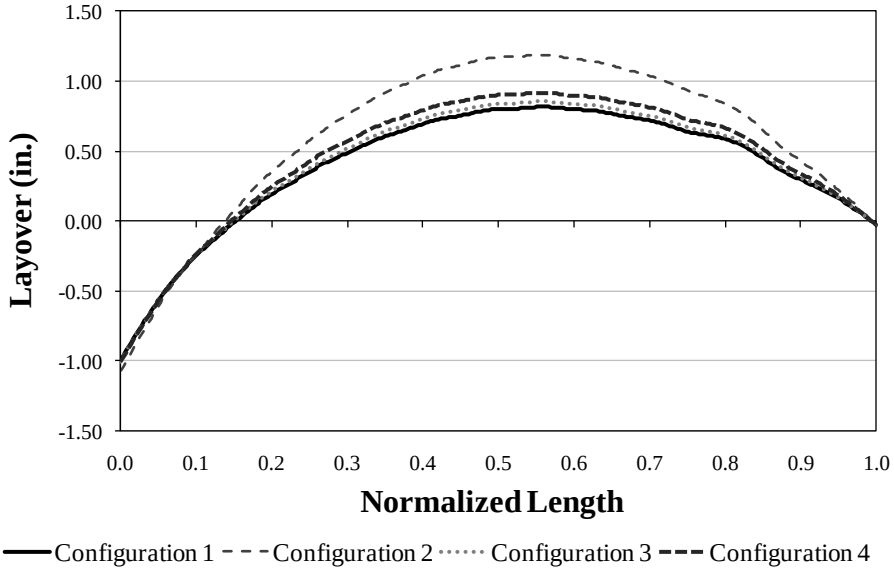


b) Layovers

Figure 4.50. Comparison of displacement predictions in the top flange of girder G1 of Bridge EISCS3

The above comparisons show that any of the studied configurations can be used in the design of the bridge without affecting its structural behavior significantly. However,

the number of intermediate cross-frames that would be used for the analysis with Configuration 1, 65, can be reduced to 51 or 30, if either Configuration 3 or 4 is chosen, respectively. The complication with implementing the lean-on systems proposed for Configurations 3 and 4 is that it is more difficult to predict and control the profile of the structure during the deck placement. For this reason, Configuration 2 is considered as the optimum solution among the four possibilities. The bracing properties of this configuration are sufficient to stabilize the girders, and as shown in Section 4.2.2.2 is a potential solution to relax the undesired transverse stiffness of the bridge during its construction.

### 4.3.3. Case study III: Simple span straight and skewed I-girder bridge (EISSS3)

The last case study is the SR1003 (Chicken Road) bridge over US 74, Robeson Co., NC, introduced in Section 3.1.2. The layout of the structure is shown in Figure 4.51. This bridge was instrumented to monitor its behavior during construction. The field measurements and the analytical studies are documented in Morera (2010). A particular aspect of this bridge is that the intermediate cross-frames are inverted V-type without top chords. The flexural stiffness of this type of cross-frame is substantially smaller than in any other configuration; therefore, its ability to provide stability bracing needs to be investigated during the design process.

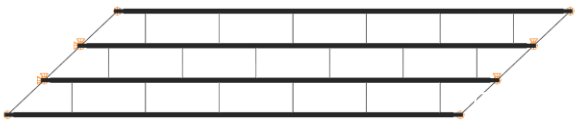

$L$ = 133 ft / $w$= 30.1 ft / $\theta_1 = 46.2^0$, $\theta_2 = 46.2^0$

Figure 4.51. EISCS3 Bridge Layout – Case Study 3

To investigate the influence of the top chord on the structural behavior, two cross-frame models were considered. In the first analysis, the bridge is modeled to represent the as-built condition, without intermediate cross-frame top chords. In the second analysis, the top chords are included. Figure 4.52 shows the 3D view of both models.

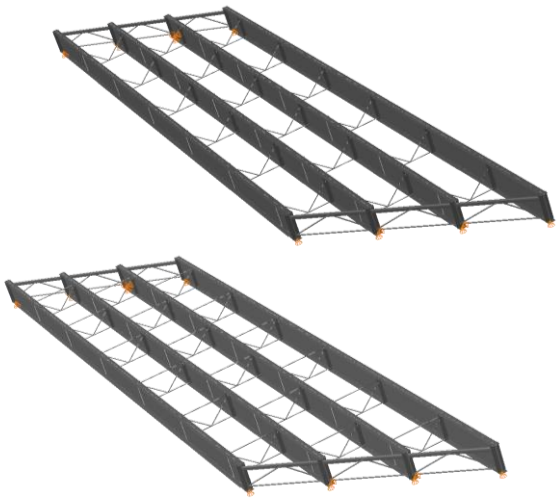

Figure 4.52. Intermediate cross-frame configurations implemented in the analyses – Case Study 3

As observed in the stress and layover plots for the fascia girder, G1, in Figure 4.53, the flange lateral bending response of the bridge is severely affected by the presence of the top chord. The results from the analysis conducted with the first configuration shows that large lateral displacements may occur in this girder due to the lack of bracing in the top flange. Similarly, the levels of flange lateral bending stress are very high in the segment between 0.30 and 0.65 of the girder length. These two responses indicate that if the incidental contributions from components such as stay-in-place forms, ties between the girders provided by the contractor, and other devices provided to facilitate the concrete placement are not considered, the bridge exhibits substantial second order

amplifications, at the TDL level. The influence of these non-structural components on the behavior of I-girder bridges is studied in detail in Chapter 6.

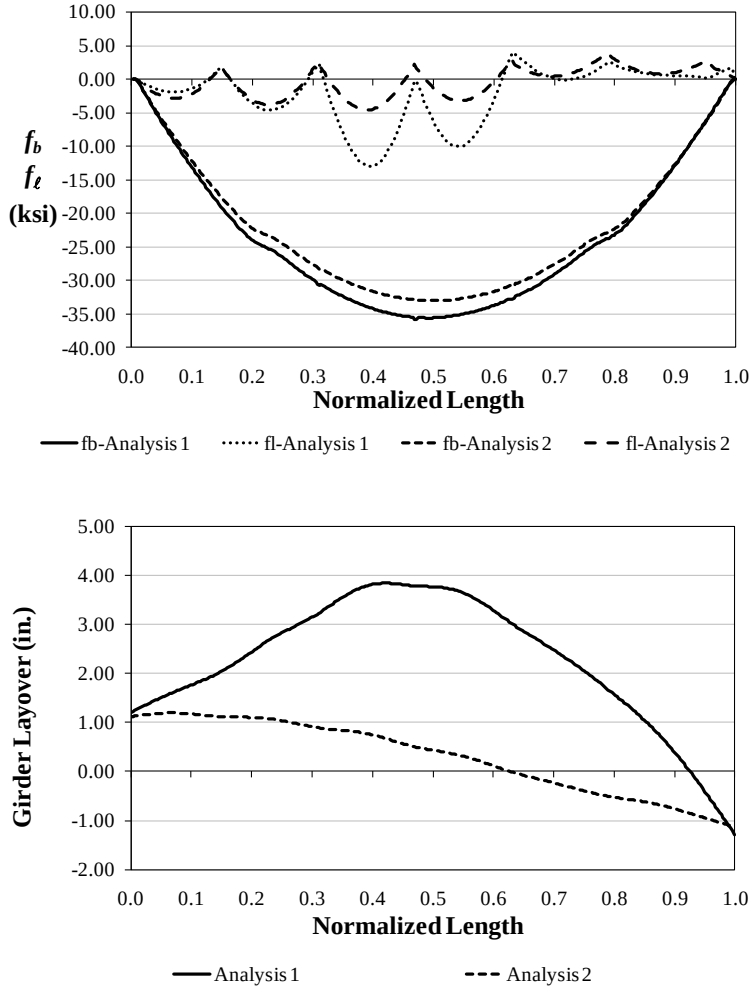


Figure 4.53. Comparison of stresses and layovers in girder G1 – Case 3

As discussed in Morera (2010), the stay-in-place metal deck forms had a significant participation in the deflected geometry of this bridge. It is possible that this observation is a consequence of the relatively small stability bracing provided by this cross-frame configuration. As shown in the results of the analysis conducted with

Configuration 2, the bridge does not exhibit large flange lateral bending responses when it is properly braced.

The results of the analyses conducted for this bridge demonstrate that the absence of the top chord in the V-configuration changes the structural behavior significantly. The lack of these bracing elements in the top flange of the I-girders increases their susceptibility to stability problems. This is of particular importance during the deck placement, when the construction loads are supported only by the steel structure. As a result, lateral deflections, susceptibility to lateral-torsional buckling, and magnification of the second order effects can occur. At this point, the performance and influence of nonstructural elements not considered in the design need to be examined. Namely, the stay-in-place metal deck forms, the formwork, and other attachments done to facilitate the construction may contribute to prevent the system from failure. Since the stiffness contributions from these components may vary widely even for situations where the components are nominally the same, this can result in significant sensitivities of the bridge responses during construction. Careful consideration should be given when relying on these elements for structural purposes. At the current time (2011), Section 6.7.4.1 of AASHTO (2010) prohibits the use of the metal deck forms as a means to provide bracing during construction.

### 4.3.4. Summary of the Influence of Cross-Frame Configurations on the Behavior of I-Girder Bridges

The studies conducted in the above three bridges demonstrate that the cross-frames have fundamental roles on the behavior of curved and/or skewed I-girder bridges. The two first cases reveal that modifications that reduce the number of elements in the

cross-frame can be implemented without modifying the system response. The changes in the bridge behavior due to modifications in the cross-frames configuration can be negligible if a distribution that provides adequate bracing is identified. In skewed bridges, the use of an X-type cross-frame without a top chord is a modification that can be implemented to achieve a better structural performance. The results obtained for the bridges analyzed in this section and the case study discussed in Section 4.2.2.2 show that this configuration provides the stiffness to brace the girders and relaxes the transverse stiffness of the structure. However, although in the two curved bridges analyzed in this section, the X-type cross-frame without top chord proved to be an efficient solution, the use of this configuration should be limited for use in straight and skewed structures. The main reason is that in highly curved bridges the load transfer that occurs from the interior girder to the exterior girder (i.e., the V-loads and the corresponding horizontal forces) can be too large for the X-type cross-frame without top chord to perform properly.

Another cross-frame configuration that is commonly used is the V-type cross-frame without top chords. However, the practice of removing the top chord in V-type cross-frames, as shown for the third case study, can affect severely the structural performance. The elimination of the top chord in girders connected with this type of cross-frames may result in large response amplifications due to second order effects. The reason is that with this modification, the cross-frames lose their ability to provide efficient bracing since their in-plane stiffness is reduced drastically. The structural stability of a bridge of these characteristics during the deck placement may depend on other factors such as the contribution of the metal deck forms, as discussed in Chapter 6.

# CHAPTER V

# IMPROVEMENTS FOR THE ANALYSIS OF I-GIRDER BRIDGES USING 2D-GRID MODELS

A general description of 2D-grid models was presented in Section 4.1.2. In the present section, the 2D-grid analysis techniques are studied in more detail. The current methods commonly used in practice to construct a grid model for the analysis and design of steel I-girder bridges are discussed first to highlight their limitations and how they can affect the response predictions. Next, improved modeling techniques that can be implemented in 2D-grid analysis software for a better representation of the structural behavior of I-girder bridges are introduced.

## 5.1. Analytical Representation of the Torsion Properties in I-Sections

In a thin-walled open-section member, there are two contributions to the torsional resistance, namely the St. Venant or pure torsion resistance and the flange warping resistance. Horizontal curvature, support skew, and overhang eccentric loads subject steel I-girders to torsion. Hence, capturing properly the torsion properties in a curved and/or skewed steel I-girder bridge is essential to obtain an accurate prediction of the structure's performance during construction. Unfortunately, most of the commercial software packages used to construct 2D-grid models do not have the ability to properly represent the torsion properties of I-section girders. Generally, they only implement the St. Venant torsion component, which results in a misrepresentation of some of the structural responses of interest during the structure's construction for the reasons discussed next.

Consider a cantilever beam subject to the external torque, $M_z$, shown in Figure 6.1(a). Due to the applied torque, the free end of the beam rotates an angle $\phi$, and the flanges displace laterally the quantity $u_f = \phi \cdot h/2$, assuming small rotations, where $h$ is the distance between flange centroids. In the I-section beam, the total internal torque is equal to

$$M_z(z) = M_s(z) + M_w(z) \qquad \text{(Eq. 5.1)}$$

The first component, $M_s$, corresponds to the Saint Venant torsion; the second component, $M_w$, is the warping torsion. The first component is defined as

$$M_s(z) = GJ\frac{d\phi}{dz} \qquad \text{(Eq. 5.2)}$$

where $G$ is the steel shear modulus of elasticity and $J$ is the torsion constant of the girder cross-section. To obtain the warping contribution to the internal torque, it is necessary to analyze the flanges as if they were subjected to lateral bending. The warping torque along the longitudinal axis of the beam, $z$, can be decomposed and represented by a force couple such that $M_w(z) = V_\ell(z) \cdot h$. Hence, the forces $V_\ell(z)$, which have an opposite sign in each flange, subject the flanges to lateral bending (see Figure 5.1(b)).

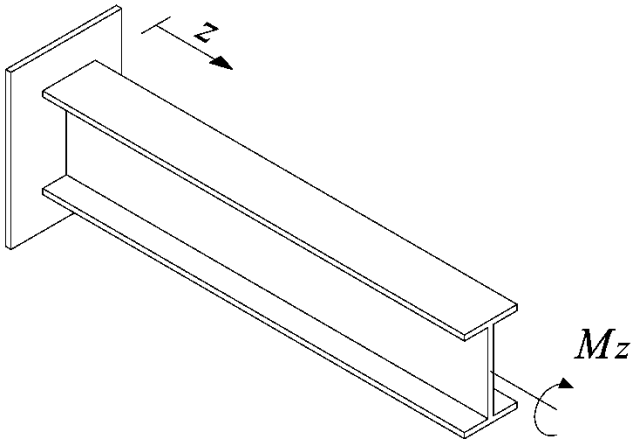


(a) Cantilever beam subject to torque $M_z$

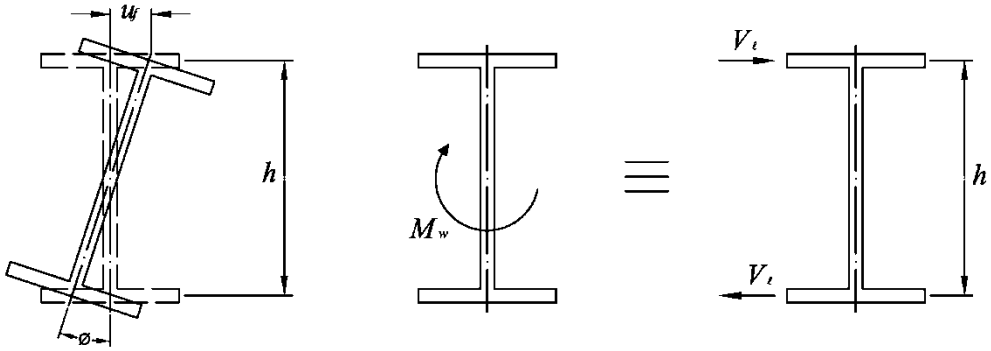


(b) Decomposition of the warping moment, $M_w$, in an equivalent force couple

Figure 5.1. Warping torsion in a cantilever beam

The governing differential equation for bending in one of the flanges is used to determine the flange lateral bending moment, $M_\ell(z)$, and the shear force $V_\ell(z)$,

$$EI_f \frac{d^2u_f(z)}{dz^2} = EI_f \frac{h}{2}\frac{d^2\phi(z)}{dz^2} = -M_\ell(z) \qquad \text{(Eq. 5.3)}$$

$$V_\ell = \frac{dM_\ell(z)}{dz} = -EI_f \frac{h}{2}\frac{d^3\phi(z)}{dz^3} \qquad \text{(Eq. 5.4)}$$

where $E$ is the modulus of elasticity of the steel, and $I_f$ is the flange moment of inertia about the strong axis. Hence, the warping torsion component is

$$M_w = V_\ell h = -EC_w \frac{d^3\phi(z)}{dz^3} \quad \text{(Eq. 5.5)}$$

In the above equation, $C_w$ is the warping constant, which is defined as

$$C_w = I_f \frac{h^2}{2} \quad \text{(Eq. 5.6)}$$

The governing differential equation in a straight I-section girder subject to torsion is found by substituting Eqs. 5.2 and 5.5 in Eq. 5.1 such that

$$M_z(z) = GJ \frac{d\phi}{dz} - EC_w \frac{d^3\phi(z)}{dz^3} \quad \text{(Eq. 5.7)}$$

As shown in Eq. 5.7, the twist angle and the applied torsion moment in an I-section beam are related through a third order linear differential equation. This equation is not suitable for implementation using an element with six dofs per node. Hence, an alternate solution is to ignore the term related to flange warping, and assume that the response is dominated by St. Venant's torsion. With this simplification, the governing differential equation is reduced to

$$M_z(z) = GJ \frac{d\phi}{dz} \quad \text{(Eq. 5.8)}$$

If the applied torque is constant, Eq. 5.8 can be integrated over the beam length (or bracing points) to obtain a linear relationship between $M_z$, and $\phi$, so that

$$M_z = \frac{GJ}{L}\phi \quad \text{(Eq. 5.9)}$$

The term $GJ/L$ is the torsional stiffness of the beam ignoring the warping contribution. The coefficients needed to formulate the stiffness matrix of a beam or frame element can be formulated with the torsional stiffness represented in this form. This is the

methodology used in most of software packages to develop the elements used to analyze I-girder bridges.

In members with closed hollow sections, pure torsion dominates the response, so the warping effects are minor. Contrary to closed-type shapes, in an I-section beam the torsion resistance is dominated by flange warping. In general, in members with thin-walled open sections, the effects of warping must be included to properly capture the torsion response. Curved and skewed steel I-girder bridges are inherently subjected to torsion. Therefore, the accuracy of the results obtained from the 2D-grid analysis of a curved and/or skewed bridge can be affected by the assumptions considered when representing the girder torsional stiffness. In Section 5.4 several cases of bridge structures are studied to observe the influence of the torsion models on the behavior of curved and skewed I-girder bridges predicted with 2D-grid analyses.

A better representation of the I-girder torsion properties is implemented in some computer programs via an additional dof that is provided at each node of the frame element, as shown in Figure 5.2. This type of element has seven dofs per node, and it is formulated based on thin-walled open-section beam theory (TWOS). The torsional response is represented by the torsional rotation dofs $u_4$ and $u_{11}$ and by the flange warping dofs $u_7$ and $u_{14}$. Chang (2006), Huang (1996) and others have demonstrated that an element formulated with 14 dofs that includes the warping deformations can be used to construct grid models that accurately represent the physical behavior of curved and skewed I-girder bridges. The Engineer must be warned that in exceptional cases, the TWOS element does not provide the same results as a 3D FEA analysis, where the flexibility of the girder webs is captured using shell elements (Chang 2006). The TWOS

formulation used in the 14-dof elements generally does not account for distortion of the I-girder webs into an S-shape. However, except for the torsional response of composite girders in their final constructed condition, web distortion typically has a a minor effect on the structural response. When the concrete deck of a composite girder hardens, it restrains the lateral displacement of the top flange, while the bottom flange is still able to move due to the web out-of-plane flexibility. Hence, the lateral displacements and lateral bending stresses, $f_\ell$, may not be properly captured in the bottom flange by the TWOS analysis. As discussed in Chang (2006), other complexities that are difficult to handle in the implementation of TWOS analysis include the modeling of the continuity conditions at cross-section transitions and at bifurcated girders (three girder elements framing into a common node).

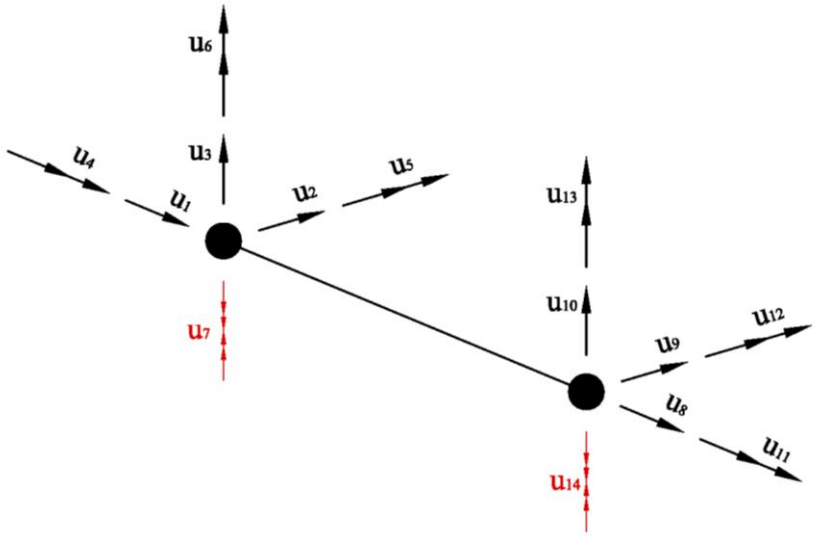


Figure 5.2. Two-node element with 14 dofs implemented in computer programs to represent the torsional properties of an I-girder in 2D-grid models

Another technique that can be implemented to better capture the torsional properties of an I-girder in a 2D-grid model is the use of an equivalent torsion constant, $J_{eq}$, as proposed by Ahmed and Weisgerber (1996). The determination of the equivalent torsion constant is discussed next. The general solution of the governing differential equation when the applied torque is constant between the beam supports (or bracing points) is

$$\phi(z) = \frac{M_z z}{GJ} + A_1 \sinh(pz) + A_2 \cosh(pz) + A_3 \qquad \text{(Eq. 5.10)}$$

in which

$$p^2 = \frac{GJ}{EC_w} \qquad \text{(Eq. 5.11)}$$

In Eq. 5.11, the constants $A_1$, $A_2$, and $A_3$, depend upon the end boundary conditions. For a beam with the flanges fixed against at warping at its ends, these boundary conditions are $\phi(0) = 0$ and $\phi'(0) = \phi'(L) = 0$. Applying these boundary conditions to Eq. 5.10 gives the following results:

$\phi(0) = 0$: $\quad A_2 + A_3 = 0$

$\phi'(0) = 0$: $\quad A_1 p + \frac{M_z(z)}{GJ} = 0$

$\phi'(L) = 0$: $\quad A_1 p \cosh(pL) + A_2 p \sinh(pL) + \frac{M_z}{GJ} = 0$

and

$$A_1 = -\frac{M_z}{GJp}$$

$$A_2 = \frac{M_z}{GJ}\frac{\cosh(pL)-1}{p\sinh(pL)}$$

$$A_3 = -\frac{M_z}{GJ}\frac{\cosh(pL)-1}{p\sinh(pL)}$$

Substituting the constants $A_1$, $A_2$, and $A_3$ in Eq. 5.10, the twist angle in a beam with warping fixed flanges and subjected to a constant torque is equal to

$$\phi(z) = \frac{M_z z}{GJ} - \frac{M_z}{GJp}\sinh(pz) + \frac{M_z}{GJ}\frac{\cosh(pL)-1}{p\sinh(pL)}\cosh(pz) - \frac{M_z}{GJ}\frac{\cosh(pL)-1}{p\sinh(pL)} \quad \text{(Eq. 5.12)}$$

From the above equation, the relative angle of rotation between the beam ends is

$$\phi = \frac{M_z}{GJ}\left[L - \frac{\sinh(pL)}{p} + \frac{\cosh(pL)-1}{p\sinh(pL)}\cdot\cosh(pL) - \frac{\cosh(pL)-1}{p\sinh(pL)}\right] \quad \text{(Eq. 5.13)}$$

or

$$\phi = M_z\frac{L}{GJ_{eq}} \quad \text{(Eq. 5.14)}$$

where $J_{eq}$ is the equivalent torsion constant for the case where flange warping is fully fixed at the beam ends, defined as

$$\begin{aligned} J_{eq(fx-fx)} &= J\left[1 - \frac{\sinh(pL)}{pL} + \frac{\cosh(pL)-1}{pL\sinh(pL)}\cdot\cosh(pL) - \frac{\cosh(pL)-1}{pL\sinh(pL)}\right]^{-1} \\ &= J\left[1 - \frac{\sinh(pL)}{pL} + \frac{\left[\cosh(pL)-1\right]^2}{pL\sinh(pL)}\right]^{-1} \end{aligned} \quad \text{(Eq. 5.15)}$$

With the equivalent torsion constant, $J_{eq(fx\text{-}fx)}$, it is possible to simulate the torsional stiffness of an I-girder with warping-fixed ends. This equivalent torsional

stiffness provides the linear relationship between the rotation angle and the applied torque required to determine the torsional stiffness coefficient. Notice that it is possible to directly obtain the stiffness coefficient from Eq. 5.14 by inverting the torsional flexibility because the torsion response is not coupled to any other dof of the frame element.

The above derivation generally provides a significantly improved estimate of the torsional rigidity of the girder segments between any two intermediate cross-frames. However, at the girder ends, the flanges are free to warp. For the end segments, defined between the exterior and the first interior cross-frame, the equivalent torsion stiffness could be determined assuming that at the segment ends, the warping boundary conditions are free-fixed. For this case, the boundary conditions necessary to determine the constants $A_1$, $A_2$, and $A_3$ are $\phi(0) = 0$ and $\phi''(0) = \phi'(L) = 0$. Applying these boundary conditions to Eq. 5.10 gives the following results:

$\phi(0) = 0$: $A_2 + A_3 = 0$

$\phi''(0) = 0$: $A_2 p^2 = 0$

$\phi'(L) = 0$: $A_1 p \cosh(pL) + \frac{M_z}{GJ} = 0$

and

$$A_1 = -\frac{M_z}{GJ}\frac{1}{p\cosh(pL)}$$

$$A_2 = A_3 = 0$$

Substituting these constants in Eq. 5.10, the rotation angle in a beam with free-fixed warping conditions subject to a constant torque is equal to

$$\phi(z) = \frac{M_z z}{GJ} - \frac{M_z}{GJ}\frac{\sinh(pz)}{p\cosh(pz)} \qquad \text{(Eq. 5.16)}$$

and

$$\phi = \frac{M_z L}{GJ}\left(1 - \frac{\sinh(pL)}{pL\cosh(pL)}\right) \qquad \text{(Eq. 5.17)}$$

Therefore, for an exterior girder segment, the equivalent torsion constant is equal to

$$J_{eq(fr-fx)} = J\left(1 - \frac{\sinh(pL)}{pL\cosh(pL)}\right)^{-1} \qquad \text{(Eq. 5.18)}$$

The implementation of the equivalent torsion constant represents a simple method to approximately capture the torsion properties of I-girders. For the analysis of an I-girder bridge, $J_{eq}$ is calculated taking $L$ as the distance between the cross-frames. Then the torsion constant $J$ can be redefined using the calculated value of $J_{eq}$. With this technique, the 12-dof frame element or the 6-dof grid element available in commercial programs can be used to construct traditional 2D-grid models that are a closer representation of the real structure than the models constructed using current practices, where the flange warping contributions are neglected.

Even though the use of the equivalent torsion constant represents a potential improvement for 2D-grid modeling techniques, it has two limitations that have to be considered. The first limitation is that, in reality, warping is not fully fixed at the girder bracing points (i.e., the relative flange lateral bending rotations are not zero at the bracing locations). In a particular flange segment defined by the distance between bracing points,

warping restraint is provided by the continuity with adjacent segments. In reality, at the segment ends, the flange warping resembles a partially restrained condition. Unfortunately, it is not practical to provide further guidelines on how to determine the equivalent torsion coefficient other than assuming fixed-fixed warping for interior girder segments and free-fixed for the exterior segments. In general, it is not feasible to capture the girder torsional stiffness exactly unless the actual flange warping displacements at the nodes of the analysis model are known. However, as shown in Section 5.4, the response predictions obtained from 2D analyses with equivalent torsion constants calculated based on fixed-fixed and pinned-fixed warping conditions are significantly more accurate than the responses obtained from analyses that ignore the warping contributions for bridges with challenging geometries and complex bracing systems.

The other limitation pertains to the unbraced length required to compute the equivalent torsion constant. Figure 5.3 shows some variations in the cross-frame layout that are commonly used in steel bridges. For the calculations, it is assumed that the unbraced length is defined as the distance between cross-frames, regardless of whether there are cross-frames on both sides of the web (contiguous pattern) or on only one side (staggered pattern). Hence, for Segments 1 and 2, the equivalent torsion constant computed with Eqs. 5.15 is the same since $L_{b1} = L_{b2} = L$. Clearly, the end conditions at the ends of Segment 1 are not the same as in the right end of Segment 2. In the later segment, the warping constraint will deviate from the fully-fixed condition more than when the girder is braced with contiguous cross-frames. Furthermore, the distance between cross-frames varies depending on how the Engineer configures the bracing system in the bridge. For instance, Segments 2 and 3 have different unbraced lengths, so

an equivalent torsion constant should be determined for each segment. In a skewed bridge, different unbraced lengths are common near the skewed supports, as shown in the case studies presented in the previous sections. Therefore, it is necessary to compute a $J_{eq}$ for each of the different unbraced lengths.

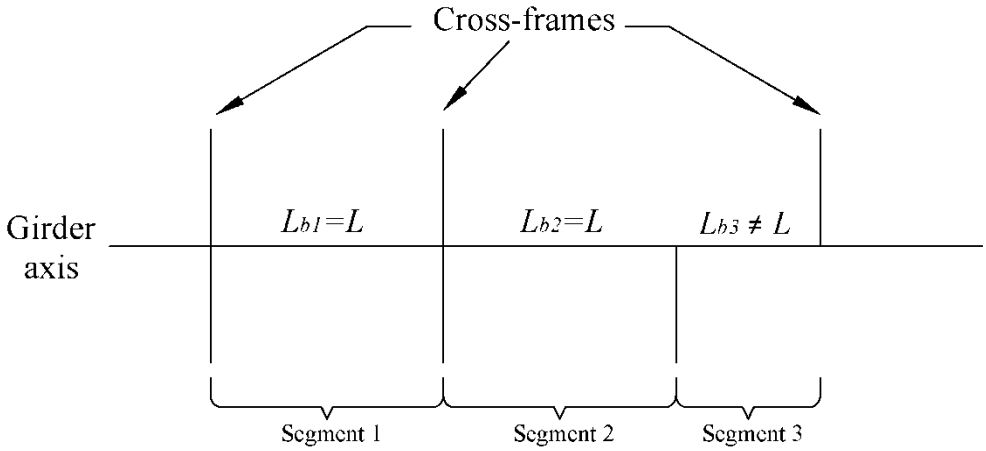


Figure 5.3. Definition of unbraced length for computation of the effective torsion constant, $J_{eq}$

### 5.1.1. Influence of the Girder Torsion Model in the Prediction of Flange Lateral Bending Responses and Cross-Frame Forces

As stated in the previous section, the torsion model used in the 2D-grid analyses may have a considerable influence on the predicted behavior of a steel I-girder bridge. This impacts the prediction of the cross-frame forces. Figure 5.4 shows that the bending dofs for the cross-frames correspond to the torsional dofs of the girders. Only these rotational dofs are shown in the figure to simplify the sketch. Nodes 2 and 3 are connected; therefore, the bending moments in the cross-frames, $M_{1\text{-}CF}$, and the torsional moments in the girders, $T_{2\text{-}G}$, must balance with one another at this common joint. The joint depicted in the figure can represent the behavior at the end bearing-line cross-frames

of a bridge, but in general, other girder and cross-frame elements may be connected into this common joint.

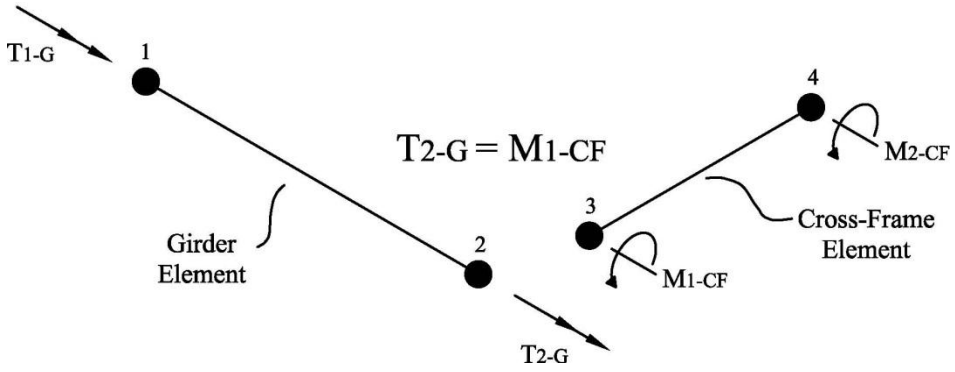


Figure 5.4. Interaction between the torsion dofs in the girders and the major-axis bending dofs in the cross-frames

Generally, due to the limited capabilities of 2D-grid models to represent the actual torsional stiffness of the bridge girders, the results obtained for $T_{2\text{-}G}$ and $M_{1\text{-}CF}$, will defer from their physical values. This is because of the overall coupling of the stiffnesses between the girders and the cross-frames in the structural analysis model. It is clear that if only the pure torsion contribution is included in the element formulation, the torsional stiffness of the girders in the model will be significantly smaller than the torsional stiffness of the real girders. Hence, the torsion moments predicted in the girder element shown in the figure, $T_{1\text{-}G}$ and $T_{2\text{-}G}$, will be much smaller than in the physical girders. From equilibrium, the girder torsional moment is equal to the cross-frame major-axis bending moment, $M_{1\text{-}CF}$. If the torsional response in the girders is not properly captured, the associated cross-frame element forces cannot be captured either.

The poor estimate of the cross-frame bending moments not only results in a false prediction of the cross-frame forces. Also, it results in a poor prediction of the girder

flange lateral bending stresses, and in some cases, the major-axis bending responses. A decomposition of the joint forces obtained from the 2D-grid model show the effects of not capturing the cross-frame moments properly. Figure 5.5 shows the equivalence between the nodal forces obtained from a 2D-grid analysis and the element forces in the physical cross-frame. As shown in the figure, the forces, *P*, *V* and *M*, at Joints *i* and *j* are decomposed in the *element* forces $F_{TC1}$, $F_{BC1}$, $F_{D1}$, and $F_{D1}$. Also, the *nodal* forces, *A, B, C*, and *D* that act at the connections between the cross-frames and the girders can be calculated from the element forces. In an analysis where only the noncomposite dead load is applied to the structure, the axial joint forces, $P_i$ and $P_j$, obtained from the 2D-grid analysis, are generally negligible since there are no external lateral forces that act in the system. Hence, the accuracy of the computed *element* and *nodal* forces depends on the accuracy of the shears and moments obtained from the analysis. Since the bending moments in the cross-frames depend on how the grid model captures the torsional response of the girders, the element and nodal forces also depend on this parameter. If the torsional stiffness model of the girders is based only on the pure torsion contributions, ignoring the flange warping component, the joint shears and moments, *V* and *M*, the cross-frame element forces, and the nodal forces will be underestimated.

As discussed in Section 4.2, the horizontal components of the nodal forces cause the lateral bending of the flanges and the associated girder layovers and $f_\ell$ stresses; while the vertical components add to the gravity loads to define the major-axis bending response of the girders. For this reason, given that the horizontal components of the nodal forces at the cross-frame locations are necessary to evaluate the flange lateral bending

stresses, a poor prediction of the girder torsional response would result in a misrepresentation of the $f_\ell$ stresses.

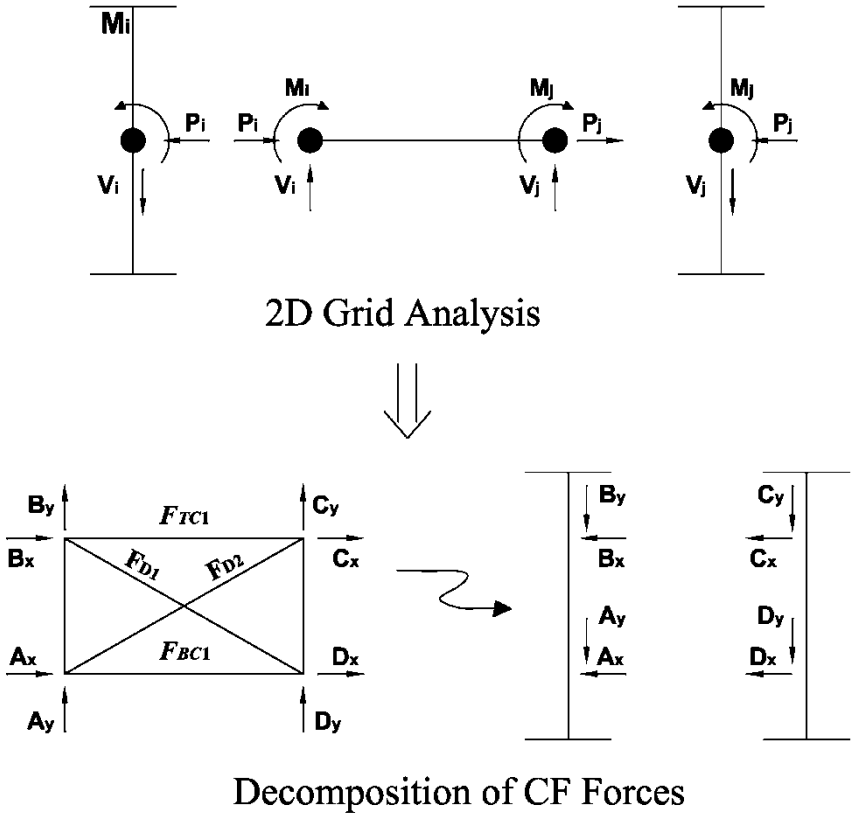


Figure 5.5. Decomposition of cross-frame forces from the results obtained from a 2D-grid analysis

Because of the above reasons, the cross-frame forces are severely underestimated with the current practices used to conduct 2D-grid analyses. This is illustrated by the case studies presented in Section 5.4. Therefore, common 2D-grid models of skewed bridges are not able to capture the flow of the transverse forces due to the skew effects (see Section 4.2.2). This is a substantial limitation of the 2D-grid models. The analysis does not highlight possible structural complications that may result due to large cross-frame forces or high levels of $f_\ell$ stresses.

Besides affecting the predictions of the flange lateral bending response and the cross-frame forces, a poor representation of the girder torsion stiffness can also affect the overall behavior prediction of the structural system. In a bridge, the cross-frames are the components that link the girders to make them work as a system rather than as individual elements. However, in 2D analyses where the warping torsion contributions are ignored, the interaction between the girders and the cross-frames is not accurately captured. In fact, as discussed in detail in Section 5.4, the response predictions obtained from a 1D line-girder analysis of a straight and skewed bridge, which has no information regarding the contributions of the cross-frames to the system response, does not differ significantly from the predictions obtained from a 2D-grid analysis. Hence, in a 2D model constructed with a poor representation of the girder torsion rigidity, the girders behave as if they were disconnected, or the cross-frames where not present in the model.

The above discussion highlights the importance of implementing a more realistic representation of the girder torsional properties that not only captures the contribution from pure torsion but also the warping contributions. The most accurate results could be obtained from an analysis where the girders are modeled using 14-dof elements. Alternatively, the substitution of the girder torsion constant, $J$, by the equivalent torsion constant, $J_{eq}$, is a simple method that can be used in traditional grid models to alleviate these limitations and improve the response predictions, as shown in the case studies presented in Section 5.4.

## 5.2. Representation of Cross-Frames in 2D-Grid Models

In this section, the modeling techniques used to represent the cross-frames in 2D-grid analyses are studied. First, the current practices are presented and analyzed, emphasizing on their accuracy and their limitations in representing the physical behavior of the cross-frames in a bridge. Next, two-node elements that capture the physical behavior of the X-type, V-type and inverted V-type cross-frames are developed and implemented in a commercial program used for the design of steel bridges.

### 5.2.1. Cross-Frame Modeling Techniques Currently used in 2D-Grid Models

In current 2D-grid analysis, the cross-frames are modeled using the same type of element used to model the girders. The frame element based on the Euler-Bernoulli beam theory is commonly used to represent what in reality is a group of elements with the configuration of a truss. Figure 5.6 shows the 2D-grid model and 3D FEA representation of Bridge XICSS7. As shown in the figure, the chords and diagonals that constitute the cross-frame are modeled as a single line element. The section properties of the line element used to represent the cross-frames are determined using ad hoc procedures, such as discussed in Coletti and Yadloski (2007) and NHI/FHWA (2011).

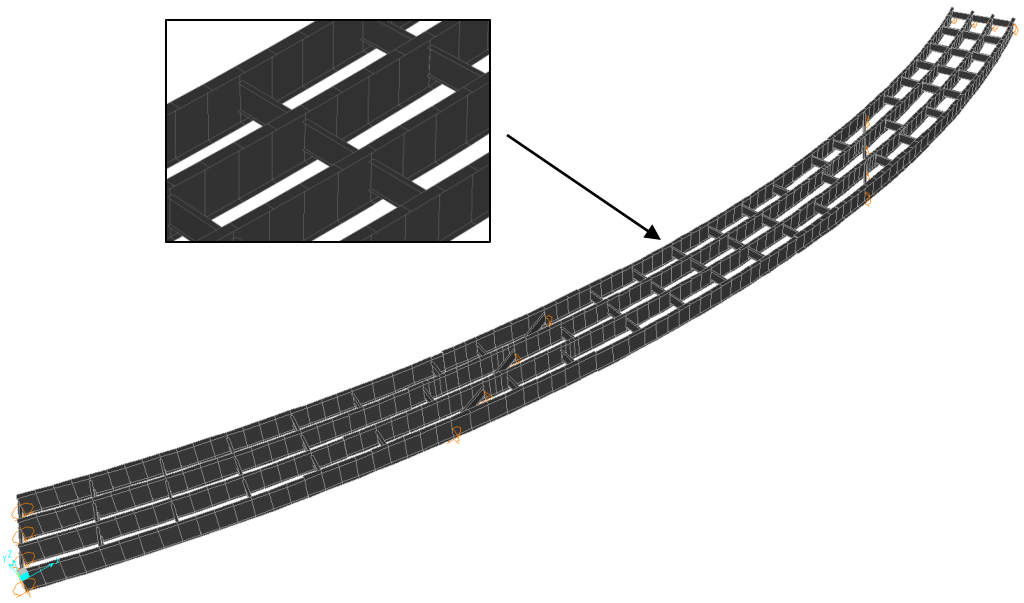

a) 2D Grid model (rendered view)

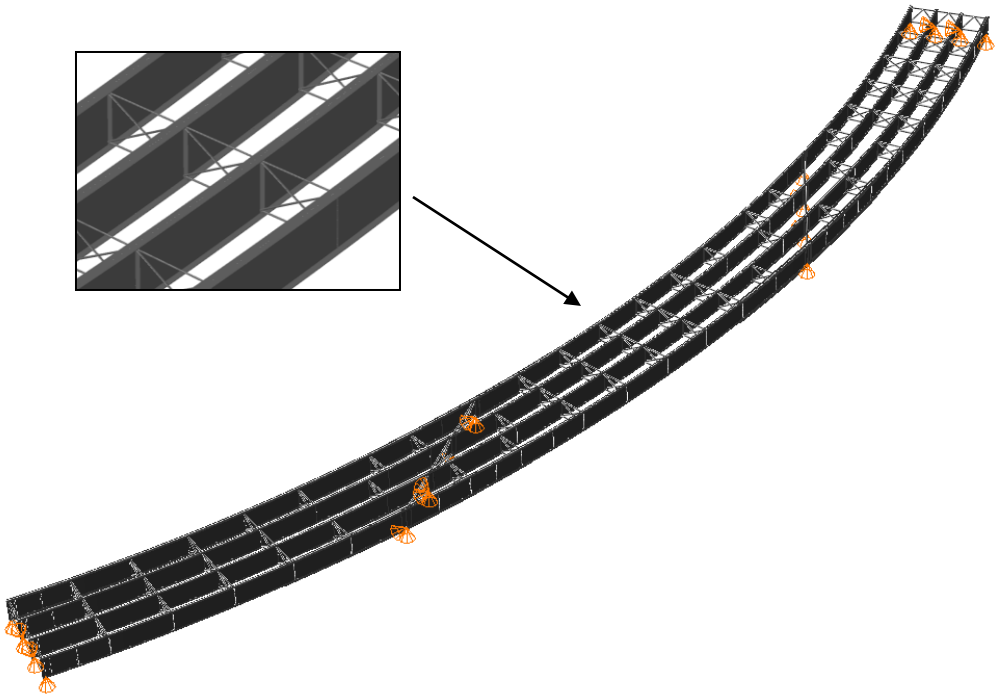

b) 3D FEA model

Figure 5.6. 2D-grid and 3D FEA models of XICSS7

One procedure that is used to determine the moment of inertia, $I_{eq}$, of the equivalent beam element is based on the flexure of the cross-frame. As depicted in Figure 5.7, a model of the cross-frame is constructed with boundary conditions that resemble a propped cantilever beam. A force couple is applied to Nodes 1 and 2 of the cross-frame, resulting in the horizontal displacements $\Delta_t$ and $\Delta_b$. Then the rotation angle, $\phi$ , is calculated as $\phi = (\Delta_t + \Delta_b)/d$. In the equivalent beam element, the moment $M = P \cdot d$ is applied at Node 1. It is required that the rotation in this node be equal to the rotation $\phi$ obtained from the analysis of the cross-frame. If shear deformations are ignored, the rotation angle in the equivalent beam is defined as $\phi = (M \cdot L)/(4EI_{eq})$. Hence, the moment of inertia of the equivalent beam using the flexure stiffness method is:

$$I_{eq} = \frac{ML}{4E\phi} \qquad \text{(Eq. 5.19)}$$

The equivalent moment of inertia found from this expression is used in the definition of the elements that represent the cross-frames in the 2D model of the bridge.

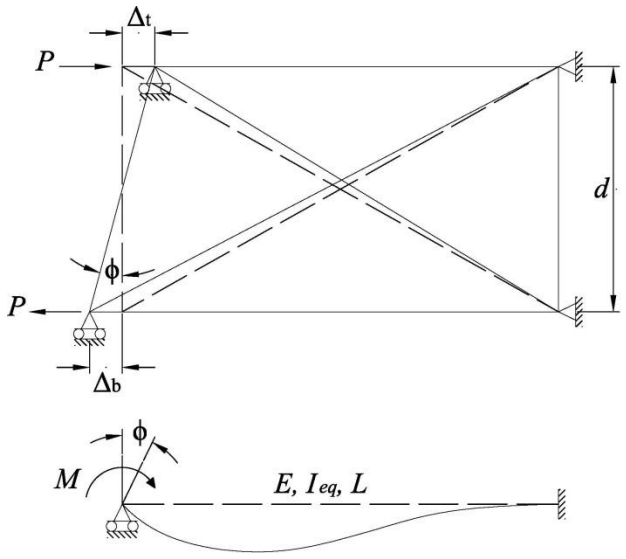


Figure 5.7. Flexure model used in standard practice to find the moment of inertia of the equivalent beam (Adapted from Coletti and Yadlosky (2007))

Another approximate procedure used to determine the moment of inertia of the equivalent beam elements is the shear stiffness method. As depicted in Figure 5.8, in this method, the cross-frame is modeled with boundary conditions that allow only the vertical displacement of one of the ends. The force *P* is applied at the end that is free to move and the vertical deflection is captured. In the equivalent beam, the deflection due to this load is equal to $\Delta = (PL^3)/(12EI_{eq})$. Therefore, the moment of inertia used in the 2D-grid models to represent the cross-frames based on this method is:

$$I_{eq} = \frac{PL^3}{12E\Delta} \qquad \text{(Eq. 5.20)}$$

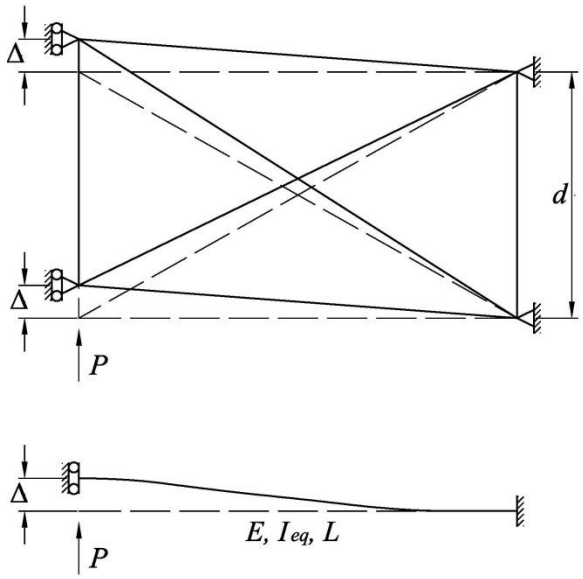


Figure 5.8. Shear model used in standard practice to find the moment of inertia of the equivalent beam (Adapted from Coletti and Yadlosky (2007))

These procedures are highly approximate. It is clear that they give two different equivalent moments of inertia, depending on which model is used. Both the flexure and shear stiffness methods only capture a part of the structural behavior of the cross-frames and are not necessarily a realistic representation of these bridge components.

In spite of the above shortcomings, some of the responses predicted by 2D models constructed using the above procedures often are close to the benchmark solutions obtained from 3D FEA analyses. As shown in Section 5.4, even for bridges with complex geometries, the approximate representation of the cross-frames does not result in significant differences with respect to the 3D FEA predictions. In particular, the major-axis bending responses of the girders obtained from 2D-grid models constructed with these standard practices are generally a close representation of the benchmark solutions. The reason for this incongruence is that in many cases, the cross-frame in-plane rigidity is much larger than the girder torsional rigidity of the I-girders. As demonstrated in Section 4.3, the girder responses only vary when the stiffness of the cross-frames is significantly reduced by for example, by removing the top chord in the V-type cross-frames. The removal of a top-chord or a diagonal in an X-type cross-frame, which supposes a decrease of the cross-frame in-plane stiffness, tends to not have a significant impact on the major-axis bending behavior of many bridges. In the 2D-grid models, the properties of the equivalent beams obtained with either the flexure or shear stiffness result in elements with rigidities that are considerably larger than the rigidities of the girders. Although the cross-frame in-plane stiffnesses obtained with each method can be substantially different, they are all much larger than the girder stiffness. Hence, the coarse representation of the cross-frames does not influence the girder major-axis bending response predictions significantly.

The response affected the most by modeling the cross-frames with these ad hoc procedures is the internal forces in the cross-frame elements, which also affect the flange lateral bending responses in the bridge. To properly capture the flow of the transverse

forces that results from the horizontal curvature and the support skew and the associated lateral bending response of the girders, it is necessary to perform the analysis with a more realistic model of the cross-frames. As discussed in Section 4.2, the forces at the joints of the cross-frame elements are decomposed to obtain the horizontal components of the nodal forces (see Figure 4.16 and Figure 5.5). These components are the forces that cause flange lateral bending stresses in the girders. If the cross-frame forces are not computed accurately, it is not possible to obtain an accurate prediction of the $f_\ell$ stresses.

The current practices used to model the cross-frames along with the poor representation of the torsion stiffness of the I-girders are the most significant limitations of the current methods used to conduct 2D-grid analysis. In the next section, simple two-node elements that are a more realistic representation of the cross-frame contributions to the system behavior are developed.

### 5.2.2. Improved Representation of the Cross-Frames in 2D-Grid Models

With the current methods used to model the cross-frames, the structural properties of these components are not properly captured. It is evident that in order to overcome the limitations of the equivalent beam elements used to model the cross-frames, it is required to capture their physical contributions to the system response. This can be done by applying the direct stiffness method to the cross-frame and recovering the coefficients that constitute its stiffness matrix. For this purpose, consider the X-type cross-frame depicted in Figure 5.9(a) and its line element representation. For simplicity only the in-plane representation (3-dof per node) in shown in the figure. If the connection plates are assumed to be rigid, and the element connections in the plane of the cross-frame are

assumed to be pinned, it is possible to apply unit displacements to each of these dofs to recover the stiffness coefficients as shown in Figure 5.9(b). Since in the cross-frame plane the chords and the diagonals are idealized as pin-connected, the coefficients depend exclusively on the axial stiffness of the cross-frame elements. Notice that for the formulation of the stiffness matrix, it is necessary to consider that the top chord, bottom chord, and the diagonals can have different cross-sections, i.e., different areas, $A_t$, $A_b$, $A_{d1}$, and $A_{d2}$, respectively. It is important to formulate the two-node element considering these characteristics, so it can handle cases such as cross-frames without top-chords (i.e., $A_t$ = 0), or without a diagonal (i.e., $A_{d1}$ or $A_{d2}$ = 0). The generality of an element formulated considering different element cross-sections is also beneficial when modeling the bearing line cross-frames. The top-chord of these cross-frames generally has a larger section than the rest of the elements since it supports the deck and wheel loads applied directly over it (see Figure 2.6).

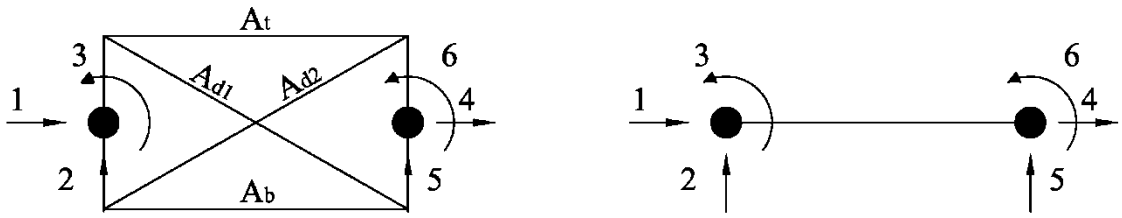


Physical Cross-Frame Two-Node Element Representation

a) Reduction of the physical cross-frame to a two-node element

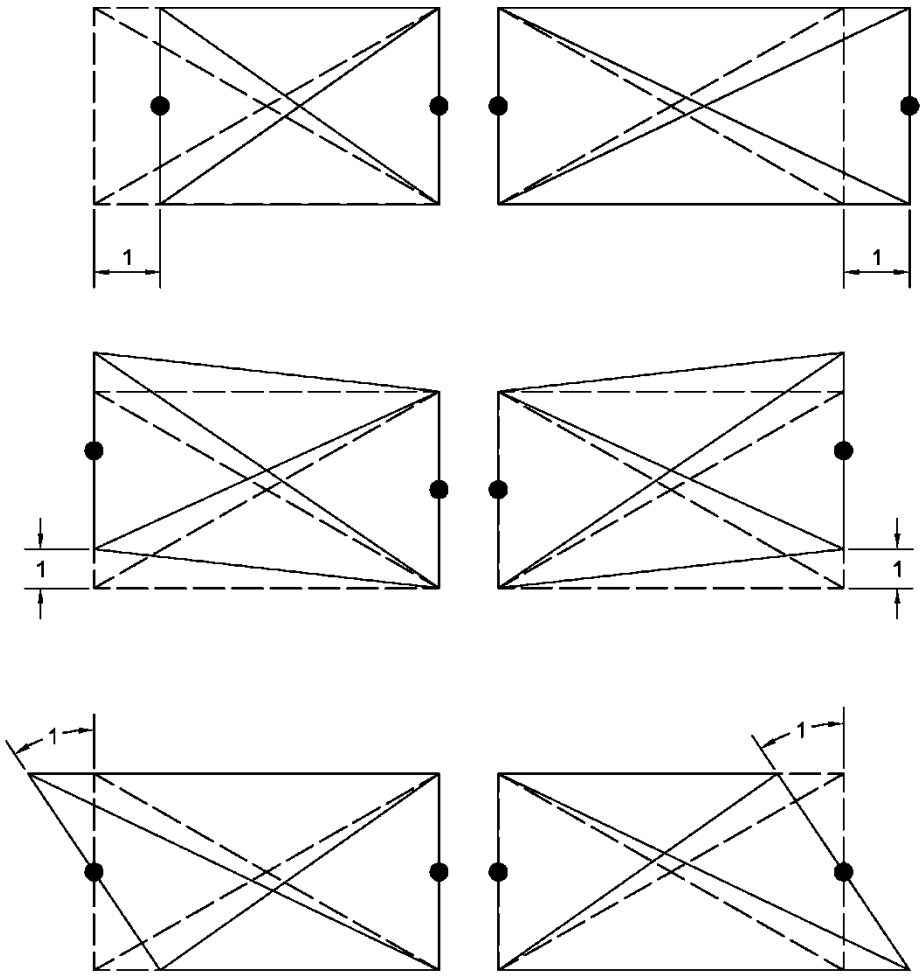


b) Unit displacements for the determination of the stiffness matrix coefficients

Figure 5.9. Determination of the stiffness matrix to represent the X-type cross-frame with a two-node beam element

The coefficients of the first column of the stiffness matrix are determined by applying a unit displacement at dof 1. The forces in the cross-frame elements due to the

applied displacement are shown in Figure 5.10. The coefficients are recovered from this free-body diagram, as shown in the same figure. Applying the same methodology to the other eleven dofs, it is possible to form the 12-by-12 stiffness matrix to represent the three-dimensional two-node element.  shows the six-by-six stiffness matrix of the X-type cross-frame corresponding to its in-plane behavior. The stiffness coefficients for the twelve dofs needed to form the 12-by-12 matrix are included in Appendix A.

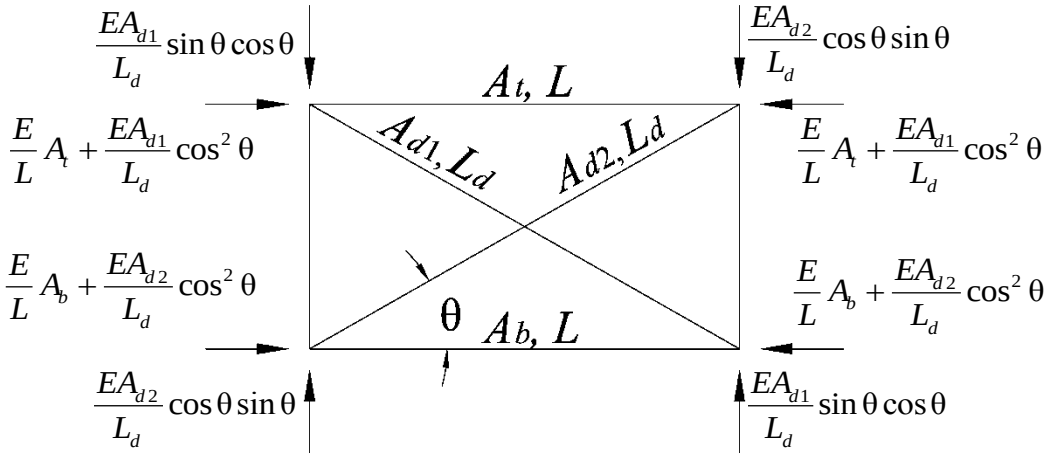


$$k_{11}: \quad \frac{E}{L}\left(A_b + A_t\right) + \frac{EL^2}{L_d^3}\left(A_{d1} + A_{d2}\right)$$

$$k_{21}: \quad \frac{ELh}{L_d^3}\left(A_{d2} - A_{d1}\right)$$

$$k_{31}: \quad \frac{Eh}{2L}\left(A_b - A_t\right) + \frac{EhL^2}{2L_d^3}\left(A_{d2} - A_{d1}\right)$$

$$k_{41}: \quad -\frac{E}{L}\left(A_b + A_t\right) - \frac{EL^2}{L_d^3}\left(A_{d1} + A_{d2}\right)$$

$$k_{51}: \quad \frac{ELh}{L_d^3}\left(A_{d1} - A_{d2}\right)$$

$$k_{61}: \quad \frac{Eh}{2L}\left(A_t - A_b\right) + \frac{EhL^2}{2L_d^3}\left(A_{d2} - A_{d1}\right)$$

Figure 5.10. Stiffness coefficients associated with Dof 1 – X-type cross-frame

The above two-node element is an accurate representation of the contributions of the X-type cross-frame to the system behavior. Contrary to the equivalent beam elements introduced previously, this element captures all the sources of deformation in the cross-frames, and also, it considers the coupling between the different dofs. Given that its formulation considers the possibility of cross-frames with different component cross-sections, it can handle situations such as cross-frames without top-chords or with a single diagonal. Due to its simplicity, it has the ability to capture the physical cross-frame behavior via a line element. This element can be implemented in any computer software to conduct 2D-grid analyses of I-girder bridges and overcome the limitations of the current models.

shows the stiffness matrix of a two-node element based on Euler-Bernoulli beam theory. By comparing the matrix of this beam element and the matrix of the X-type cross-frame, it is evident that the equivalent beam cannot capture the real behavior of these structural components. The cross-frame stiffness matrix has eight independent coefficients ($k_{11}$, $k_{12}$, $k_{13}$, $k_{16}$, $k_{22}$, $k_{23}$, $k_{33}$, and $k_{36}$). In , these coefficients are equated to the coefficients of the beam element to determine the section properties of the equivalent beam. From the equation for $k_{11}$, it is possible to calculate an equivalent area $A_{eq}$. The non-zero off-diagonal terms $k_{12}$, $k_{13}$, and $k_{16}$, however, cannot be represented by the Euler-Bernoulli beam matrix. These terms will be zero only if the cross-frames have equal chords and equal diagonals. In cases such as cross-frames without top chords or a single diagonal, these coupling terms are not zero. However, the equivalent beam cannot capture the interaction between the different dofs.

$$k=E\begin{bmatrix}
\frac{1}{L}(A_b+A_t)+\frac{L^2}{{L_d}^3}(A_{d1}+A_{d2}) & \frac{Lh}{{L_d}^3}(A_{d2}-A_{d1}) & \frac{h}{2L}(A_b-A_t)+\frac{hL^2}{2{L_d}^3}(A_{d2}-A_{d1}) & -\frac{1}{L}(A_b+A_t)-\frac{L^2}{{L_d}^3}(A_{d1}+A_{d2}) & \frac{Lh}{{L_d}^3}(A_{d1}-A_{d2}) & \frac{h}{2L}(A_t-A_b)+\frac{hL^2}{2{L_d}^3}(A_{d2}-A_{d1}) \\
\frac{Lh}{{L_d}^3}(A_{d2}-A_{d1}) & \frac{h^2}{{L_d}^3}(A_{d1}+A_{d2}) & \frac{h^2L}{2{L_d}^3}(A_{d1}+A_{d2}) & \frac{Lh}{{L_d}^3}(A_{d1}-A_{d2}) & -\frac{h^2}{{L_d}^3}(A_{d1}+A_{d2}) & \frac{h^2L}{2{L_d}^3}(A_{d1}+A_{d2}) \\
\frac{h}{2L}(A_b-A_t)+\frac{hL^2}{2{L_d}^3}(A_{d2}-A_{d1}) & \frac{h^2L}{2{L_d}^3}(A_{d1}+A_{d2}) & \frac{h^2}{4L}(A_b+A_t)+\frac{h^2L^2}{4{L_d}^3}(A_{d1}+A_{d2}) & \frac{h}{2L}(A_t-A_b)+\frac{hL^2}{2{L_d}^3}(A_{d1}-A_{d2}) & -\frac{h^2L}{2{L_d}^3}(A_{d1}+A_{d2}) & -\frac{h^2}{4L}(A_b+A_t)+\frac{h^2L^2}{4{L_d}^3}(A_{d1}+A_{d2}) \\
-\frac{1}{L}(A_b+A_t)-\frac{L^2}{{L_d}^3}(A_{d1}+A_{d2}) & \frac{Lh}{{L_d}^3}(A_{d1}-A_{d2}) & \frac{h}{2L}(A_t-A_b)+\frac{hL^2}{2{L_d}^3}(A_{d1}-A_{d2}) & \frac{1}{L}(A_b+A_t)+\frac{L^2}{{L_d}^3}(A_{d1}+A_{d2}) & \frac{Lh}{{L_d}^3}(A_{d2}-A_{d1}) & \frac{h}{2L}(A_b-A_t)+\frac{hL^2}{2{L_d}^3}(A_{d1}-A_{d2}) \\
\frac{Lh}{{L_d}^3}(A_{d1}-A_{d2}) & -\frac{h^2}{{L_d}^3}(A_{d1}+A_{d2}) & -\frac{h^2L}{2{L_d}^3}(A_{d1}+A_{d2}) & \frac{Lh}{{L_d}^3}(A_{d2}-A_{d1}) & \frac{h^2}{{L_d}^3}(A_{d1}+A_{d2}) & -\frac{h^2L}{2{L_d}^3}(A_{d1}+A_{d2}) \\
\frac{h}{2L}(A_t-A_b)+\frac{hL^2}{2{L_d}^3}(A_{d2}-A_{d1}) & \frac{h^2L}{2{L_d}^3}(A_{d1}+A_{d2}) & -\frac{h^2}{4L}(A_b+A_t)+\frac{h^2L^2}{4{L_d}^3}(A_{d1}+A_{d2}) & \frac{h}{2L}(A_b-A_t)+\frac{hL^2}{2{L_d}^3}(A_{d1}-A_{d2}) & -\frac{h^2L}{2{L_d}^3}(A_{d1}+A_{d2}) & \frac{h^2}{4L}(A_b+A_t)+\frac{h^2L^2}{4{L_d}^3}(A_{d1}+A_{d2})
\end{bmatrix}$$

Figure 5.11. Two-node element stiffness matrix, two-dimensional representation of the X-type cross-frame

$$k=E\begin{bmatrix}
\frac{A_{eq}}{L} & 0 & 0 & -\frac{A_{eq}}{L} & 0 & 0 \\
0 & \frac{12I_{eq}}{L^3} & \frac{6I_{eq}}{L^2} & 0 & -\frac{12I_{eq}}{L^3} & \frac{6I_{eq}}{L^2} \\
0 & \frac{6I_{eq}}{L^2} & \frac{4I_{eq}}{L} & 0 & -\frac{6I_{eq}}{L^2} & \frac{2I_{eq}}{L} \\
-\frac{A_{eq}}{L} & 0 & 0 & \frac{A_{eq}}{L} & 0 & 0 \\
0 & -\frac{12I_{eq}}{L^3} & -\frac{6I_{eq}}{L^2} & 0 & \frac{12I_{eq}}{L^3} & -\frac{6I_{eq}}{L^2} \\
0 & \frac{6I_{eq}}{L^2} & \frac{2I_{eq}}{L} & 0 & -\frac{6I_{eq}}{L^2} & \frac{4I_{eq}}{L}
\end{bmatrix}$$

$k_{11}$: $A_{eq}=(A_b+A_t)+\left(L^3/{L_d}^3\right)(A_{d1}+A_{d2})$

$k_{12}$: $0=\left(Lh/{L_d}^3\right)(A_{d2}-A_{d1})$

$k_{13}$: $0=(h/2L)(A_b-A_t)+\left(hL^2/2{L_d}^3\right)(A_{d2}-A_{d1})$

$k_{16}$: $0=(h/2L)(A_t-A_b)+\left(hL^2/2{L_d}^3\right)(A_{d2}-A_{d1})$

$k_{22}$: $I_{eq}=\left(h^2L^3/12{L_d}^3\right)(A_{d1}+A_{d2})$

$k_{23}$: $I_{eq}=\left(h^2L^3/12{L_d}^3\right)(A_{d1}+A_{d2})$

$k_{33}$: $I_{eq}=\left(h^2/16\right)(A_b+A_t)+\left(h^2L^3/16{L_d}^3\right)(A_{d1}+A_{d2})$

$k_{36}$: $I_{eq}=\left(-h^2/8\right)(A_b+A_t)+\left(h^2L^3/8{L_d}^3\right)(A_{d1}+A_{d2})$

Figure 5.12. Comparison of the stiffness matrices of the X-type cross-frame and the Euler-Bernoulli beam

Each of the next four terms, $k_{22}$, $k_{23}$, $k_{33}$, and $k_{36}$, may be used to compute an equivalent moment of inertia, $I_{eq}$. From the equations obtained for these terms, it is observed that three different values of $I_{eq}$ are necessary to capture the cross-frame behavior (notice that the required $I_{eq}$ from terms $k_{22}$ and $k_{23}$ is the same). In current practice, when the cross-frames are modeled with beam elements based on the shear stiffness model, the equivalent moment of inertia is calculated from the equation for the term $k_{22.}$ Similarly, when the flexure stiffness method is used to determine the beam properties, $I_{eq}$ is calculated from the equation for $k_{33}$. Hence, instead of constructing a model of the cross-frame to determine the equivalent moment of inertia from Eqs. 19 or 20, $I_{eq}$ can be directly computed from the equations obtained from the terms $k_{22}$ or $k_{33}$, respectively. However, as demonstrated in this section, this practice yields a poor representation of the physical cross-frame.

Another type of element that is sometimes used to represent the cross-frames is based on the Timoshenko beam theory. This element incorporates the contributions of the beam shear deformations to the response. Figure 5.13 shows the stiffness matrix of the line element formulated with this theory. In this element, an additional variable, the shear area, $A_v$, can be manipulated in conjunction with $I_{eq}$ to model the cross-frames with equivalent beams. However, this is not sufficient to fully capture the cross-frame behavior. As mentioned before, there are three additional equations defined by the independent terms $k_{22}$, $k_{23}$, $k_{33}$, and $k_{36}$ that would have to be represented with the properties of the equivalent beam to fully capture the cross-frame response. Since there are only two properties, $A_v$ and $I_{eq}$, which can be modified in the cross-section to affect the flexural stiffness characteristics, the Timoshenko beam theory is insufficient to model

an X-type cross-frame. Furthermore, for the cases when the other off-diagonal terms are not zero, the Timoshenko beam has the same limitations as the Euler-Bernoulli beam.

The above discussion shows that neither the Euler-Bernoulli beam nor the Timoshenko beam have the characteristics required for a proper representation of the X-type cross-frames. The two approximate methods used in current practice yield different cross-frame properties that capture only one part of the cross-frame behavior. Therefore, the equivalent beam concept is not sufficient to represent the physical response of these components. A more realistic representation can be obtained by implementing the proposed model in the 2D-grid analyses. The case studies shown in Section 5.4 demonstrate that the responses of the cross-frames and the overall structural behavior of an I-girder bridge is predicted more accurately when the proposed element is implemented in the analyses.

$$k = E\begin{bmatrix}
\frac{A_{eq}}{L} & 0 & 0 & -\frac{A_{eq}}{L} & 0 & 0 \\
0 & \frac{12A_vGI_{eq}}{L\left(A_vGL^2+12EI_{eq}\right)} & \frac{6A_vGI_{eq}}{A_vGL^2+12EI_{eq}} & 0 & -\frac{12A_vGI_{eq}}{L\left(A_vGL^2+12EI_{eq}\right)} & \frac{6A_vGI_{eq}}{A_vGL^2+12EI_{eq}} \\
0 & \frac{6A_vGI_{eq}}{A_vGL^2+12EI_{eq}} & \frac{4I_{eq}\left(A_vGL^2+3EI_{eq}\right)}{L\left(A_vGL^2+12EI_{eq}\right)} & 0 & -\frac{6A_vGI_{eq}}{A_vGL^2+12EI_{eq}} & \frac{2I_{eq}\left(A_vGL^2-6EI_{eq}\right)}{L\left(A_vGL^2+12EI_{eq}\right)} \\
-\frac{A_{eq}}{L} & 0 & 0 & \frac{A_{eq}}{L} & 0 & 0 \\
0 & -\frac{12A_vGI_{eq}}{L\left(A_vGL^2+12EI_{eq}\right)} & -\frac{6A_vGI_{eq}}{A_vGL^2+12EI_{eq}} & 0 & \frac{12A_vGI_{eq}}{L\left(A_vGL^2+12EI_{eq}\right)} & -\frac{6A_vGI_{eq}}{A_vGL^2+12EI_{eq}} \\
0 & \frac{6A_vGI_{eq}}{A_vGL^2+12EI_{eq}} & \frac{2I_{eq}\left(A_vGL^2-6EI_{eq}\right)}{L\left(A_vGL^2+12EI_{eq}\right)} & 0 & -\frac{6A_vGI_{eq}}{A_vGL^2+12EI_{eq}} & \frac{4I_{eq}\left(A_vGL^2+3EI_{eq}\right)}{L\left(A_vGL^2+12EI_{eq}\right)}
\end{bmatrix}$$

Figure 5.13. Stiffness matrix of a beam element including shear deformations (Timoshenko beam)

### 5.2.3. Formulation of the Two-Node Elements used to Represent V-Type and Inverted V-Type Cross-Frames

In the previous section, a two-node element is derived that can be implemented in a grid analysis to model X-type cross-frames. The stiffness coefficients necessary to formulate the stiffness matrix of this element are obtained by applying unit displacements at each of the six dofs that define the in-plane behavior of the cross-frame. This procedure cannot be applied directly to recover the matrix coefficients of the elements used to model the V-type and inverted V-type cross-frames. Since the diagonals frame into a middle node, it is not possible to directly calculate the element forces when these cross-frames are subject to unit displacements at the specified dofs. To overcome this difficulty in the V-type cross-frame, the matrix is first formulated considering the dofs of System A, as depicted in Figure 5.14. The translational and rotational dofs associated with the middle node, $u_7$, $u_8$, and $u_9$, are then condensed out to obtain the 6-by-6 stiffness matrix (System B). Finally, the matrix of the two-node element is formulated by expressing the dofs of System B as two orthogonal translations and one rotation at each end of the two-node element. Notice that since in the element development it is assumed that the girder connection plates are rigid, in Systems A and B, the vertical dofs at the top and bottom nodes at each end of the cross-frame are the same. This assumption helps eliminate two dofs from the formulation. The rigid plate assumption also serves to express the horizontal displacements of the nodes in System B as rotations in System C.

Another aspect to consider in the derivation of the line element is the inclusion of the rotational dof, $u_9$. This dof must be included in the development of the element used to model the V-type cross-frame. In the formulation, the bottom chords are modeled as

beam elements that are pin-connected to the connection plates. The top chord and the diagonals are modeled as truss elements. It is evident that if the top chord is removed, the in-plane rigidity of the cross-frame depends exclusively on the bending stiffness of the bottom chord, which is captured via the rotational dof, $u_9$.

The stiffness matrix of the V-type cross-frame is shown in Figure 5.15. Due to the complexity of the matrix, only the 3-by-3 matrix that represents the co-rotational dofs is shown in the figure. The other stiffness coefficients required to form the 6-by-6 matrix are shown as a function of the co-rotational dofs. Except for the variable $I$, which represents the in-plane moment of inertia of the bottom chord, the other variables are the same as those previously defined for the X-type cross-frame.

By inspecting the matrix in Figure 5.15, it is observed that the Euler-Bernoulli formulation is a poor representation of the V-type cross-frame. For example, the complexity of the bending stiffness of this cross-frame represented by the element $k_{33}$ cannot be captured by the $k_{33} = 4EI_{eq}/L$ term in the Euler-Bernoulli beam. Similarly, the off-diagonal terms in the equivalent beam matrix are equal to zero and do not capture the coupling of the different dofs of the cross-frame. It is clear that the physical V-type cross-frame is better represented by the proposed model. The complete matrix of the two-node line element including the out-of-plane stiffness terms is presented in Appendix B.

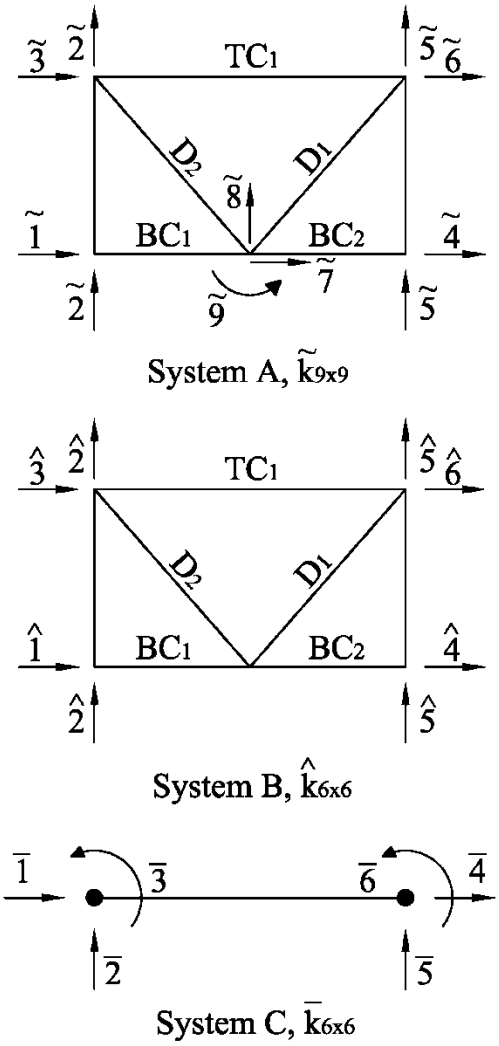


Figure 5.14. System transformation required to formulate the 6-by-6 stiffness matrix of the two-node element, V-type cross-frame

$$k = E\begin{bmatrix} \frac{A_b+A_t}{L}+\frac{3A_d IL^2}{A_d L^3 h^2+24IL_d{}^3} & 0 & -\frac{h\left[3A_d IL^2 h-(A_b-A_t)\left(24IL_d{}^3+A_d L^3 h^2\right)\right]}{2L\left(A_d L^3 h^2+24IL_d{}^3\right)} \\ 0 & \frac{4A_b A_d h^2}{A_d L^3+8A_b L_d{}^3} & \frac{2A_b A_d Lh^2}{A_d L^3+8A_b L_d{}^3} \\ -\frac{h\left[3A_d IL^2 h-(A_b-A_t)\left(24IL_d{}^3+A_d L^3 h^2\right)\right]}{2L\left(A_d L^3 h^2+24IL_d{}^3\right)} & \frac{2A_b A_d Lh^2}{A_d L^3+8A_b L_d{}^3} & \frac{h^2\left[(A_b+A_t)\left(8A_b A_d L^3 L_d{}^3 h^2+192A_b IL_d{}^6\right)+A_d{}^2 L^6 h^2(5A_b+A_t)+A_d IL^3 L_d{}^3(144A_b+24A_t)+3A_d{}^2 IL^6\right]}{4L\left(A_d L^3 h^2+24IL_d{}^3\right)\left(A_d L^3+8A_b L_d{}^3\right)} \end{bmatrix}$$

$$k_{11} = -k_{14} = -k_{41} = k_{44}$$

$$k_{13} = -k_{16} = k_{31} = -k_{34} = -k_{43} = k_{46} = -k_{61} = k_{64}$$

$$k_{22} = -k_{25} = -k_{52} = k_{55}$$

$$k_{33} = -k_{36} = -k_{63} = k_{66}$$

$$k_{23} = k_{26} = k_{32} = -k_{35} = -k_{53} = -k_{56} = k_{62} = -k_{65}$$

$$k_{12} = k_{15} = k_{21} = k_{24} = k_{42} = k_{45} = k_{51} = k_{54} = 0$$

Figure 5.15. Two-node element stiffness matrix, two-dimensional representation of the V-type cross-frame (System C)

The third cross-frame type implemented via a two-node element is the inverted V-configuration. As in the V-type cross-frame, the matrix is first formulated in System A with the eight dofs depicted in Figure 5.16. Next, the dofs associated with the middle node are condensed out, and the element matrix is transformed to the dofs of System B. Finally, the matrix is modified to represent the cross-frame with a line element with a horizontal, a vertical, and a rotational dof at each node (System C). It is worth noting that in the formulation of this element, the rotational dof at the middle node is not included since all the cross-frame components are modeled as truss elements in the plane of the cross-frame. Contrary to the V-type cross-frame, it is not common to remove any of the chords from this cross-frame configuration. Therefore, it is sufficient to capture the axial deformations of the cross-frame elements to properly represent its in-plane behavior.

The 6-by-6 stiffness matrix of the inverted V-type cross-frame is shown in Figure 5.17. In the matrix formulation, it is assumed that the diagonals have the same cross-section, i.e., $A_d$. This type of configuration is usually used at bearing lines. Commonly, the top-chord has a larger section than the bottom chord since it supports the deck joint, as previously depicted in Figure 2.6. Since in many cases the chords are different, i.e., $A_t \neq A_b$, the off-diagonal terms in the matrix, such as $k_{31}$, are not zero. As in the previous cases, the equivalent beam model cannot represent this behavior. Hence, the proposed two-node element could be implemented in a 2D analysis to more accurately represent the inverted V-type cross-frames. The coefficients to form the 12-by-12 matrix of this cross-frame are presented in Appendix C.

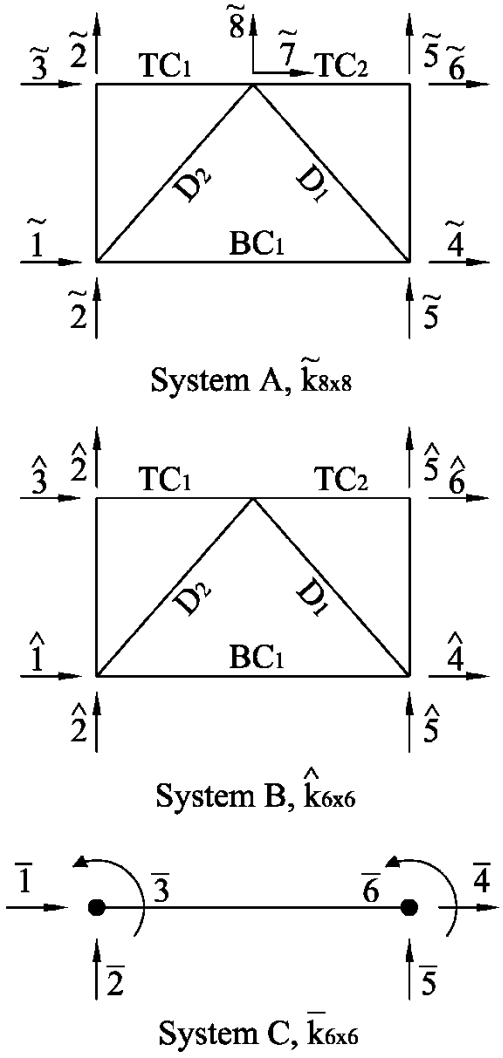


Figure 5.16. System transformation required to formulate the 6-by-6 stiffness matrix of the two-node element, inverted V-type cross-frame

$$k = E\begin{bmatrix}
\frac{A_b + A_t}{L} & 0 & \frac{(A_b - A_t)h}{2L} & -\frac{A_b + A_t}{L} & 0 & -\frac{(A_b - A_t)h}{2L} \\
0 & \frac{4A_d A_t h^2}{A_d L^3 + 8A_t L_d{}^3} & \frac{2A_d A_t L h^2}{A_d L^3 + 8A_t L_d{}^3} & 0 & -\frac{4A_d A_t h^2}{A_d L^3 + 8A_t L_d{}^3} & \frac{2A_d A_t L h^2}{A_d L^3 + 8A_t L_d{}^3} \\
\frac{(A_b - A_t)h}{2L} & \frac{2A_d A_t L h^2}{A_d L^3 + 8A_t L_d{}^3} & \frac{h^2\left(8A_t{}^2 L_d{}^3 + 5A_d A_t L^3 + 8A_b A_t L_d{}^3 + A_b A_d L^3\right)}{4L\left(A_d L^3 + 8A_t L_d{}^3\right)} & -\frac{(A_b - A_t)h}{2L} & -\frac{2A_d A_t L h^2}{A_d L^3 + 8A_t L_d{}^3} & \frac{A_d A_t L^2 h^2}{A_d L^3 + 8A_t L_d{}^3} - \frac{(A_t + A_b)h^2}{4L} \\
-\frac{A_b + A_t}{L} & 0 & -\frac{(A_b - A_t)h}{2L} & \frac{A_b + A_t}{L} & 0 & \frac{(A_b - A_t)h}{2L} \\
0 & -\frac{4A_d A_t h^2}{A_d L^3 + 8A_t L_d{}^3} & -\frac{2A_d A_t L h^2}{A_d L^3 + 8A_t L_d{}^3} & 0 & \frac{4A_d A_t h^2}{A_d L^3 + 8A_t L_d{}^3} & -\frac{2A_d A_t L h^2}{A_d L^3 + 8A_t L_d{}^3} \\
-\frac{(A_b - A_t)h}{2L} & \frac{2A_d A_t L h^2}{A_d L^3 + 8A_t L_d{}^3} & \frac{A_d A_t L^2 h^2}{A_d L^3 + 8A_t L_d{}^3} - \frac{(A_t + A_b)h^2}{4L} & \frac{(A_b - A_t)h}{2L} & -\frac{2A_d A_t L h^2}{A_d L^3 + 8A_t L_d{}^3} & \frac{h^2\left(8A_t{}^2 L_d{}^3 + 5A_d A_t L^3 + 8A_b A_t L_d{}^3 + A_b A_d L^3\right)}{4L\left(A_d L^3 + 8A_t L_d{}^3\right)}
\end{bmatrix}$$

Figure 5.17. Two-node element stiffness matrix, two-dimensional representation of the inverted V-type cross-frame (System C)

### 5.2.4. Decomposition of the Nodal Forces in Cross-Frame Element Forces

In 2D-grid models, the primary analysis output is the joint displacements. These displacements are multiplied by the corresponding stiffness coefficients to calculate the joint forces. To obtain the forces in the chords and diagonals of the cross-frames in current practice, the joint forces typically are decomposed as shown in Figure 5.18. The $V_i$ and $V_j$ shears are essentially the same; the difference between them is equal to the weight of the cross-frame. This effect is negligible, so the largest of these forces is selected and equally divided between the top and bottom nodes of the cross-frame. In most of cases, the axial loads, $P_i$ and $P_j$, are negligible. In the case that they are considered for computing the element forces, they are also equally divided between the top and bottom nodes. The left and right moments, $M_i$ and $M_j$, are decomposed into force couples with magnitude equal to $M/h$ and applied to the cross-frame nodes. Then, the forces in the chords and the diagonals are obtained from statics.

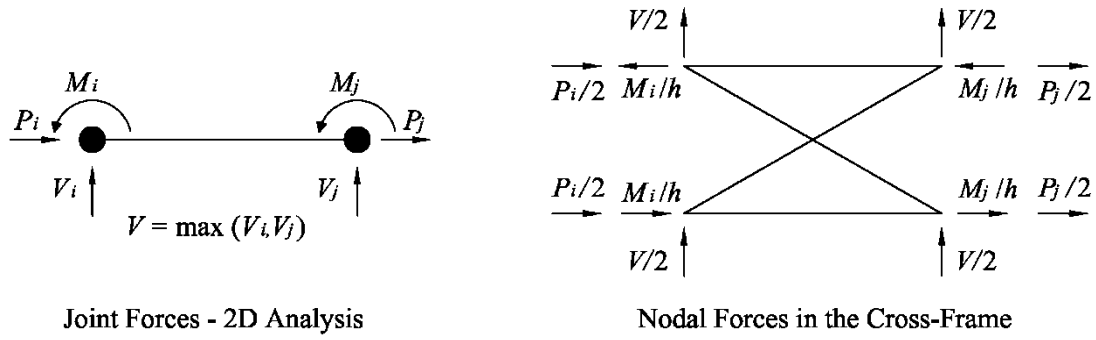


Figure 5.18. Current practices for determination of cross-frame forces from 2D-grid analysis results

It is worth mentioning that this approximate procedure to calculate the element forces satisfies equilibrium, but the distribution of $P$, $V$, and $M$ in the physical cross-frame can be significantly different. For example, if the top-chord is removed, it is clear

that $P$ and $M$ are not distributed equally between the top and bottom nodes. This incongruence in the decomposition of forces is another limitation of current practices.

In the recommended two-node element, the forces in the chords and diagonals of the cross-frames are calculated considering the fundamental force-displacement relationship. The forces are computed by recovering the joint displacements to determine the element deformations. The deformations are then multiplied by the corresponding stiffness coefficients to obtain the element forces. Applying this criterion, the forces in the chords and the diagonals of an X-type cross-frame are equal to:

$$F_{TC} = \frac{E \cdot A_t}{L}\left[\left(u_4 - u_1\right) + \frac{h}{2}\left(u_3 - u_6\right)\right] \quad \text{(Eq. 5.21)}$$

$$F_{BC} = \frac{E \cdot A_b}{L}\left[\left(u_4 - u_1\right) + \frac{h}{2}\left(u_6 - u_3\right)\right] \quad \text{(Eq. 5.22)}$$

$$F_{D1} = \frac{E \cdot A_{d1}}{2L_d^{\,2}}\left[2L\left(u_4 - u_1\right) + 2h\left(u_2 - u_5\right) + Lh\left(u_3 + u_6\right)\right] \quad \text{(Eq. 5.23)}$$

$$F_{D2} = -\frac{E \cdot A_{d2}}{2L_d^{\,2}}\left[2L\left(u_1 - u_4\right) + 2h\left(u_2 - u_5\right) + Lh\left(u_3 + u_6\right)\right] \quad \text{(Eq. 5.24)}$$

where $u_i$ is the displacement at dof $i$. Figure 5.9(a) shows the dof numbering associated with the displacements as well as the orientation of Diagonals 1 and 2. Similarly, for the V-type cross-frame, the element forces can be calculated from the following equations:

$$F_{TC} = \frac{E \cdot A_t}{2L}\left[2\left(u_4 - u_1\right) + h\left(2u_3 - u_6\right)\right] \quad \text{(Eq. 5.25)}$$

$$F_{D1} = \frac{EA_d L_d \left[ c_1 \left( u_4 - u_1 \right) + c_2 \left( u_5 - u_2 \right) + c_3 u_3 + c_4 u_6 \right]}{\left( A_d L^3 h^2 + 24 I L_d{}^3 \right) \left( A_d L^3 + 8 A_t L_d{}^3 \right)}$$

$$\begin{aligned} c_1 &= 6 A_d I L^4 + 48 A_b I L L_d{}^3 \\ c_2 &= 96 A_b I L_d{}^3 h + 4 A_b A_d L^3 h^3 \\ c_3 &= 2 A_d A_b L^4 h^3 - 3 A_d I L^4 h + 24 A_b I L L_d{}^3 h \\ c_4 &= 3 A_d I L^4 h + 72 A_b I L L_d{}^3 h + 2 A_b A_d L^4 h^3 \end{aligned} \qquad \text{(Eq. 5.26)}$$

$$F_{D2} = \frac{EA_d L_d \left[ d_1 \left( u_1 - u_4 \right) + d_2 \left( u_2 - u_5 \right) + d_3 u_3 + d_4 u_6 \right]}{\left( A_d L^3 h^2 + 24 I L_d{}^3 \right) \left( A_d L^3 + 8 A_t L_d{}^3 \right)}$$

$$\begin{aligned} d_1 &= -6 A_d I L^4 - 48 A_b I L L_d{}^3 \\ d_2 &= 96 A_b I L_d{}^3 h + 4 A_b A_d L^3 h^3 \\ d_3 &= 2 A_d A_b L^4 h^3 + 3 A_d I L^4 h + 72 A_b I L L_d{}^3 h \\ d_4 &= 24 A_b I L L_d{}^3 h + 2 A_b A_d L^4 h^3 - 3 A_d I L^4 h \end{aligned} \qquad \text{(Eq. 5.27)}$$

$$F_{BC1} = \frac{-E \cdot A_b}{2L \left( A_d L^3 + 8 A_t L_d{}^3 \right)} \left[ e_1 \left( u_1 - u_4 \right) + e_2 \left( u_2 - u_5 \right) + e_3 u_3 + e_4 u_6 \right]$$

$$\begin{aligned} e_1 &= 2 A_d L^3 + 16 A_t L_d{}^3 \\ e_2 &= 4 A_d L^2 h \\ e_3 &= 3 A_d L^3 h + 8 A_b L_d{}^3 h \\ e_4 &= A_d L^3 h - 8 A_b L_d{}^3 h \end{aligned} \qquad \text{(Eq. 5.28)}$$

$$F_{BC2} = \frac{E \cdot A_b}{2L \left( A_d L^3 + 8 A_t L_d{}^3 \right)} \left[ f_1 \left( u_4 - u_1 \right) + f_2 \left( u_2 - u_5 \right) + f_3 u_3 + f_4 u_6 \right]$$

$$\begin{aligned} f_1 &= 2 A_d L^3 + 16 A_t L_d{}^3 \\ f_2 &= 4 A_d L^2 h \\ f_3 &= A_d L^3 h - 8 A_b L_d{}^3 h \\ f_4 &= 3 A_d L^3 h + 8 A_b L_d{}^3 h \end{aligned} \qquad \text{(Eq. 5.29)}$$

Figure 5.14 shows the position of the components BC1, BC2, D1, and D2. Finally, the forces in the inverted V-type cross-frame are computed from:

$$F_{TC1} = \frac{E \cdot A_t \left[ a_1 \left( u_4 - u_1 \right) + a_2 \left( u_2 - u_5 \right) + a_3 u_3 + a_4 u_6 \right]}{2L \left( A_d L^3 + 8 A_t L_d{}^3 \right)}$$

$$a_1 = 2A_d L^3 + 16 A_t L_d{}^3$$
$$a_2 = 4A_d L^2 h \qquad \text{(Eq. 5.30)}$$
$$a_3 = 3A_d L^3 h + 8 A_t L_d{}^3 h$$
$$a_4 = A_d L^3 h - 8 A_t L_d{}^3 h$$

$$F_{TC2} = \frac{-E \cdot A_t \left[ b_1 \left( u_1 - u_4 \right) + b_2 \left( u_2 - u_5 \right) + b_3 u_3 + b_4 u_6 \right]}{2L \left( A_d L^3 + 8 A_t L_d{}^3 \right)}$$

$$b_1 = 2A_d L^3 + 16 A_t L_d{}^3$$
$$b_2 = 4A_d L^2 h \qquad \text{(Eq. 5.31)}$$
$$b_3 = A_d L^3 h - 8 A_t L_d{}^3 h$$
$$b_4 = 3A_d L^3 h + 8 A_t L_d{}^3 h$$

$$F_{D1} = \frac{2EA_t A_d L_d h}{A_d L^3 + 8 A_t L_d{}^3} \left[ 2 \left( u_2 - u_5 \right) + L \left( u_3 + u_6 \right) \right] \qquad \text{(Eq. 5.32)}$$

$$F_{D2} = -\frac{2EA_t A_d L_d h}{A_d L^3 + 8 A_t L_d{}^3} \left[ 2 \left( u_2 - u_5 \right) + L \left( u_3 + u_6 \right) \right] \qquad \text{(Eq. 5.33)}$$

$$F_{BC} = \frac{EA_b}{2L} \left[ 2 \left( u_4 - u_1 \right) + h \left( u_6 - u_3 \right) \right] \qquad \text{(Eq. 5.34)}$$

The orientation of the diagonals and chords is depicted in Figure 5.16.

These equations can be directly implemented in the computer program used to conduct the analysis; otherwise, the forces can be calculated outside the program by exporting the analysis results and the cross-section properties of the elements to a spreadsheet. Finally, it is important to note that the element forces calculated with the above equations are in equilibrium with the joint forces obtained from the two-node element ($P_i$, $P_i$, $V_i$, $V_j$, $M_i$, and $M_j$).

One particular aspect of 2D-grid analyses is that the nodal axial displacements, $u_1$ and $u_4$, due to the noncomposite dead loads are not captured. A study of the results obtained from a 2D model will show that these displacements are zero in all the nodes since only gravity loads are applied to the system. Fortunately, except for some bearing line cross-frames, the axial forces, $P_i$ and $P_j$, are negligible, that is, the axial deformation of a cross-frame is small, as compared to the shear and bending deformations that it undergoes due to the skew effects. At a skewed support, however, when the bearings of two adjacent girders restrain the lateral displacements, these axial forces can be of considerable magnitude, and can induce large forces in the cross-frames that connect these girders.

The following procedure can be used to compute the change in length in a cross-frame located at a skewed support. In Figure 5.19, line $L_o$ represents the initial cross-frame length measured at its mid-height. The figure also shows the major-axis bending rotation, $\phi_y$, and the associated longitudinal displacement, $u_b$, that a girder undergoes as a result of applying the gravity loads. Ozgur and White (2007) show that the layover at a bearing line can be obtained as:

$$u_{lat} = u_b \cdot \tan(\theta) \qquad \text{(Eq. 5.35)}$$

where $u_{lat}$ is the layover of the girder top flange, and $\theta$ is the skew angle. The lateral and longitudinal displacements of the two girders can be calculated to locate the final position of the cross-frame and determine it final length, $L_f$. Hence, the axial deformation on the cross-frame is approximately equal to $u_4 - u_1 = L_f - L_o$. This stretch can be used in Eqs. 5.21 to 5.34 to include the contribution of the axial deformation in the cross-frame forces.

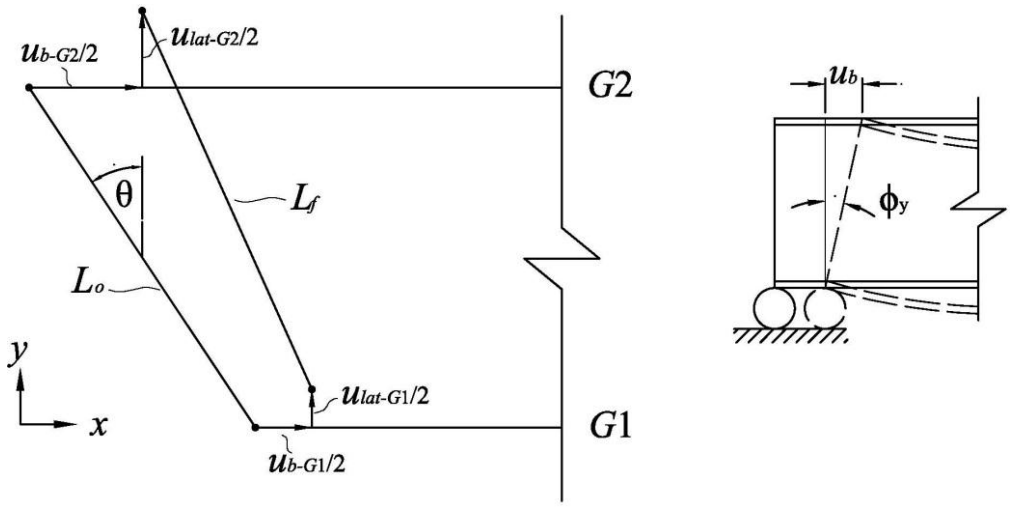


Figure 5.19. Girder lateral displacements and length change in the cross-frame at bearing locations

### 5.2.5. Displacement Transformation Matrix for Calculation of Cross-Frame Element Forces

As described in the previous section, the forces in the cross-frame elements are computed from the displacements obtained from a 2D-grid analysis. In cases where the cross-frame local coordinate system does not coincide with the global coordinate system, the displacements obtained from the analysis need to be transformed before the element forces can be calculated. Figure 5.20 shows a cross-frame oriented at an angle θ and the displacements obtained from the analysis in the global system. This case could represent a cross-frame in a bearing line where the skew angle is equal to θ.

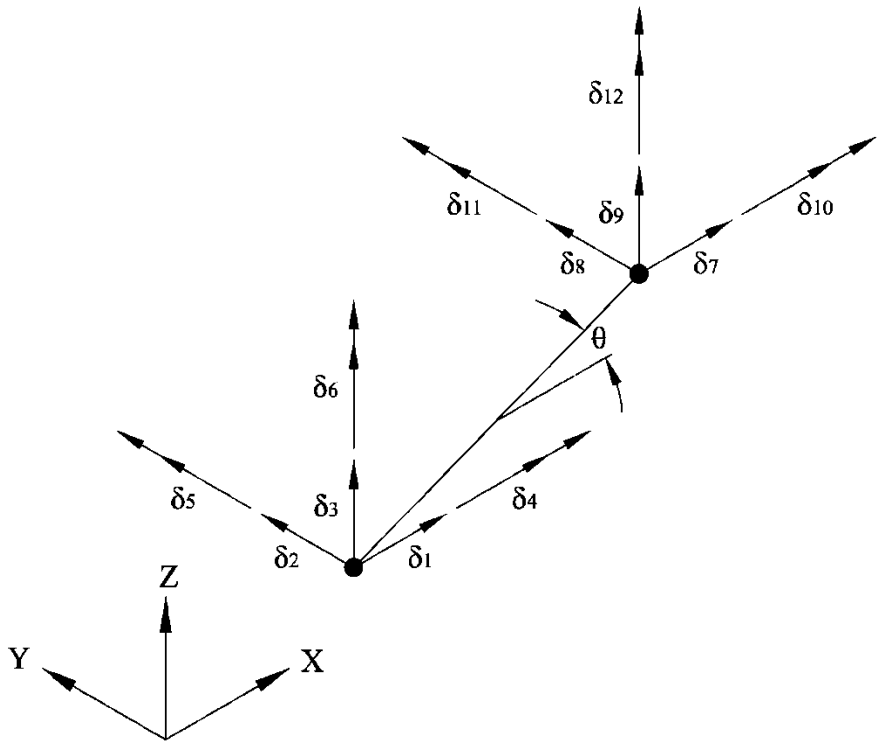


Figure 5.20. Cross-frame element displacements in the global coordinate system

To compute the chord and diagonal forces using Eqs. 5.21 to 5.34, it is required to transform the global displacements, $\delta_i$, to local displacements, $u_i$. This transformation is accomplished via the transformation matrix *T*, such that

$$u_{6x1} = T_{6x12}\delta_{12x1} \qquad \text{(Eq. 5.36)}$$

where *u* is the vector that contains the displacements in the local system (System C for the V-type and inverted V-type cross-frames), *T* is the transformation or rotation matrix shown in Figure 5.21, and δ is the displacement vector in the global coordinates.

$$T(\theta)=\begin{bmatrix} \cos\theta & \sin\theta & 0 & 0 & 0 & 0 & 0 & 0 & 0 & 0 & 0 & 0 \\ 0 & 0 & 1 & 0 & 0 & 0 & 0 & 0 & 0 & 0 & 0 & 0 \\ 0 & 0 & 0 & \sin\theta & -\cos\theta & 0 & 0 & 0 & 0 & 0 & 0 & 0 \\ 0 & 0 & 0 & 0 & 0 & 0 & \cos\theta & \sin\theta & 0 & 0 & 0 & 0 \\ 0 & 0 & 0 & 0 & 0 & 0 & 0 & 0 & 1 & 0 & 0 & 0 \\ 0 & 0 & 0 & 0 & 0 & 0 & 0 & 0 & 0 & \sin\theta & \cos\theta & 0 \end{bmatrix}$$

Figure 5.21. Displacement transformation matrix

The development of the two-node elements, along with the displacement rotation matrix and the equations to compute the internal forces are the tools needed to conduct a 2D-grid analysis with a more accurate representation of the cross-frames. In the next section, the proposed two-node elements are tested under several loading conditions to determine their ability to capture the real behavior of a cross-frame.

### 5.2.6. Comparison of the Current and Proposed Techniques used for Cross-Frame Modeling

In this section, numerical examples of an X-type cross-frame subjected to different load actions is introduced to highlight the virtues of the proposed cross-frame model and compare it to the results obtained from the equivalent beam elements. As depicted in Figure 5.22, three loading cases are considered for the tests. The benchmark analysis is conducted by modeling the cross-frame explicitly and restraining the translational dofs at the left end. The displacements in the cross-frame, $u_x$, $u_y$, and $\theta$, are captured at the node located at mid-height of the right end. In the simplified model, the cross-frame is represented with a line element, and the boundary conditions are represented with a fixed support. The displacements are captured at the right node.

The loading cases selected for the analyses test the capability of the models to capture the three basic sources of deformation in the cross-frame, axial, shear, and bending deformation. In the first test, an axial load, $F_x$, is divided in equal fractions and applied at the top and bottom nodes, as shown in the figure for Loading Case 1 (LC1). Similarly, in the second test the vertical load, $F_y$, is divided between these two nodes. In the third test, a force couple equal to $P \cdot h$ is applied at the top and bottom nodes. In the simplified line element, this force couple is represented with the moment $M$. The forces $F_x$, $F_y$, and $P$ are set in the analyses so that the force in at least one elements is equal to the yielding force of the L6x6x1/2 angle used to model the cross-frames, i.e, 288.5 kips.

In addition to the three loading cases discussed above, variations in the cross-frame geometry are implemented to study the capabilities of the line element. The most basic case is Cross-Fame Configuration 1 (CFC1), where the two chords and two diagonals are included in the model. In CFC2 the cross-frame geometry is modified by removing Diagonal 2 (see Figure 5.9(a)). Finally, in the last configuration, CFC3, the top-chord is removed from the cross-frame.

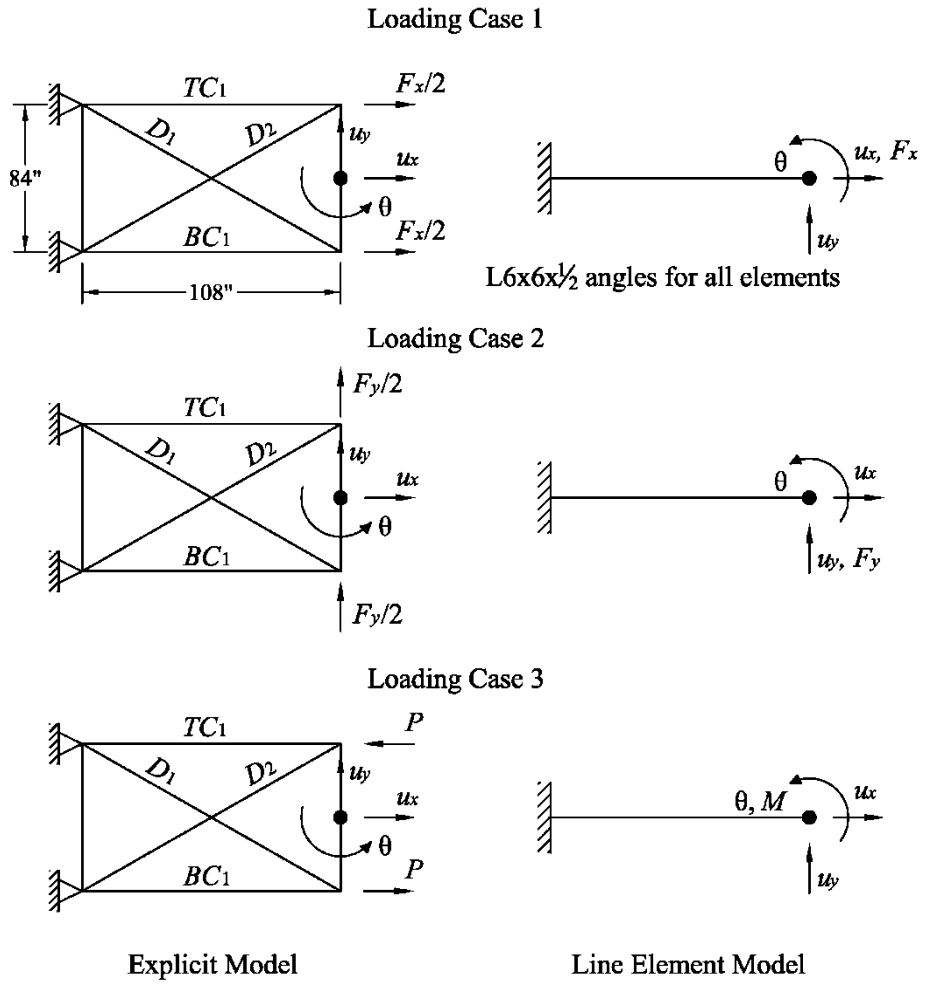


Figure 5.22. Loading cases considered in the tests of the proposed two-node element for the representation of X-type cross-frame

Table 5.1 shows the results of the tests that compare the responses obtained from the explicit model of the cross-frame and the proposed two-node element. As shown in the table, both the displacements and element forces are matched exactly by the line element. The different sources of deformation, as well as the variations in the cross-frame geometry are well represented with this element.

Several of the characteristics of the line element can be studied from the results shown in the table. In the most basic test, CFC1 is subject to LC1. As a result, the

monitored node moves to the right 0.186 in., but it does not displace vertically or rotate. In this test, all the elements are subject to tension, and the forces in both chords and both diagonals are the same. Due to the symmetry of the cross-frame geometry and loading, this case is the simplest scenario of all the tests conducted. A more challenging case to test the capabilities of the line element occurs when the top-chord is removed (CFC3-LC1). In this case, the monitored node not only moves horizontally (0.299 in.) but it also experiences a vertical displacement of -0.384 in. and a rotation of -0.007 rad. This test shows the coupling that exists among the different dofs and the ability of the proposed element to capture this behavior. As shown in the table the simple line element is an exact representation of the explicit cross-frame model. The accuracy of the proposed model can be verified for other challenging cases such as CFC2-LC3, where the cross-frame minus one diagonal is subject to a force couple. In all cases, the explicit and simplified models yield the same results.

Table 5.1. Comparison of force and displacement responses obtained from the tests of the cross-frame explicit model and the proposed two-node element

| | Forces (kips) | | | | Displacements (in, rad) | | |
|---|---|---|---|---|---|---|---|
| Cross-Frame Configuration | TC | BC | D1 | D2 | $u_x$ | $u_y$ | $\theta$ |
| Loading Case 1 | | | | | | | |
| Cross-Frame (Explicit Model) | | | | | | | |
| 1 | 288.5 | 288.5 | 179.8 | 179.8 | 0.186 | 0.000 | 0.000 |
| 2 | 288.5 | 288.5 | 0.0 | NA | 0.186 | 0.239 | 0.000 |
| 3 | NA | 0.0 | 288.5 | 288.5 | 0.299 | -0.384 | -0.007 |
| Two-Node Element - Proposed Model | | | | | | | |
| 1 | 288.5 | 288.5 | 179.8 | 179.8 | 0.186 | 0.000 | 0.000 |
| 2 | 288.5 | 288.5 | 0.0 | NA | 0.186 | 0.239 | 0.000 |
| 3 | NA | 0.0 | 288.5 | 288.5 | 0.299 | -0.384 | -0.007 |
| Loading Case 2 | | | | | | | |
| Cross-Frame (Explicit Model) | | | | | | | |
| 1 | -227.7 | 227.7 | -288.5 | 288.5 | 0.000 | 0.573 | 0.004 |
| 2 | 0.0 | 227.7 | -288.5 | NA | 0.073 | 0.573 | 0.002 |
| 3 | NA | 227.7 | -288.5 | 0.0 | -0.150 | 0.573 | 0.007 |
| Two-Node Element - Proposed Model | | | | | | | |
| 1 | -227.7 | 227.7 | -288.5 | 288.5 | 0.000 | 0.573 | 0.004 |
| 2 | 0.0 | 227.7 | -288.5 | NA | 0.073 | 0.573 | 0.002 |
| 3 | NA | 227.7 | -288.5 | 0.0 | -0.150 | 0.573 | 0.007 |
| Loading Case 3 | | | | | | | |
| Cross-Frame (Explicit Model) | | | | | | | |
| 1 | -288.5 | 288.5 | 0.0 | 0.0 | 0.000 | 0.239 | 0.004 |
| 2 | -288.5 | 288.5 | 0.0 | NA | 0.000 | 0.239 | 0.004 |
| 3 | NA | 288.5 | -182.7 | -182.7 | -0.189 | 0.483 | 0.009 |
| Two-Node Element - Proposed Model | | | | | | | |
| 1 | -288.5 | 288.5 | 0.0 | 0.0 | 0.000 | 0.239 | 0.004 |
| 2 | -288.5 | 288.5 | 0.0 | NA | 0.000 | 0.239 | 0.004 |
| 3 | NA | 288.5 | -182.7 | -182.7 | -0.189 | 0.483 | 0.009 |

The second set of tests compares the responses predicted by the explicit model and the equivalent beams based on the flexure and shear stiffness models. Table 5.2 shows the nodal displacements obtained from the analyses. Inspecting the results shown in the table, it is clear that the approximate models are not capable of predicting the

benchmark responses. For example, the equivalent beam models cannot capture the dof interaction that exists for the CFC2 and CFC3 cases when they are loaded under LC1. The results of the analyses conducted with these models only report a horizontal displacement of the right end of the cross-frame, but do not capture the vertical displacement and rotation that also occur in the node. Similarly, for LC2, the equivalent beam models do not capture the horizontal displacement in the monitored node for the cases when either a diagonal or the top-chord is removed from the cross-frame. For these tests, a comparison of the element forces is not included. The cantilever beam used to represent the cross-frame is a statically determinate system, so the nodal forces do not depend on the properties of the beam element.

Table 5.2. Comparison of the displacement responses obtained from the explicit cross-frame model and the equivalent beam models

| | Displacements (in., rad) | | | | | | | | |
|---|---|---|---|---|---|---|---|---|---|
| | Load Case 1 | | | Load Case 2 | | | Load Case 3 | | |
| Cross-Frame Configuration | $u_x$ | $u_y$ | $\theta$ | $u_x$ | $u_y$ | $\theta$ | $u_x$ | $u_y$ | $\theta$ |
| Explicit & Proposed Model | | | | | | | | | |
| 1 | 0.186 | 0.000 | 0.000 | 0.000 | 0.573 | 0.004 | 0.000 | 0.239 | 0.004 |
| 2 | 0.186 | 0.239 | 0.000 | 0.073 | 0.573 | 0.002 | 0.000 | 0.239 | 0.004 |
| 3 | 0.299 | -0.384 | -0.007 | -0.150 | 0.573 | 0.007 | -0.189 | 0.483 | 0.009 |
| Equivalent Beam Model (Flexure Stiffness) | | | | | | | | | |
| 1 | 0.186 | 0.000 | 0.000 | 0.000 | 0.676 | 0.010 | 0.000 | 0.642 | 0.012 |
| 2 | 0.150 | 0.000 | 0.000 | 0.000 | 0.405 | 0.006 | 0.000 | 0.769 | 0.014 |
| 3 | 0.148 | 0.000 | 0.000 | 0.000 | 0.508 | 0.007 | 0.000 | 0.483 | 0.009 |
| Equivalent Beam Model (Shear Stiffness) | | | | | | | | | |
| 1 | 0.186 | 0.000 | 0.000 | 0.000 | 1.537 | 0.021 | 0.000 | 1.460 | 0.027 |
| 2 | 0.150 | 0.000 | 0.000 | 0.000 | 1.537 | 0.021 | 0.000 | 2.921 | 0.054 |
| 3 | 0.148 | 0.000 | 0.000 | 0.000 | 0.768 | 0.011 | 0.000 | 0.730 | 0.013 |

## 5.3. Summary of the Proposed Improvements for the Analysis of I-Girder Bridges using 2D-Grid Analysis

The previous sections highlight the characteristics of the 2D-grid models and the limitations of the current techniques to properly represent the behavior of an I-girder bridge during construction. Essentially, there are two modeling practices that can considerably affect the accuracy of the analyses. The first practice is related to the representation of the torsion properties of the I-girders. In computer programs commonly used for 2D-grid modeling, the torsional resistance of the I-girders is formulated considering only the pure or St. Venant torsion contributions. Even though it is well known that for a thin-walled open-section member, the torsion resistance is dominated by the flange warping contributions, these are not included in the analyses. Therefore, curved and skewed bridges, which are inherently subjected to torsion, may not be properly represented with a 2D-grid model due to the poor representation of the torsion properties of the I-girders.

Beyond affecting the girder responses, the lack of a model that includes the warping contributions also affects the prediction of the cross-frame forces and their overall participation in the system behavior. The behavior of these components is directly related to the torsional response of the I-girders. If the girders are too flexible in torsion, in a 2D-grid model, the forces in the cross-frames will be underpredicted. In curved and/or skewed bridges this can cause a poor prediction of the responses since in these structures there is a transverse load path that must be included in the analysis. Hence, it is necessary to implement a more realistic model of the torsion resistance of the I-girders. For this purpose, the equivalent torsion constant is a concept that may be considered as a

possible option. This technique is a simple solution that includes the contributions of flange warping and only requires redefining the torsion constant in the model. As shown in the case studies of Section 5.4, this modeling practice can increase significantly the accuracy of the approximate 2D-grid models.

The other factor that can affect the response predictions of a 2D-grid analysis is the model used to represent the cross-frames. In most of cases, the cross-frames are modeled using an equivalent beam element, which is based on the Euler-Bernoulli beam theory. The section properties of the equivalent beam are obtained from ad hoc procedures such as the flexure stiffness and the shear stiffness methods. The cross-frame responses predicted with each of the methods can be different since they only capture part of their structural behavior and none of them are an accurate representation of these components. The equivalent beam concept is even more limited when representing configurations such as cross-frames without top-chords or a single diagonal.

A better representation of the cross-frames can be accomplished by formulating two-node elements that consider all the stiffness contributions to the system response. In this section line elements that are a simple and accurate representation of the cross-frames and that can be implemented in 2D-grid models where developed and tested to study their accuracy. The results show that the proposed models can be a potential improvement to the current practices used to conduct 2D-grid analyses.

Finally, it is necessary to highlight that even though the implementation of the proposed techniques can result in better predictions of the system responses, there are other important aspects of the structural behavior that are not modeled in a 2D-grid

analysis. This approximate method has no depth information of the bridge. Hence scenarios where the web flexibility contributes significantly to the behavior of a structure are not captured. Similarly, the proposed cross-frame model assumes that the horizontal axis of the cross-frames is located at the centroid of the girders, which is not necessarily the right. In many instances, this approximation and others related to the depth information may not have a considerable impact on the bridge behavior, but it is worth for the Engineer to be cognizant of these limitations, and recognize conditions where they can affect the system performance.

## 5.4. Case Studies of Bridges Modeled with Improved Analysis Techniques

In this section, three structures are analyzed to study the ability of the traditional and improved 2D-grid models to capture the behavior of I-girder bridges with challenging geometries. The two first case studies are the NISSS14 and NISSS16 straight and skewed bridges. The third case is XICSS7, which is a continuous curved and skewed bridge.

The 2D-grid analyses for the three structures are conducted using the LARSA 4D software (LARSA 2010). This software package is selected for the study because of its versatility to handle custom element definitions. The program architecture allows the implementation of the two-node elements developed in Section 5.2 to represent the cross-frames, so they can be used in the analyses of the case studies.

### 5.4.1. Case Study I: Simple Span Straight and Skewed Bridge (NISSS16)

This structure was introduced in Section 3.1.4. It is a nine girder 150 ft long bridge with the left support skewed $50^{o}$ and the right support oriented normal to the

longitudinal girder axis. All the cross-frames in this bridge are of the inverted V-type. Its plan view is shown in Figure 5.23. This bridge was studied in Section 4.2.2.1 to implement potential mitigation schemes that could reduce the collateral effects of the skew. With a skew index equal to 0.59, this system is a good case to test the ability of the 2D-grid models for capturing the behavior of a structure with a challenging geometry.

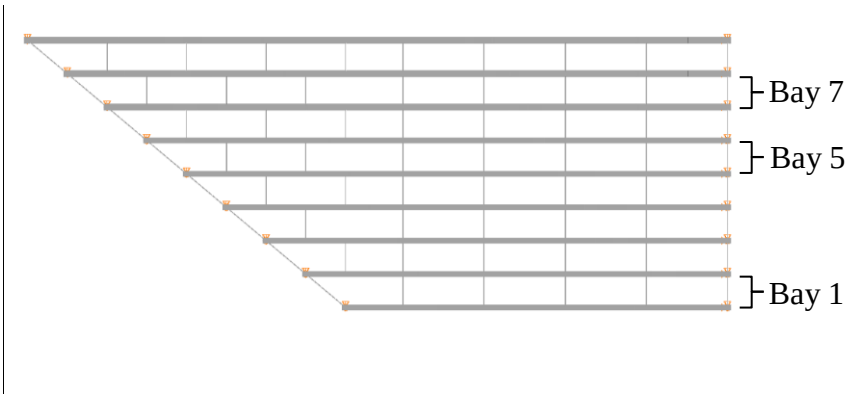


Figure 5.23. Framing plan of bridge NISSS16

The bridge is studied using five analyses: a 3D geometric nonlinear FEA model, a 1D line-girder model, and three 2D-grid models with different characteristics. The plots in Figure 5.24 and Figure 5.25 show the major-axis bending stresses, $f_b$, at the top flange of the girders and the vertical displacements, respectively. The responses are predicted at the TDL level.

The results labeled 2D-M1 are obtained from a 2D-grid analysis conducted using current modeling practices. In this analysis, the torsion properties of the girders are modeled neglecting the warping contributions. The cross-frames are modeled with line elements. The section properties of the beam elements are determined using the shear stiffness model discussed in Section 5.2.1.

The 2D-M2 model implements the first of the two proposed recommendations to improve the behavior predictions obtained from 2D-grid analyses. In this model, the girder cross-sections are defined using the equivalent torsion constant concept introduced in Section 5.1. By using the equivalent torsional constants, $J_{eq}$, the warping contributions to the girder torsional stiffness are included, assuming that flange warping is fixed at the interior bracing points. For the girder end segments, the equivalent torsion constants are calculated assuming that the flanges are free to warp at the supports. The cross-frames in this model have the same characteristics as in 2D-M1.

The third 2D-grid model, 2D-M3, includes the two recommendations proposed to improve the predictions obtained from this analysis method. The model is constructed considering the improved girder torsional stiffness representation via the equivalent torsion constants. The inverted V-type cross-frames are modeled using the two-node element definitions introduced in Section 5.2.3.

The plots show that the major-axis bending responses, $f_b$ stresses and vertical displacements, are accurately predicted by the approximate models. The 1D line-girder and the 2D-grid models accurately capture the benchmark response obtained from the 3D FEA. These results suggest that the cross-frame actions have a negligible influence in these responses. This implies that the effects of the vertical force components induced in the girders by the cross-frames ($A_y$, $B_y$, $C_y$, and $D_y$ in Figure 4.16) have little significance, as compared to the effects of the gravity loads (TDL). For this reason, although it does not have any information regarding the cross-frame forces, the 1D line-girder model is able to capture the girder responses. In the case of the 2D-grid models, the results show

that whether the recommended practices are implemented or not, the major-axis bending behavior of the bridge is properly captured by the three models.

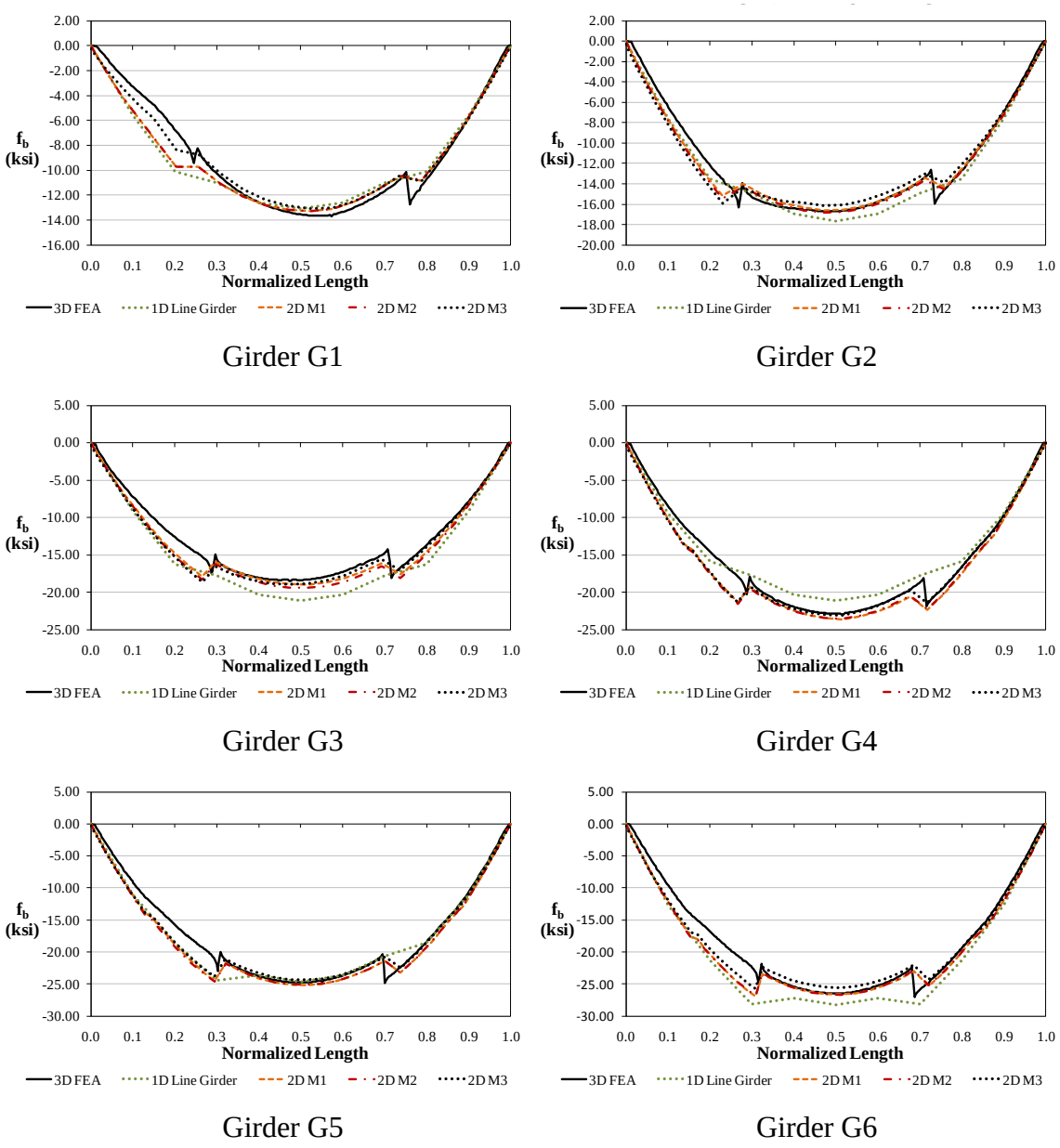


Figure 5.24. Major-axis bending stress responses at the top flange obtained from different analysis methods in bridge NISSS16, TDL level

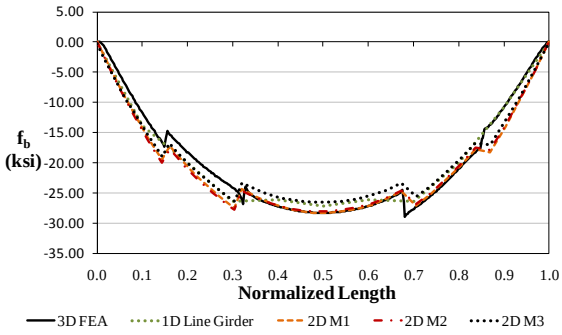


Girder G7

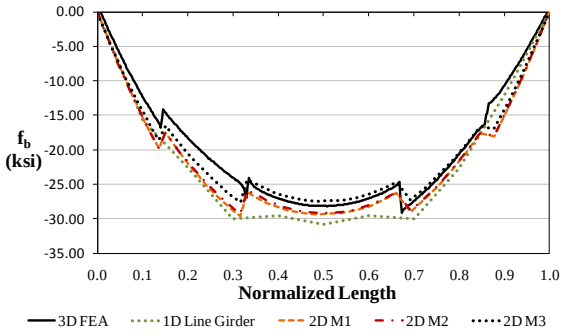


Girder G8

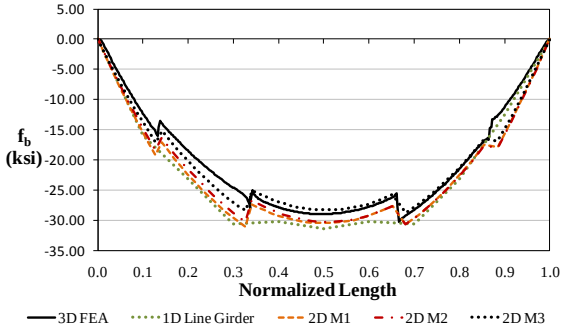


Girder 9

Figure 5.24. Major-axis bending stress responses at the top flange obtained from different analysis methods in bridge NISSS16, TDL level (continued)

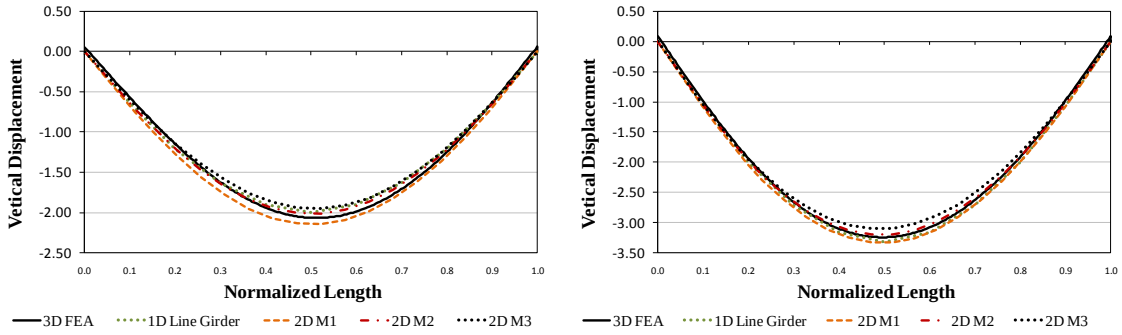


Girder G1




Girder G2

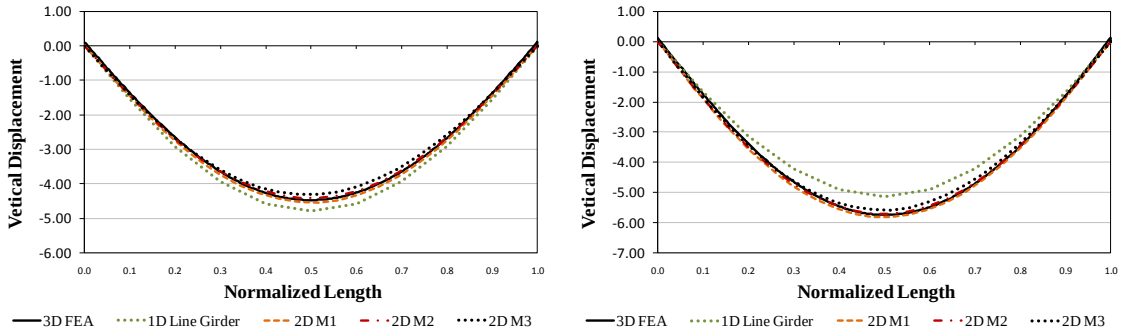


Girder G3




Girder G4

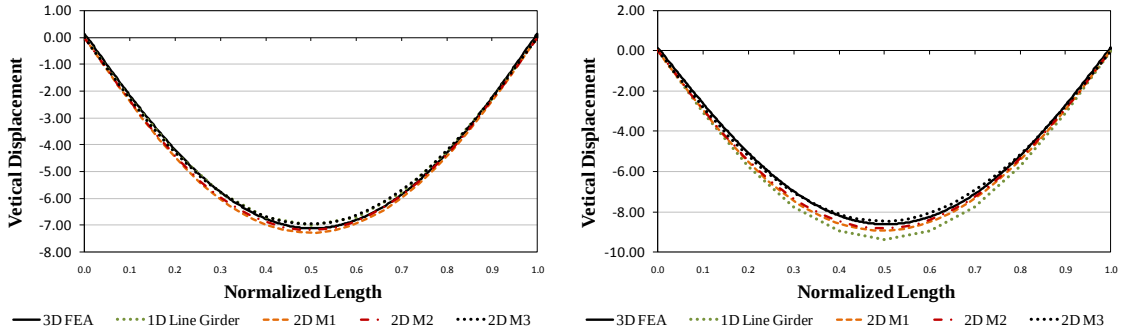


Girder G5




Girder G6

Figure 5.25. Girder vertical displacement obtained from different analysis methods in bridge NISSS16, TDL level

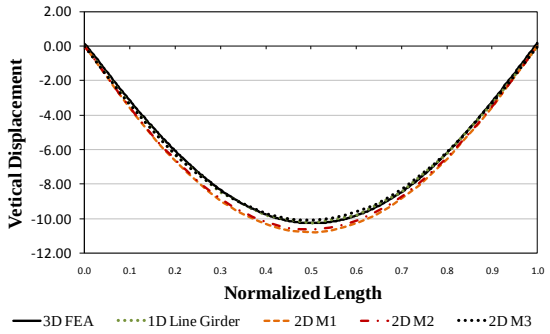


Girder G7

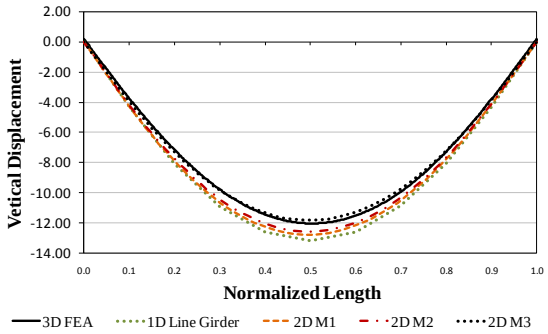


Girder G8

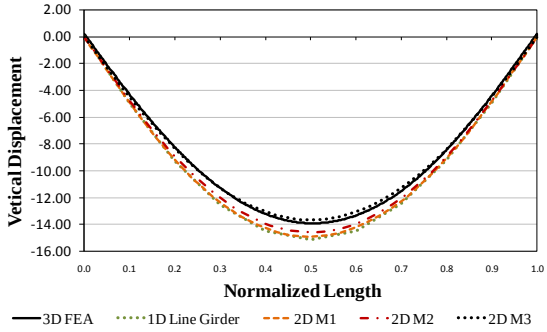


Girder G9

Figure 5.25. Girder vertical displacement obtained from different analysis methods in bridge NISSS16, TDL level (continued)

In the case of the cross-frame force predictions, the results obtained from the approximate models do not show the same accuracy. In the 2D-grid models, the nodal displacements at the cross-frame locations are collected and used in Eq. 5.21 to 5.34 to determine the forces in the cross-frame elements. To compare the predictions of the 2D models to the 3D FEA, the element cross-frame forces are expressed as bending moments, $M_i$ and $M_j$, and shear forces, $V_i$ and $V_j$, as shown in Figure 5.26. In the case of NISSS16, all the cross-frames are of the inverted V-type; however, the element forces in X-type and V-type cross frames can be illustrated in terms of shear forces and bending moments, as well.

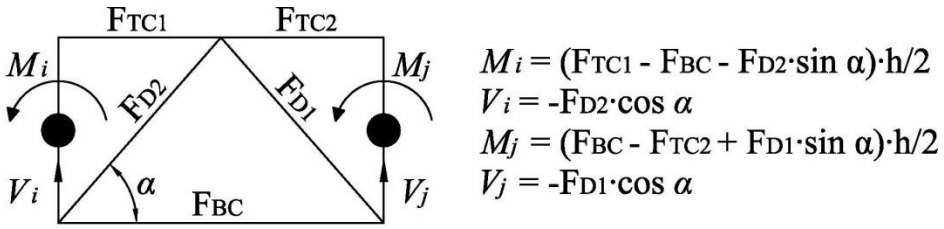


Figure 5.26. Representation of the cross-frame element forces as shear forces and bending moments

Figure 5.27 shows the cross-frame shears and moments in Bays 1, 5, and 7 (see Figure 5.23). The plots contain the predictions obtained from the three 2D-grid analyses described previously and the refined 3D FEA. The cross-frame responses are plotted versus the cross-frame number. For instance, in Bay 1, between girders G1 and G2, there are six cross-frames, where 1 and 6 are the cross-frames at the left and right support, respectively. Only the plot of the shear force at the left end of the cross-frame (Node *i*) is shown in the figure since the shear at Node *j* is essentially the same. The data presented in the plots is discrete; the dotted lines are included only to facilitate the visualization of the responses and identify trends.

These plots show that 2D-M3, the 2D-grid model conducted with the proposed representation of the cross-frames and the girder torsion properties accurately capture the responses predicted by the refined 3D model. The other two models, 2D-M1 and 2D-M2, do not capture the cross-frame actions. The plots show that both the bending moments and the shear forces are severely underestimated. The predictions show that these models do not capture the development of the cross-frame forces due to the skew effects and the transverse flow of those forces in the system. This means that in these two grid models, the girders are effectively behaving as if they were disconnected and working individually rather than as a system. Another response of interest, which is affected by

the underestimation of the cross-frame forces, is the girder lateral bending stress. It is not possible to recover the stress responses directly from a 2D-grid analysis. However, since the lateral bending stresses in the girder flanges, $f_\ell$, depend on the magnitude of the cross-frame forces, the models 2D-M1 and 2D-M2 also are not able to provide the required information to capture this response. A method to predict the $f_\ell$ stresses and the girder layovers based on the results obtained from a 2D-grid analysis with the suggested improvements is discussed in Section 5.5.

This study shows that to obtain a good prediction of the cross-frame forces and the associated girder flange lateral bending response from a 2D-grid analysis, it is necessary to implement the recommendations discussed in Sections 5.1 and 5.2. A better representation of the torsion properties of the girders and of the cross-frames is fundamental to capture these responses. Additionally, the implementation of the recommended improvements is important to properly predict the major-axis bending responses in bridges where the vertical components of the nodal forces ($A_x$, $B_x$, $C_x$, and $D_x$ in Figure 4.16) are large. In this case study, these components are not large enough to cause significant changes in the $f_b$ stresses and the vertical displacements. However, in cases where the skew index is larger than 0.65, such as Bridge NISSS14 ($I_{SE}$ = 1.36), the vertical force components have a considerable participation in the major-axis bending responses, as shown in Section 4.2.1.6.

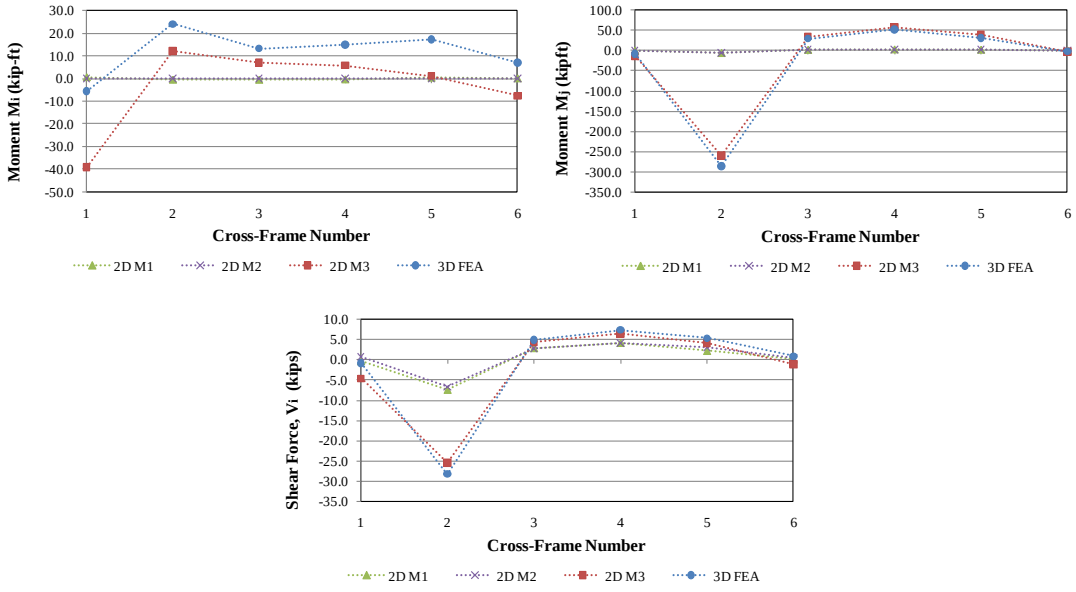


**Bay 1 (Girders G1-G2)**

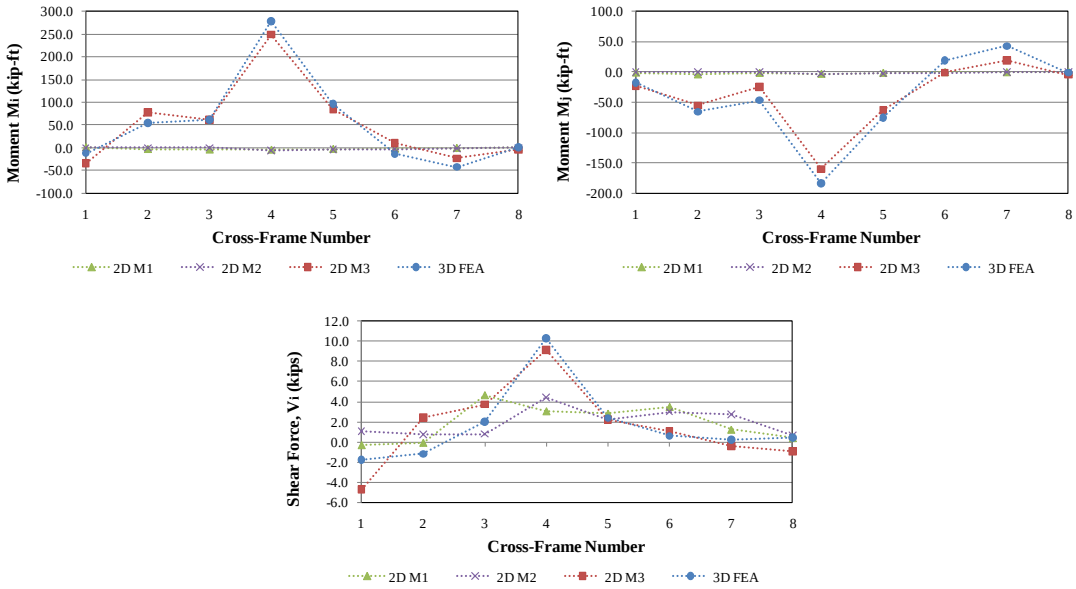


**Bay 5 (Girders G5-G6)**

Figure 5.27. Forces in cross-frame elements obtained from different analysis methods in bridge NISSS16, TDL level

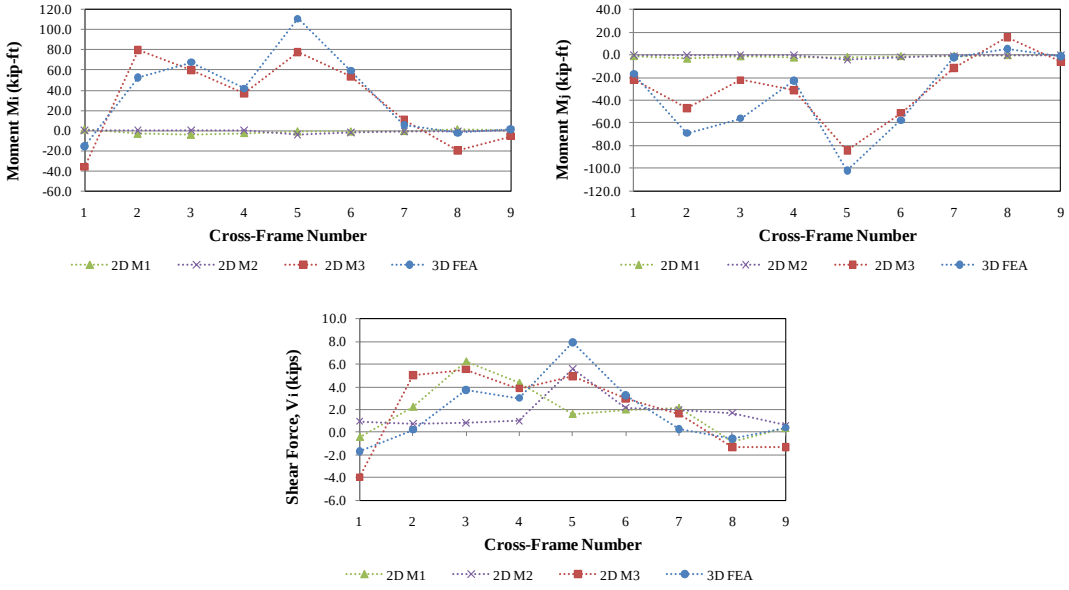


**Bay 7 (Girders G7-G8)**

Figure 5.27. Forces in cross-frame elements obtained from different analysis methods in bridge NISSS16, TDL level (continued)

### 5.4.2. Case Study II: Continuous Span Straight and Skewed Bridge (NICSS16)

The second case study is Bridge NICSS16, shown in Figure 5.28. This structure was introduced in Sections 4.2.1.5 and 4.2.2.2 to study the effects of the skew on straight and continuous bridges and methods to mitigate them. The structure has nine girders with parallel skews oriented at 70 degrees. All the cross-frames in this structure are of the inverted V-type. With skew indices equal to 1.69, 1.36, and 1.36 for Spans 1, 2 and 3, respectively, this system is considered as severely skewed. Hence, it is an ideal case to test the capability of the current and improved 2D-grid models to capture its behavior during construction.

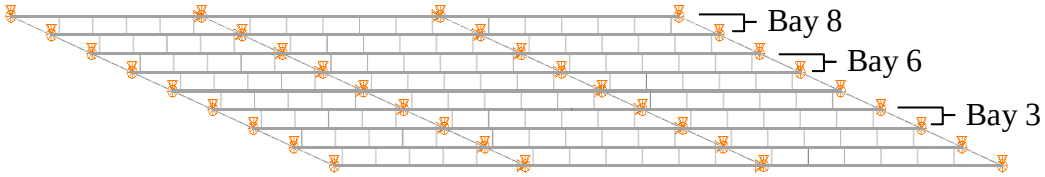


Figure 5.28. Framing plan of NICSS16

Four models were constructed for this bridge. The first is a 3D FE model with all the components of the structure modeled explicitly. The behavior of the structure captured by the nonlinear 3D FE model is the benchmark. Its responses are used as reference to study the accuracy of the results obtained from the approximate 1D and 2D models.

The second analysis is conducted using a 1D line-girder analysis. As previously described, in this model the girders are analyzed independently from each other. The loads applied on a particular girder are determined based on tributary areas. The line-girder analysis does not consider the participation of the cross-frames on the behavior of the structure. Therefore, this model cannot capture the effects of the skew and the associated flow of transverse forces on the system performance.

The third model, named 2D-M1, is a 2D-grid model constructed using current practices. In this model, girders and cross-frames are modeled using beam elements. The torsion properties of the elements used to represent the girders are based only on St. Venant's torsion, neglecting the flange warping contributions. For the cross-frames, the section properties are determined using the approximate shear stiffness model introduced in Section 5.2.1.

The fourth model, 2D-M2, is constructed implementing the practices recommended in Section 5.1 and 5.2. In this model, the warping contributions to the girder torsional stiffness are included via an equivalent torsion constant, $J_{eq}$. For the determination of the equivalent torsion constants, the girders are assumed to be warping fixed at the bracing points, and warping free at the abutments. The inverted V-type cross-frames are modeled with the two-node element developed in Section 5.2.3.

Figure 5.29 shows the plots of the major-axis bending stresses, $f_b$, predicted by the different models at the TDL level. As shown in these plots, the responses predicted by the 1D line-girder and 2D-M1 models are different to those that result from the 3D model; especially in Spans 1 and 3. It is important to notice that the 1D model predictions for girders G1 and G9 are the same. This is also the case for the results obtained from this analysis for girders G2 to G8. The reason is that if only the effects of the gravity loads are considered in the analysis, the responses in the fascia girders must coincide. Similarly, since the skews are parallel, the predictions obtained for the interior girders must match.

As shown in the plots, the 2D-M1 model results are the same as those obtained from the 1D line-girder model. This suggests that the 2D-grid model constructed with current practices is not capable of capturing the interaction that exists between the girders and the cross-frames in this highly skewed structure. The results indicate that in this 2D-grid model, the girders perform as if they are disconnected. The reasons for this behavior are related to the poor representation of the cross-frames and the girder torsion properties in the model. As discussed in Section 5.1.1, the torsional dofs of the girders are coupled to the bending dofs in the cross-frames. If only pure torsion contributions are considered in the elements used to represent the girders, the girders in the model will be more

flexible than in reality. Hence, the forces transferred to the cross-frame elements will be significantly underestimated. The cross-frame forces are transferred to the girders through the connection plates in the form of nodal forces. The *vertical* components of such forces add to the noncomposite dead loads to define the major-axis bending response of the structure. If the cross-frame forces are underestimated, so are the nodal forces. This is the main reason why the predictions obtained for NICSS16 from the 2D-M1 model coincide with those obtained from the 1D line-girder analysis. In many cases, such as the case study studied in Section 5.4.1, the cross-frame force vertical components are too small compared to the gravity loads to cause significant changes in the $f_b$ stress response. However, in bridges with a large skew index, these forces are not negligible.

The predictions obtained from the 2D-M2 model show that a better representation of the cross-frames and the girder torsion properties are necessary to capture the expected response predicted by the 3D model. As shown in the plots, the $f_b$ stress responses are properly represented by the improved 2D-grid model. These results imply that the 2D-M2 model is able to capture the cross-frame actions in the system behavior.

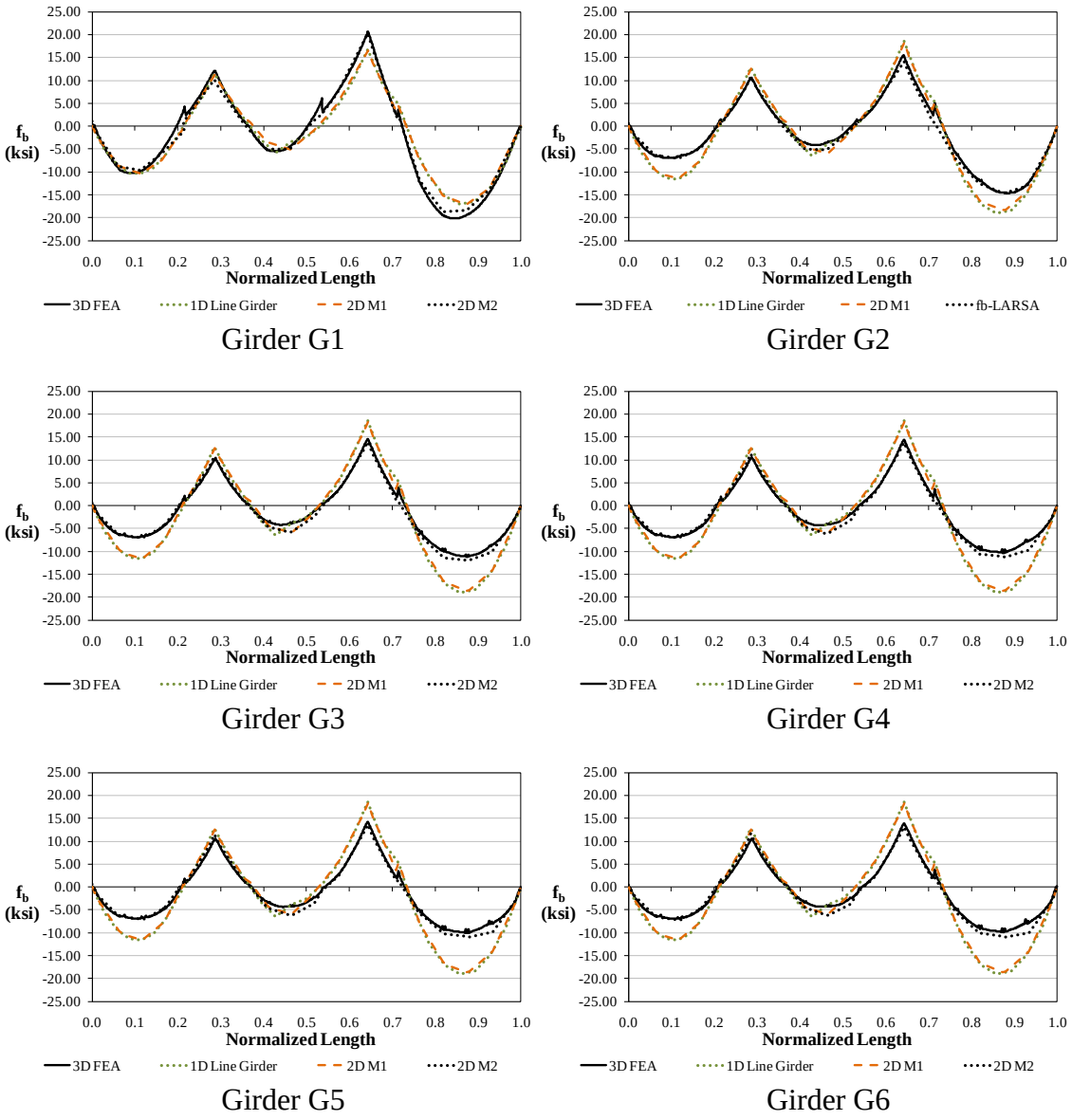


Figure 5.29. Major-axis bending stress responses at the top flange obtained from different analysis methods in bridge NICSS16, TDL level

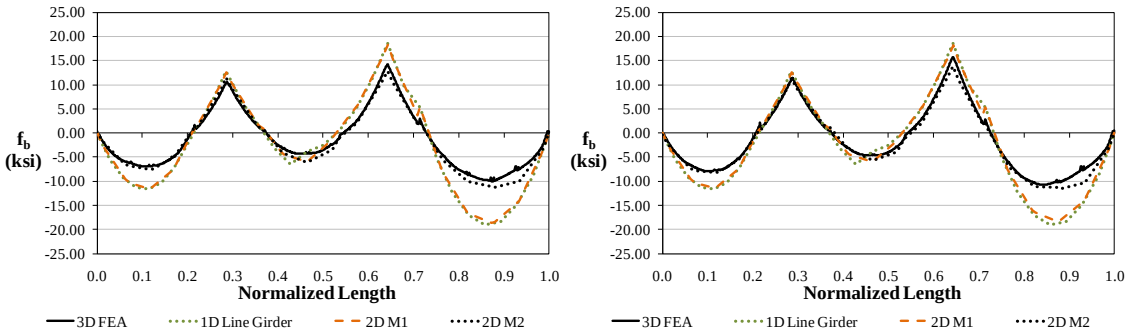


Girder G7 Girder G8

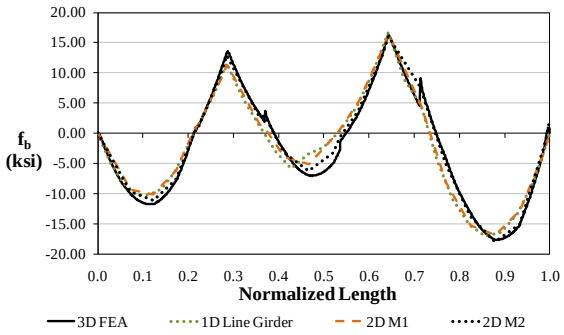


Girder G9

Figure 5.29. Major-axis bending stress responses at the top flange obtained from different analysis methods in bridge NICSS16, TDL level (continued)

The plots shown in Figure 5.30 correspond to the vertical displacements in the girders at the same load level, TDL. As in the case of the major-axis bending stresses, the girder deflections are poorly predicted by the 1D line-girder model and the 2D-M1 grid model. Especially in the girders G3 to G8, the displacements in Span 3 are significantly overpredicted by these approximate models. A more accurate representation is obtained when the improvements suggested for representing the cross-frames and the girder torsion properties are implemented in the 2D-grid model. As shown in the plots, the

responses obtained from the 2D-M2 model match almost exactly the benchmark responses obtained from the 3D FEA.

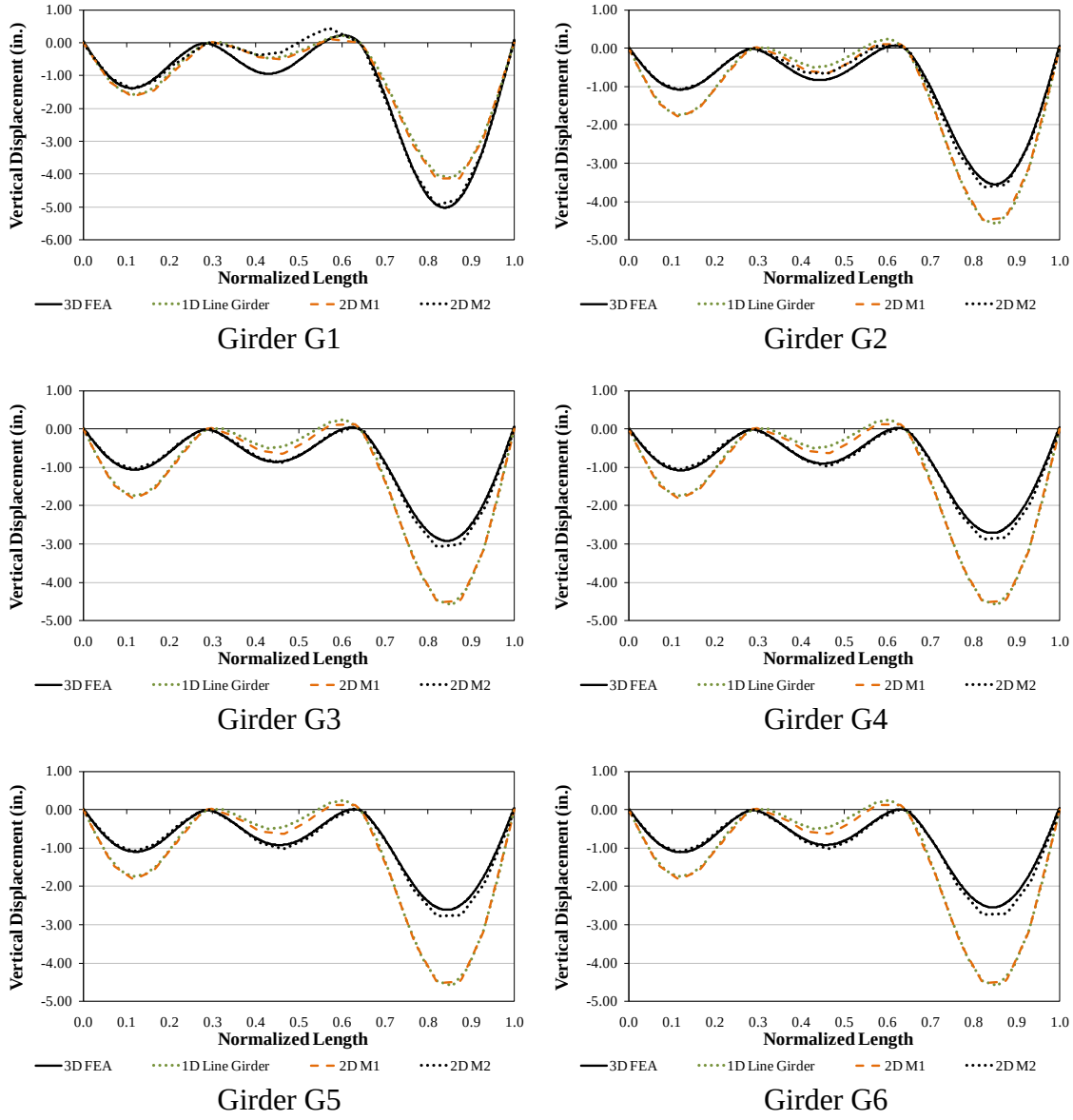


Figure 5.30. Girder vertical displacement obtained from different analysis methods in bridge NICSS16, TDL level

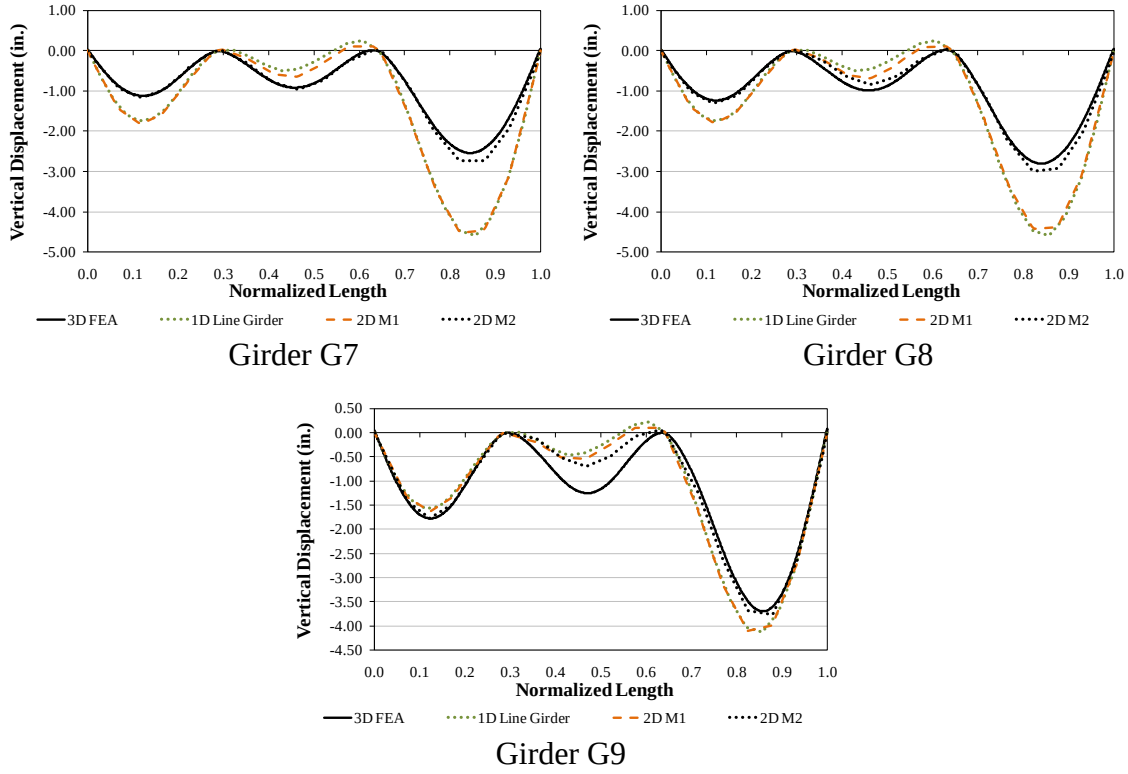


Figure 5.30. Girder vertical displacement obtained from different analysis methods in bridge NICSS16, TDL level (continued)

Finally, a comparison of the cross-frame forces obtained from the different analyses is shown in Figure 5.31. The figure shows the results for three of the eight bays of the bridge. The forces are shown in terms of bending moments and shear forces acting at the cross-frame ends. The plots only include the predictions obtained from the 2D-grid models and the 3D FEA. There are no predictions for the 1D line-girder analysis since this method cannot capture the cross-frame actions.

As depicted in the plots, the 2D-M1 results are very poor. The forces obtained from the 2D-grid model constructed using current practices are severely underpredicted. Both the shear forces and the bending moments are essentially zero in this model. As

previously concluded from studying the $f_b$ stress responses, this is equivalent to saying that in this model the girders are behaving as independent elements. However, significant improvements are obtained when the recommended representation of the cross-frames and the girder torsional stiffnesses are included in the analysis, as shown in the results of the 2D-M2 grid model. The forces predicted by this 2D-grid model are an acceptable representation of the forces predicted by the more rigorous 3D FEA.

The studies conducted on this bridge show that the skew effects may not be captured by 2D-grid analyses constructed with current practices. The transverse force flow which is a consequence of the skew can be captured only with a valid model of the torsional girder stiffness and the cross-frame contributions. Therefore, to obtain a more accurate representation of the system behavior, it is necessary to implement in the 2D-grid model the recommendations discussed in Sections 5.1 and 5.2. These recommendations not only improve the 2D-grid model response predictions in terms of major-axis bending stresses, $f_b$, and vertical displacements but also provide the information necessary to predict the flange lateral bending stresses, $f_\ell$, and girder layovers. As discussed later in Section 5.5, proper representations of these two responses can be computed by using the results of a 2D-grid analysis.

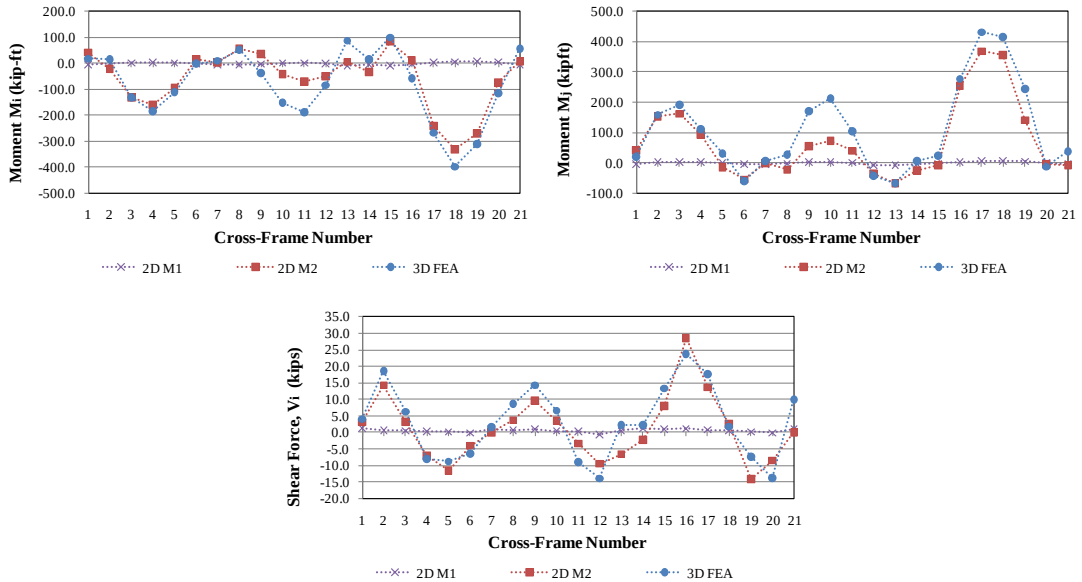


**Bay 3 (Girders G3-G4)**

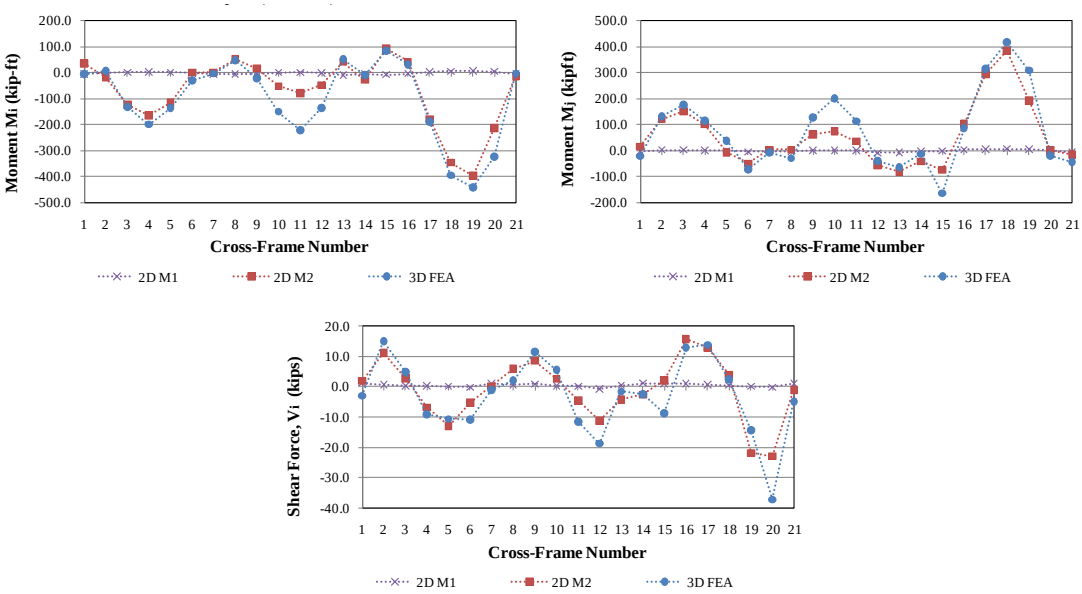


**Bay 6 (Girders G6-G7)**

Figure 5.31. Forces in cross-frame elements obtained from different analysis methods in bridge NICSS16, TDL level

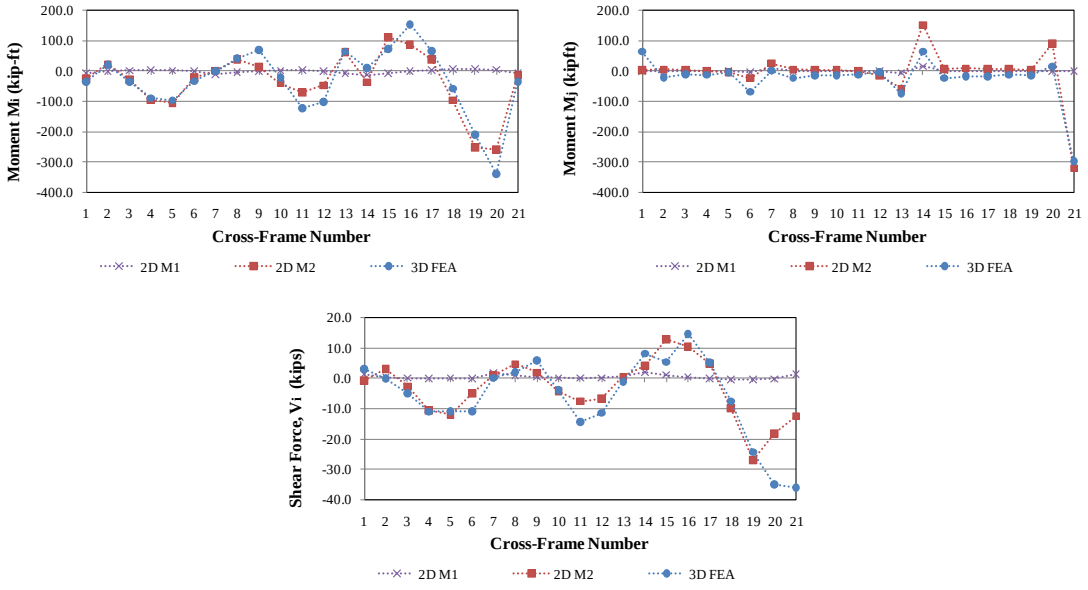


**Bay 8 (Girders G8-G9)**

Figure 5.31. Forces in cross-frame elements obtained from different analysis methods in bridge NICSS16, TDL level (continued)

### 5.4.3. Case Study III: Continuous Span Curved and Skewed Bridge (XICSS7)

The third case study is Bridge XICSS7. This structure was previously introduced in Section 4.3.1 to analyze the influence of different cross-frame configurations. The layout of the structure is reproduced in Figure 5.32. Due to its complex geometry, this continuous curved and skewed bridge represents a convenient scenario to study the capabilities of the 2D-grid models.

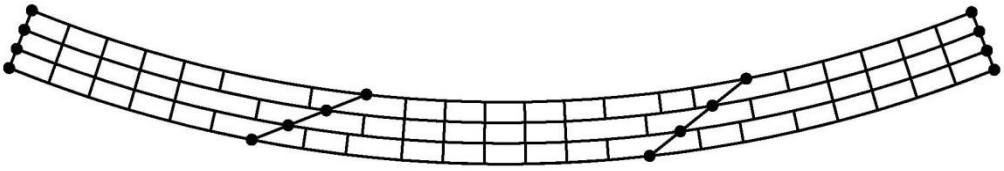

$L_1$ = 160 ft, $L_2$ = 210 ft, $L_3$ = 160 ft / $R$ = 700 ft / $w$ = 40.5 ft / $\theta_1$= 0 ˚, $\theta_2$= -60 ˚, $\theta_3$= -60˚, $\theta_4$= 0˚

Figure 5.32. Framing plan of XICCS7

Three different analyses are conducted for this bridge. The first is a 3D FEA, which is the most rigorous representation of the physical structure. The other two are 2D-grid analyses, 2D-M1 and 2D-M2, conducted following the current and improved modeling techniques, respectively. Figure 5.33 shows the major-axis bending stresses, $f_b$, predicted by the different models. As depicted in the plots, the results of model 2D-M2 are slightly closer to the 3D model predictions than the results obtained from 2D-M1, but in general, both 2D-grid models are an accurate representation of the benchmark.

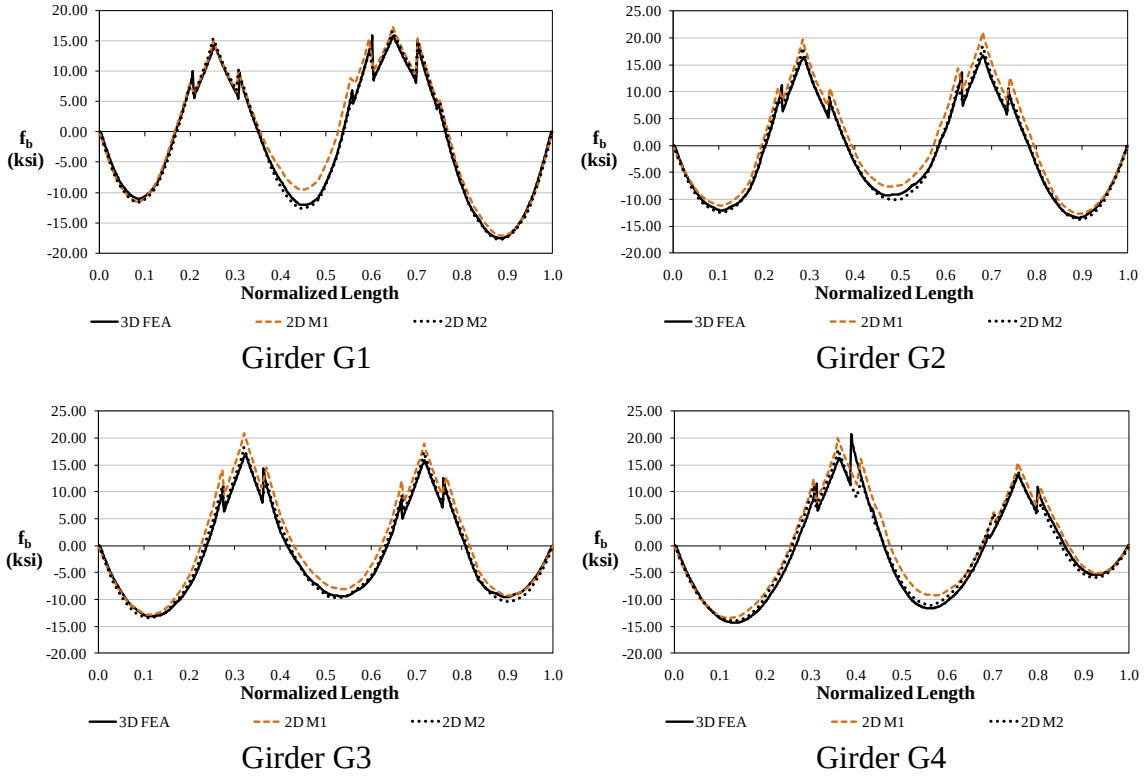


Figure 5.33. Major-axis bending stress responses at the top flange obtained from different analysis methods in bridge XICCS7, TDL level

In the case of the vertical displacements, the response correlation between the different methods is not the same as for the $f_b$ stresses. As shown in Figure 5.34, the vertical displacements obtained from the 2D-M1 model are significantly different than

the expected values. This inaccurate representation of the girder behavior is related to the poor torsion model characteristics of the elements used to model the I-girders. Usually, in a 2D-grid analysis of a curved bridge, the displacements are over-predicted when the contributions of flange warping are not included in the element formulation. This is an interesting characteristic of a curved bridge. While the major-axis bending stress response is commonly insensitive to the curvature and the torsion properties of the girders, the vertical displacements are highly dependent on these parameters. Hence, the displacement results obtained from a 2D-grid model constructed with current techniques may lead to inaccurate predictions of the system behavior during construction. For example, the use of the potentially incorrect vertical displacement predictions for determination of camber diagrams may complicate the control of the bridge geometry during deck placement.

When the 2D-grid model is improved by the techniques discussed in Sections 5.1 and 5.2, the vertical displacement responses are accurately captured. As shown in the plots of Figure 5.34, the predictions obtained from the 2D-M2 model are a close match of the results obtained from the refined 3D model.

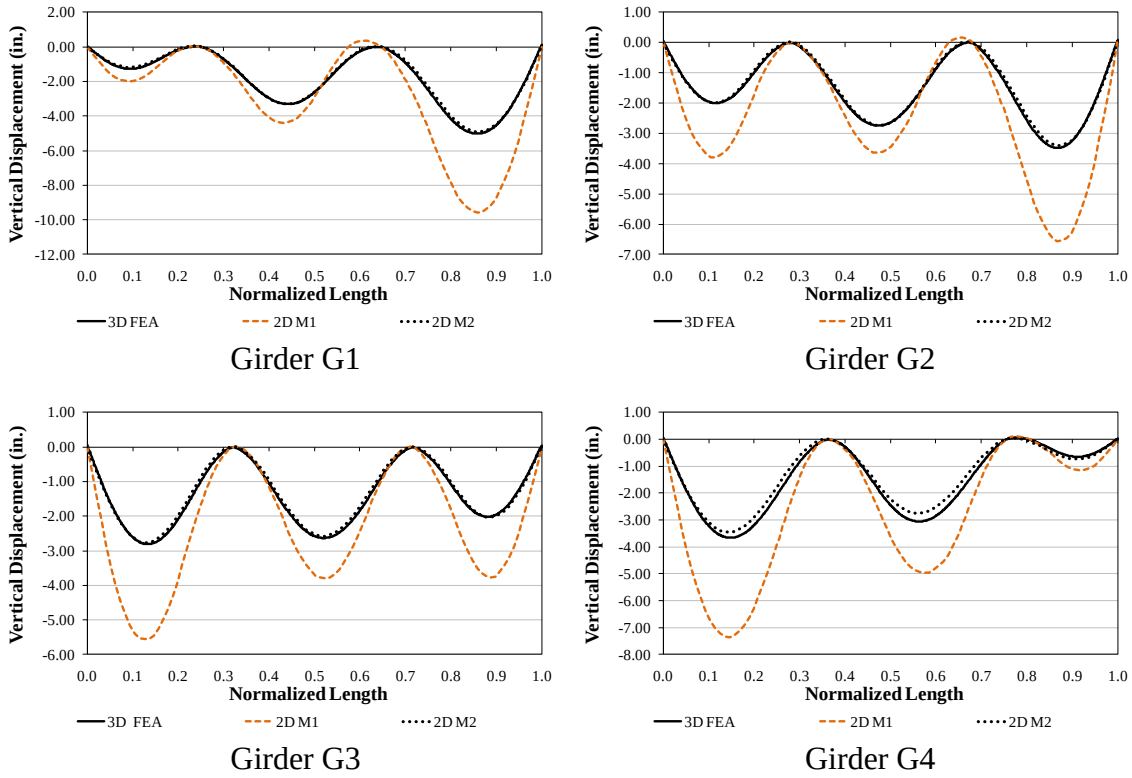


Figure 5.34. Girder vertical displacement obtained from different analysis methods in bridge XICCS7, TDL level

Another response that is of particular interest in curved bridges is the girder layovers. Figure 5.35 shows the response predictions obtained from the different methods. Similar to the vertical displacements, the layover predictions captured by the 2D-M1 model are a poor representation of the benchmark. The plots show that at the bracing points, the layovers obtained from this model are relatively close to the 3D model results. However, within the unbraced length, the response prediction is disproportionate. This is another effect of the limited model used to represent the torsion stiffness of the I-girders. The "bumps" in the traces indicate that the girder model is excessively flexible in torsion. A better prediction of the girder layovers is obtained by implementing the equivalent torsion constant in the definition of the cross-section properties of the girders and the proposed two-node elements to represent the cross-frames. As shown in the plots,

the results of the 2D-M2 model are very close to the layovers obtained from the 3D model.

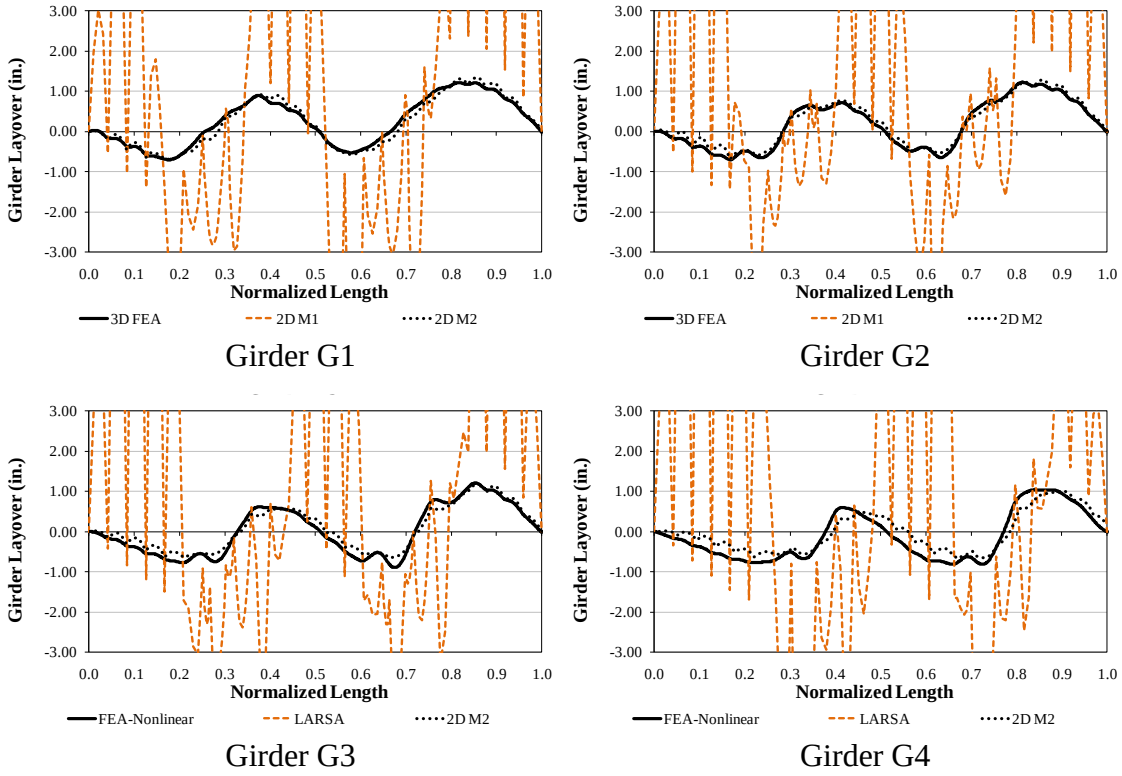


Figure 5.35. Girder layovers obtained from different analysis methods in bridge XICCS7, TDL level

The last responses studied in this bridge are the cross-frame forces. As in the previous case studies, the forces in Figure 5.36 are shown in terms of bending moments and shear forces applied at the cross-frame ends. The plots show that for this structure, both 2D-grid models capture the predictions of the refined 3D model. In this case, the load transfer from the interior girder G4 to the exterior girder G1 that occurs due to the horizontal curvature (see Section 4.1.1.1) is properly captured by both 2D models. Hence, for the prediction of the cross-frame forces in this particular structure, the limitations of model 2D-M1 do not have a major effect. However, as shown in the previous two case

studies, the limitations of the cross-frame and girder torsional stiffness models can have a considerable impact in the prediction of the cross-frame forces. For this reason, when the construction of an I-girder bridge is studied with a 2D-grid analysis, the designer should consider implementing the modeling techniques recommended in Sections 5.1 and 5.2.

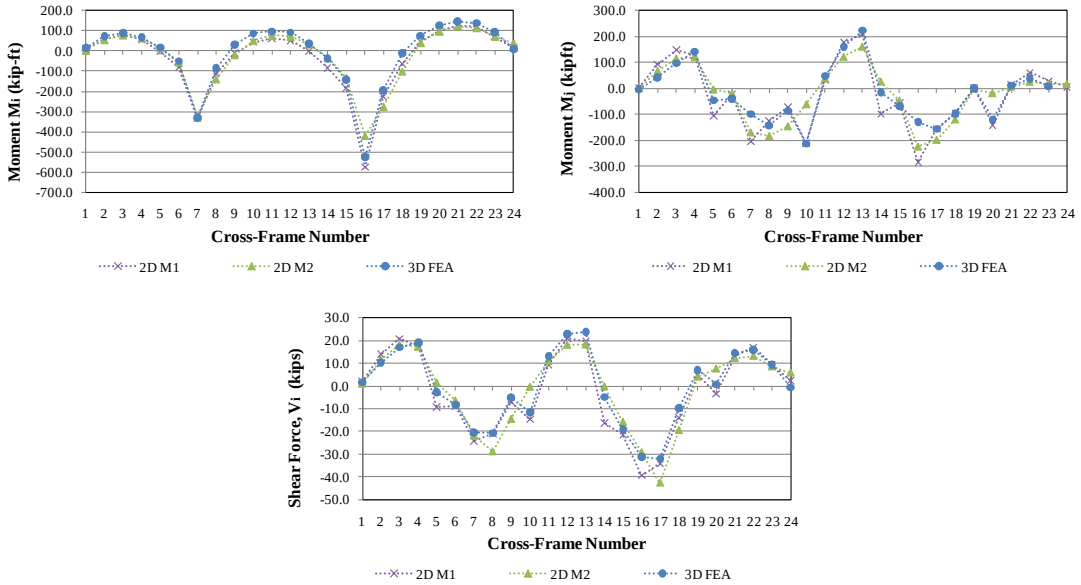


**Bay 1 (Girders G1-G2)**

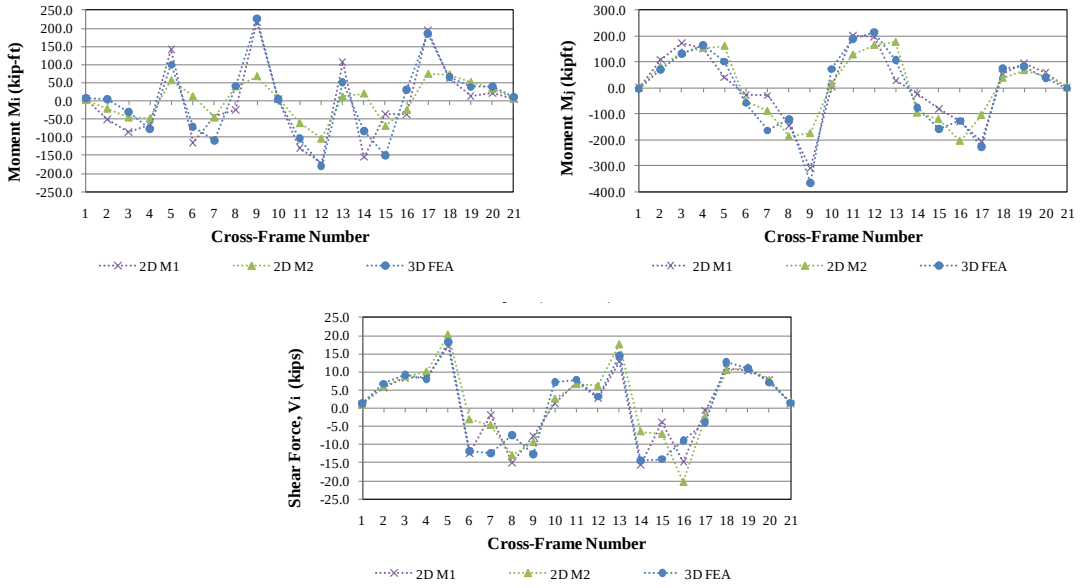


**Bay 2 (Girders G2-G3)**

Figure 5.36. Forces in cross-frame elements obtained from different analysis methods in bridge XICCS7, TDL level

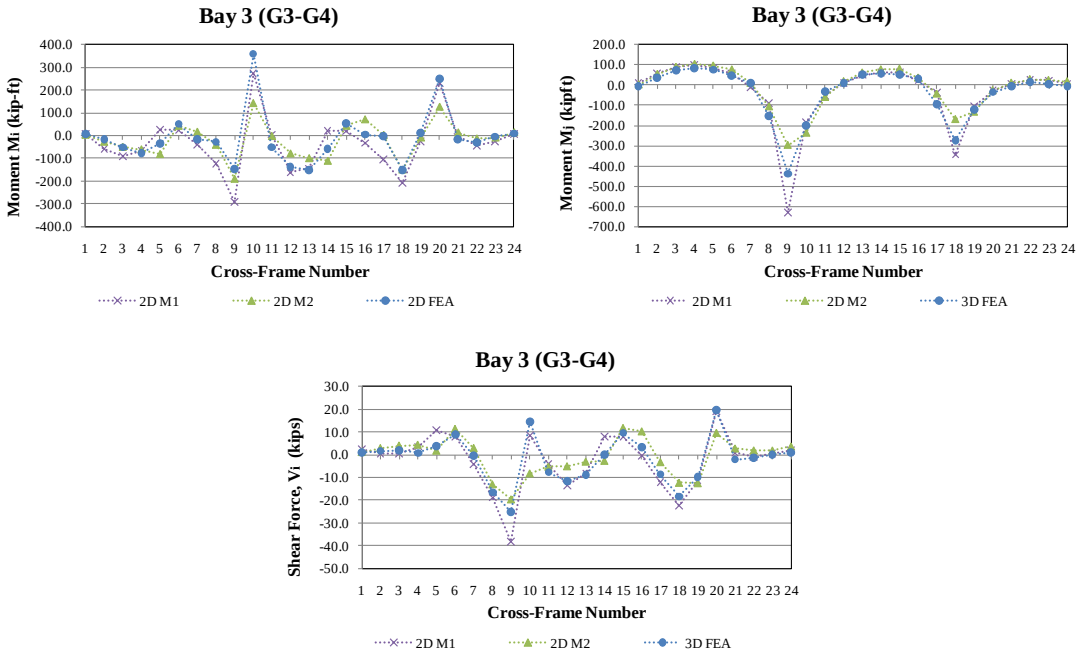


**Bay 3 (Girders G3-G4)**

Figure 5.36. Forces in cross-frame elements obtained from different analysis methods in bridge XICCS7, TDL level (continued)

## 5.5. Determination of I-Girder Flange Lateral Bending Responses due to Skew Effects

Two of the most important collateral effects of the skew are the flange lateral bending stresses and the girder layovers. It is necessary to have an estimate of the stresses, so they can be considered in the dimensioning of the I-girders. Besides, the prediction of the girder layovers is required to control the geometry of the structure during its construction. Currently, there is little guidance on how to evaluate these responses. In this section procedures to determine the flange lateral bending stresses and the girder layovers of I-girder bridges during construction are provided.

### 5.5.1. Procedure to Compute Flange Lateral Bending Stresses

In a steel girder bridge, the flange lateral bending stresses, $f_\ell$, that result from the horizontal curvature and the skew effects must be considered in the design of the structure. As required by the AASHTO Bridge Specifications (AASHTO 2010), these stresses are combined with the major-axis bending stresses to conduct the strength checks in the noncomposite and composite structure. However, at present, there is limited information on how to determine the $f_\ell$ stresses associated with the skew.

In a skewed bridge, the cross-frames induce forces in the I-girders, subjecting their flanges to lateral bending stresses, $f_\ell$. Currently, the only accurate methods to compute these forces and stresses are via refined "3D" grid models that explicitly include the warping stiffness contributions (see Section 4.1.2) or a rigorous 3D FEA. However, with some exceptions, these analysis methods are predominantly used for research purposes. As discussed in Section 4.1, they can require significant effort to construct the model and post-process the results.

To obtain the $f_\ell$ stress responses, it is necessary to have an accurate prediction of the cross-frame forces. In the approximate 1D line-girder analysis, the forces in the cross-frames due to the skew are not captured; therefore, it is not feasible to determine the $f_\ell$ stresses associated with this parameter. Similarly, as shown in the case studies of Section 5.4, due to the poor representation of the cross-frames and the torsion model of the I-girders, the 2D-grid models constructed with current techniques do not capture the cross-

frame forces. For these reasons, the AASHTO Bridge Specifications (AASHTO 2010), Section C6.10.1 state that:

"In the absence of calculated values of $f_\ell$ from a refined analysis, a suggested estimate for the total $f_\ell$ in a flange at a cross-frame or diaphragm due to the use of discontinuous cross-frame or diaphragm lines is 10.0 ksi for interior girders and 7.5 ksi for exterior girders. These estimates are based on a limited examination of refined analysis results for bridges with skews approaching 60 degrees from normal and an average $D/b_f$ ratio of approximately 4.0. In regions of the girders with contiguous cross-frames or diaphragms, these values need not be considered. Lateral flange bending in the exterior girders is substantially reduced when cross-frames or diaphragms are placed in discontinuous lines over the entire bridge due to the reduced cross-frame or diaphragm forces. A value of 2.0 ksi is suggested for $f_\ell$, for the exterior girders in such cases, with the suggested value of 10 ksi retained for the interior girders. In all cases, it is suggested that the recommended values of $f_\ell$ be proportioned to dead and live load in the same proportion as the unfactored major-axis dead and live load stresses at the section under consideration. An examination of cross-frame or diaphragm forces is also considered prudent in all bridges with skew angles exceeding 20 degrees."

The variety of geometries of highway bridges is extensive, including a large range of skew, length, width, number of spans, and curvature combinations. Therefore, the above recommendations are coarse estimates that provide the Engineer with stress values that may be used to consider the skew effects in design.

In this section, a method to estimate the $f_\ell$ stresses in straight and skewed bridges is introduced. For this purpose, the bridge analyzed in Section 5.4.1 to demonstrate the applicability of the improved 2D-grid methods of analysis, NISSS16, is revisited. Figure 5.37(a) shows the plan view of the bridge. It is intended to capture the flange lateral bending stress response in the top flange of girder G6. As discussed in Section 4.2, due to the noncomposite dead loads, in a skew bridge there is a transverse flow of forces that is transferred by the cross-frames. Figure 5.37(b) shows the free-body diagram of the second cross-frame in Bay 6, B6-CF2. The cross-frame forces are transferred to the girders in the form of nodal forces. The horizontal and vertical components of the vertical loads are determined by applying the equilibrium equations at nodes A to D, such that:

$$\begin{aligned} A_x &= -F_{BC} - F_{D2}\cos(\theta) \\ A_y &= -F_{D2}\sin(\theta) \\ B_x &= -F_{TC} - F_{D1}\cos(\theta) \\ B_y &= F_{D1}\sin(\theta) \\ C_x &= F_{TC} + F_{D2}\cos(\theta) \\ C_y &= F_{D2}\sin(\theta) \\ D_x &= F_{BC} + F_{D1}\cos(\theta) \\ D_y &= -F_{D1}\sin(\theta) \end{aligned} \qquad \text{(Eq. 5.37)}$$

where θ is the angle between the chords and the diagonals. Next, the flange is isolated from the rest of the structure and subjected to the horizontal components of the nodal forces, as illustrated in Figure 5.37(c). Notice that the $C_x$ force components of the cross-frames in Bay 5 are applied on one side of the flange, while the $B_x$ components of the Bay 6 cross-frames are applied on the other side. The magnitudes of the forces acting on the flange in discussion are included in the figure. They are computed with Eqs. 5.37, by using the cross-frame force estimates obtained from the improved 2D-grid analysis of this

bridge (see Section 5.4.1). To recognize the fact that there is an offset between the cross-frame chords and the flange locations, the nodal forces shown in Figure 5.37(c) are factored by $h/h_o$, where $h$ is the height of the cross-frame and $h_o$ is the distance between flange centroids.

These nodal force lateral components are the source of the lateral bending in the flange; however, only those forces that are acting in the region where the cross-frames are staggered can cause large stresses. As shown in Figure 5.37(c), the forces in the region where the cross-frames are contiguous can be larger than those where they are staggered, but they tend to cancel each other out. For example, in the intermediate contiguous cross-frame line close to the skewed support, the forces are 26.67 kips in B5-CF4 and -25.36 kips in B6-CF5, and the resultant is 1.31 kips. Hence, although the nodal forces are larger than in other parts of the flange, the force resultant causes a minor effect on the lateral bending. The connections between the cross-frames and the girders, however, must be designed considering these forces. Another important aspect to consider regarding this approximate procedure is that the nodal forces are not completely balanced. In the case of the flange under consideration in Figure 5.37(c), the unbalance calculated by adding all the lateral forces acting in the flange is -2.58 kips. The reason is that only the forces originated by the cross-frames are considered in the analysis. In reality, some lateral forces are transferred to the flange via the web. If these forces are added to the nodal forces, the flange would be in equilibrium.

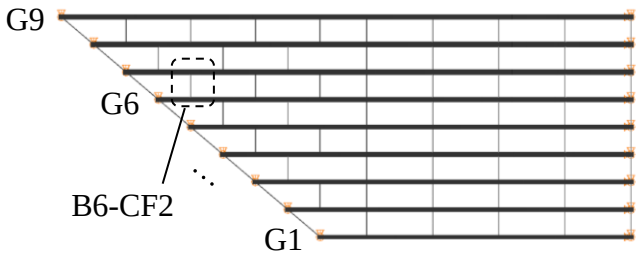


(a) Plan view of Bridge NISSS16

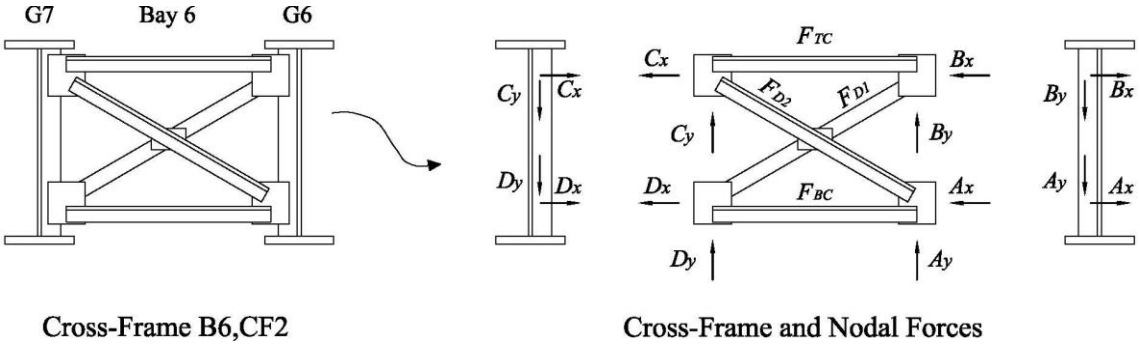


(b) Forces transferred from cross-frame B6-CF2 to girders G6 and G7

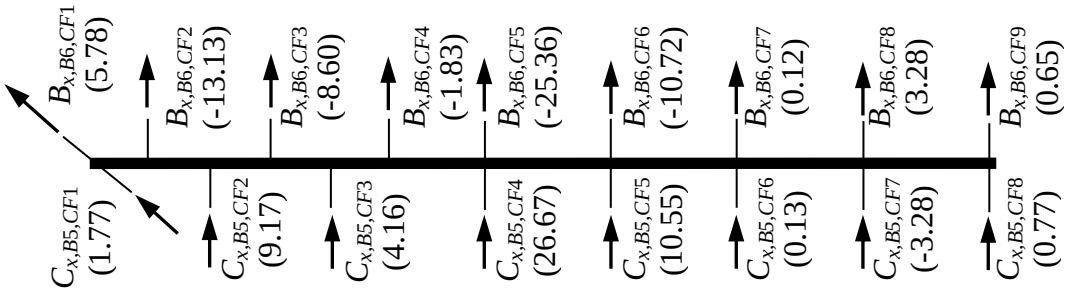


(c) Top flange of girder G6 subject to the horizontal components of the nodal forces

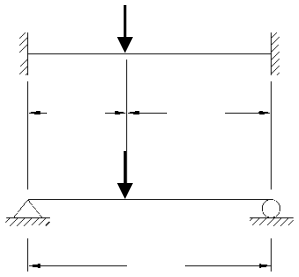

$$M_{\ell\,(F)} = \frac{2Pa^2b^2}{L^3}$$

$$M_{\ell\,(P)} = \frac{Pab}{L}$$

(d) Lateral bending moment, $M_\ell$, in a flange segment under different support conditions

Figure 5.37. Procedure to determine the flange lateral bending stresses in the top flange of girder G6, NISSS16, at TDL level

The next step in the procedure is to obtain the lateral bending moment, $M_\ell$, at each cross-frame location. For this purpose, a flange segment is isolated and analyzed as an equivalent beam subject to a point load, as depicted in Figure 5.37(d). Accurate evaluation of the $M_\ell$ values from the free-body diagram in Figure 5.37(c) is not possible since the location of the above out-of-balance forces (summing to -2.58 kips) is not known. Hence, any minor error in approximating the forces coming from the web accumulates and leads to a large error in the calculation of $M_\ell$ as one moves along the length of the girder.

In Figure 5.37(d), the variables *a* and *b* are the distances between the point load and the two adjacent cross-frames. In the equivalent beam, the boundary conditions depend on the level of rotational restraint provided by the adjacent flange segments. Unfortunately, it is not practical to determine precisely the flange rotations at the ends of the segment under consideration. Instead, bounds for the lateral bending moment can be determined by assuming the ends are either fully fixed or simply-supported. From these results, the $f_\ell$ stresses are estimated by dividing the lateral bending moments by the corresponding elastic section modulus of the flange.

Figure 5.38 shows the plots of the response predictions obtained using this approach and the results obtained from the 3D FEA for the top flange of Girders G1, G3, and G6. The plots include the responses for fully fixed and simply supported end conditions. Additionally, a trace that represents the average between these two responses is included. As shown in these plots, the estimates obtained with the proposed approach

and using the results derived from the improved 2D-grid model are a reasonable representation of the benchmark. The responses predicted by the FEA lay between the predictions determined assuming fully fixed and pinned ends, and are estimated reasonably well by taking the average of the last two predictions.

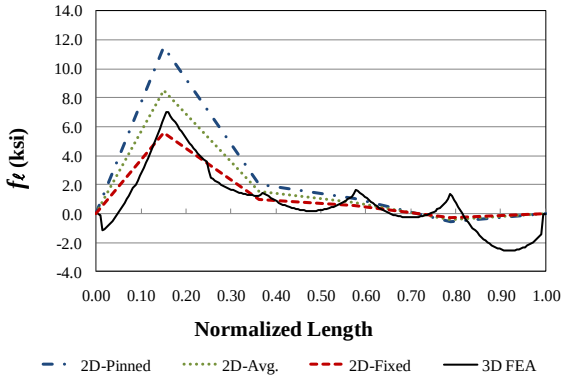


**Girder G1**

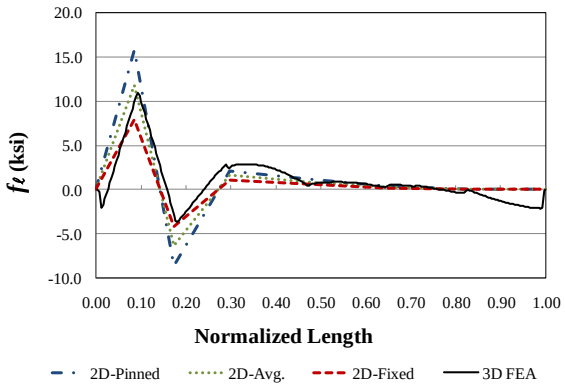


**Girder G3**

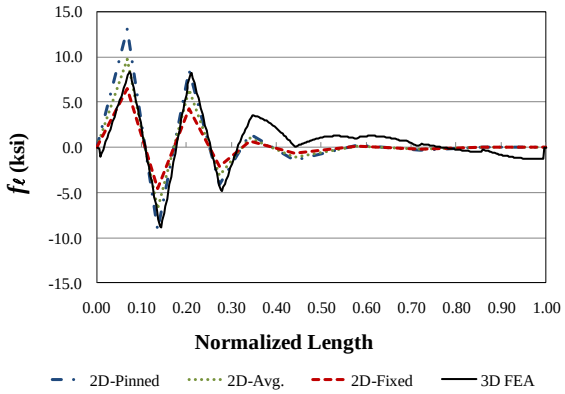


**Girder G6**

Figure 5.38. Flange lateral bending stresses in Bridge NISSS16 at TDL level

To further study the applicability of the proposed procedure, the flange lateral bending stress responses in girders G1, G3, and G6 of Bridge NICSS16 are shown in Figure 5.39. This structure is an ideal case study due to the high levels of flange lateral bending encountered during its construction. As depicted in the plots, the approximate analysis provides a reasonable representation of the $f_\ell$ stress responses. As in the previous case, the 3D FEA response is confined between the predictions obtained using the two extreme support conditions. The average of these two responses is close to the solution obtained from the refined model.

The method proposed to calculate the flange lateral bending stresses in skewed bridges provides the bounds for this response. The Engineer can determine the maximum and minimum stress levels expected in a skewed structure. The average of the two bound responses may be considered as a reasonable estimate of the expected response. This is a similar criterion to the one used to predict the $f_\ell$ stresses due to curvature effects. As described in Section 4.1 for the calculation of the lateral bending stresses at the cross-frame positions, a factor of 10 may be used instead of 12 in the denominator of Eq. 4.5 to recognize the fact that the flange rotations are not fully fixed at the brace points. Similar to this factor, the average response in the above calculations is an empirical approximation of the physical behavior of the structure.

It should be emphasized that in order to predict the flange lateral bending stresses using the proposed method, it is necessary to first have an accurate prediction of the cross-frame forces. Hence, the results of a 2D-grid analysis conducted with current practices cannot be used for this purpose. The cross-frame forces should be obtained from

an analysis where the recommendations of Sections 5.1 and 5.2 are implemented in the model. Finally, in curved and skewed I-girder bridges, the $f_\ell$ stresses calculated with the procedure described above to consider the skew effects can be added to the $f_\ell$ stresses calculated with Eqs. 4.1 and 4.5 to include the eccentric overhang loads and the curvature effects respectively.

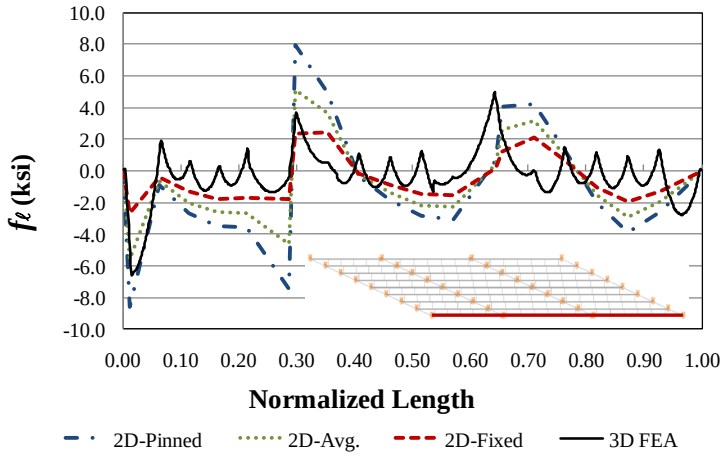


**Girder G1**

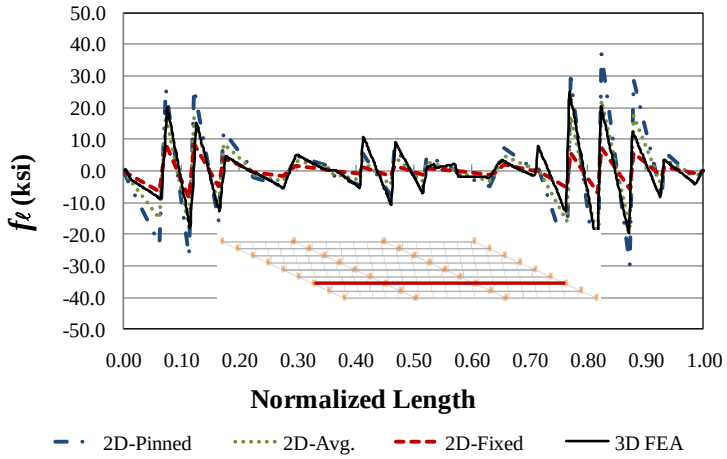


**Girder G3**

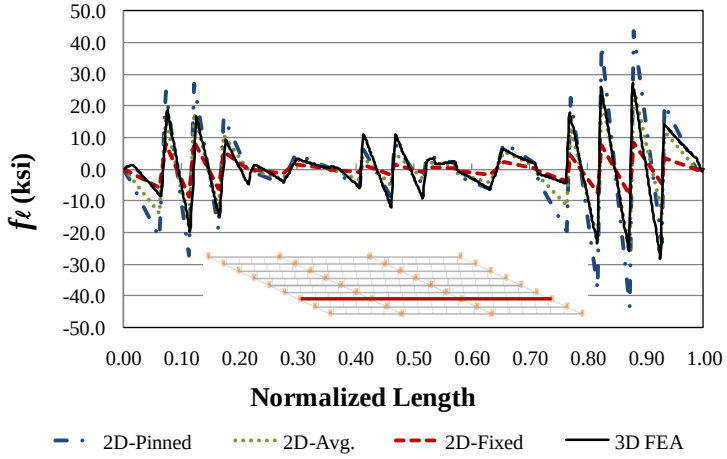


**Girder G6**

Figure 5.39. Flange lateral bending stresses in Bridge NICSS16 at TDL level

### 5.5.2. Procedure to Compute Girder Layovers

The girder lateral displacements in a skewed bridge can be predicted at the cross-frame locations based on the major-axis bending response. If the vertical displacements are known, the geometry of the bridge can be used to determine the rotation of the girders at the braced locations. Figure 5.40 shows the undeflected and deflected positions in a two-girder system, when it is subject to gravity loadings.

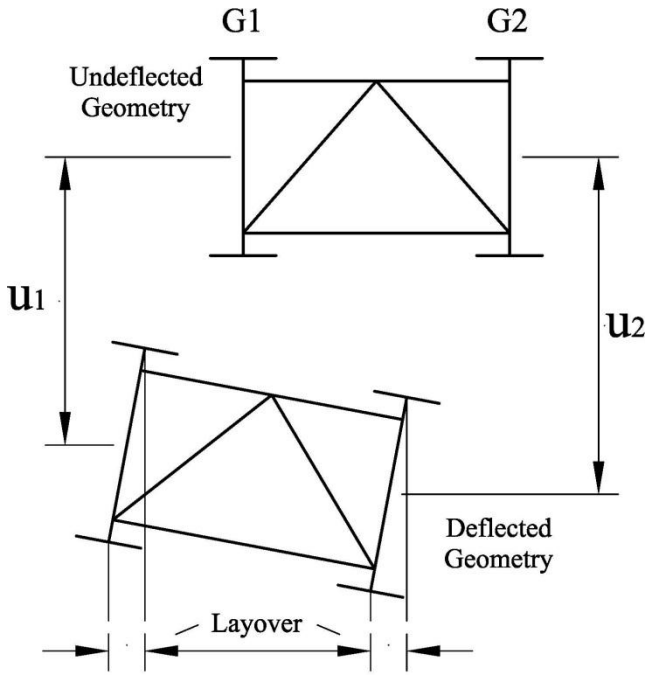


Figure 5.40. Vertical displacements and girder layover in a two-girder system with skewed supports

As shown in the figure, the girders have to rotate to accommodate the differential deflections. Thus, the relative lateral displacement between the top flange and the bottom flange or girder layover is given by

$$\text{layover} = \frac{u_2 - u_1}{s} d \qquad \text{(Eq. 5.38)}$$

where $d$ is the web depth, $s$ is the distance between girders, and $u_1$ and $u_2$ are the vertical displacements of girders G1 and G2, respectively. Two assumptions need to be considered when determining the layovers based on Eq. 5.38. First, it is assumed that the webs of the girders do not deform. Since at the cross-frame positions the connection plates are rigidly attached to the web and flanges, it is possible to assume that the girder webs remain straight. The second assumption is that as the girders deflect, the cross-frame moves as a rigid body, so the rotations in two adjacent girders are the same. Since the in-plane stiffness of the cross-frames is significantly larger that the torsional stiffness of the girders, the cross-frames displace as quasi-rigid bodies. Hence, this assumption is valid for most practical cases.

In addition, to apply this formula, it is required that the cross-frames are oriented perpendicular to the girders. At the supports, however, the cross-frames are generally oriented parallel to the skewed bearing line. As discussed in Section 5.2.4, Ozgur and White (2007) propose a method to compute the layover at the bearing lines that is based on the compatibility of displacements between the girders and the bearing line cross-frames. According to the researchers, the girder layovers at the bearing lines can be calculated with Eq. 5.35, which is reproduced here for convenience:

$$u_{lat} = u_b \cdot \tan(\theta) \qquad \text{(Eq. 5.39)}$$

where $u_{lat}$ is the layover of the girder top flange, $u_b$ is the difference of the longitudinal deflection of the top and bottom flanges due to the major-axis bending rotation at the bearing line, and $\theta$ is the skew angle.

Eqs. 5.38 and 5.39 can be used to predict the girder layover at the bracing points. In many cases, these values should be sufficient to predict the geometry of the bridge during construction and the expected values of out-of-plumbness in the girder webs. Within the unbraced lengths, this response is dominated by the torsional rigidity of the girders. For design purposes it could be assumed that the lateral displacements vary linearly between the cross-frames. In properly braced bridges, this assumption should be sufficient. If large lateral displacements in the unbraced length are observed, the structural stability of the girders should be studied since the structure may be undergoing large second order amplifications.

The above recommendations are applied to predict the girder layover in Bridge NISSS16. Figure 5.41 shows the vertical displacements in the girders due to the total noncomposite dead load, TDL. The girder deflections are obtained from a 2D-grid analysis conducted following the recommendations discussed in Sections 5.1 and 5.2. In the plot, the girders are shifted in the horizontal axis to depict their relative position with respect to the longest girder, G9. This plot is equivalent to an elevation view of the deflected shape of the bridge. The cross-frame positions have also been included in the plot to observe the differential deflections that these components accommodate through girder rotations. As shown in the figure, large differential deflections are introduced by the skew and girder length difference. The largest values are observed at the cross-frame line 9, CF9. There is a 13.6-in. difference between the deflection of the shortest girder, G1, and the deflection of the longest girder, G9.

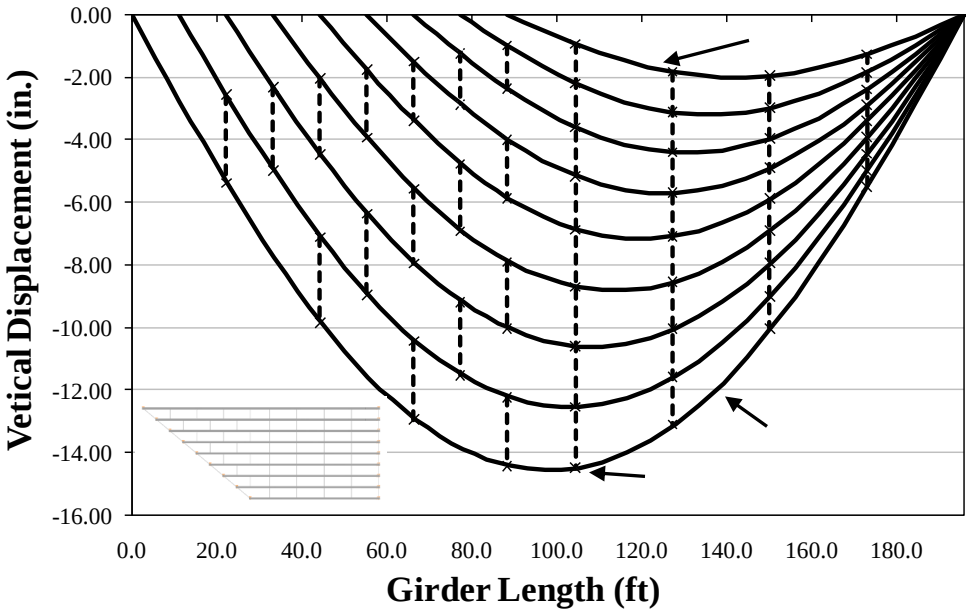


Figure 5.41. Girder vertical deflections in Bridge NISSS16 at TDL level

Before applying the recommendations to compute girder layovers, it is convenient to examine the relative lateral displacement response of the girders obtained from the 3D FEA. The responses plotted in Figure 5.42 show that the layover of the girders at the bracing locations is practically the same. As shown in the figure, the responses between two adjacent girders meet at the bracing positions. This implies that the approximation that the cross-frames do not experience large in-plane deformations is valid for this structure. Another aspect in this plot that deserves attention is the response of the girders between the bracing points. As depicted in the plot, the layover between the cross-frames varies almost linearly for all the girders. This is an expected result, given that this bridge is properly braced, with cross-frames every 15 to 22.5 ft.

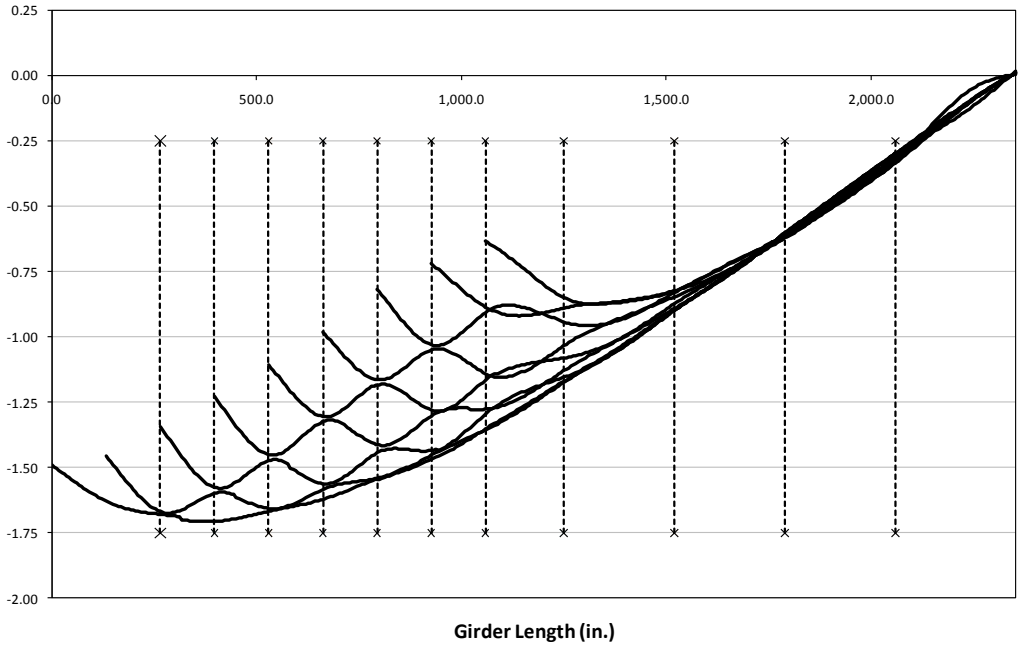


Figure 5.42. Girder layover in Bridge NISSS 16 at the TDL level

The plots that compare the layovers obtained from the refined analysis versus the approximate results for girders G2, G5, and G9 are shown in Figure 5.43. The plots show that the predictions of the girder layovers using the above recommendations fit the benchmark responses accurately.

The proposed procedure can be applied to any type of skewed bridge, including straight and curved bridges. Its accuracy depends on the accuracy of the predicted vertical displacements. In this example, the girder layovers were calculated based on the vertical deflections obtained from an improved 2D-grid model. However, if the structure has a small skew index, the layovers could also be obtained from a 1D line-girder analysis.

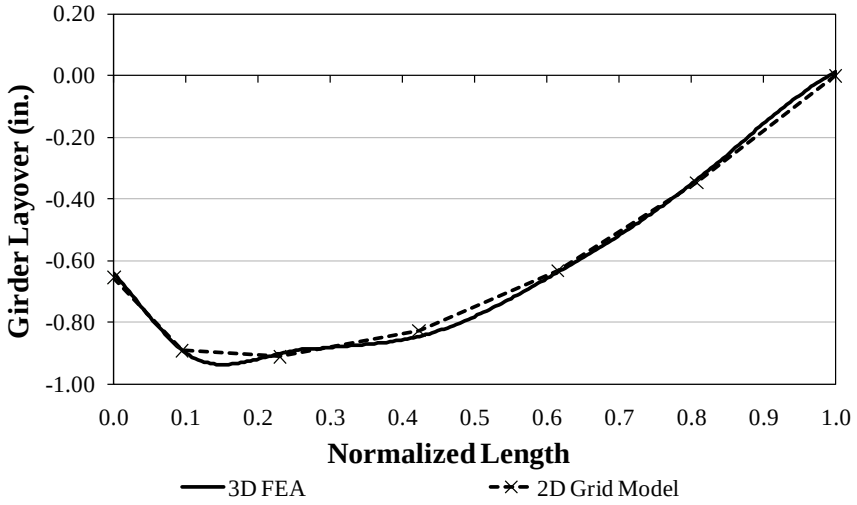


**Girder G2**

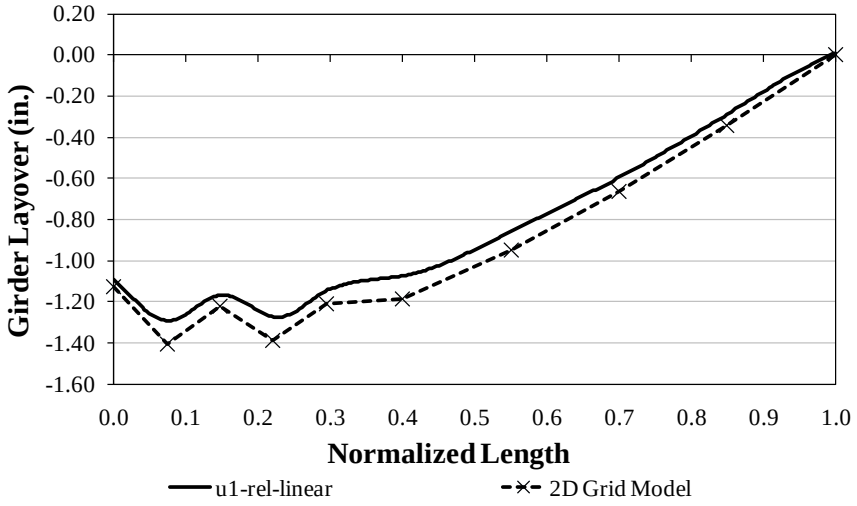


**Girder G5**

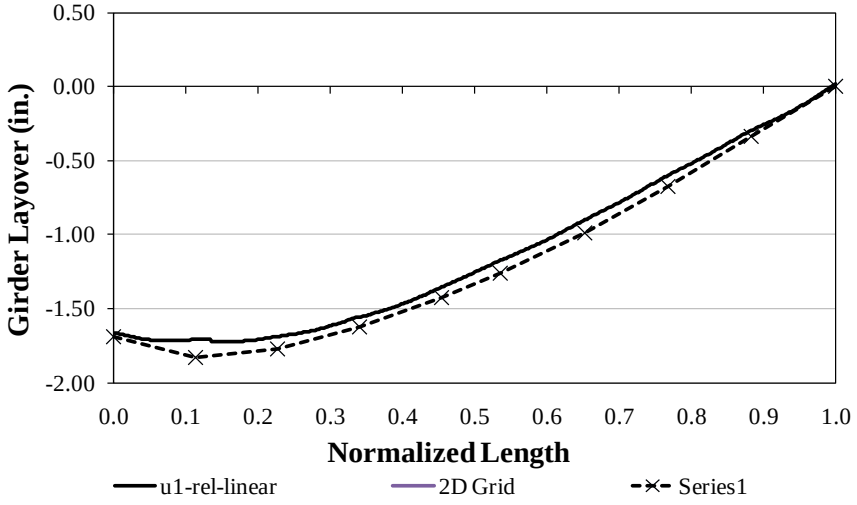


**Girder G9**

Figure 5.43. Girder layovers in Bridge NICSS16 at TDL level

# CHAPTER VI

# EFFECTS OF PERMANENT METAL DECK FORMS ON THE BEHAVIOR OF I-GIRDER BRIDGES

## 6.1. Background

Traditionally, in the engineering of steel bridges the use of stay-in-place (SIP) metal deck forms as a means to brace the girders during construction has been prohibited. In fact, AASHTO (2010), Section 6.7.4.1 states that the use of SIP forms for these purposes is not allowed. On the other hand, in the steel building industry, metal deck forms have been considered as an effective method to provide stability bracing in floor beams. It is important, however, to recognize that there are differences between these applications. The methods to attach the forms to the steel members in bridges are different than the used for buildings. In steel bridges, the forms are connected between the top flanges of two adjacent girders (see Figure 6.1) with a detail that facilitates the control of the deck profile prior to its placement. This detail, however, decreases the form's efficiency for bracing purposes, as discussed in Section 6.2. In steel buildings, the SIP form-flange attachment is done with puddle welds or self-drilling screws that do not interrupt the continuity of the forms over the flanges. When the form flutes are perpendicular to the beams, the forms impede the top flange lateral displacement, stabilizing the beams during the slab casting.

Figure 6.1. SIP forms in a bridge prior deck placement

Another difference between bridge and building applications is the type of loading actions during the noncomposite state. The dead loads and construction loads in these types of structures are significantly different. The strength requirements and therefore the bracing requirements in a bridge girder are much larger than in a floor beam.

The participation of the SIP metal deck forms on the structural behavior of steel bridges is a topic that has caught the interest of researchers and practitioners in recent years. The need of systems that enhance the structural performance and reduce the construction costs has resulted in several research efforts to study the bracing properties of these traditionally non-structural components. The most relevant research conducted in this field is summarized in Section 6.2. These studies show that unless enhanced details are used to attach the forms to the girder flanges, the SIP forms do not serve as an efficient means for girder bracing. On the other hand, researchers have recognized that even though the metal deck forms may not be used for bracing purposes, they are part of the structural system. Therefore, they can affect the control of the bridge geometry during

construction. Section 6.3 discusses some of the previous work conducted to evaluate the influence of the SIP forms on the structural responses. Section 6.4 presents studies conducted in two structures that, due to their specific characteristics, are sensitive to the stiffness contributions of the SIP forms. The studies are used to recognize situations where the influence of the forms on the system response may not be negligible.

## 6.2. Diaphragm Bracing of I-Girders

### 6.2.1. Construction Practices

In bridge construction, the practices used to connect SIP forms to the girder top flanges are aimed to facilitate the control of the deck profile prior to its placement. Figure 6.2 illustrates two of the most common details. In the first case, the light gage support angle is welded to the flange, and the forms are attached to the outstanding leg using self-screwing fasteners. When welding directly to the flange is not permitted, a strap angle is used to connect the support angles at each side, and hold-down clips are provided to tighten the support angles to the girder. The practices to attach the support and strap angles to the flanges vary from contractor to contractor, but the concepts shown in Figure 6.2 are essentially kept the same.

The main advantage of these details is that by varying the level at which the support angle is placed relative to the flange, the positioning of the SIP forms can be adjusted to obtain an adequate deck profile. This is a method to smooth out the differential deflections that may exist between girders due to the fabrication and erection procedures, and also, to accommodate the elevation differences due to changes in flange thicknesses and superelevation.

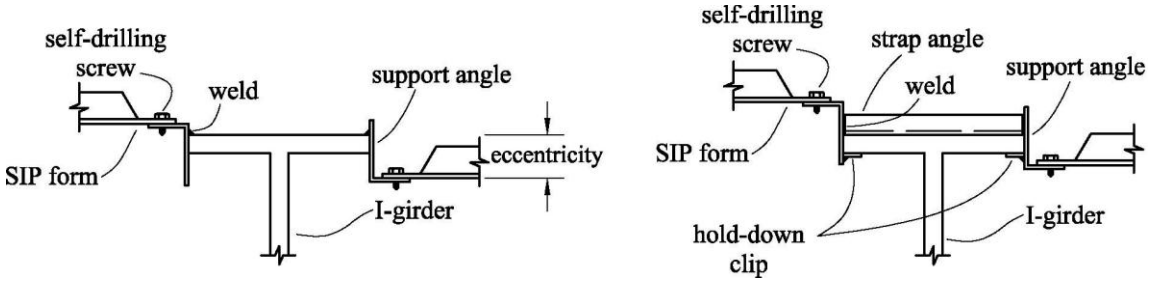


(a) Angle - flange weld permitted (b) Angle - flange weld prohibited

Figure 6.2. Details used to connect SIP forms to the top flange

### 6.2.2. Structural Properties of SIP Forms

In the last two decades, extensive experimental programs have been conducted to determine the structural properties of SIP forms used in bridge construction, and the feasibility of using them for bracing purposes. Most of these experiments have been conducted at the University of Texas at Austin and the University of Houston, and their results are summarized in the next paragraphs. The research in this field has significantly contributed to understand the performance of the panels and to determine the aspects that control their structural properties.

The structural characteristics of SIP forms or panels are normally characterized in terms of their shear stiffness. The resistance to shear racking is considered to be the largest source of stiffness in the panels. The test setup commonly implemented to determine the properties of SIP forms is depicted in Figure 6.3. In these tests, a panel is connected to a frame that is subjected to a lateral force, *P*. This force creates a compression and a tension field in the panel that resembles the behavior of a truss system. From the test, an effective shear modulus, $G'$, is determined as

$$G' = \frac{PL^2}{fw\Delta} \qquad \text{(Eq. 6.1)}$$

The variables in this equation are defined in Figure 6.3.

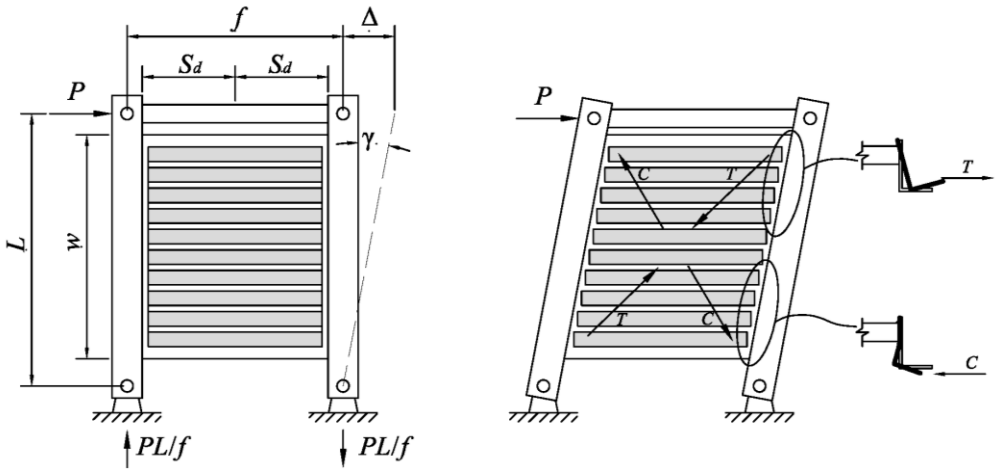


Figure 6.3. Shear test frame (adapted from Egilmez et al. 2007 and Egilmez et al. 2009)

Several research efforts have been conducted to test SIP forms used in bridge construction. Currah (1993) tested a number of panels of different gage and with different connection details to capture their shear stiffness properties. Similarly, Jetann (2003) and Lowery (2003) conducted shear tests in SIP forms that extended the experimental data available. The three researchers arrived at the same fundamental conclusion regarding the feasibility of using SIP forms for bracing purposes. They concluded that the flexibility of the connection detail used to attach the forms to the top flange reduces drastically the effective stiffness properties of the panels. As depicted in Figure 6.2 and Figure 6.3, there is an eccentricity between the weld and the panel level. In the region where the panel develops a tension field, the support angle pulls away from the flange, rotating about the weld as essentially a rigid body. In the region where the panel is subject to compression, the angle bents under the flange tip. Currah (1993) reports that due to this eccentricity,

the effective shear stiffness reduction can be larger than 80 % versus the case where the weld and the panel level are collinear (i.e., no eccentricity).

Egilmez et al. (2009) conducted a different set of tests to determine the bracing properties of the SIP forms. As depicted in Figure 6.4, a twin-girder system subject to three different load conditions was used to measure the stiffness properties of the panels. The advantage of this setup versus the typical shear frame test is that the SIP forms are tested under conditions that better represent real applications. In the two-girder system the deformations of the SIP panels vary along the length of the girders, as it occurs in real bridges. From these tests, the researchers determined that shear deformations in the SIP forms are larger near the supports, while near mid-span, the larger deformations are due to flexure. Hence, the stiffness properties determined from these tests are more representative of the actual structural conditions than the properties obtained from shear tests.

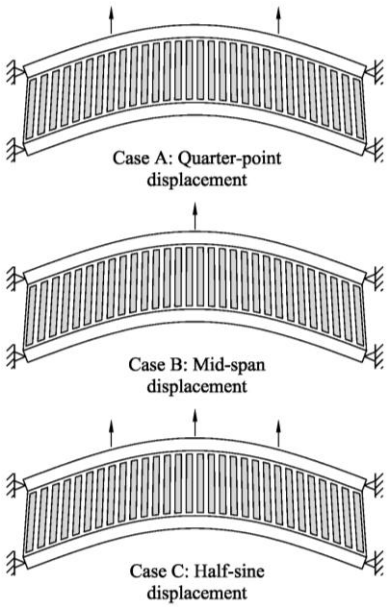


Figure 6.4. Lateral loading tests conducted in a twin-girder system (adapted from Egilmez (2009))

Similar to previous studies, Egilmez (2005) and Egilmez et al. (2009) concluded that the eccentricity of the support angle attachment severely decreases the bracing capabilities of the SIP forms. In addition to the support angle eccentricity, they determined that the effective shear stiffness of the panels depends significantly on the following parameters:

- The thickness and dimensions of the support angle.
- The top flange thickness.
- The level of dead load that the SIP forms support.
- The SIP form thickness.

In summary, the studies show that unless special details are provided to eliminate the significance of these variables, especially, the incidence of the support angle eccentricity, the SIP forms may not provide adequate bracing to stabilize the girders during deck placement. Also of major importance is the fact that the stiffness contributions of the forms to the system are highly variable given that in a bridge, all the parameters described above vary along the structure's span. Therefore, it is difficult to predict accurately the participation of the forms in the structural responses.

### 6.3. Participation of SIP Forms on the Bridge Geometry Control

During recent years, studies have been conducted to determine the factors that influence the deformed shape of a bridge during construction, especially, during deck placement. It is important to conduct an accurate assessment of girder deflections since the successful construction of the concrete deck largely depends on the control of the deformed geometry of the bridge. Some of the difficulties that contractors may face

during construction when the bridge displacements do not correspond to those anticipated by the analysis include: undercutting or over-running of the deck thickness, inadequate distance between the deck surface and the head of the shear studs, and non-uniform deck thicknesses.

One of the factors that have been studied to observe its influence on girder deflections is the participation of the SIP forms. Field measurements and analytical studies have shown that even though SIP forms may not be used for stability bracing purposes, they are part of the system, and their contributions, in some cases, should be considered in the analysis to properly capture girder deflections. In particular, the studies conducted at North Carolina State University in several research efforts support the conclusion that the SIP forms can influence the girder deflections, and therefore, the overall geometry control of the structure. Whisenhunt (2004) and Fisher (2006) report the deflections measured during deck placement of nine straight and skewed I-girder bridges and one straight bridge with normal supports. According to their studies, the numerical simulations represent more accurately the field measurements when the SIP forms are included in the analyses. Further investigations conducted by Morera (2010) in two straight and skewed I-girder bridges show that the SIP forms can be a contributor to the bridge responses. Similar to Whisenhunt (2004) and Fisher (2006), Morera (2010) concludes that the results of the FE models constructed to reproduce the field observations are more representative of the measured vertical deflections and girder layovers when the SIP forms are included in the analyses.

In practical terms, the effective stiffness of the panel-connection system can vary substantially with the parameters discussed previously in Section 6.2. In a bridge

structure, the top flange thickness, the support angle eccentricity, and the detail to attach the support angle to the flange vary along the span. Since all these parameters have an influence on the effective stiffness of the SIP panels, it is not feasible to accurately represent their participation in a computer model for a given situation. The design engineer does not have any control over these detailed parameters. Therefore, it is difficult to recognize the influence of the SIP forms by comparing the results of a computer model to field measurements.

Due to the limitations to properly represent the SIP form contributions in 2D or 3D models and the significant increase in time required to include them in the model, it may be desirable to eliminate them from the analysis. For this purpose it is necessary to recognize the conditions where the SIP panels may be contributing to the structural responses of an I-girder bridge during construction. In the next section, two existing bridges that are susceptible to the participation of the SIP forms are analyzed. The studies conducted in these structures serve to identify potential reasons for the participation of the SIP forms in the structural behavior.

## 6.4. Influence of SIP Forms on the Structural Responses of I-Girder Bridges

Section 3.2 discusses the procedures and techniques used to construct the 3D FEA models used in this research. In that section, the type of finite elements implemented to represent the different components of structure such as girders, cross-frames, stiffeners, and connection plates are presented. Also, methods to conduct virtual tests by including residual stresses and initial imperfections due to fabrication processes are discussed. In addition to the simulation procedures presented in Section 3.2, in this part of the research

it is necessary to model the SIP forms in the structural system. Section 6.4.1 introduces techniques to represent SIP forms in 3D FEA models. These 3D FEA procedures are implemented in the studies of the bridges discussed in Sections 6.4.2 and 6.4.3 to investigate the participation of the SIP forms on the system performance.

### 6.4.1. Modeling Techniques used in FEA Models to Represent SIP Forms

As discussed in Section 6.2.2, the structural properties of the SIP forms are commonly represented in terms of their shear stiffness, calculated from Eq. 6.1. Once the effective shear stiffness, $G^{'}$, is known, the diaphragm shear rigidity, $Q$, is calculated as

$$Q = G^{'} S_d = G^{'} \left( \frac{n_g - 1}{n_g} S \right) \qquad \text{(Eq. 6.2)}$$

where $S_d$ is the tributary width of diaphragm bracing a single girder, $n_g$ is the number of girders connected to SIP forms (or diaphragms), and $S$ is the panel width. The units of $Q$ are [Force/rad], so it represents the force required to cause a rotation of one radian in the shear test frame. This concept is further illustrated in Figure 6.3. In the context of this figure, $Q = P/\gamma$. If any other stiffness contributions of the SIP panels are ignored, their structural properties are given by $Q$.

One of the most common strategies to include the SIP forms in FEA is to model them as an equivalent truss. This technique has been implemented in various studies conducted to determine the structural properties of the SIP forms, leading to accurate predictions of laboratory tests (Egilmez 2005, Helwig and Yura 2008). As depicted in Figure 6.5, the SIP forms are modeled in the 3D FEA as a sequence of truss panels. In the above FEA models, truss diagonals are provided every two SIP panels.

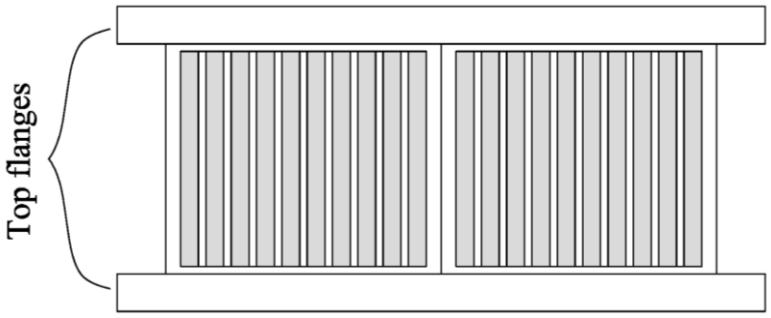


SIP forms spanning between flanges

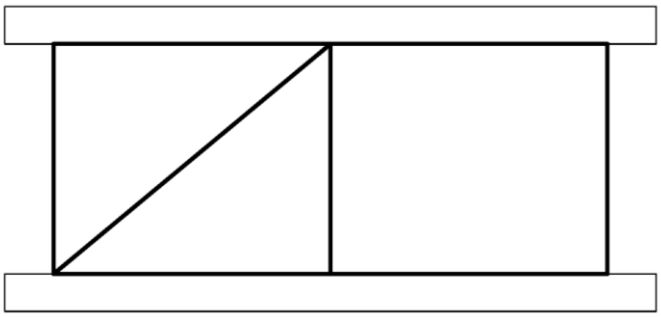

Representation of the SIP forms with equivalent truss panels

Figure 6.5. Equivalent truss concept implemented in FEA to represent the SIP forms

As shown in Yura (2001), the in-plane shear stiffness of a truss panel with a single diagonal is equal to

$$\beta_b = \frac{AES^2 h_b^2}{2L_c^3 + S^3} \quad \text{(Eq. 6.3)}$$

where $A$ is the area of the struts and the diagonal (assuming they are the same), $E$ is the steel modulus of elasticity, $h_b$ is the SIP panel length, and $L_c$ is the diagonal length. As shown in Yura and Helwig (2008), the equivalent shear rigidity is equal to

$$Q = \frac{\beta_b}{2h_b} \quad \text{(Eq. 6.4)}$$

Eqs. 6.2, 6.3, and 6.4 are used to determine the area of the struts and the diagonals in the equivalent truss that is implemented in the 3D FE models. From these equations, the truss element area is

$$A = \frac{G' S_d \left(4 L_c^{\,3} + 2 S^3\right)}{E S^2 h_b} \qquad \text{(Eq. 6.5)}$$

Except for $E$ (which is equal to 29000 ksi for steel) and $G$', all the variables in Eq. 6.5 are obtained from the geometry of the SIP forms and the bridge structure. The effective shear stiffness, $G'$, must be determined based on experimental data from tests conducted in shear frames or from tests in twin-girder systems, as the ones reported in Egilmez (2005). The second method is the most reliable since it best represents the deformations that real structures experience during the deck placement. The challenge of determining a value of $G'$ that can be used in analytical models is that it depends in several factors that cannot be controlled during the construction of a bridge, as discussed in Section 6.2. For the studies conducted in this research, the values of $G'$ are obtained from the lateral loading tests in a twin-girder system reported in Egilmez (2005) and Egilmez et al. (2009).

The SIP forms used in the construction of the bridges discussed in Sections 6.4.2 and 6.4.3 are made from ASTM A-653 material, and have a thickness of 0.91 mm (20 ga). From the tests reported in Egilmez et al. (2009), $G'$ for SIP forms of these characteristics is equal to 1787 KN/m-rad (10.18 kip/in.-rad). This value of $G'$ is used as reference in the next sections to develop the truss models that represent the SIP forms in the 3D FEAs of the case studies.

### 6.4.2. Case Study I: Simple Span Straight and Skewed I-Girder Bridge (EISSS3)

The first structure considered for this study is Bridge EISSS3, introduced in Section 3.1.2. This is a four I-girder bridge with V-type cross-frames without top-chords. Figure 6.6 shows the bridge in perspective and its key dimensions. This bridge is considered for the analyses conducted in this section because of the type of bracing system utilized in the design. In Section 4.3.3, this structure is studied to observe the influence of different cross-frame configurations on the structural behavior. The results of the analyses discussed in Section 4.3.3 show that V-type cross-frames without top-chords may not provide the required bracing to prevent excessive second-order amplifications of girder responses. For this reason, this bridge is selected to conduct further investigations in this section. It is necessary to investigate this bridge and study the sensitivity of the structural behavior to the SIP form contributions and other modifications in the bracing system.

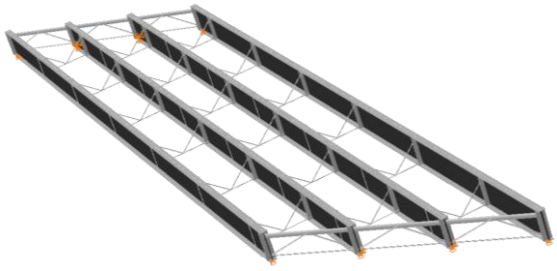

$L$ = 133 ft / $w$= 30.1 ft / $\theta_1 = 46.2^0$, $\theta_2 = 46.2^0$

Figure 6.6. Perspective view of Bridge EISSS3

Two approaches are considered in the analyses to model the SIP forms in the 3D FEAs. The first approach follows the procedures discussed in Section 6.4.1 to model the SIP forms as equivalent truss panels. For this purpose, it is necessary to determine the

area of the elements in the truss, $A$, using Eq. 6.5. From Section 6.4.1, $G^{'}$ = 10.18 kip/in.-rad. In this bridge, the distance between girders is 9.84 ft and the average top flange width is 14.17 in. Hence, $S$ = 9.84·12-14.17=103.91 in. The panel width, $h_b$, is 6 ft (72 in.), so the diagonal length, $L_c$, is equal to 126.42 in. Finally, the tributary width of diaphragm bracing a single girder, $S_d$ = [(4-1)/4]103.91 = 77.93 in. Substituting these values in Eq. 6.5, the area of the elements in the equivalent truss panel is

$$A = \frac{10.18 \times 77.93\left(4 \times 126.42^3 + 2 \times 103.91^3\right)}{29000 \times 103.91^2 \times 72} = 0.36 \text{ in}^2$$

This area is relatively small, if the equivalent truss system is thought of as a top flange level bracing system. For example, the smallest hot-rolled angle available is an L2x2x1/8 and has an area of 0.484 in$^2$. Figure 6.7 shows the perspective and the plan view of the bridge with the equivalent truss panels included. In this figure, the intermediate cross-frames are not shown to facilitate the visualization of the truss panels.

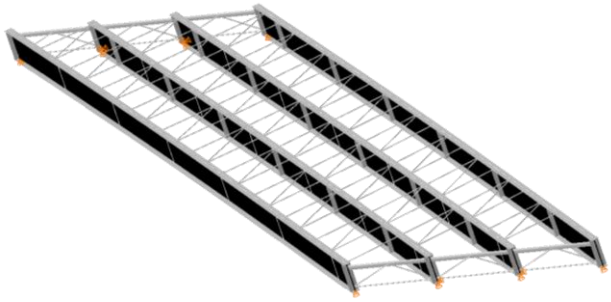

(a) Perspective view

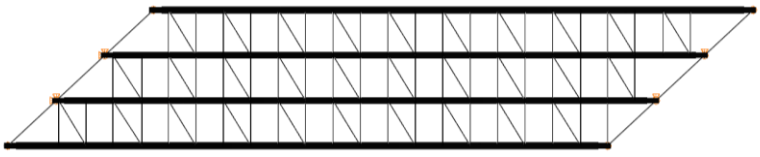

(b) Plan view

Figure 6.7. Equivalent truss panels used to model the SIP forms in Bridge EISSS3

In the second approach, the SIP forms are modeled in the 3D FEAs with membrane elements. A membrane is an element that has in plane strength, but does not have out-of-plane bending stiffness, which is the case of the SIP forms. ABAQUS 6.10 (Dassault Systèmes 2010) has a comprehensive library of triangular and quadrilateral membrane elements that can be used for the purpose of these studies. The element selected to simulate the SIP forms is the M3D4 membrane.

There is an advantage of modeling the SIP forms with membranes rather than with equivalent truss panels. A membrane element can be defined to have orthotropic mechanical properties, which is the type of behavior exhibited by SIP forms. In the SIP forms, the axial stiffness is different in two orthogonal directions. As shown in Figure Figure 6.8, in the direction that is parallel to the flutes, the effective stiffness of the SIP form, $k_{d1}$, depends on the cross-section properties of the form and the flexibility of the connection between the top flange and the form. In the direction perpendicular to the flutes, the stiffness of the forms is negligible ($k_{d2} \approx 0$) since the forms deform as an accordion. Finally, the SIP forms have an effective in-plane shear stiffness, $k_s$, that depends on its resistance to shear racking and the detail of the connection, as discussed in Section 6.2. In a membrane element, these three mechanical properties can be defined independently to best represent the SIP form stiffness contributions.

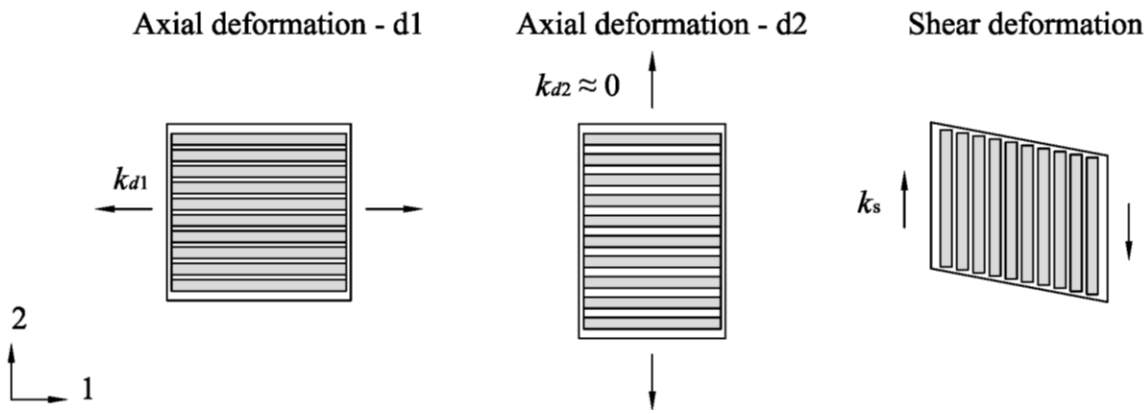


Figure 6.8. Deformation patterns in an SIP form

When equivalent truss panels are used to model the SIP panels, the area of the truss elements is calibrated to represent only their shear stiffness. In this calculation, the axial stiffness properties in the two orthogonal directions are not considered. Hence, the equivalent truss model may induce sources of stiffness that in the context of the system strength may not have a considerable influence. However, in this research, it is desired to observe the influence of the SIP panels in the bridge deformed geometry, so a more accurate representation of their contributions is necessary. Modeling the SIP panels with membranes not only eliminates possible sources of spurious stiffnesses but also serves to compare and validate the results obtained from models that use equivalent truss systems to represent the forms.

To include the panels using membrane elements instead of truss panels, it is necessary to determine the thickness of the elements. For this purpose, an FE model of an equivalent truss panel with $A = 0.36$ in$^2$ is constructed to simulate the shear frame test depicted in Figure 6.9. Then, the panel is subjected to the point load $P$ that causes the lateral displacement $\Delta$. A separate analysis is conducted using a membrane element instead of the equivalent truss panel, and the thickness of the element is calibrated to

match the lateral displacement obtained from the previous tests. From this test, it is determined that the thickness of the membrane element needed to represent the shear stiffness of the equivalent truss panel is 0.004 in.

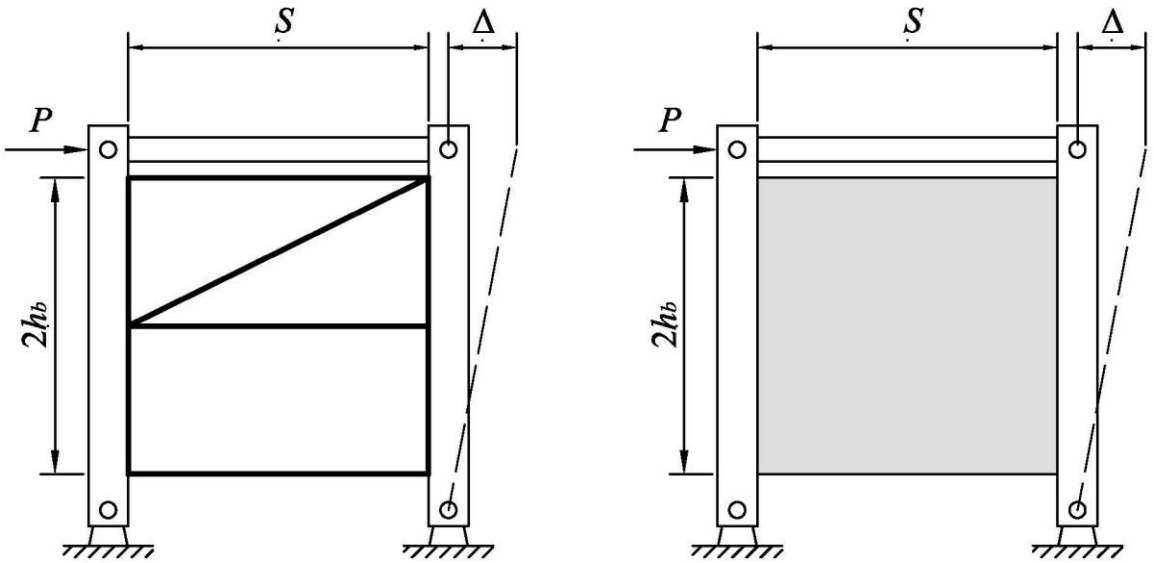


Equivalent truss panel Membrane element

Figure 6.9. Tests to determine the thickness of the membrane elements used to represent the SIP forms

6.4.2.1. Analysis Results

In the studies conducted in Bridge EISSS3, seven types of analyses are conducted to observe the participation of the SIP forms on the system responses. Table 6.1 shows the different scenarios considered for the studies. The first model, M1, corresponds to the case where the SIP forms are not included in the analysis, and the cross-frames are modeled as V-type without top-chord. In the second analysis, M2, the top-chords of the cross-frames are included in the analyses to observe the changes on the bridge behavior due to the presence of these components. Similar to the first case, in M2 the SIP forms are not considered in the analysis. Model M3 is one of the two models that better represent the as-built conditions of the structure. In this analysis, the SIP forms are

included in the model by representing them with equivalent truss panels. The area of the truss elements is determined previously in this section and is equal to 0.36 $in^2$. As in the real bridge, the cross-frames are modeled without top-chords. The fourth model, M4, is the same as M3, but in this case, the SIP forms are modeled with equivalent trusses with an area two times larger than the one used in M3, i.e., $A$ = 0.72 $in^2$. The intention of increasing the area of the truss elements is to determine the sensitivity of the structure to different stiffness contributions of the SIP forms. As mentioned previously in Section 6.3, it is difficult to accurately capture the participation of the SIP forms given that their stiffness contributions depend on several variables and changes on which location of the bridge span it is measured. Therefore, it is desirable to investigate the sensitivity of the system to changes in the form stiffness.

Model M5 is the same as model M4 with the difference that in this case the cross-frame top chords are included in the analysis. As in previous cases, it is desired to observe possible changes in the structural responses due to the inclusion of the top chord, but also considering the contributions of the SIP forms. In the sixth model, M6, the truss elements are modeled with elements that have ten times the area of the elements in model M3. The truss components have an area equal to 3.60 $in^2$, which is close to the area of L4x4x1/2 angles ($A$ = 3.75 $in^2$). The truss system in the M6 model resembles a top flange level bracing system that is provided in some cases to increase the global buckling capacity of a bridge and also, to increase the resistance to lateral loads such as wind or seismic loads. Model M6 is an extreme scenario to observe the influence of structural members provided at the top flange level on the behavior of a bridge subject to gravity loads during construction. The last model, M7 similarly to M3 is a close representation of

the bridge as-built condition. In model M7, the SIP forms are modeled with membrane elements, as described previously in this section. The advantage of using membrane elements rather than equivalent trusses is that with membranes is possible to model the orthotropic properties of the SIP forms. Since the use of membranes is a more refined method to represent the SIP forms, the results of model M7 are used to validate the predictions obtained from M3 and therefore, the other truss panel models.

Table 6.1. Description of analyzed cases, Bridge EISSS3

| Model | Top-Chord | SIP form model | Membrane thickness or truss element area |
|---|---|---|---|
| M1 | - | - | - |
| M2 | Y | - | - |
| M3 | - | Equivalent truss | 0.36 $in^2$ |
| M4 | - | Equivalent truss | 0.72 $in^2$ |
| M5 | Y | Equivalent truss | 0.72 $in^2$ |
| M6 | Y | Equivalent truss | 3.60 $in^2$ |
| M7 | - | Membrane | 0.004 in. |

In all the seven FE models linear and nonlinear analyses were conducted since it is important to observe the response amplifications due to second-order effects. Figure 6.10 shows the plots of the girder layovers and the vertical displacements of the fascia girder G1 at the TDL level. As shown in the plot of the girder layovers, in M1 the amplifications in the response due to second-order effects are important. At mid-span the layover predicted by the linear analysis is equal to 1.70 in., while the nonlinear analysis predicts a 3.77 in. layover. This shows that if the system is analyzed with the considerations of model M1 (no cross-frame top chords, no SIP form participation), it exhibits significant nonlinear behavior. In fact, a separate nonlinear analysis conducted to

determine the ultimate capacity of the structure shows that the collapse load is 1.05 TDL, which is less than the 1.5TDL design load required by the STRENGTH IV load combination.

The layovers for the fascia girder G1 obtained from the other six models for both linear and nonlinear analyses are essentially the same, as depicted in Figure 6.10(a). There are several conclusions that can be drawn from these results. First, the results of model M2 show that when the top chord is included in the intermediate cross-frames, the system is dominated by first-order actions. This analysis shows that when the girders are braced properly with V-type cross-frames that include top chords, the layovers are reduced drastically and the second-order effects are negligible.

The results of model M3 show that in this bridge, the participation of the SIP forms in the girder layovers (and in the control of the bridge deformed geometry) is significant. In this structure, the SIP forms are participating in conjunction with the cross-frames to provide stability bracing. The SIP forms are preventing the large rotations of the girder that are observed in the results of model M1. In addition, a comparison of the responses of models M3 and M4 show that the system is insensitive to variations of the SIP form stiffness contributions since duplicating the area of the equivalent truss element does not result in significant changes in the girder layovers.

Similar to the other analyses, the importance of second-order effects in the girder layovers of model M5 is negligible. Additionally, a comparison of the M4 and M5 model results shows that when the top-chords are included in the cross-frames, the contribution of the SIP forms to the layover is irrelevant. This behavior demonstrates that when the in-

plane stiffness of the cross-frames is large enough to brace the girders and minimize the local second-order effects associated with the girder unbraced length, the SIP forms can be ignored in the structural analysis. The results of the studies discussed in this chapter, as well as, the analyses discussed in Section 4.3 show that except for the case of V-type cross-frames without top chords, all the cross-frame configurations commonly used in the design of steel girder bridges have sufficient in-plane stiffness to meet the stability bracing requirements.

The results of model M6 show that even when the bridge is analyzed with an equivalent truss that resembles a top flange level bracing system, the layovers in girder G1 remain essentially the same. As in the previous cases, this highlights the relevance of the cross-frame top chords on the system behavior. Finally, model M7 shows the results obtained with a different representation of the SIP forms. The response obtained from model M7 imply that the contributions of the in-plane axial stiffness of the SIP forms ($k_{d1}$ and $k_{d2}$ in Figure 6.8) to the layovers of girder G1 are irrelevant since it provides the same predictions as model M3.

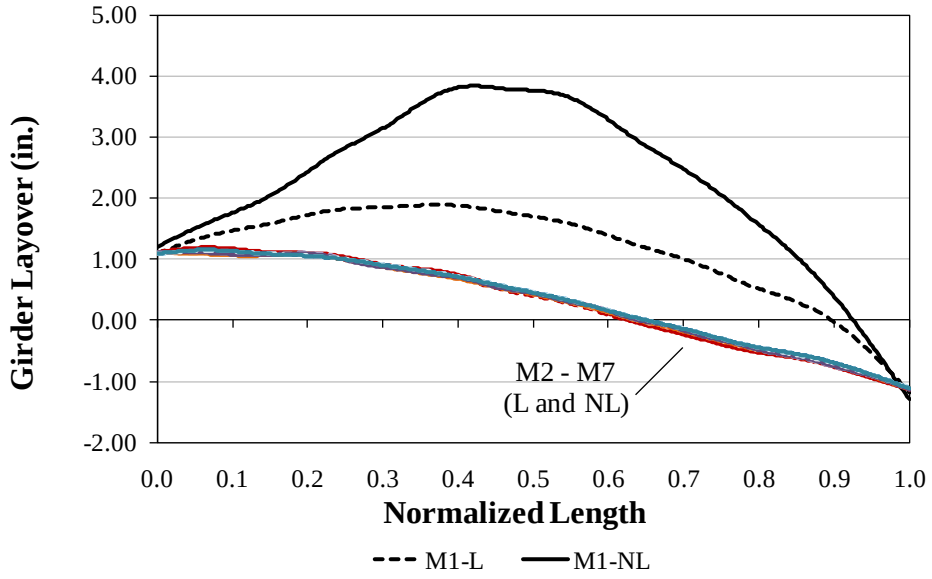


(a) Girder layovers

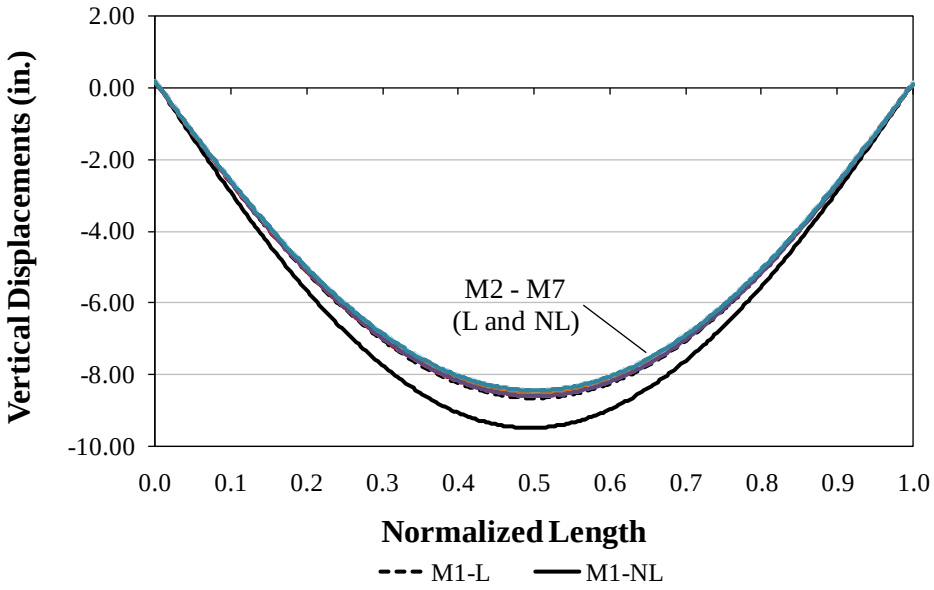


(b) Vertical displacements

Figure 6.10. Displacement responses in the fascia girder G1 at the TDL level

The vertical displacement predictions obtained for girder G1. shown in Figure 6.10(b), follow the same trend as the girder layovers. In the case of the vertical displacements, the second-order effects are less noticeable that in the girder layovers, but

it is evident that except for the results of model M1, the other six models yield essentially the same predictions. Figure 6.11 shows the layovers and vertical displacement predictions obtained for the interior girder G2. Similar to girder G1, except for M1, in this interior girder the analyses show that the responses are dominated by first-order actions, and the contributions of SIP forms are insignificant when the system is braced with V-type cross-frames that include top chords.

A particular aspect that is observed in the plots of the girder layovers is that, at the bearing lines, all the analyses predict almost the same values. In girder G1, the layovers are 1.2 in. and -1.3 in. at the left and right supports, respectively. In girder G2, the values are 1.0 in. and -1.0 in. As discussed in Chapter 4, the layovers at the supports are controlled by a "global effect" that depends on the skew angle and the major axis-bending rotation of the girders at these locations. Similarly, at the intermediate bracing points, the layovers are function of the differential deflections between adjacent girders if the cross-frames behave as rigid bodies. The discussions of Chapter 4 shown that due to the global effect, in skewed bridges the largest girder layovers generally occur at the bearing lines. As shown later in this section, the cross-frame in-plane deformations in V-type cross-frames without top chords can be significant, so the assumption of the cross-frames being rigid does not apply for model M1. This is the reason for the layovers being considerable larger in the interior of girders G1 and G2, according to the solutions obtained from M1.

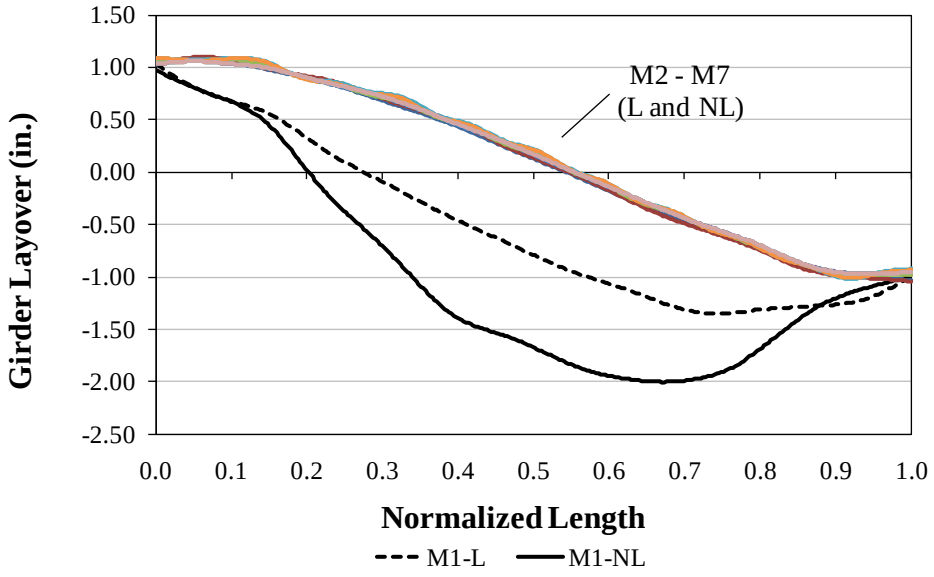


(a) Girder layovers

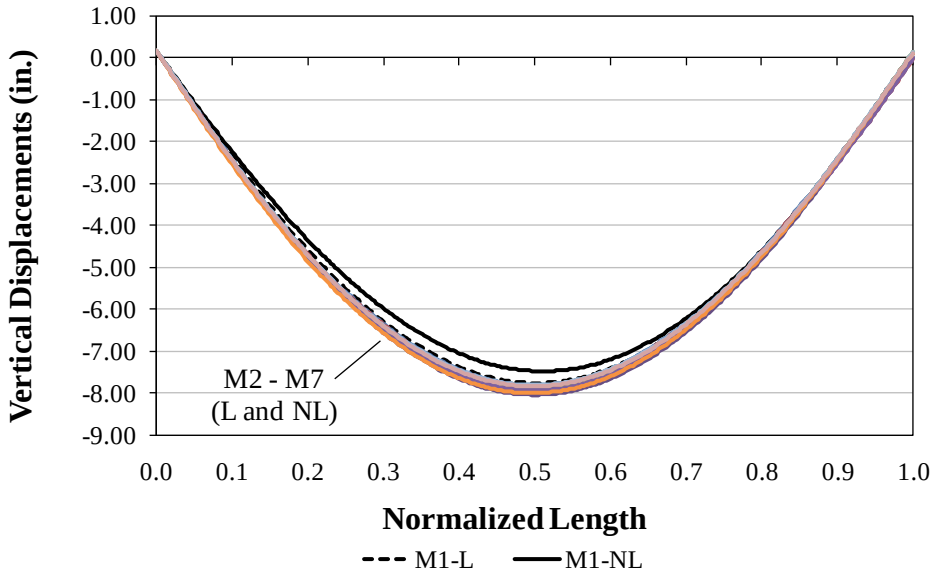


(b) Vertical displacements

Figure 6.11. Displacement responses in the first interior girder G2 at the TDL level

To further illustrate the importance of the top chord and the SIP forms in the control of the deformed geometry of Bridge EISSS3 under the gravity loads, Figure 6.12 depicts the structure in its deflected position. This figure shows the perspective of the

structure obtained from models M1, M2, and M3, amplified by a factor of ten to facilitate the visualization. As shown in Figure 6.12(a), the cross-frame diagonals rotate about their intersection with the bottom chord. Hence, the in-plane stiffness of the intermediate cross-frames depends mostly on the flexural stiffness of the bottom chord rather than in the axial stiffness of the chords and diagonals. Due to the poor bracing properties of this type of cross-frame configuration, the girder experience large second-order amplifications, which result in excessive girder layovers. When the top chords are included, the girders layovers are reduced and the girders deflect more uniformly, as depicted in Figure 6.12(b). In this case (M2), the cross-frames are stiffer than in the first case (m1) and brace the girders, so they behave as a unit. Finally, Figure 6.12(c) shows that the SIP forms participate bracing the girders and reducing the effects of not providing cross-frame the top chords.

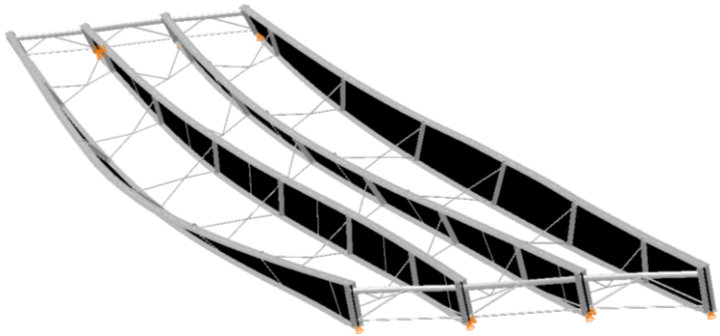

(a) Model M1 (V-type cross-frames without top chords, SIP forms not included)

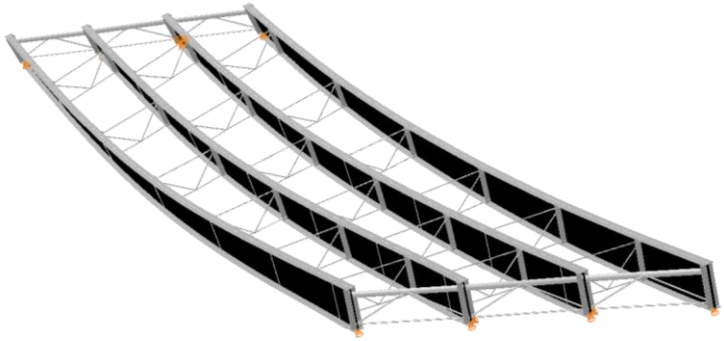

(b) Model M2 (V-type cross-frames with top chords, SIP forms not included)

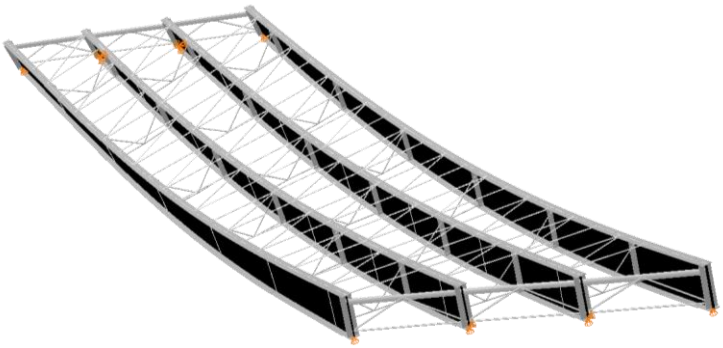

(c) Model M3 (V-type cross-frames without top chords, SIP forms included)

Figure 6.12. Deflected geometry of Bridge EISSS3 at the TDL level (x10)

In addition to the girder displacements, it is important to investigate the stress responses obtained from the different models. Figure 6.13 shows the major-axis bending, $f_b$, and flange lateral bending stresses, $f_\ell$, in girder G1. In Figure 6.13(b), only the predictions from models M1, M2, and M7 are included to facilitate the visualization of

results. For this response, the predictions captured by these three models are sufficient to investigate the influence of the SIP forms and the cross-frame top chord in the structural behavior.

The results in Figure 6.13(a) show that the major-axis bending stress response is almost insensitive to the variations included in the models. The stress predictions obtained from model M1-NL are slightly larger than in M1-L, showing that the amplifications due to second-order effects in $f_b$ is minor. In the case of $f_\ell$, the differences are more evident. The solution for M1-NL shows that in the third and fourth girder segments the levels of $f_\ell$ are large. The amplifications associated with nonlinear behavior in this response are considerable. However, when top chords are provided in the intermediate cross-frames, the levels of flange lateral bending stress experience a substantial decrement. Model M7, which closely represents the as-built condition, shows that the SIP forms participate reducing the $f_\ell$ levels, especially within the girder unbraced lengths.

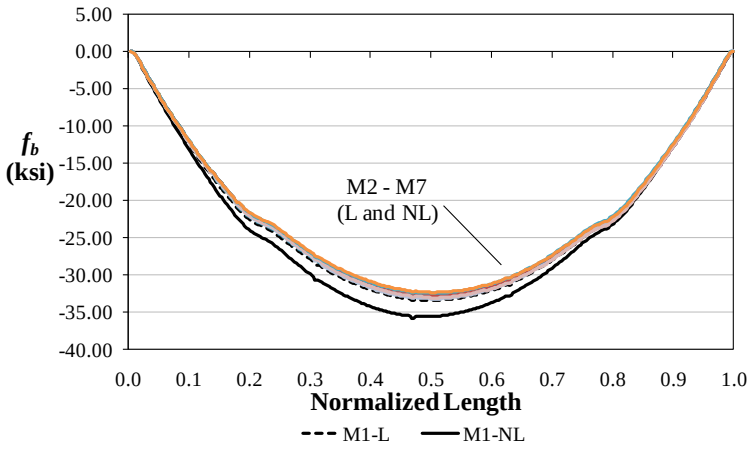


(a) Major-axis bending stresses

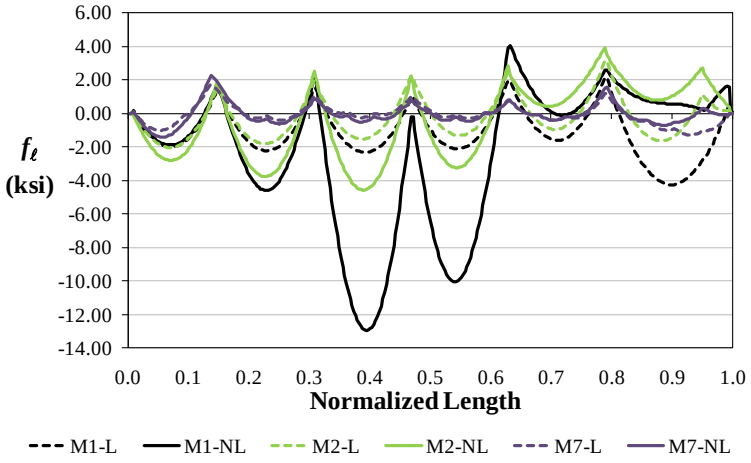


(b) Flange lateral bending stresses

Figure 6.13. Stress responses in the fascia girder G1 at the TDL level

The results obtained from the different analyses conducted of this bridge show that under certain circumstances the SIP forms influence the system performance. The displacement responses demonstrate that the control of the deformed geometry during construction is sensitive to the presence of the SIP forms only if the cross-frame top chords are not included in the bridge. When the top chords are included in the models, the significance of considering or not the SIP forms in the analyses is negligible. In addition,

the results show that the system is insensitive to fluctuations in the SIP form stiffness when the in-plane stiffness of the cross-frames is sufficient to brace the girders properly. In conclusion, the studies conducted of this bridge suggest that the use of V-type cross-frames without top chords may lead to an unexpected behavior of the structure during construction, which includes a participation of the SIP forms. When the cross-frames are stiff enough to integrate the girders and make them work as a unit, the participation of the SIP forms may be insignificant.

### 6.4.3. Case Study II: Simple Span Curved and Skewed I-Girder Bridge (EISCS4)

In certain situations, steel I-girder bridges can be vulnerable to stability related failures during their construction. I-girder bridge units with large span-to-width ratios may be susceptible to global stability problems rather than cross-section or individual unbraced length strength limit states as the experienced by Bridge EISSS3 (see Section 6.4.2). In fact, due to a global second-order lateral-torsional amplification of the displacements and stresses, the limit of the structural resistance may be reached well before the theoretical elastic buckling load. Therefore, in structures sensitive to global second-order effects, simply ensuring that the loads for a given configuration are below an estimated global elastic buckling load is not sufficient. In addition, large displacement amplifications can make it difficult to predict and control the structure's geometry during construction. Possible situations with these characteristics include widening projects of existing bridges, pedestrian bridges with twin girders, phased construction, and erection stages where only a few girders of a bridge unit are in place, and thus the unit is relatively long-and-narrow.

Bridge EISCS4 is an existing structure with these characteristics. This structure is introduced in Section 3.1.8. It is three-girder unit with a span of 256 ft that experienced large global second-order amplifications during its construction. The unit was the third phase of a construction project erected next to an I-girder system consisting of 14 girders that had been previously constructed. Figure 6.14(a) shows the plan view of the 17 girder bridge, and Figure 6.14(b) shows a perspective view of EISCS 4, the three-girder unit (G15 to G 17) studied in this section.

During the concrete placement on Phase III, it was observed that the vertical deflections were larger than in the girders of Phase II. By the time that approximately two thirds of the concrete deck had been placed, the top-of-slab on Phase III was considerably lower than the corresponding location on Phase II. At this point, it was decided to stop the deck placement. The bridge had deformed more than expected and was potentially at a point of incipient instability. Sanchez and White (2011) present analytical studies conducted in this structure to address the structural behavior of the three-girder unit and also propose a method to predict potential undesired global second-order amplifications in a bridge of these characteristics.

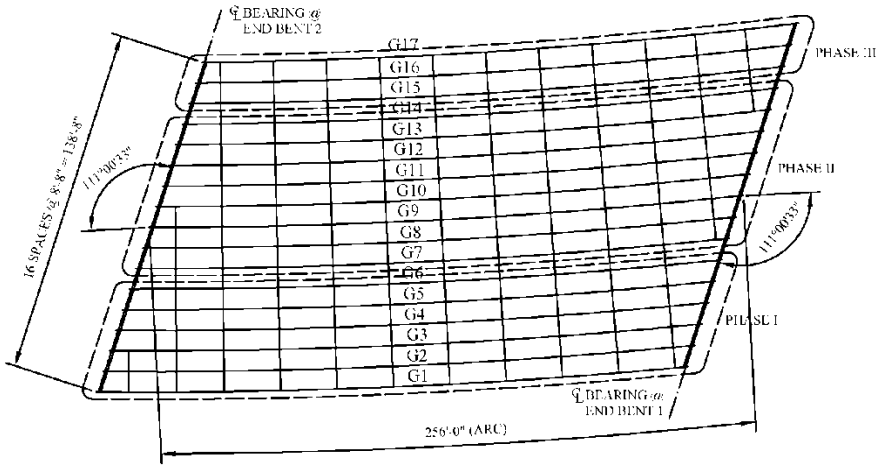


(a) Plan view of the 17 I-girder bridge

$L_1$ = 252 ft / $R$ = 2269 ft / $w$ = 26.6 ft / $\theta_1$ = -24.71°, $\theta_2$ = -18.36°, 3 girders

(b) Three-girder unit (Phase III)

Figure 6.14. Plan view if the 17 I-girder bridge and the three girder unit (Bridge EISCS4)

The relevance of the global second-order effects in this structure is depicted in Figure 6.15, which shows the responses in girder G15 (the girder in Phase III adjacent to the closure pour) obtained from elastic linear and geometrically nonlinear FEAs. In these analyses the participation of the SIP forms is not included. Figure 6.15(a) shows the results for the top flange major-axis bending stress, $f_b$, normalized with respect to the yield strength of the steel ($F_y$ = 70 ksi). Figure 6.15(b) show the vertical displacements,

with the vertical axis truncated at 40.0 inches to facilitate the comparisons. The maximum deflection at midspan predicted by the nonlinear FEA is 216 inches. As shown in these plots, the response amplifications in both $f_b$ and the vertical displacements due to geometric nonlinearity are substantial. The results obtained from the nonlinear analysis are shown at 0.85TDL since this is the limit load predicted by the elastic nonlinear FEA.

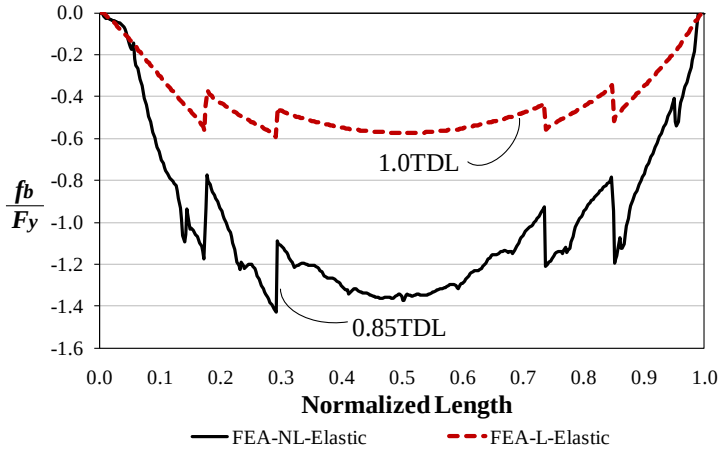


(a) Major-axis bending stresses

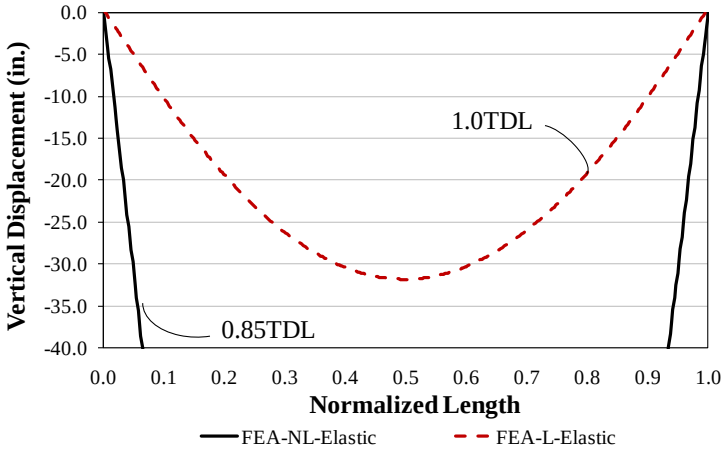


(b) Vertical displacements

Figure 6.15. Responses predicted in girder G15 of Bridge EISCS4 by elastic linear and nonlinear FEAs

Similar to the analyses conducted in Bridge EISSS3, in this section the influence of the SIP forms in the structural performance of the three-girder unit is studied. It is intended to observe the participation of the forms on the behavior of a long-and-narrow bridge under construction. For this purpose, the SIP forms are included in the 3D FEA models as membrane elements, following the techniques discussed in Sections 6.2 and 6.4.1.

To represent the SIP forms with membrane elements it is necessary to determine the membrane dimensions that represent the mechanic properties of the forms. As in the previous case study, the membrane thickness is obtained by comparing its shear stiffness to the stiffness of an equivalent truss panel. For this purpose, the area of the truss elements, *A*, is calculated using Eq. 6.5. The SIP panels in this structure are the same as those used in the construction of Bridge EISSS3, so the same shear stiffness $G^{'}$ = 10.18 kip/in.-rad and panel width, $h_b$ = 6 ft (72 in.) are used. In this structure, the girder spacing is 8.67 ft, and the average top flange thickness is 24.0 in. Hence, the panel width, *S*, is equal to 8.67–24.0/12 = 6.67 ft (80.04 in.). The tributary width of diaphragm bracing is $S_d$ = [(3-1)/3]6.67 = 4.45 ft (53.36 in.). Finally, with $h_b$ = 6 ft and *S* = 6.67 ft, the diagonal length, $L_c$, is equal to 8.97 ft (107.66 in.). Substituting these values in Eq. 6.5, the area of the elements in the equivalent truss panel is

$$A = \frac{10.18 \times 53.36\left(4 \times 107.66^3 + 2 \times 80.04^3\right)}{29000 \times 80.04^2 \times 72} = 0.24 \text{ in}^2$$

Similar to the procedure described in Section 6.4.1, the thickness of the membrane elements used to represent the SIP forms is determined from simulations of the shear frame test. From this analysis, it is determined that a membrane element with a thickness

of 0.0032 in. is needed to obtain the same shear stiffness of a truss panel with $A$ = 0.24 in$^2$. Figure 6.16 shows the models with and without the SIP forms.

(a) Model without the SIP forms

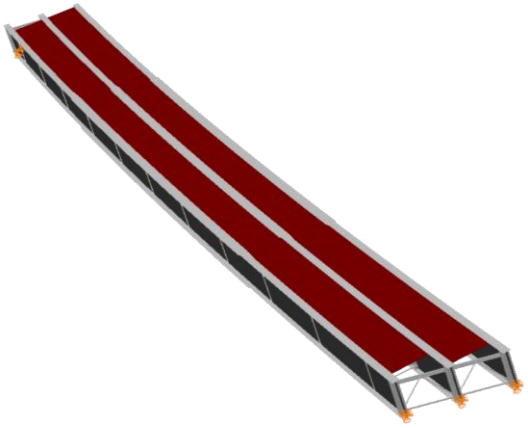

(b) SIP forms modeled with membrane elements

Figure 6.16. Perspective view of the two models used in the studies of Bridge EISCS4

In addition to the elastic models described previously, this bridge was analyzed with full nonlinear FEA following the procedures discussed in Section 3.2.2. The full nonlinear FEA captures the plastic deformations in the system, considering the effects of the residual stresses that result from the fabrication of the I-girders. Due to these characteristics, this analysis is the closest representation of the structural performance of the physical bridge. The intent of conducting a full nonlinear FEA is to determine the

influence of the SIP forms in the control of the deflected geometry of the bridge and also in prediction of the failure load.

Figure 6.17 shows the fraction of the TDL plotted versus the lateral displacement of girder G15 at mid-span for the linear and nonlinear elastic analyses, as well, as for the full nonlinear FEAs. In the plot, the dotted horizontal line corresponds to the fraction of the TDL where the theoretical elastic structure reaches its load limit, i.e., 0.85TDL. The dot-dash line represents the fraction of TDL that corresponds to the steel structure's self-weight, i.e., 0.33TDL. As shown in this figure, the SIP forms have a minor participation in this response. In general, for a given load level, the SIP forms participate reducing the vertical deflections of the girder. In the case of the limit load, the results from the full nonlinear FEAs show that when the forms are included in the analysis the collapse load increase slightly from 0.70TDL to 0.72TDL.

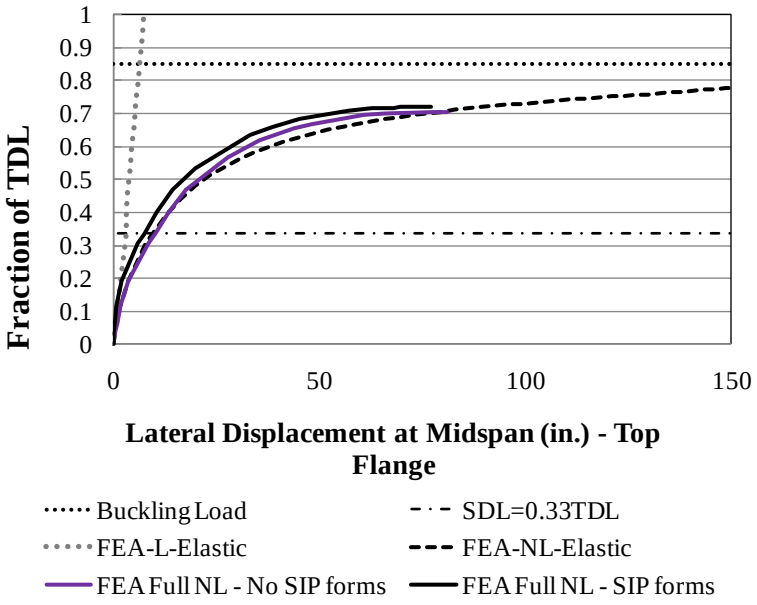


Figure 6.17. TDL fraction vs. flange lateral displacement of girder G15

Another response that is of interest in this study is the girder vertical displacements. Figure 6.18 shows the vertical displacements at mid-span of girder G15 plotted versus the fraction of the TDL. Similar to the previous plot, the differences between the responses predicted by the full nonlinear models are is minor.

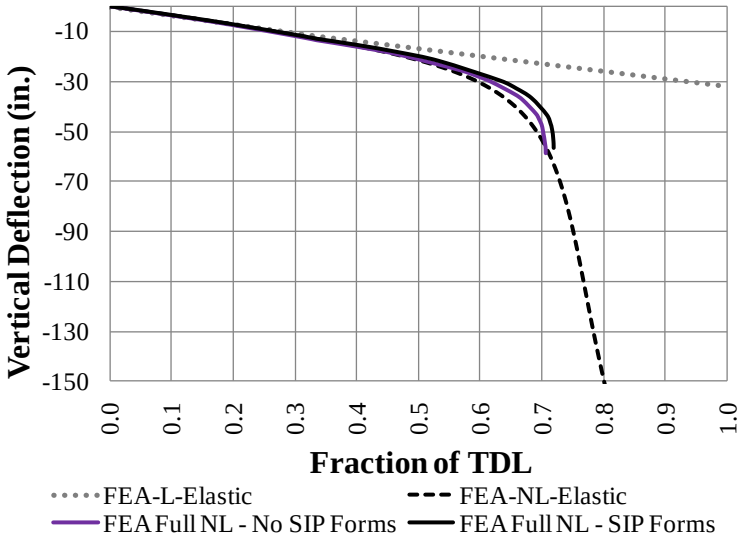


Figure 6.18. Vertical deflection at mid-span of girder G15 in Bridge EISCS4

The results obtained from the analyses conducted in this bridge show that the SIP forms have a negligible effect on the structural responses. In this case study, the SIP forms do not reduce the displacement amplifications associated with geometric nonlinear behavior. From these results, it is apparent that the forms do not participate significantly on the control of the deformed geometry of a bridge that is susceptible to global second-order effects. Finally, the analyses conducted in this long-and-narrow structure show that the SIP panels do not have any significant effect on the limit load. As shown for this bridge the collapse load only increased from 0.70 to 0.72 when the SIP forms are included in the model.

## 6.5. Summary

In this chapter, the influence of the SIP forms on the behavior of two steel I-girder bridges is studied by observing the changes in the structural responses when their contributions are included in the analyzes. The two bridges discussed in this chapter were selected for the studies because they are susceptible to large response amplifications due to second-order effects.

In Bridge EISSS3, the nonlinear behavior is associated with the poor stability bracing provided by the intermediate V-type cross-frames without top chords. The analyses of this bridge show that when the in-plane stiffness of the cross-frames is not sufficient to integrate the girders and make them work as a unit, the SIP forms can have a considerable participation in the control of the deformed geometry of the structure. However, when the girders are connected at sufficient locations with cross-frames that do not experience large deformations during the deck placement, the influence of the SIP forms is negligible. In the context of analysis and design of I-girder bridges, this means that the SIP forms may not need to be included in the analyses if the intermediate cross-frames are stiff enough to conserve their geometry during the deck placement. Fortunately, except for V-type cross-frame without top chords, all the cross-frame configurations commonly used in the design of I-girder bridges satisfy this requirement.

In Bridge EISCS4, the reasons for the second-order amplifications observed in the system responses are due to different reasons than in Bridge EISSS3. Long-and-narrow structures can exhibit nonlinear behavior due to global stability effects rather than the individual unbraced length problems observed in bridges that are poorly braced. However, in bridges susceptible to global nonlinear behavior, the participation of the SIP

forms may not be as significant as in bridges with response amplifications due to local second-order effects. The results of Bridge EISCS4 show that the forms do not have a considerable influence in the girder deflections or in the system strength.

# CHAPTER VII

# SUMMARY AND CONCLUSIONS

## 7.1. Summary and Conclusions

Bracing systems have a fundamental role on the behavior of curved and skewed I-girder bridges during construction. This research focuses on the identification of the structural functions and the participation of the bracing systems on the responses of I-girder bridges during the various stages of the construction process. The studies conducted in this thesis illustrate the factors that need to be considered to layout the cross-frames in bridges with complex geometries. In addition, an investigation of current simplified analysis methods used for the design of curved and/or skewed I-girder bridges show that, in many cases, they are insufficient to capture the structural behavior. Based on this investigation, techniques are developed that can be implemented to improve the response predictions obtained from 2D-grid models. Finally, this research addresses the influence of the SIP forms on the performance of I-girder bridges during deck placement. The following sections summarize and highlight the findings documented in this thesis.

### 7.1.1. Skew Effects and Mitigation Schemes

In straight and skewed I-girder bridges, the bracing system can be configured to reduce the undesired collateral effects of skew. The analyses conducted in this research demonstrate that the coupling between the major-axis bending deflections and the skew angle induce a layover in the girders that can be interpreted as the global effect of skew. Studies conducted in highly skewed structures show that the structural performance can

be improved by placing the intermediate cross-frames in a way that they do not interfere with the global girder twist imposed by the bearing line cross-frames. When the girders are connected at points that have approximately the same layovers, the forces in the cross-frames experience a considerable reduction relative to the case where the cross-frames are framed perpendicular to the girder longitudinal axes. The cross-frame force reduction also results in lower levels of flange lateral bending stress. In conclusion, in the design of a bridge, the intermediate cross-frames can be oriented and spaced so that the effects of skew are reduced substantially relative to ordinary current practice.

By recognizing that the bracing system can be oriented to enhance the bridge performance, two methods are proposed to mitigate the skew effects. In the first method, the intermediate cross-frames are oriented to minimize their influence on the girder twist imposed by the cross-frames at the supports. Studies are conducted on a straight bridge with one of the supports skewed at $50^o$ and the other oriented perpendicular to the girder longitudinal axes ($0^o$ skew) to investigate the structural behavior using different cross-frame layouts. The studies demonstrate that by orienting the intermediate cross-frames in a fanned configuration, the structural performance is significantly improved. In addition, the studies show that it is not necessary to provide any more continuous cross-frame lines than that required to control the bridge profile during the deck placement. For stability bracing purposes, it is sufficient to connect the girders in pairs rather than with a continuous cross-frame line. This practice relaxes the transverse stiffness of the bridge, reducing the skew effects and improving the system performance.

In the second method, the bracing properties of the X-type cross-frame are analyzed to determine the influence of the chords and diagonals in the system response.

Analyses conducted for a highly skewed bridge demonstrate that the top chord of X-type cross-frames can be removed to relax the transverse stiffness of the bridge, without affecting significantly the structural performance of the system. This practice can reduce the flange lateral bending stress levels more than a 50% with respect to the case where the top chords are included.

### 7.1.2. Methods to Determine the Influence of the Skew Effects on Straight Bridges

The studies conducted in straight and skewed bridges show that the layout of the cross-frames has a direct impact on the structural performance. Furthermore, in addition to the cross-frame layout, the magnitude of the skew effects depends on the relationship between the skew angle, the span length, and the bridge width. These three parameters are considered to propose an index that is used to separate those bridges where the skew effects are a major contributor to the structural responses from those where their participation is minor or negligible. The studies conducted on 24 straight and skewed steel I-girder bridges show that two possible limits that can be used to categorize a bridge in terms of the skew index, $I_S$, are 0.30 and 0.65.

In structures with a skew index above 0.30, the ratio $f_\ell$ / $f_b$ is considerably larger than in bridges with indices below this limit. Another aspect of bridges with $I_S \geq 0.30$ relates to the magnitude of the cross-frame forces. Even though there is no definite limit to determine when the cross-frame forces are large, in structures with indices above 0.30 these forces can be significantly larger than in other bridges.

The second limit, 0.65, serves to identify bridges where not only the $f_\ell$ and cross-frame force levels are significant but also the skew effects can significantly influence the major-axis bending responses of the bridge. In bridges with $I_S \geq 0.65$, the cross-frame forces are sufficiently large to have an effect on the girder vertical deflections and the associated major-axis bending stresses. The analyses conducted of bridges with indices above this limit show that the vertical components of the cross-frame forces should be considered in combination with the gravity loads to predict the vertical displacements and the $f_b$ stresses in the girders.

In addition to highlighting bridges that due to their geometry may be susceptible to considerable skew effects, the skew index can be used to determine when an approximate 1D line-girder analysis may not be sufficient to properly capture the behavior of a bridge during construction. A straight line-girder model does not have any information regarding the participation of the cross-frames in the bridge behavior. The predictions obtained from analyses conducted with this approximate method are based only on the gravity loads acting on the girders and neglect the cross-frame contributions. Furthermore, line-girder analyses do not provide any predictions of the cross-frame forces and $f_\ell$ levels. For these reasons, it is recommended to limit the use of 1D line-girder analysis to bridges with $I_S \leq 0.30$. Bridges with skew indices above this limit should be analyzed using 3D FEA or 2D-grid models constructed with the techniques developed in this research.

### 7.1.3. Improvements for the Analysis of I-Girder Bridges using 2D-Grid Models

The studies conducted in this thesis to assess the virtues and limitations of 2D-grid models constructed with current practices demonstrate that in certain situations their predictions are not a proper representation of the physical behavior of a bridge. The model used to represent the torsional stiffness of the I-girders and the techniques used to represent the cross-frame contributions have two limitations that can potentially result in inaccurate predictions of the system responses.

Due to their geometry characteristics, curved and skewed bridges are inherently subjected to torsion. Therefore, it is essential to properly capture the torsion properties of the I-girders to obtain an accurate prediction of the structure's performance. Unfortunately, in most of computer programs used for the design of steel girder bridges, the I-girders are modeled with elements that only consider the Saint Venant or pure torsion contributions. The formulation of the torsional stiffness of these elements neglects the warping contributions, which is the main source of torsional resistance in thin-walled open sections.

Rather than just affecting the girder responses, a model that does not include the warping contributions also influences the cross-frame force predictions since the behavior of these components is directly related to the torsional response of the I-girders. If the girders are excessively flexible in torsion, the forces in the cross-frames will be excessively underpredicted. Due to these limitations, in straight and skewed bridges, 2D-grid models cannot capture the interaction between girders and cross-frames. In bridges of these characteristics, essentially, there is no difference between the results obtained from a 2D-grid and a simple 1D line-girder model.

In the case of the cross-frames, it is common in current practice to model them with the same type of elements used to model the girders. Often an element based on Euler-Bernoulli classical beam theory is used to represent what in reality is a group of elements that exhibit the typical behavior of a truss. The properties of the equivalent beam are determined using ad hoc procedures that approximately capture the structural properties of the cross-frame; however, in bridges such as some of those studied in this research these techniques can lead to inaccurate predictions.

In this thesis, techniques that can be used in the construction of 2D models are developed to overcome these two limitations. First, an equivalent torsion constant that simulates the contributions of warping to the girder torsional stiffness is implemented in the models. In the case of the cross-frame models, two-node elements that accurately represent the stiffness contributions of these components are developed for the three cross-frame configurations commonly used in the design of I-girder bridges (i.e., X-type, V-type, and inverted V-type cross-frames). The tests conducted to validate the formulations show that these line elements can properly capture the behavior of cross-frames subjected to axial, shear, and bending deformations.

The results obtained for three case studies of bridges with challenging geometries demonstrate that with the implementation of the equivalent torsion constant and the cross-frame models developed in this research, the improvements in the predictions obtained from 2D-grid analyses are substantial. An advantage of the proposed techniques is that they can be easily included in 2D-grid models. The implementation of the equivalent constant requires a simple manipulation in the definition of the girder cross-section properties. Similarly, the line elements developed to represent the cross-frames

can be included in the library of any software package used for bridge design. As such, these developments in the field of 2D-grid analysis can be readily implemented and used for the design of steel I-girder bridges.

### 7.1.4. Development of Methods to Predict Flange Lateral Bending Stresses and Girder Layovers in Straight and Skewed Bridges

In a skewed bridge, the cross-frames induce forces in the I-girders, subjecting their flanges to lateral bending stresses, $f_\ell$. For the design of I-girder bridges, the AASHTO LRFD Specifications require conducting the strength checks in a girder segment (defined by the distance between bracing points) considering both $f_b$ and $f_\ell$. In current practice (2011), however, flange lateral bending stresses, $f_\ell$, in straight and skewed bridges can only be predicted using refined 3D FEA. In light of this limitation, the Specifications provide estimates of $f_\ell$ that can be used to determine the strength of the girders during construction. For bridges with skews of up to $60^o$ with staggered cross-frames and a web depth-to-flange width ratio of up to 4.0, it is suggested to assume that $f_\ell$ is equal to 10.0 ksi for interior girders and 7.5 ksi for exterior girders. These coarse estimates provide guidance on how to include $f_\ell$ for the construction checks; however, the large diversity of geometries found in highway bridges makes it difficult to cover all the possible scenarios with these two values.

In this research a technique to compute $f_\ell$ due to skew effects that more properly capture this response and that can be used in lieu of the above estimates is developed. For this purpose, it is necessary to conduct 2D-grid analysis following the recommendations discussed in Chapter 5 and summarized in the previous section. The results of the 2D-grid analysis serve to compute cross-frame forces that are decomposed in forces that are applied to the flanges. Then, each flange segment, which is defined as the distance between three cross-frames (or the sum of two unbraced lengths), is analyzed as a beam subjected to a point load. The supports of the beam are located at the ends of the segment, and the point load is applied at the location of the middle cross-frame. The results obtained for two case studies that were analyzed with this method demonstrate that the $f_\ell$ stresses computed using this technique properly represent the predictions obtained from rigorous 3D FE models.

In addition to the prediction of $f_\ell$, in this research, a method to calculate the girder layovers in straight and skewed bridges is developed. The method consists on determining the layovers at the cross-frame locations using the girder vertical displacement predictions obtained from either a 1D line girder or a 2D-grid analysis. The displacements at a given connection point are used to calculate the rotations needed to accommodate the differential deflections between two adjacent girders. Similar to the $f_\ell$ predictions, the girder layovers in a highly skewed bridge are predicted using the 3D FEA and the proposed method. The results of the analyses show that this method provides accurate estimates of this response at the cross-frame locations.

### 7.1.5. Participation of SIP Forms on the Bridge Geometry Control

Traditionally, the use of SIP metal deck forms as a means to provide stability bracing to the girders during deck placement has been prohibited by the AASHTO Bridge Design Specifications. Based on field measurements and analytical studies, design provisions adopted by some DOTs suggest that even though the SIP panels do not meet the requirements for stability bracing, they are part of the system, and their contributions may have an effect in the control of the bridge deformed geometry. For this purpose, ad hoc procedures have been developed in the past to include the participation of the forms in girder deflections.

In this research, the influence of the SIP forms on the behavior of I-girder bridges is studied in two structures that due to their characteristics are susceptible to large second-order response amplifications. The studies documented in Chapter 6 demonstrate that the participation of the SIP forms may be important only in those bridges that are not adequately braced with cross-frames that have the required in-plane stiffness. In particular, in bridges where the girders are connected with V-type cross-frames without top chords, the stiffness contributions of SIP forms can be considerable. The studies show that in systems where the cross-frames are sufficiently stiff to brace the girders as the structure deflects, the participation of the SIP forms is negligible and can be ignored in the structural analysis.

## 7.2. Future Work

The studies conducted in this research show that the configuration of the bracing system is a key factor that defines the behavior of a steel I-girder bridge. In addition to

the cross-frame layouts studied in this thesis, other configurations that may enhance the structural performance and facilitate the construction should be investigated. For example, the configuration shown in Figure 7.1 is and option that may be used in long-span bridges that require flange level lateral bracing in some regions to increase their resistance to lateral loads. As depicted in the figure, inclined cross-frames may be used to replace the lateral level bracing. When the cross-frames are inclined they not only stabilize the girders but also increase the transverse stiffness of the bridge since the structure behaves as a space truss system. This alternative could be studied to optimize the design while reducing fabrication costs.

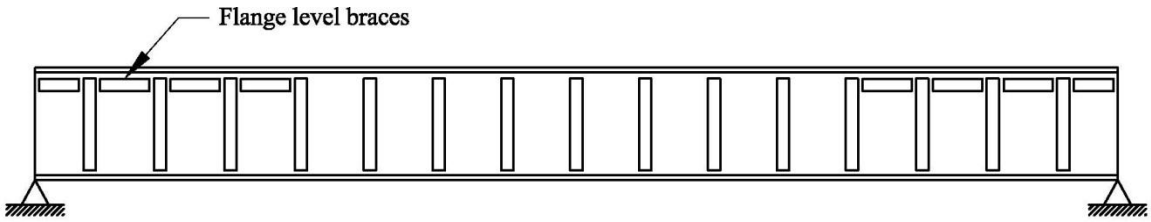


(a) Bridge with flange level bracing system

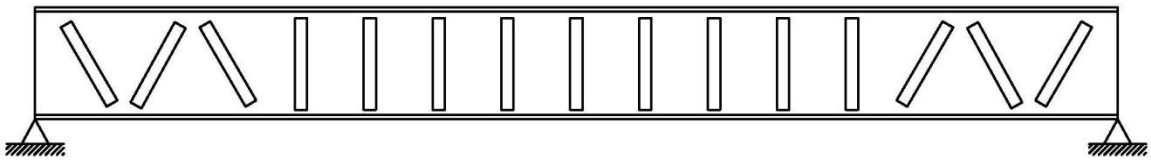

(b) Bridge with inclined cross-frames

Figure 7.1. Schematic representation of a long-span bridge with inclined cross-frames

Another aspect related to this research that requires further investigation is the method to connect the cross-frames to the girder webs. The studies conducted in this research focused on methods to orient the cross-frames so that the structural behavior is improved. However, these configurations require the cross-frame to be skewed at angles larger than $20^{o}$, which is the limit specified by the LRFD AASHTO Specifications. One

of the main reasons for this requirement is that at angles larger than this, it is more difficult to weld the connection plates. For this reason, in future research, it is recommended to study connection details that can be used to overcome this limitation without decreasing the bracing properties of the cross-frames.

Finally, in the context of structural analysis, the developments in the 2D-grid analysis techniques documented in this thesis can be extended to include cross-frame detailing. Currently, the only analysis method that can be used to study the effects of detailing the cross-frames for a given load condition (e.g. steel dead load fit) is 3D FEA. The two-node cross-frame elements formulated in Chapter 5 may be modified to extend the capabilities of 2D-grid models. With this improvement, the fit-up forces can be calculated in a bridge detailed for dead-load-fit.

# APPENDIX A

# CALCULATION OF THE STIFFNESS COEFFICIENTS FOR THE X-TYPE CROSS-FRAME ELEMENT

The formulation of the two-node element used to represent X-type cross-frames was introduced in Chapter 5. In Section 5.2.2, the ability of the proposed element to capture the physical behavior of this type of cross-frame is illustrated; however, only the in-plane properties of the element are considered in the discussions. This appendix provides the stiffness coefficients for the three-dimensional representation of the element. As shown in Figure A.1, the element has six dofs per node. The 12-by-12 stiffness matrix defined by these coefficients can be implemented in computer programs used for the analysis of steel girder bridges. Figure A.2 shows the dimensions and element properties required to calculate the coefficients.

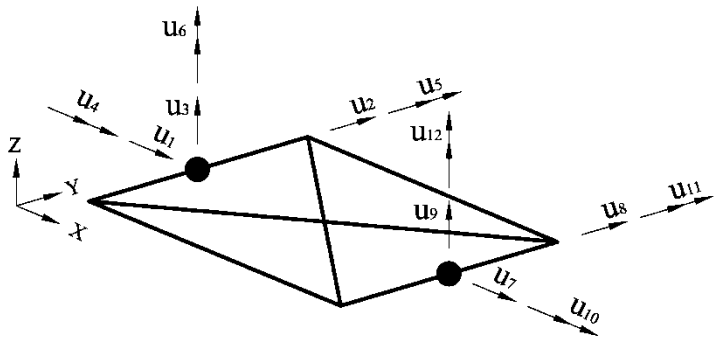


Figure A.1. Schematic representation of the two-node element developed to represent X-type cross-frames in 2D-grid models

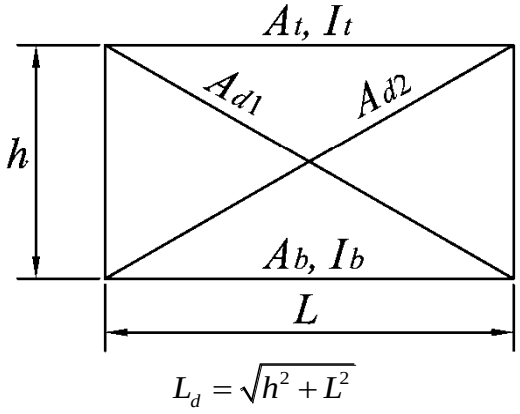


Figure A.2. Properties and dimensions required to calculate the coefficients of the X-type cross-frames stiffness matrix

| Column 1 | Column 2 |
|---|---|
| $k_{1,1}: \quad \frac{E}{L}(A_b + A_t) + \frac{EL^2}{L_d^3}(A_{d1} + A_{d2})$ | $k_{1,2}: \quad \frac{ELh}{L_d^3}(A_{d2} - A_{d1})$ |
| $k_{2,1}: \quad \frac{ELh}{L_d^3}(A_{d2} - A_{d1})$ | $k_{2,2}: \quad \frac{Eh^2}{L_d^3}(A_{d1} + A_{d2})$ |
| $k_{3,1}: \quad 0$ | $k_{3,2}: \quad 0$ |
| $k_{4,1}: \quad 0$ | $k_{4,2}: \quad 0$ |
| $k_{5,1}: \quad 0$ | $k_{5,2}: \quad 0$ |
| $k_{6,1}: \quad \frac{Eh}{2L}(A_b - A_t) + \frac{EhL^2}{2L_d^3}(A_{d2} - A_{d1})$ | $k_{6,2}: \quad \frac{Eh^2L}{2L_d^3}(A_{d2} + A_{d1})$ |
| $k_{7,1}: \quad -\frac{E}{L}(A_b + A_t) - \frac{EL^2}{L_d^3}(A_{d1} + A_{d2})$ | $k_{7,2}: \quad \frac{ELh}{L_d^3}(A_{d1} - A_{d2})$ |
| $k_{8,1}: \quad \frac{ELh}{L_d^3}(A_{d1} - A_{d2})$ | $k_{8,2}: \quad -\frac{Eh^2}{L_d^3}(A_{d1} + A_{d2})$ |
| $k_{9,1}: \quad 0$ | $k_{9,2}: \quad 0$ |
| $k_{10,1}: \quad 0$ | $k_{10,2}: \quad 0$ |
| $k_{11,1}: \quad 0$ | $k_{11,2}: \quad 0$ |
| $k_{12,1}: \quad \frac{Eh}{2L}(A_t - A_b) + \frac{EhL^2}{2L_d^3}(A_{d2} - A_{d1})$ | $k_{12,2}: \quad \frac{Eh^2L}{2L_d^3}(A_{d1} + A_{d2})$ |

Column 3

$k_{1,3}:\ 0$

$k_{2,3}:\ 0$

$k_{3,3}:\ \frac{12E}{L^3}\left(I_b + I_t\right)$

$k_{4,3}:\ \frac{6Eh}{L^3}\left(I_t - I_b\right)$

$k_{5,3}:\ -\frac{6Eh}{L^2}\left(I_t + I_b\right)$

$k_{6,3}:\ 0$

$k_{7,3}:\ 0$

$k_{8,3}:\ 0$

$k_{9,3}:\ -\frac{12E}{L^3}\left(I_b + I_t\right)$

$k_{10,3}:\ \frac{6Eh}{L^3}\left(I_b - I_t\right)$

$k_{11,3}:\ -\frac{6Eh}{L^2}\left(I_t + I_b\right)$

$k_{12,3}:\ 0$

Column 4

$k_{1,4}:\ 0$

$k_{2,4}:\ 0$

$k_{3,4}:\ \frac{6Eh}{L^3}\left(I_t - I_b\right)$

$k_{4,4}:\ \frac{3Eh^2}{L^3}\left(I_t + I_b\right)$

$k_{5,4}:\ \frac{3Eh}{L^2}\left(I_b - I_t\right)$

$k_{6,4}:\ 0$

$k_{7,4}:\ 0$

$k_{8,4}:\ 0$

$k_{9,4}:\ \frac{6Eh}{L^3}\left(I_b - I_t\right)$

$k_{10,4}:\ -\frac{3Eh^2}{L^3}\left(I_t + I_b\right)$

$k_{11,4}:\ \frac{3Eh}{L^2}\left(I_b - I_t\right)$

$k_{12,4}:\ 0$

Column 5

$k_{1,5}:\quad 0$

$k_{2,5}:\quad 0$

$k_{3,5}:\quad -\frac{6E}{L^2}\left(I_b+I_t\right)$

$k_{4,5}:\quad \frac{3Eh}{L^2}\left(I_b-I_t\right)$

$k_{5,5}:\quad \frac{4E}{L}\left(I_b+I_t\right)$

$k_{6,5}:\quad 0$

$k_{7,5}:\quad 0$

$k_{8,5}:\quad 0$

$k_{9,5}:\quad \frac{6E}{L^2}\left(I_b+I_t\right)$

$k_{10,5}:\quad \frac{3Eh}{L^2}\left(I_t-I_b\right)$

$k_{11,5}:\quad \frac{2E}{L}\left(I_b+I_t\right)$

$k_{12,5}:\quad 0$

Column 6

$k_{1,6}:\quad \frac{Eh}{2L}\left(A_b-A_t\right)+\frac{EhL^2}{2L_d{}^3}\left(A_{d2}-A_{d1}\right)$

$k_{2,6}:\quad \frac{Eh^2L}{2L_d{}^3}\left(A_{d1}+A_{d2}\right)$

$k_{3,6}:\quad 0$

$k_{4,6}:\quad 0$

$k_{5,6}:\quad 0$

$k_{6,6}:\quad \frac{Eh^2}{4L}\left(A_b+A_t\right)+\frac{Eh^2L^2}{4L_d{}^3}\left(A_{d1}+A_{d2}\right)$

$k_{7,6}:\quad \frac{Eh}{2L}\left(A_t-A_b\right)+\frac{EhL^2}{2L_d{}^3}\left(A_{d1}-A_{d2}\right)$

$k_{8,6}:\quad -\frac{Eh^2L}{2L_d{}^3}\left(A_{d1}+A_{d2}\right)$

$k_{9,6}:\quad 0$

$k_{10,6}:\quad 0$

$k_{11,6}:\quad 0$

$k_{12,6}:\quad \frac{Eh^2}{4L}\left(A_b+A_t\right)-\frac{Eh^2L^2}{4L_d{}^3}\left(A_{d1}+A_{d2}\right)$

| Column 7 | Column 8 |
| --- | --- |
| $k_{1,7}: \quad -\frac{E}{L}\left(A_b + A_t\right) - \frac{EL^2}{L_d^{\,3}}\left(A_{d1} + A_{d2}\right)$ | $k_{1,8}: \quad \frac{EhL}{L_d^{\,3}}\left(A_{d1} - A_{d2}\right)$ |
| $k_{2,7}: \quad \frac{EhL}{L_d^{\,3}}\left(A_{d1} - A_{d2}\right)$ | $k_{2,8}: \quad -\frac{Eh^2}{L_d^{\,3}}\left(A_{d1} + A_{d2}\right)$ |
| $k_{3,7}: \quad 0$ | $k_{3,8}: \quad 0$ |
| $k_{4,7}: \quad 0$ | $k_{4,8}: \quad 0$ |
| $k_{5,7}: \quad 0$ | $k_{5,8}: \quad 0$ |
| $k_{6,7}: \quad \frac{Eh}{2L}\left(A_t - A_b\right) + \frac{EhL^2}{2L_d^{\,3}}\left(A_{d1} - A_{d2}\right)$ | $k_{6,8}: \quad -\frac{Eh^2L}{2L_d^{\,3}}\left(A_{d1} + A_{d2}\right)$ |
| $k_{7,7}: \quad \frac{E}{L}\left(A_b + A_t\right) + \frac{EL^2}{L_d^{\,3}}\left(A_{d1} + A_{d2}\right)$ | $k_{7,8}: \quad \frac{EhL}{L_d^{\,3}}\left(A_{d2} - A_{d1}\right)$ |
| $k_{8,7}: \quad \frac{EhL}{L_d^{\,3}}\left(A_{d2} - A_{d1}\right)$ | $k_{8,8}: \quad \frac{Eh^2}{L_d^{\,3}}\left(A_{d1} + A_{d2}\right)$ |
| $k_{9,7}: \quad 0$ | $k_{9,8}: \quad 0$ |
| $k_{10,7}: \quad 0$ | $k_{10,8}: \quad 0$ |
| $k_{11,7}: \quad 0$ | $k_{11,8}: \quad 0$ |
| $k_{12,7}: \quad \frac{Eh}{2L}\left(A_b - A_t\right) + \frac{EhL^2}{2L_d^{\,3}}\left(A_{d1} - A_{d2}\right)$ | $k_{12,8}: \quad -\frac{Eh^2L}{2L_d^{\,3}}\left(A_{d1} + A_{d2}\right)$ |

Column 9

$k_{1,9}: \quad 0$

$k_{2,9}: \quad 0$

$k_{3,9}: \quad -\frac{12E}{L^3}\left(I_t + I_b\right)$

$k_{4,9}: \quad \frac{6Eh}{L^3}\left(I_b - I_t\right)$

$k_{5,9}: \quad \frac{6E}{L^2}\left(I_t + I_b\right)$

$k_{6,9}: \quad 0$

$k_{7,9}: \quad 0$

$k_{8,9}: \quad 0$

$k_{9,9}: \quad \frac{12E}{L^3}\left(I_t + I_b\right)$

$k_{10,9}: \quad \frac{6Eh}{L^3}\left(I_t - I_b\right)$

$k_{11,9}: \quad \frac{6E}{L^2}\left(I_t + I_b\right)$

$k_{12,9}: \quad 0$

Column 10

$k_{1,10}: \quad 0$

$k_{2,10}: \quad 0$

$k_{3,10}: \quad \frac{6Eh}{L^3}\left(I_b - I_t\right)$

$k_{4,10}: \quad -\frac{3Eh^2}{L^3}\left(I_b + I_t\right)$

$k_{5,10}: \quad \frac{3Eh}{L^2}\left(I_t - I_b\right)$

$k_{6,10}: \quad 0$

$k_{7,10}: \quad 0$

$k_{8,10}: \quad 0$

$k_{9,10}: \quad \frac{6Eh}{L^3}\left(I_t - I_b\right)$

$k_{10,10}: \quad \frac{3Eh^2}{L^3}\left(I_b + I_t\right)$

$k_{11,10}: \quad \frac{3Eh}{L^2}\left(I_t - I_b\right)$

$k_{12,10}: \quad 0$

Column 11

$k_{1,11}: \quad 0$

$k_{2,11}: \quad 0$

$k_{3,11}: \quad -\frac{6E}{L^2}\left(I_t + I_b\right)$

$k_{4,11}: \quad \frac{3Eh}{L^2}\left(I_b - I_t\right)$

$k_{5,11}: \quad \frac{2E}{L}\left(I_t + I_b\right)$

$k_{6,11}: \quad 0$

$k_{7,11}: \quad 0$

$k_{8,11}: \quad 0$

$k_{9,11}: \quad \frac{6E}{L^2}\left(I_t + I_b\right)$

$k_{10,11}: \quad \frac{3Eh}{L^2}\left(I_t - I_b\right)$

$k_{11,11}: \quad \frac{2E}{L}\left(I_t + I_b\right)$

$k_{12,11}: \quad 0$

Column 12

$k_{1,12}: \quad \frac{Eh}{2L}\left(A_b - A_t\right) + \frac{EhL^2}{2L_d^{\,3}}\left(A_{d2} - A_{d1}\right)$

$k_{2,12}: \quad \frac{Eh^2L}{2L_d^{\,3}}\left(A_{d1} + A_{d2}\right)$

$k_{3,12}: \quad 0$

$k_{4,12}: \quad 0$

$k_{5,12}: \quad 0$

$k_{6,12}: \quad -\frac{Eh^2}{4L}\left(A_b + A_t\right) + \frac{Eh^2L^2}{4L_d^{\,3}}\left(A_{d1} + A_{d2}\right)$

$k_{7,12}: \quad \frac{Eh}{2L}\left(A_b - A_t\right) + \frac{EhL^2}{2L_d^{\,3}}\left(A_{d1} - A_{d2}\right)$

$k_{8,12}: \quad -\frac{Eh^2L}{2L_d^{\,3}}\left(A_{d1} + A_{d2}\right)$

$k_{9,12}: \quad 0$

$k_{10,12}: \quad 0$

$k_{11,12}: \quad 0$

$k_{12,12}: \quad \frac{Eh^2}{4L}\left(A_b + A_t\right) + \frac{Eh^2L^2}{4L_d^{\,3}}\left(A_{d1} + A_{d2}\right)$

# APPENDIX B

# CALCULATION OF THE STIFFNESS COEFFICIENTS FOR THE V-TYPE CROSS-FRAME ELEMENT

The formulation of the two-node element used to represent V-type cross-frames was introduced in Chapter 5. In Section 5.2.3, the ability of the proposed element to capture the physical behavior of this type of cross-frame is illustrated; however, only the in-plane properties of the element are considered in the discussions. This appendix provides the stiffness coefficients for the three-dimensional representation of the element. As shown in Figure B.1, the element has six dofs per node. The 12-by-12 stiffness matrix defined by these coefficients can be implemented in computer programs used for the analysis of steel girder bridges. Figure B.2 shows the dimensions and element properties required to calculate the coefficients.

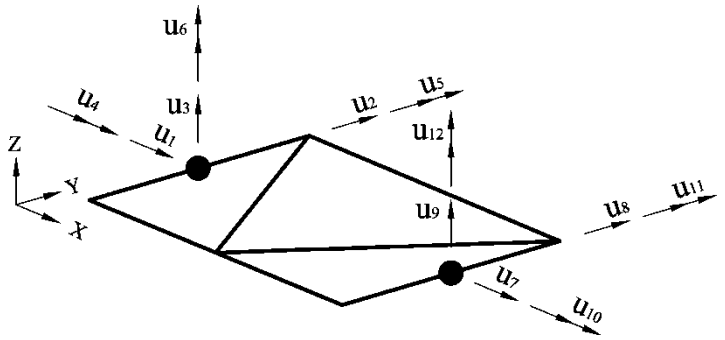


Figure B.1. Schematic representation of the two-node element developed to represent V-type cross-frames in 2D-grid models

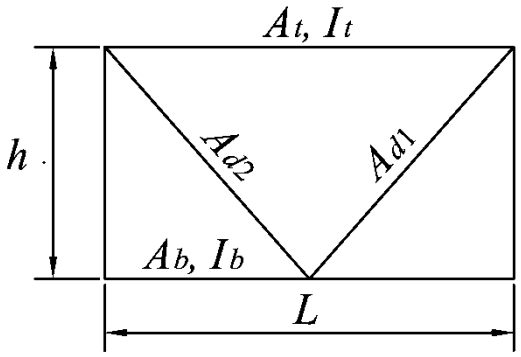


$$L_d = \sqrt{h^2 + (L/2)^2}$$

Figure B.2. Properties and dimensions required to calculate the coefficients of the V-type cross-frames stiffness matrix

Column 1

$$k_{1,1}: \quad \frac{E}{L}(A_b + A_t) + \frac{3A_d I_b L^2}{A_d L^3 h^2 + 24 I_b L_d{}^3}$$

$$k_{2,1}: \quad 0$$

$$k_{3,1}: \quad 0$$

$$k_{4,1}: \quad 0$$

$$k_{5,1}: \quad 0$$

$$k_{6,1}: \quad -\frac{Eh\left[3A_d I_b L^2 h - (A_b - A_t)\left(24 I_b L_d{}^3 + A_d L^3 h^2\right)\right]}{2L\left(A_d L^3 h^2 + 24 I_b L_d{}^3\right)}$$

$$k_{7,1}: \quad -\frac{E}{L}(A_b + A_t) + \frac{3A_d I_b L^2}{A_d L^3 h^2 + 24 I_b L_d{}^3}$$

$$k_{8,1}: \quad 0$$

$$k_{9,1}: \quad 0$$

$$k_{10,1}: \quad 0$$

$$k_{11,1}: \quad 0$$

$$k_{12,1}: \quad \frac{Eh\left[3A_d I_b L^2 h - (A_b - A_t)\left(24 I_b L_d{}^3 + A_d L^3 h^2\right)\right]}{2L\left(A_d L^3 h^2 + 24 I_b L_d{}^3\right)}$$

Column 2

$k_{1,2}:\ 0$

$k_{2,2}:\ \dfrac{4EA_bA_dh^2}{A_dL^3+8A_bL_d{}^3}$

$k_{3,2}:\ 0$

$k_{4,2}:\ 0$

$k_{5,2}:\ 0$

$k_{6,2}:\ \dfrac{2EA_bA_dLh^2}{A_dL^3+8A_bL_d{}^3}$

$k_{7,2}:\ 0$

$k_{8,2}:\ -\dfrac{4EA_bA_dh^2}{A_dL^3+8A_bL_d{}^3}$

$k_{9,2}:\ 0$

$k_{10,2}:\ 0$

$k_{11,2}:\ 0$

$k_{12,2}:\ \dfrac{2EA_bA_dLh^2}{A_dL^3+8A_bL_d{}^3}$

Column 3

$k_{1,3}:\ 0$

$k_{2,3}:\ 0$

$k_{3,3}:\ \dfrac{12E}{L^3}\left(I_b+I_t\right)$

$k_{4,3}:\ \dfrac{6Eh}{L^3}\left(I_t-I_b\right)$

$k_{5,3}:\ -\dfrac{6Eh}{L^2}\left(I_t+I_b\right)$

$k_{6,3}:\ 0$

$k_{7,3}:\ 0$

$k_{8,3}:\ 0$

$k_{9,3}:\ -\dfrac{12E}{L^3}\left(I_b+I_t\right)$

$k_{10,3}:\ \dfrac{6Eh}{L^3}\left(I_t-I_b\right)$

$k_{11,3}:\ -\dfrac{6Eh}{L^2}\left(I_t+I_b\right)$

$k_{12,3}:\ 0$

Column 4

$k_{1,4}: \quad 0$

$k_{2,4}: \quad 0$

$k_{3,4}: \quad \frac{6Eh}{L^3}\left(I_t - I_b\right)$

$k_{4,4}: \quad \frac{3Eh^2}{L^3}\left(I_t + I_b\right)$

$k_{5,4}: \quad \frac{3Eh}{L^2}\left(I_b - I_t\right)$

$k_{6,4}: \quad 0$

$k_{7,4}: \quad 0$

$k_{8,4}: \quad 0$

$k_{9,4}: \quad \frac{6Eh}{L^3}\left(I_b - I_t\right)$

$k_{10,4}: \quad -\frac{3Eh^2}{L^3}\left(I_t + I_b\right)$

$k_{11,4}: \quad \frac{3Eh}{L^2}\left(I_b - I_t\right)$

$k_{12,4}: \quad 0$

Column 5

$k_{1,5}: \quad 0$

$k_{2,5}: \quad 0$

$k_{3,5}: \quad -\frac{6E}{L^2}\left(I_b + I_t\right)$

$k_{4,5}: \quad \frac{3Eh}{L^2}\left(I_b - I_t\right)$

$k_{5,5}: \quad \frac{4E}{L}\left(I_b + I_t\right)$

$k_{6,5}: \quad 0$

$k_{7,5}: \quad 0$

$k_{8,5}: \quad 0$

$k_{9,5}: \quad \frac{6E}{L^2}\left(I_b + I_t\right)$

$k_{10,5}: \quad \frac{3Eh}{L^2}\left(I_t - I_b\right)$

$k_{11,5}: \quad \frac{2E}{L}\left(I_b + I_t\right)$

$k_{12,5}: \quad 0$

Column 6

$$k_{1,6}: \quad -\frac{Eh\left[3A_d I_b L^2 h-\left(A_b-A_t\right)\left(24I_b {L_d}^3+A_d L^3 h^2\right)\right]}{2L\left(A_d L^3 h^2+24I_b {L_d}^3\right)}$$

$$k_{2,6}: \quad \frac{2EA_b A_d L h^2}{A_d L^3+8A_b {L_d}^3}$$

$$k_{3,6}: \quad 0$$

$$k_{4,6}: \quad 0$$

$$k_{5,6}: \quad 0$$

$$k_{6,6}: \quad \frac{Eh^2\left[\left(A_b+A_t\right)\left(8A_b A_d L^3 {L_d}^3 h^2+192A_b I_b {L_d}^6\right)+{A_d}^2 L^6 h^6\left(5A_b+A_t\right)+A_d I_b L^3 {L_d}^3\left(144A_b+24A_t\right)+3{A_d}^2 I_b L^6\right]}{4L\left(A_d L^3 h^2+24I_b {L_d}^3\right)\left(A_d L^3+8A_b L_d h^3\right)}$$

$$k_{7,6}: \quad \frac{Eh\left[3A_d I_b L^2 h-\left(A_b-A_t\right)\left(24I_b {L_d}^3+A_d L^3 h^2\right)\right]}{2L\left(A_d L^3 h^2+24I_b {L_d}^3\right)}$$

$$k_{8,6}: \quad -\frac{2EA_b A_d L h^2}{A_d L^3+8A_b {L_d}^3}$$

$$k_{9,6}: \quad 0$$

$$k_{10,6}: \quad 0$$

$$k_{11,6}: \quad 0$$

$$k_{12,6}: \quad -\frac{Eh^2\left[\left(A_b+A_t\right)\left(8A_b A_d L^3 {L_d}^3 h^2+192A_b I_b {L_d}^6\right)+{A_d}^2 L^6 h^6\left(5A_b+A_t\right)+A_d I_b L^3 {L_d}^3\left(144A_b+24A_t\right)+3{A_d}^2 I_b L^6\right]}{4L\left(A_d L^3 h^2+24I_b {L_d}^3\right)\left(A_d L^3+8A_b L_d h^3\right)}$$

Column 7

$$k_{1,7}: \quad -\frac{E}{L}\left(A_b + A_t\right) - \frac{3A_d I_b L^2}{A_d L^3 h^2 + 24 I_b {L_d}^3}$$

$$k_{2,7}: \quad 0$$

$$k_{3,7}: \quad 0$$

$$k_{4,7}: \quad 0$$

$$k_{5,7}: \quad 0$$

$$k_{6,7}: \quad \frac{Eh\left[3A_d I_b L^2 h - \left(A_b - A_t\right)\left(24 I_b {L_d}^3 + A_d L^3 h^2\right)\right]}{2L\left(A_d L^3 h^2 + 24 I_b {L_d}^3\right)}$$

$$k_{7,7}: \quad \frac{E}{L}\left(A_b + A_t\right) + \frac{3A_d I_b L^2}{A_d L^3 h^2 + 24 I_b {L_d}^3}$$

$$k_{8,7}: \quad 0$$

$$k_{9,7}: \quad 0$$

$$k_{10,7}: \quad 0$$

$$k_{11,7}: \quad 0$$

$$k_{12,7}: \quad -\frac{Eh\left[3A_d I_b L^2 h - \left(A_b - A_t\right)\left(24 I_b {L_d}^3 + A_d L^3 h^2\right)\right]}{2L\left(A_d L^3 h^2 + 24 I_b {L_d}^3\right)}$$

Column 8

$k_{1,8}:\ 0$

$k_{2,8}:\ -\frac{4EA_bA_dh^2}{A_dL^3+8A_b{L_d}^3}$

$k_{3,8}:\ 0$

$k_{4,8}:\ 0$

$k_{5,8}:\ 0$

$k_{6,8}:\ -\frac{2EA_bA_dLh^2}{A_dL^3+8A_b{L_d}^3}$

$k_{7,8}:\ 0$

$k_{8,8}:\ \frac{4EA_bA_dh^2}{A_dL^3+8A_b{L_d}^3}$

$k_{9,8}:\ 0$

$k_{10,8}:\ 0$

$k_{11,8}:\ 0$

$k_{12,8}:\ -\frac{2EA_bA_dLh^2}{A_dL^3+8A_b{L_d}^3}$

Column 9

$k_{1,9}:\ 0$

$k_{2,9}:\ 0$

$k_{3,9}:\ -\frac{12E}{L^3}\left(I_t+I_b\right)$

$k_{4,9}:\ \frac{6Eh}{L^3}\left(I_b-I_t\right)$

$k_{5,9}:\ \frac{6E}{L^2}\left(I_t+I_b\right)$

$k_{6,9}:\ 0$

$k_{7,9}:\ 0$

$k_{8,9}:\ 0$

$k_{9,9}:\ \frac{12E}{L^3}\left(I_t+I_b\right)$

$k_{10,9}:\ \frac{6Eh}{L^3}\left(I_t-I_b\right)$

$k_{11,9}:\ \frac{6E}{L^2}\left(I_t+I_b\right)$

$k_{12,9}:\ 0$

Column 10

$k_{1,10}:\quad 0$

$k_{2,10}:\quad 0$

$k_{3,10}:\quad \frac{6Eh}{L^3}\left(I_b - I_t\right)$

$k_{4,10}:\quad -\frac{3Eh^2}{L^3}\left(I_b + I_t\right)$

$k_{5,10}:\quad \frac{3Eh}{L^2}\left(I_t - I_b\right)$

$k_{6,10}:\quad 0$

$k_{7,10}:\quad 0$

$k_{8,10}:\quad 0$

$k_{9,10}:\quad \frac{6Eh}{L^3}\left(I_t - I_b\right)$

$k_{10,10}:\quad \frac{3Eh^2}{L^3}\left(I_b + I_t\right)$

$k_{11,10}:\quad \frac{3Eh}{L^2}\left(I_t - I_b\right)$

$k_{12,10}:\quad 0$

Column 11

$k_{1,11}:\quad 0$

$k_{2,11}:\quad 0$

$k_{3,11}:\quad -\frac{6E}{L^2}\left(I_t + I_b\right)$

$k_{4,11}:\quad \frac{3Eh}{L^2}\left(I_b - I_t\right)$

$k_{5,11}:\quad \frac{2E}{L}\left(I_t + I_b\right)$

$k_{6,11}:\quad 0$

$k_{7,11}:\quad 0$

$k_{8,11}:\quad 0$

$k_{9,11}:\quad \frac{6E}{L^2}\left(I_t + I_b\right)$

$k_{10,11}:\quad \frac{3Eh}{L^2}\left(I_t - I_b\right)$

$k_{11,11}:\quad \frac{2E}{L}\left(I_t + I_b\right)$

$k_{12,11}:\quad 0$

Column 12

$$k_{1,12}: \quad \frac{Eh\left[3A_d I_b L^2 h-\left(A_b-A_t\right)\left(24I_b L_d{}^3+A_d L^3 h^2\right)\right]}{2L\left(A_d L^3 h^2+24I_b L_d{}^3\right)}$$

$$k_{2,12}: \quad \frac{2EA_b A_d L h^2}{A_d L^3+8A_b L_d{}^3}$$

$$k_{3,12}: \quad 0$$

$$k_{4,12}: \quad 0$$

$$k_{5,12}: \quad 0$$

$$k_{6,12}: \quad -\frac{Eh^2\left[\left(A_b+A_t\right)\left(8A_b A_d L^3 L_d{}^3 h^2+192A_b I_b L_d{}^6\right)+A_d{}^2 L^6 h^6\left(5A_b+A_t\right)+A_d I_b L^3 L_d{}^3\left(144A_b+24A_t\right)+3A_d{}^2 I_b L^6\right]}{4L\left(A_d L^3 h^2+24I_b L_d{}^3\right)\left(A_d L^3+8A_b L_d h^3\right)}$$

$$k_{7,12}: \quad -\frac{Eh\left[3A_d I_b L^2 h-\left(A_b-A_t\right)\left(24I_b L_d{}^3+A_d L^3 h^2\right)\right]}{2L\left(A_d L^3 h^2+24I_b L_d{}^3\right)}$$

$$k_{8,12}: \quad -\frac{2EA_b A_d L h^2}{A_d L^3+8A_b L_d{}^3}$$

$$k_{9,12}: \quad 0$$

$$k_{10,12}: \quad 0$$

$$k_{11,12}: \quad 0$$

$$k_{12,12}: \quad \frac{Eh^2\left[\left(A_b+A_t\right)\left(8A_b A_d L^3 L_d{}^3 h^2+192A_b I_b L_d{}^6\right)+A_d{}^2 L^6 h^6\left(5A_b+A_t\right)+A_d I_b L^3 L_d{}^3\left(144A_b+24A_t\right)+3A_d{}^2 I_b L^6\right]}{4L\left(A_d L^3 h^2+24I_b L_d{}^3\right)\left(A_d L^3+8A_b L_d h^3\right)}$$

# APPENDIX C

# CALCULATION OF THE STIFFNESS COEFFICIENTS FOR THE INVERTED V-TYPE CROSS-FRAME ELEMENT

The formulation of the two-node element used to represent inverted V-type cross-frames was introduced in Chapter 5. In Section 5.2.3, the ability of the proposed element to capture the physical behavior of this type of cross-frame is illustrated; however, only the in-plane properties of the element are considered in the discussions. This appendix provides the stiffness coefficients for the three-dimensional representation of the element. As shown in Figure C.1, the element has six dofs per node. The 12-by-12 stiffness matrix defined by these coefficients can be implemented in computer programs used for the analysis of steel girder bridges. Figure C.2 shows the dimensions and element properties required to calculate the coefficients.

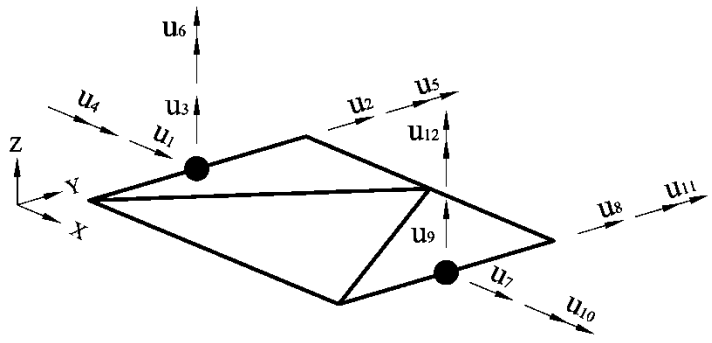


Figure C.1. Schematic representation of the two-node element developed to represent inverted V-type cross-frames in 2D-grid models

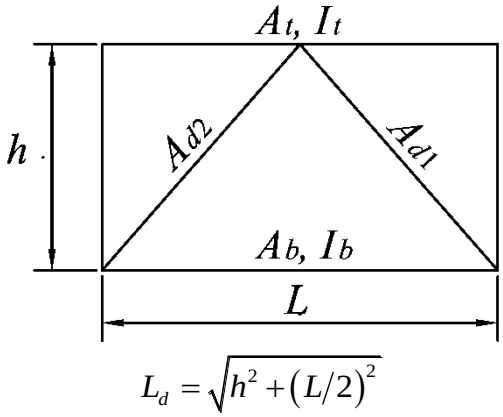


Figure C.2. Properties and dimensions required to calculate the coefficients of the inverted V-type cross-frames stiffness matrix

| Column 1 | Column 2 |
|---|---|
| $k_{1,1}: \quad \frac{E}{L}(A_b + A_t)$ | $k_{1,2}: \quad 0$ |
| $k_{2,1}: \quad 0$ | $k_{2,2}: \quad \frac{4EA_dA_th^2}{A_dL^3 + 8A_t{L_d}^3}$ |
| $k_{3,1}: \quad 0$ | $k_{3,2}: \quad 0$ |
| $k_{4,1}: \quad 0$ | $k_{4,2}: \quad 0$ |
| $k_{5,1}: \quad 0$ | $k_{5,2}: \quad 0$ |
| $k_{6,1}: \quad \frac{Eh}{2L}(A_b - A_t)$ | $k_{6,2}: \quad \frac{2EA_dA_tLh^2}{A_dL^3 + 8A_t{L_d}^3}$ |
| $k_{7,1}: \quad -\frac{E}{L}(A_b + A_t)$ | $k_{7,2}: \quad 0$ |
| $k_{8,1}: \quad 0$ | $k_{8,2}: \quad -\frac{4EA_dA_th^2}{A_dL^3 + 8A_t{L_d}^3}$ |
| $k_{9,1}: \quad 0$ | $k_{9,2}: \quad 0$ |
| $k_{10,1}: \quad 0$ | $k_{10,2}: \quad 0$ |
| $k_{11,1}: \quad 0$ | $k_{11,2}: \quad 0$ |
| $k_{12,1}: \quad -\frac{Eh}{2L}(A_b - A_t)$ | $k_{12,2}: \quad \frac{2EA_dA_tLh^2}{A_dL^3 + 8A_t{L_d}^3}$ |

Column 3

$k_{1,3}: \quad 0$

$k_{2,3}: \quad 0$

$k_{3,3}: \quad \frac{12E}{L^3}\left(I_b + I_t\right)$

$k_{4,3}: \quad \frac{6Eh}{L^3}\left(I_t - I_b\right)$

$k_{5,3}: \quad -\frac{6Eh}{L^2}\left(I_t + I_b\right)$

$k_{6,3}: \quad 0$

$k_{7,3}: \quad 0$

$k_{8,3}: \quad 0$

$k_{9,3}: \quad -\frac{12E}{L^3}\left(I_b + I_t\right)$

$k_{10,3}: \quad \frac{6Eh}{L^3}\left(I_b - I_t\right)$

$k_{11,3}: \quad -\frac{6Eh}{L^2}\left(I_t + I_b\right)$

$k_{12,3}: \quad 0$

Column 4

$k_{1,4}: \quad 0$

$k_{2,4}: \quad 0$

$k_{3,4}: \quad \frac{6Eh}{L^3}\left(I_t - I_b\right)$

$k_{4,4}: \quad \frac{3Eh^2}{L^3}\left(I_t + I_b\right)$

$k_{5,4}: \quad \frac{3Eh}{L^2}\left(I_b - I_t\right)$

$k_{6,4}: \quad 0$

$k_{7,4}: \quad 0$

$k_{8,4}: \quad 0$

$k_{9,4}: \quad \frac{6Eh}{L^3}\left(I_b - I_t\right)$

$k_{10,4}: \quad -\frac{3Eh^2}{L^3}\left(I_t + I_b\right)$

$k_{11,4}: \quad \frac{3Eh}{L^2}\left(I_b - I_t\right)$

$k_{12,4}: \quad 0$

Column 5

$k_{1,5}:\ 0$

$k_{2,5}:\ 0$

$k_{3,5}:\ -\frac{6E}{L^2}\left(I_b+I_t\right)$

$k_{4,5}:\ \frac{3Eh}{L^2}\left(I_b-I_t\right)$

$k_{5,5}:\ \frac{4E}{L}\left(I_b+I_t\right)$

$k_{6,5}:\ 0$

$k_{7,5}:\ 0$

$k_{8,5}:\ 0$

$k_{9,5}:\ \frac{6E}{L^2}\left(I_b+I_t\right)$

$k_{10,5}:\ \frac{3Eh}{L^2}\left(I_t-I_b\right)$

$k_{11,5}:\ \frac{2E}{L}\left(I_b+I_t\right)$

$k_{12,5}:\ 0$

Column 6

$k_{1,6}:\ \frac{Eh}{2L}\left(A_b-A_t\right)$

$k_{2,6}:\ \frac{2EA_dA_tLh^2}{A_dL^3+8A_t{L_d}^3}$

$k_{3,6}:\ 0$

$k_{4,6}:\ 0$

$k_{5,6}:\ 0$

$k_{6,6}:\ \frac{Eh^2\left(8{A_t}^2{L_d}^3+5A_dA_tL^3+8A_bA_t{L_d}^3+A_bA_dL^3\right)}{4L\left(A_dL^3+8A_t{L_d}^3\right)}$

$k_{7,6}:\ -\frac{Eh}{2L}\left(A_b-A_t\right)$

$k_{8,6}:\ -\frac{2EA_dA_tLh^2}{A_dL^3+8A_t{L_d}^3}$

$k_{9,6}:\ 0$

$k_{10,6}:\ 0$

$k_{11,6}:\ 0$

$k_{12,6}:\ \frac{EA_dA_t{L}^2h^2}{A_dL^3+8A_t{L_d}^3}-\frac{E\left(A_t+A_b\right)h^2}{4L}$

Column 7

$k_{1,7}: \quad -\frac{E}{L}\left(A_b + A_t\right)$

$k_{2,7}: \quad 0$

$k_{3,7}: \quad 0$

$k_{4,7}: \quad 0$

$k_{5,7}: \quad 0$

$k_{6,7}: \quad \frac{Eh}{2L}\left(A_t - A_b\right)$

$k_{7,7}: \quad \frac{E}{L}\left(A_b + A_t\right)$

$k_{8,7}: \quad 0$

$k_{9,7}: \quad 0$

$k_{10,7}: \quad 0$

$k_{11,7}: \quad 0$

$k_{12,7}: \quad -\frac{Eh}{2L}\left(A_t - A_b\right)$

Column 8

$k_{1,8}: \quad 0$

$k_{2,8}: \quad -\frac{4EA_dA_th^2}{A_dL^3 + 8A_t{L_d}^3}$

$k_{3,8}: \quad 0$

$k_{4,8}: \quad 0$

$k_{5,8}: \quad 0$

$k_{6,8}: \quad -\frac{2EA_dA_tLh^2}{A_dL^3 + 8A_t{L_d}^3}$

$k_{7,8}: \quad 0$

$k_{8,8}: \quad \frac{4EA_dA_th^2}{A_dL^3 + 8A_t{L_d}^3}$

$k_{9,8}: \quad 0$

$k_{10,8}: \quad 0$

$k_{11,8}: \quad 0$

$k_{12,8}: \quad -\frac{2EA_dA_tLh^2}{A_dL^3 + 8A_t{L_d}^3}$

Column 9

$k_{1,9}: \quad 0$

$k_{2,9}: \quad 0$

$k_{3,9}: \quad -\frac{12E}{L^3}\left(I_t + I_b\right)$

$k_{4,9}: \quad \frac{6Eh}{L^3}\left(I_b - I_t\right)$

$k_{5,9}: \quad \frac{6E}{L^2}\left(I_t + I_b\right)$

$k_{6,9}: \quad 0$

$k_{7,9}: \quad 0$

$k_{8,9}: \quad 0$

$k_{9,9}: \quad \frac{12E}{L^3}\left(I_t + I_b\right)$

$k_{10,9}: \quad \frac{6Eh}{L^3}\left(I_t - I_b\right)$

$k_{11,9}: \quad \frac{6E}{L^2}\left(I_t + I_b\right)$

$k_{12,9}: \quad 0$

Column 10

$k_{1,10}: \quad 0$

$k_{2,10}: \quad 0$

$k_{3,10}: \quad \frac{6Eh}{L^3}\left(I_b - I_t\right)$

$k_{4,10}: \quad -\frac{3Eh^2}{L^3}\left(I_b + I_t\right)$

$k_{5,10}: \quad \frac{3Eh}{L^2}\left(I_t - I_b\right)$

$k_{6,10}: \quad 0$

$k_{7,10}: \quad 0$

$k_{8,10}: \quad 0$

$k_{9,10}: \quad \frac{6Eh}{L^3}\left(I_t - I_b\right)$

$k_{10,10}: \quad \frac{3Eh^2}{L^3}\left(I_b + I_t\right)$

$k_{11,10}: \quad \frac{3Eh}{L^2}\left(I_t - I_b\right)$

$k_{12,10}: \quad 0$

Column 11

$k_{1,11}:\ 0$

$k_{2,11}:\ 0$

$k_{3,11}:\ -\frac{6E}{L^2}\left(I_t+I_b\right)$

$k_{4,11}:\ \frac{3Eh}{L^2}\left(I_b-I_t\right)$

$k_{5,11}:\ \frac{2E}{L}\left(I_t+I_b\right)$

$k_{6,11}:\ 0$

$k_{7,11}:\ 0$

$k_{8,11}:\ 0$

$k_{9,11}:\ \frac{6E}{L^2}\left(I_t+I_b\right)$

$k_{10,11}:\ \frac{3Eh}{L^2}\left(I_t-I_b\right)$

$k_{11,11}:\ \frac{2E}{L}\left(I_t+I_b\right)$

$k_{12,11}:\ 0$

Column 12

$k_{1,12}:\ -\frac{Eh}{2L}\left(A_b-A_t\right)$

$k_{2,12}:\ \frac{2EA_dA_tLh^2}{A_dL^3+8A_t{L_d}^3}$

$k_{3,12}:\ 0$

$k_{4,12}:\ 0$

$k_{5,12}:\ 0$

$k_{6,12}:\ \frac{EA_dA_tL^2h^2}{A_dL^3+8A_t{L_d}^3}-\frac{E\left(A_t+A_b\right)h^2}{4L}$

$k_{7,12}:\ \frac{Eh}{2L}\left(A_b-A_t\right)$

$k_{8,12}:\ -\frac{2EA_dA_tLh^2}{A_dL^3+8A_t{L_d}^3}$

$k_{9,12}:\ 0$

$k_{10,12}:\ 0$

$k_{11,12}:\ 0$

$k_{12,12}:\ \frac{Eh^2\left(8{A_t}^2{L_d}^3+5A_dA_tL^3+8A_bA_t{L_d}^3+A_bA_dL^3\right)}{4L\left(A_dL^3+8A_t{L_d}^3\right)}$

# REFERENCES


AASHTO (2010). *LRFD* Bridge *Design Specifications*, 5th Edition, American Association of State Highway and Transportation Officials, Washington, DC.

AASHTO/NSBA (2011). Guidelines for the Analysis of Steel Girder Bridges, G13.1, AASHTO/NSBA Steel Bridge Collaboration, American Association of State Highway and Transportation Officials, Washington, DC and National Steel Bridge Alliance, Chicago, IL.

AISC (2010). Code of Standard Practice for Steel Buildings and Bridges, AISC 303-10, American Institute of Steel Construction, IL.

AISI (1997). Four LRFD Examples of Steel Highway Bridges, American Iron and Steel Institute, Washington, DC.

Ahmed, M.Z. and Weisberger, F.E. (1996). "Torsion Constant for Matrix Analysis of Structures Including Warping Effect," International Journal of Solids and Structures, Elsevier, 33(3), 361-374.

Berglund, E.M. and Schultz, A.E. (2006). "Girder Differential Deflection and Distortion-Induced Fatigue in Skewed Steel Bridges," Journal of Bridge Engineering, ASCE, 11(2), 169-177.

Chang, C.-J. (2006). "Construction Simulation for Curved Steel I-Girder Bridges," Ph.D. Dissertation, Georgia Institute of Technology, Atlanta, GA, 340 pp.

Chavel, B.W. (2008). "Construction and Detailing Methods of Horizontally Curved Steel I-Girder Bridges," Ph.D. Dissertation, Swanson School of Engineering, University of Pittsburgh, PA, 357 pp.

Currah, R.M. (1993). "Shear Strength and Shear Stiffness of Permanent Steel Bridge Deck Forms," M.S. Thesis, University of Texas at Austin, Austin, TX, 100 pp.

Dassault Systèmes (2010). ABAQUS/Standard Version 6.10, Dassault Systèmes, Inc. Providence, RI, http://www.simulia.com/

Dexter, R.J. and Wright, J.W. (2004). "Fatigue and Fracture of Steel Girders," Journal of Bridge Engineering, ASCE, 9(3), 278-286.

Egilmez, O.O. (2005). "Lateral Bracing of Steel Bridge Girders by Permanent Metal Deck Forms," Ph.D. Dissertation, University of Houston, Houston, TX, 309 pp.

Egilmez, O.O., Helwig, T.A., Jetann, C.A. and Lowery, R. (2007). "Stiffness and Strength of Metal Bridge Deck Forms," Journal of Bridge Engineering, ASCE, 12(4), 429-437.

Egilmez, O.O., Herman, R.S. and Helwig, T.A. (2009). "Lateral Stiffness of Steel I-Girder Braced by Metal Deck Forms," Journal of Bridge Engineering, ASCE, 14(1), 17-25.

Fasl, J., Romage, M., Helwig., T.A., Herman, R. and Frank, K.H. (2009). "Field Measurements on Steel Girder Bridge with Skewed Supports Utilizing Lean-On Bracing," Proceedings, Structures Congress, ASCE, 125-134.

Fisher, J.W. and Keating, P.B. (1989). "Distortion-Induced Fatigue Cracking of Bridge Details with Web Gaps," Journal of Constructional Steel Research, Elsevier, 215-228.

Fisher, S.T. (2006). "Development of a Simplified Procedure to Predict Dead Load Deflections of Skewed and Non-Skewed Steel Plate Girder Bridges," M.S. Thesis, School of Civil Engineering, North Carolina State University, Raleigh, NC, 360 pp.

Grubb, M. (1984). "Horizontally Curved I-Girder Bridge Analysis: V-Load Method," Transportation Research Record, Transportation Research Board, N982, 26-36

Helwig, T.A. and Yura, J.A. (2008). "Shear Diaphragm Bracing of Beams. I: Stiffness and Strength Behavior," Journal of Structural Engineering, ASCE, 134(3), 348-356.

Huang, W.-H. (1996). "Curved I-Girder Systems," Ph.D. Dissertation, Department of Civil and Environmental Engineering, University of Minnesota, Minneapolis, MN, 305 pp.

Jetann, C.A. (2003). "Stiffness and Strength of Metal Bridge Deck Forms with Stiffened Connection Details," M.S. Thesis, University of Houston, Houston, TX, 200 pp.

Jung, S.-K. (2006). "Inelastic Strength Behavior of Horizontally Curved Composite I-Girder Bridge Structural Systems," Ph.D. Dissertation, School of Civil and Environmental Engineering, Georgia Institute of Technology, Atlanta, GA, 811 pp.

Kim, Y.D. (2010). "Behavior and Design of Metal Building Frames using General Prismatic and Web-Tapered Steel I-Section Members," Ph.D. Dissertation, School of Civil and Environmental Engineering, Georgia Institute of Technology, Atlanta, GA, 528 pp.

Kupricka, G., and Poellot, B. (1993). "Nuisance Stiffness," Bridgeline, HDR Engineering, Inc., 4(1), 3 pp.

LARSA (2010). "LARSA 4D, The Complete Package for Bridge Design and Construction," http://www.larsa4d.com.

Lowery, R.K. (2003). "Shear Stiffness and Strength Properties of Permanent Metal Deck Forms for Bridge Applications," M.S. Thesis, University of Houston, Houston, TX, 150 pp.

Morera, F.J. (2010). "Lateral Flange Bending in Heavily Skewed Steel Bridges." Ph.D. Dissertation, School of Civil Engineering, North Carolina State University, Raleigh, NC, 408 pp.

NCHRP/TRB (2007), Simplified Live Load Distribution Factor Equations, NCHRP Report 592, National Cooperative Highway Research Program, Washington, DC, and Transportation Research Board, Washington, DC.

NCHRP/TRB (2011), Guidelines for Analytical Methods and Erection Engineering of Curved and Skewed Steel Deck-Girder Bridges, NCHRP 12-79, National Cooperative Highway Research Program, Washington, DC, and Transportation Research Board, Washington, DC.

NHI/FHWA (2011a). Load and Resistance Factored Design and Analysis of Skewed and Curved Steel Bridges, Design Manual, NHI Course No. 130095, Publication No. FHWA-NHI-10-087, National Highway Institute, Federal Highway Administration, 1476 pp.

NHI/FHWA (2011b). Load and Resistance Factored Design and Analysis of Skewed and Curved Steel Bridges, Participant Workbook, NHI Course No. 130095, Publication No. FHWA-NHI-10-086, National Highway Institute, Federal Highway Administration, 1476 pp.

Ozgur, C. and White, D.W. (2007). "Behavior and Analysis of a Curved Steel I-Girder Bridge," Proceedings, World Steel Bridge Symposium, National Steel Bridge Alliance, Chicago, IL, 18 pp.

Ozgur, C. (2011). "Influence of Cross-Frame Detailing on Curved and Skewed Steel I-Girder Bridges," Ph.D. Dissertation, Georgia Institute of Technology, Atlanta, GA. 382 pp.

Poellot, W.N. (1987). "Computer-Aided Design of Horizontally Curved Girders by the V-Load Method," Engineering Journal, AISC, 24(1), 42-50.

Prawel, S.P., Morrell, M.L. and Lee, G.C. (1974). "Bending and Buckling Strength of Tapered Structural Members," Welding Research Supplement, Vol. 53, February, 75-84.

Quadrato, C., Battistini, A., Frank, K, Helwig, T., and Engelhardt, M. (2010). "Improved Cross-Frame Connection Details for Steel Bridges with Skewed Supports," Transportation Research Record, No. 2200, 29-35.

Sanchez, T.A. and White, D.W. (2011). "Stability of Curved Steel I-Girder Bridge during Construction," Structural Engineering, Mechanics, and Materials Report No. 77,

School of Civil and Environmental Engineering, Georgia Institute of Technology, Atlanta, GA.

Stallings, J.M., Cousins, T.E. and Stafford, T.E. (1999). "Removal of Diaphragms from Three-Span Steel Girder Bridge," Journal of Bridge Engineering, ASCE, 4(1), 63-70.

Wang, L. and Helwig, T.A. (2008). "Stability Bracing Requirements for Steel Bridge Girders with Skewed Supports," Journal of Bridge Engineering, ASCE, 13(2), 149-157.

Whisenhunt, T.W. (2004). "Measurements and Finite Element Modeling of the Non-Composite Deflections of Steel Plate Girder Bridges," M.S. Thesis, School of Civil Engineering, North Carolina State University, Raleigh, NC, 203 pp.

White, D.W. and Jung, S.-K. (2007), "Effect of Web Distortion on the Buckling Strength of Noncomposite Discretely-Braced I-Beams," Engineering Structures, Elsevier, 29, 1872-1888.

Yang, Y. and McGuire, W. (1984). "A Procedure for Analyzing Space Frames with Partial Warping Restraint," International Journal of Numerical Methods in Engineering, 20, 1377-1398.

Yura, J.A. (2001), "Fundamentals of Beam Bracing," Engineering Journal, AISC, 38(1), 11-26.

# VITA

Telmo Andres Sanchez Grunauer was born to Telmo Alejandro Sanchez Gonzalez and Mercy del Pilar Grunauer Alvear in Quito, Ecuador on December 3, 1979. He spent most of his childhood traveling in his father's truck, transporting machinery for oil exploration from the Ecuadorian coast to the Amazon jungle. In 2003, he obtained a Bachelor of Science degree in Mechanical Engineering from Escuela Politecnica del Ejercito. After working for four years for a steel fabricator, he joined the graduate program of Virginia Polytechnic Institute and State University, where he obtained the degree of Masters of Science in Civil Engineering. In 2008, he enrolled into the Ph.D. program in the School of Civil and Environmental Engineering at Georgia Institute of Technology. Upon graduation, Andres will join HDR Engineering, Inc. in Pittsburgh, PA, where he will be designing bridges and maybe, running a marathon.